U.PORTO

BIOTECNOLOGIA MOLECULAR E CELULAR APLICADA ÀS CIÊNCIAS DA SAÚDE

# Multifunctional lipid nanoparticles for breast cancer treatment

Andreia Almeida Granja

**D**
**2022**

U.PORTO

**Andreia Almeida Granja**. Multifucntional lipid nanoparticles for breast cancer treatment

**D**.ICBAS **2022**

**Multifucntional lipid nanoparticles for breast cancer treatment**

Andreia Almeida Granja

SEDE ADMINISTRATIVA

INSTITUTO DE CIÊNCIAS BIOMÉDICAS ABEL SALAZAR
FACULDADE DE FARMÁCIA

Andreia Almeida Granja

# Multifunctional lipid nanoparticles for breast cancer treatment

Tese de Candidatura ao grau de Doutor em Biotecnologia Molecular e Celular Aplicada às Ciências da Saúde;

Programa Doutoral da Universidade do Porto (Instituto de Ciências Biomédicas de Abel Salazar e Faculdade de Farmácia).

Orientador – Prof. Doutora Maria de La Salette de Freitas Fernandes Hipólito Reis Dias Rodrigues
Categoria – Professor Catedrático
Afiliação – Faculdade de Farmácia da Universidade do Porto

Co-orientador – Doutora Célia Tavares de Sousa
Categoria – Investigador Auxiliar
Afiliação – Instituto de Física dos Materiais da Universidade do Porto (IFIMUP).

Aos meus pais e irmão, Glória, José e Afonso Granja

*Remember to look up at the stars and not down at your feet. Try to make sense of what you see and wonder about what makes the universe exist. Be curious. And however difficult life may seem, there is always something you can do and succeed at. It matters that you don't just give up*.

Prof. Stephen Hawking

# Agradecimentos

*Happiness can be found, even in the darkest of times, if one only remembers to turn on the light*

Albus Dumbledore

Este percurso foi feito de altos e baixos, de clareza, mas também de alguma escuridão. Por isso, tenho que agradecer a todas as pessoas que me mostraram a "luz" e tornaram esta jornada muito mais feliz.

Em primeiro lugar, tenho que agradecer à minha orientadora, Professora Doutora Salette Reis que teve um papel fundamental na execução desta tese. Muito obrigada, em primeiro lugar por me ter recebido no laboratório desde o início da minha tese de mestrado em 2015, e por todo o seu apoio, incentivo, inteira disponibilidade e acompanhamento tão próximo ao longo deste percurso. Agradeço também pelo entusiasmo tão inspirador e contagiante que tem pela ciência!

À minha co-orientadora Doutora Célia Sousa pelo seu apoio, disponibilidade total, pelas discussões e partilha de conhecimento científico e pelas oportunidades que me proporcionou ao longo destes anos.

À Doutora Marina Pinheiro pelo seu apoio, partilhas e discussões científicas e pelo contributo na execução de alguns dos trabalhos práticos aqui desenvolvidos.

Ao Professor Doutor Ilídio Correia agradeço por me ter acolhido tão bem no seu laboratório, por todas as condições que me proporcionou e pela participação ativa na discussão dos trabalhos, que foram preponderantes para finalização desta tese. Agradeço também ao Doutor Duarte Diogo por todo o apoio e disponibilidade e pelo seu papel tão relevante na discussão do trabalho experimental desenvolvido no CICS-UBI. Tenho também que agradecer muito à Rita Sousa por ter sido muito mais do que uma parceira no laboratório, para além da sua enorme capacidade de trabalho, pelo seu contributo enorme no trabalho experimental, tenho também que agradecer o facto de me ter recebido tão bem na Covilhã, por me ter transmitido o seu amor pela cidade e pelas várias boleias que me deu até ao cimo da cidade. Agradeço também à Cátia Alves pelo seu contributo no trabalho experimental e pela sua simpatia e boa-disposição. Agradeço também a todos outros elementos do grupo do professor Ilídio

pela sua simpatia e por me receberem tão bem, nomeadamente à Cátia Solange, à Carolina, ao André, à Bruna, à Mariana e ao Nathanael.

Um obrigada gigante ao grupo $MB^2$ por ao longo destes anos me fazerem sentir em casa. Não poderia ter tido melhores companheiros. Um muito obrigada à Francisca Bento pelo seu contributo no trabalho experimental, pela sua simpatia e doçura e por ter confiado em mim para co supervisionar a sua tese de mestrado. Agradeço muito à Cláudia Nunes pela sua enorme generosidade e disponibilidade, pela partilha de conhecimento, pelo seu importante contributo nesta tese e pelo seu sentido de humor e gargalhada contagiantes. Agradeço também muito à Tânia Moniz pelo seu contributo na parte experimental e pela sua alegria, boa-disposição, bom-humor e partilha de experiências. Agradeço muito às minhas AA, Ana Isabel e Andreia Marinho que são para além de colegas de trabalho, grandes amigas. Obrigada pela vossa ajuda, apoio, confidências, pelos risos e pelos disparates e pelos nossos óptimos jantares! Sem dúvida que tornaram este meu percurso muito mais fácil e feliz. À Joana Magalhães pelo seu apoio incondicional, carinho, amizade e por me ter dado o "sobrinho" mais querido do mundo. Ao João Albuquerque e à Daniela Resende pela amizade, boa disposição e por todos os bons momentos. Agradeço também a todos os elementos atuais do grupo: Sofia Lima, Catarina Seabra, Filipa Soares, Zina, Daniela Loureiro, Irina, Raquel, Tomás, Marco, Ana Macedo, Mariana, Thaisa por todo o apoio. E estou grata também às pessoas que seguiram outros caminhos, mas que foram também muito importantes neste meu percurso: Pris, Catarina Pereira Leite, José, Nini, Alexandre, Luíse, Rúben, Suellen, Andreia Silva, o meu muito obrigada. Thank you so much "à minha amiga" Yong, Olfa and Abdu!

Tenho também que agradecer aos meninos dos laboratórios "do lado" Inês Ramos, Luísa, Sara, Sandia, Bruno, Renato, Sarah, Marieta, Mafalda, Sofia, Edite. E um obrigada especial à Sara Marques e à Ana Marta pelo carinho e amizade. Agradeço também muito à dona Manuela e à Vânia por todo o seu trabalho, pela sua boa-disposição e pelo carinho e a forma maternal como sempre me trataram.

Agradeço também a todas as pessoas da FCUP, Sara Freitas, João Horta Belo, Ana Silva, Mike, Rodrigo, Prof. Dr. Hélder Crespo, Prof Dr. João Pedro Araújo pela enriquecedora partilha de conhecimento de uma área científica tão diferente da minha.

Thank you to Dr María Victoria Gómez-Gaviro and all of the colleagues at Hospital Gregorio Marañón for the collaboration in the performance of the pilot *in vivo* studies.

I also have to thank for the amazing professional and personal experience that I had during my short-term scientific mission at NTNU – Trondheim, Norway. Thank you so much Prof. Dr. Mikael Lindgren and Dr. Odrun Gederaas for your generosity and hospitality. And thank you Tom for your endless kindness.

Um muito obrigada a todos os meus colegas do BiotecHealth, Mafalda, João, Joana, José, Eunice, Filipe e Rita por todo o apoio, pelos momentos de partilha e pela enorme jornada que foi a organização do Simpósio.

Às minhas "nenas", o melhor que a "Bioengenharia" me deu, Mariana, Bárbara, Lúcia, Eva, Tânia, Sofia e Rita por toda a amizade ao longo destes 10 anos, pelas partilhas e por todos os momentos de convívio que tão bem me fizeram sempre!

À Filipa Lourenço pela sua ajuda a manter a minha boa sanidade mental nestes últimos tempos.

Às minhas queridas amigas Ana, Joana, Fabiana e Xana muito obrigada pelos jantares e momentos de partilha tão importantes para mim ao longo de todos estes anos.

À minha "sis" Rita, minha companheira nesta jornada desde o início, minha melhor amiga e confidente, meu ombro amigo sempre presente em todos os momentos pessoais e profissionais, bons e maus, o meu mais sincero e profundo obrigada. Sem o teu apoio e compreensão tudo seria sido muito mais difícil. Obrigada pelas chamadas, pelos almoços e jantares sempre que algo "dava errado", pelas conversas e por toda a tua preocupação e compreensão. Thank you also Thomas for being such a nice friend, for inviting me to "game night" so many times and for your patience to "share" Rita with me.

Aos meus tios avós, Vicente, pelo seu cuidado e preocupação comigo e Baninha, que onde quer que esteja, estará feliz por mim e aos meus primos Victor, Babi, Carolina e Francisca.

À minha avó Rosa e ao meu tio Agostinho pelo carinho e cuidado e ao meu avô António que, onde quer que esteja espero que esteja orgulhoso.

À família Catarino pela imensa amizade por mim e pelos meus pais e irmão.

Aos meus avós António e Maria das Dores que me mimaram e cuidaram sempre com muito amor e que sempre serão para mim um exemplo. Estão sempre no meu pensamento e sei que onde quer que estejam, estão certamente orgulhosos de mim.

Aos meus tios e padrinhos, Helena e Francisco obrigada por todo o apoio, boa-disposição, preocupação e bons momentos de convívio. Aos meus primos Diogo e Catarina obrigada pelas boas conversas, pela vossa preocupação e interesse por este meu percurso e por me terem dado a priminha mais bem-disposta, simpática e bonita do mundo, a Leonor, que sem dúvida trouxe uma nova alegria a todos nós nestes últimos meses.

Ao meu irmão Afonso que tem tanto de enérgico como de carinhoso e que é a “luz dos meus olhos” desde que nasceu. Por último, tenho que agradecer infinitamente aos meus pais, Glória e José por tudo o que fizeram por mim ao longo destes anos, por me terem proporcionado as melhores condições para que este percurso fosse o mais fácil possível, pela sua imensa preocupação e conforto nos momentos mais difíceis e por todo o amor que sempre me deram.

# Funding

This work received financial support from PT national funds (FCT/MCTES, Fundação para a Ciência e Tecnologia and Ministério da Ciência, Tecnologia e Ensino Superior) through the project UIDB/50006/2020.

This work was also supported by FCT through the FCT PhD Programs, specifically by the BiotechHealth Program (Doctoral Program on Cellular and Molecular Biotechnology Applied to Health Sciences) with the grant PD/BI/128352/2017. I also acknowledge FCT (Fundação para a Ciência e Tecnologia) and ESF (European Social Fund) for the PhD grant SFRH/BD/130147/2017

# Publications

Ao abrigo do disposto do número 2, alínea a) do artigo 31o do Decreto-Lei no 115/2013 de 7 de Agosto, fazem parte integrante desta tese de doutoramento os seguintes trabalhos já publicados:

1. Granja, A., M. Pinheiro, C.T. Sousa, and S. Reis, *Gold nanostructures as mediators of hyperthermia therapies in breast cancer.* Biochem Pharmacol, 2021. **190**: p. 114639,10.1016/j.bcp.2021.114639.
2. Granja, A., R. Lima-Sousa, C.G. Alves, D. de Melo-Diogo, M. Pinheiro, C.T. Sousa, I.J. Correia, and S. Reis, *Mitoxantrone-loaded lipid nanoparticles for breast cancer therapy - Quality-by-design approach and efficacy assessment in 2D and 3D in vitro cancer models.* Int J Pharm, 2021. **607**: p. 121044,10.1016/j.ijpharm.2021.121044.

# Abstract

Breast cancer is the most commonly diagnosed and the deathliest cancer among women worldwide. Standard therapeutic is hindered by non-specific tumor distribution, leading to dose-limiting systemic side effects, reduced efficacy and possibility of disease recurrence. These limitations highlight the need to improve current breast cancer therapy through the design of innovative, economically viable and cancer-cell targeted strategies.

The main aim of this thesis was to use nanomedicine to improve breast cancer therapy. With that purpose, the first goal was to design, produce and optimize solid lipid nanoparticles (SLN) for the entrapment of the chemotherapeutic drug Mitoxantrone (Mito). SLN were produced using a low-cost, organic solvent-free method and optimized using a rationale Box-Behnken design. Nanoparticles showed a high drug entrapment efficiency of more than 90% and particle size around 200 nm, revealing adequate characteristics for intravenous administration and tumor passive targeting through the enhanced permeability and retention (EPR) effect. After determining the safety of the lipid nanocarrier in normal cells and in red blood cells (RBCs), the second main goal was to evaluate the anti-cancer activity of the nanosystem towards breast cancer in 2D cultures and, in tumor spherois that better mimic the complexity and heteregeneity of the tumor *in vivo*. Nanoparticles were found to be cyto and hemocompatible and were able to maintain the high anti-tumoral efficacy of the drug.

The third goal of this thesis was to explore different economically affordable functionalization strategies to improve the selectivity of the nanosystem towards cancer cells. Two different functionalization strategies were developed using hyaluronic acid (HA) and folic acid (FA), to target cancer cells overexpressing CD44 and FR receptors, respectively. Overall, the functionalization did not substantially affect the particles' main physicochemical properties, their hemocompatibility and anti-cancer efficacy. Moreover, both strategies were able to increase breast cancer cellular uptake, as assessed by flow cytometry and confocal microscopy. The findings obtained also suggested that the use of HA of a higher molecular weight may improve cancer cell internalization. Additionally, the FA-functionalized SLN were found to be internalized through clathrin-mediated endocytosis and macropynocitosis.

Due to breast cancer high heterogeneity and complexity and the fact that conventional treatment involves multiple drug of multiple therapy combination, the design of a multifunctional and multimodal nanosystem offers a great advantage in the management of

this malignancy. Therefore, the fourth goal of this thesis was to combine chemotherapy and hyperthermia, namely, photothermal therapy, to improve breast cancer therapeutic outcomes, by designing a multifunctional SLN co-loaded with Mito and gold nanorods (AuNRs). Based on the aforementioned studies, FA was selected for SLN surface decoration. The nanosystem could induce a temperature increase of more than 20˚C upon irradiation with a near-infrared (NIR) continuous laser by optimizing the irradiation exposure time (808 nm, 1.7 W $cm^{-2}$). An enhanced Mito release occurred following NIR irradiation, suggesting that the local generated heat by the plasmonic AuNRs was able to destabilize the particle's lipid matrix. Additionally, the active targeting was found to be effective, leading to a quicker and higher cancer cell internalization in breast cancer cells. This fact was corroborated by time-lapse live cell imaging uptake studies, where functionalized SLN were found to be internalized after 30 min, demonstrating a faster and higher uptake than non-functionalized SLN and free Mito. Finally, the combination of chemotherapy, thermal-induced drug release by NIR irradiation and photothermal therapy using AuNRs resulted in an enhanced breast cancer cell death.

To conclude, this thesis contributed to the development of an economically-viable nanomedicine strategy to enhance breast cancer therapy. An efficient encapsulation of Mito into SLN was obtained, along with adequate characteristics for intravenous administration. Two strategies of surface functionalization were developed to improve the selective targeting of tumor cells. Finally, two treatment modalities, chemotherapy and photothermal therapy were combined into one single multifunctional nanosystem, which can contribute to an enhanced breast cancer treatment performance and, desirably to the reduction dosages and associated side-effects of conventional chemotherapy in a future clinical application.

**Keywords:** solid lipid nanoparticles, breast cancer, Box-Behnken design, tumor spheroids, active cancer cell targeting, hyaluronic acid, folic acid, gold nanorods, photothermal therapy, multimodal therapy

# Resumo

O cancro da mama é o tipo de cancro mais comum e o mais mortal em mulheres em todo o mundo. A terapia convencional está limitada devido a uma distribuição não específica no organismo, não direcionada ao tumor, o que leva a efeitos colaterais sistémicos, que limitam as doses administradas e levam à redução da eficácia e possibilidade de doença recorrente. Estas limitações justificam a necessidade de melhorar a terapia atual do cancro da mama, através de estratégias inovadoras, economicamente viáveis e direcionadas às células cancerígenas.

O propósito principal desta tese foi recorrer à nanomedicina para melhorar a terapia atual do cancro da mama. Tendo isso em conta, o primeiro objetivo consistiu em desenhar, produzir e optimizar nanopartículas lipídicas sólidas (SLN) para a encapsulação do fármaco quimioterapêutico Mitoxantrona (Mito). As SLN foram produzidas utilizando um método de baixo custo e sem recurso a solventes orgânicos e optimizadas através de um desenho racional do tipo Box-Behnken. As nanopartículas produzidas demonstraram uma alta eficiência de encapsulação de mais de 90%, bem como características adequadas para uma administração intravenosa, , nomeadamente um tamanho de partícula aproximado de 200 nm e para acumulação na região do tumor através de direcionamento passivo, devido ao efeito da permeabilidade e retenção aumentadas (EPR). Após se avaliar a segurança do nanotransportador lipídico em células normais e em glóbulos vermelhos (RBCs), o segundo objetivo principal foi avaliar a actividade anticancerígena do nanosistema no cancro da mama em culturas 2D e em esferóides tumorais, que conseguem mimetizar de forma mais fidedigna a complexidade e a heterogeneidade do tumor. As nanopartículas demonstraram ser cito e hemocompatíveis e foram também capazes de manter a eficácia anti-tumoral do fármaco.

O terceiro objetivo desta tese foi o de explorar diferentes estratégias de funcionalização economicamente viáveis de forma a melhorar a selectividade do nanosistema para as células cancerígenas. Duas estratégias diferentes de funcionalização foram desenvolvidas usando ácido hialurónico e ácido fólico, de forma a direcionar o nanosistema para as células tumorais que sobreexpressam os receptors CD44 e os receptores de folato, respetivamente. De uma maneira geral, a funcionalização não afetou substancialmente as principais propriedades físico-químicas das partículas, bem como a sua hemocompatibiidade e a sua eficácia anti-tumoral. Para além disso, ambas as estratégias foram capazes de aumentar a internalização em células de cancro da mama, o que foi demonstrado pelos ensaios de citometria de fluxo e microscopia de confocal. Estes

resultados também sugeriram que o uso de um ácido hialurónico de maior peso molecular é mais vantajoso para o aumento da internalização em células cancerígenas. Para além disso, a internalização das nanoparticulas funcionalizadas com ácido fólico ocorreu através de endocitose mediada por clatrina e por macropinocitose.

Devido à grande heterogeneidade e complexidade do cancro da mama e ao facto da terapêutica convencional envolver geralmente a administração de vários fármacos e a combinação de múltiplas terapias, o desenho de um nanosistema multifuncional e multimodal pode oferecer uma grande vantagem no tratamento desta doença. Assim, o quarto objetivo desta tese foi o de combinar a quimioterapia com a hipertermia, nomeadamente com a terapia fototérmica, de forma a melhorar a eficácia do tratamento, através do desenvolvimento de uma SLN carregada com o fármaco Mito e com nanorods de ouro. Tendo por base os estudos anteriores, o ácido fólico foi seleccionado para a funcionalização da superfície das SLN. O nanosistema foi capaz de induzir um aumento da temperatura de mais de 20°C após irradiação com um laser contínuo de infravermelho próximo (NIR) após optimização do tempo de exposição (808 nm, 1.7 W $cm^{-2}$). O aumento da temperatura local originada pelo efeito plasmónico das nanorods de ouro levou ao aumento da libertação do fármaco Mito após irradiação com o laser NIR, o que sugere que o calor libertado pelas nanorods de ouro foi capaz de destabilizar a matriz lipídica da nanopartícula. Adicionalmente, a estratégia de direcionamento ativo baseada em ácido fólico foi eficaz, levando a uma mais rápida e maior internalização das nanopartículas nas células de cancro da mama. Este facto foi corroborado por estudos realizados em tempo-real com células vivas, onde as SLN funcionalizadas foram internalizadas após 30 min de incubação mais rapidamente e em maior quantidade do que as SLN não funcionalizadas e o fármaco livre. Por último, a combinação da quimioterapia, libertação do fármaco mediada pelo aumento da temperatura local após irradiação com luz NIR e terapia fototérmica resultou num aumento da morte das células do cancro da mama.

Concluindo, esta tese contribuiu para o desenvolvimento de uma estratégia de nanomedicina economicamente viável de forma a melhorar a terapia do cancro da mama. As SLN desenvolvidas permitiram obter uma alta eficiência de encapsulação do fármaco Mito, bem como características adequadas para uma administração por via intravenosa. Duas estratégias de funcionalização foram desenvolvidas para melhorar o direcionamento selectivo para as células tumorais. Finalmente, duas modalidades de tratamento, a quimioterapia e a terapia fototérmica, foram combinadas num único nanosistema multifuncional, o que pode contribuir para aumentar a eficiência do tratamento e

possivelmente para a redução das dosagens e dos efeitos adversos da quimioterapia convencional numa futura aplicação clínica.

**Palavras-chave:** nanopartículas lipídicas sólidas, cancro da mama, Box-Behnken, esferóides tumorais, direcionamento ativo para células cancerígenas, ácido hialurónico, ácido fólico, nanorods de ouro, terapia fototérmica, terapia multimodal.

# Table of contents

**Abstract**..... I

**List of Figures**..... IX

**List of Tables**..... XIX

**List of abbreviations and symbols**..... XXII

**Chapter 1. Thesis structure**..... 1

**Chapter 2. Theoretical background**..... 3

**2.1.** Therapeutic advances in breast cancer using lipid nanoparticles: from targeting strategies to the development of multifunctional nanosystems..... 11

**2.2.** Gold nanostructures as mediators of hyperthermia therapies in breast cancer..... 53

**Chapter 3. Motivation and objectives**..... 75

**Chapter 4. Progress Beyond the State of the Art**..... 81

**4.1.** Mitoxantrone-loaded lipid nanoparticles for breast cancer therapy – Quality-by-design approach and efficacy assessment in 2D and 3D in vitro cancer models..... 83

**4.2.** Hyaluronic acid-decorated lipid nanoparticles for enhanced delivery of mitoxantrone: assessing the influence of the polymer molecular weight on breast cancer cell targeting ability ..... 109

**4.3.** Folate receptor-mediated delivery of mitoxantrone-loaded solid lipid nanoparticles to breast cancer cells..... 137

**4.4**. Multifunctional targeted solid lipid nanoparticles for combined photothermal therapy and chemotherapy of breast cancer..... 165

**Chapter 5. Concluding remarks and future perspectives**..... 197

**Appendix**..... 203

Appendix I..... 205

Appendix II..... 209

# List of Figures

## Chapter 2. Theoretical background

**Figure 1.** Molecular structure and molecular weight (MW) of Mitoxantrone……..4

### 2.1. Therapeutic advances in breast cancer using lipid nanoparticles: from targeting strategies to the development of multifunctional nanosystems

**Figure 1.** Schematic representation of breast cancer development, progression and metastasis……. 17

**Figure 2.** Summary of the recent strategies for the management of breast cancer using lipid nanoparticles…….. 25

### 2.2. Gold nanostructures as mediators of hyperthermia therapies in breast cancer

**Fig. 1.** Summary of the effects of hyperthermia at the cellular and tumor microenvironment levels. At the cellular level, hyperthermia can elicit cancer cell death through different mechanisms. Heat induces the denaturation of several nuclear proteins, impairing different mechanisms related to DNA repair. Additionally, hyperthermia compromises the mitochondrial membrane permeability and causes endoplasmic reticulum stress, leading to intracellular Ca2+ accumulation and release of ROS, which will culminate in cell apoptosis. In the tumor microenvironment, hyperthermia can improve blood flow and perfusion enhancing the accumulation of drugs and other compounds or even immune cells in the tumor region. Heat can also directly stimulate the immune system and promote the release of immunogenic ligands and tumor antigens, leading to the activation of natural killer (NK) and dendritic cells (DCs) and, subsequently, to the activation and recruitment of cytotoxic CD8+ T cells……... 57

**Fig. 2.** Principle of PTT in cancer management. The photothermal agent is injected either intravenously or intratumorally and accumulates in the tumor tissue via EPR effect or due to active cancer cell-targeting. Tumor is then irradiated with NIR light (using either a

continuous or a pulsed laser) with a specific power intensity for a short period of time. The photothermal agent will then release heat upon NIR stimulus, leading to local hyperthermia and tumor cell death…….. 58

**Fig. 3.** Transmission electron microscopy images of different types of gold nanostructures. (A) Gold nanorods. Adapted from [106], Copyright 2019 with permission from Elsevier. (B) Gold nanostars. Adapted from [112]. (C) Spherical gold nanoparticles. Adapted from [116], Copyright 2018, with permission from Elsevier. (D) Gold nanoshells. Adapted from [77].. 60

**Fig. 4.** Summary of strategies employed for gold-mediated PTT in breast cancer. Different types of gold nanostructures have been produced including nanorods, nanostars, nanoshells, spherical nanoparticles and hybrid nanostructures comprising two or more types of nanoparticles into one single nanoplatform composed of organic or inorganic materials. Surface modification has been performed to improve the biocompatibility and circulation time of the nanoparticles, the most common being the PEGylation of the nanoparticle surface. Active cancer-cell targeting has been performed through functionalization with specificc antibodies, peptides, aptamers or small molecules. Most studies combined PTT with other therapies taking advantage of the synergistic effects between them, including chemotherapy, gene therapy, immunotherapy, photodynamic therapy and radiotherapy. Theranostic nanoplatform have also been designed using several imaging techniques for in situ tumor and nanoparticle imaging and thermal monitoring. Imaging techniques figures adapted with permission from [124,135,137], Copyright 2020, 2016, American Chemical Society, from [126,130], Copyright 2018, 2017 with permission from the Royal Society of Chemistry and [94,154], Copyright 2019, 2016 with permission from Elsevier……. 61

**Chapter 4. Progress Beyond the State of the Art**

**4.1. Mitoxantrone-loaded lipid nanoparticles for breast cancer therapy – Quality-by-design approach and efficacy assessment in 2D and 3D in vitro cancer models**

**Fig. 1.** TEM photographs of SLN (A) and SLN-Mito (B), Magnification 50000X……. 89

**Fig. 2.** Storage stability of (A) particle size, (B) PDI, (C) zeta potential and (D) EE% over 24 weeks at 4°C. Data are expressed as mean ± SD (n = 3). Differences between control (time

point 0) and other time points were performed using One-way ANOVA followed by Dunnett's test (*) denotes statistically significant differences relative to the correspondent week 0. *p<0.05, **p<0.01…….. 89

**Fig. 3.** Cumulative release of Mito at physiological (7.4) and acidic (5.0) pH. Data are expressed as mean ± SD (n = 3)……. 90

**Fig. 4.** *In vitro* hemolysis assay of SLN and SLN-Mito. (**A**) Image of the samples treated with the highest concentration (24 mg/mL) tested of SLN and SLN-Mito and controls - negative (saline solution) and positive (TX-100 - 1% v/v) following 1h incubation. (**B**) Graphic representation of the concentration-dependent hemolysis induced by SLN and SLN-Mito. Data are expressed as mean ± SD (n = 3)……. 90

**Fig. 5.** Effect of unloaded SLN on the viability of NHDF (**A**) and breast cancer cell line MCF-7 (**B**) at different lipid concentrations after 24 and 48h of incubation. Data are expressed as mean ± SD (n = 5)…….. 91

**Fig. 6.** Anti-cancer activity of SLN-Mito versus free Mito on MCF-7 cells at increasing concentrations of Mito (and corresponding lipid concentrations) after 24h (**A**) and 48h (**B**) of incubation. Differences between groups were determined using two-way ANOVA using Tukey's test. Data are expressed as mean ± SD (n = 5). ** $p$<0.01, *** $p$<0.001, **** $p$<0.0001…….. 91

**Fig. 7**. CLSM z-stacks free drug (**A**) *vs.* SLN-Mito (**B**) at a concentration of 10 μM of Mito in heterotypic spheroids at a penetration depth of 15, 45, 75 and 105 μm, and respective plots of the fluorescence intensity (F. I.) across the spheroid's diameter. Red channel: Mito. Scale bars correspond to 100 μm……..…….. 92

**Fig. 8.** Anti-cancer activity of SLN-Mito versus free Mito on heterotypic spheroids. Data are expressed as mean ± SD (n = 30). Differences between groups were determined using two-way ANOVA using Tukey's test. ** $p$<0.01…… 93

**Fig.9.** CLSM images of heterotypic spheroids after incubation with culture medium and free drug and SLN-Mito at a concentration of 21 μM of Mito following Calcein-AM/PI staining. Green channel: Calcein-AM; Red channel: PI. Scale bars correspond to 100 μm……... 93

**Supplementary data**

**Figure S1.** Correlation of the measured vs. predicted values of the dependent variables after fitting using the quadratic model. (**A**) Size (**B**) EE% (**C**) LC%..... 102

**Figure S2.** Response contour plots in two-dimensions representing the statistically significant effects (*p*-value<0.05) for each dependent variable. (**A**) Effect of the amount of Mitoxantrone and surfactant on particle size. (**B**) Effect of the amount of Mitoxantrone and surfactant on EE%. (**C**) Effect of the amount of lipid and Mitoxantrone on LC%. (**D**) Effect of the amount of lipid and surfactant on LC%..... 103

**Figure S3.** Particle size determination of SLN (A and B) and SLN-Mito (C and D) using NTA. (A) and (C) Average size distribution following 5 measurements. (B) and (D) NTA video frames…….. 104

**Figure S4.** Effect of unloaded SLN on the viability of HER-2 positive breast cancer cell line AU-565 (**B**) at different lipid concentrations after 24 and 48h of incubation. Data are expressed as mean ± SD (n = 5)…….. 106

**Figure S5.** Anti-cancer activity of SLN-Mito versus free Mito on AU-565 cells at increasing concentrations of Mito (and corresponding lipid concentrations) after 24h (**A**) and 48h (**B**) of incubation. Differences between groups were determined using two-way ANOVA using Tukey's test. Data are expressed as mean ± SD (n = 5). ****$p$<0.0001…….. 106

**Figure S6.** Dose-response curve of MCF-7 cells after 48h incubation with unloaded SLN…….....……. 107

**Figure S7.** Dose-response curves of MCF-7 cells after 24h (**A**) and 48h (**B**) incubation with free mitoxantrone and SLN-Mito……..……..... 109

## 4.2. Hyaluronic acid-decorated lipid nanoparticles for enhanced delivery of mitoxantrone: assessing the influence of the polymer molecular weight on breast cancer cell targeting ability

**Figure 1**. **NMR characterization of the DPPE-HA conjugates** (**A**) Chemical structure of HA (left) and DPPE (right) (**B**) NMR spectra of the DPPE-HA20 conjugate and their precursors DPPE (middle) and HA20 (bottom). (**C**) NMR spectra of the DPPE-HA1000 and their precursors DPPE (middle) and HA1000 (bottom)……..…… 122

**Figure 2**. ***In vitro*** **drug release assay**. Cumulative drug release of Mito from SLN HA 0 and SLN HA1000 at pH 7.4 and pH 5.0. Values represent mean ± SD (n=3)……. 124

**Figure 3. Storage stability study**. Effect of the time of storage on size (A), PDI (B), zeta potential (C) and EE& (D) of SLN DPPE-HA nanoformulations unloaded (DPPE-HA) and loaded (DPPE-HA-Mito). Values represent the mean ± SD (n=3). Differences between groups were assessed using two-way ANOVA followed by Dunnet post-hoc test *p<0.05, **p<0.01, ***p<0.001, ****<0.0001 relatively to the correspondent nanoformulation at week 0……..125

**Figure 4.** ***In vitro*** **hemolysis assay**. RBCs from three human donors were incubated with increasing concentrations of loaded and unloaded nanoformulations. Values represent mean ± SD (n=3)…….. 126

**Figure 5. Effects of the unloaded SLN on MCF-7 cell viability.** Cell viability was assessed by the resazurin assay after 24 hours of exposure to the different unloaded nanoformulations at increasing concentrations of lipid. Values represent the mean ± SD (n=3)……. 127

**Figure 6. Effects of drug-loaded SLN on MCF-7 cell viability**. (A) Cell viability was assessed by the resazurin assay after 24 hours of exposure to the different drug-loaded nanoformulations at increasing concentrations of Mito. Values represent the mean ± SD (n=3). (B) Values of $IC_{50}$ determined for each drug-loaded nanoformulation…..… 127

**Figure 7. CLSM images of the MCF-7 cellular uptake**. Cells were incubated with the different Mito-loaded SLN (SLN, SLN-HA20, SLN-HA1000) for 4h and 24h. Blue channel: Hoechst 33342 (nucleus). Green channel: LysoTracker™ Green DND-26. Red channel: Mito……128

**Figure 8. MCF-7 cellular uptake of C6-loaded SLN measured by flow cytometry.** Cells were incubated with the different nanoformulations for 1h, 4h and 24h. Data expressed as mean ± SD (n = 3). Differences between groups were assessed using two-way ANOVA followed by Dunnet post-hoc test **** p<0.0001 relatively to the non-functionalized SLN…… 129

**Supplementary data**

**Figure S1.** NTA analysis of SLN-HA20-Mito (A) and SLN-HA1000-Mito (B). Size distribution and NTA video frames…… 135

**Figure S2.** Dose-response curves of MCF-7 cells following incubation with free drug, HA-functionalized and non-functionalized Mito-loaded SLN for 24h…….. 135

## 4.3. Folate receptor-mediated delivery of mitoxantrone-loaded solid lipid nanoparticles to breast cancer cells

**Figure 1. Storage stability of SLN-FA-Mito during 6 months stored at 4˚C**: Size (**A**), PDI (**B**), Zeta potential (**C**) and EE% (**D**). Data expressed as mean ± SD (n = 3). Differences between groups were assessed using two-way ANOVA followed by Dunnet post-hoc test *p<0.05, relatively to week 0……. 149

**Figure 2. *In vitro* drug release.** Cumulative drug release of SLN-FA-Mito at pH 5.0 and 7.4. Data expressed as mean ± SD (n = 3)……..……. 150

**Figure 3. *In vitro* hemolysis assay.** Human RBCs were exposed to increasing concentrations of SLN-FA-Mito and incubated at 37˚C for 1h. Data expressed as mean ± SD using RBCs from 3 healthy donors (n=3)……..…… 150

**Figure 4. Effect of the unloaded (A) and Mito-loaded (B) nanoformulations on MCF-7 cell viability.** MCF-7 cells were treated with the different nanoformulations for 24 h and cell viability was determined by the resazurin assay. Data expressed as mean ± SD (n = 3). Differences between groups were assessed using two-way ANOVA followed by Dunnet post-hoc test **p<0.01 relatively to the free drug. ……..…….. 152

**Figure 5. Apoptosis of MCF-7 cells following incubation with the nanoformulations using the FITC Annexin V Apoptosis assay.** Cells were incubated for 24 h with the different nanoformulations and free drug at a concentration of 5 µg/mL (**A**) and 50 µg/mL of lipid (**B**), corresponding to 0.21 µM and 2.1 µM of Mito. Data expressed as mean ± SD (n = 3). Differences between each treatment and control group were assessed using two-way ANOVA followed by Dunnet post-hoc test. viable: **** p<0.0001, *** p<0.001; early apoptosis: •••• p<0.0001; late apoptosis # p<0.05; necrosis: ‡ p<0.05……153

**Figure 6. CLSM images of the MCF-7 cellular uptake of non-functionalized and functionalized Mito-loaded SLN.** Cells were incubated with the nanoformulation for 4h. Blue channel: Hoechst 33342 (nucleus). Green channel: LysoTracker™ Green DND-26. Red channel: Mito.…… 154

**Figure 7. Quantification of MCF-7 cellular uptake of C6-labelled SLN by flow cytometry**. Cells were incubated with the different nanoformulations for 1h, 4h and 24h. Data expressed as mean ± SD (n = 3). Differences between groups were assessed using two-way ANOVA followed by Sidak post-hoc test * p<0.05, **** p<0.0001 relatively to the non-functionalized SLN at each time-point.…… 155

**Figure 8. Effect of energy and different cellular uptake pathway inhibitors on MCF-7 internalization of SLN-C6 and SLN-FA-C6**. Cells were incubated with the different pathway inhibitors for 30 min prior to incubation with the nanoparticles for 1h. Fluorescence values were normalized with the values of the cells incubated at 37˚C without any inhibitor. Data expressed as mean ± SD (n = 3). Differences between groups were assessed using two-way ANOVA followed by Dunnet post-hoc test *p<0.05, **p<0.01,****p<0.0001 relatively to corresponding control SLN. ……. 157

**Supplementary data**

**Figure S1. Scatter plots of Annexin V (x-axis) vs 7-AAD (y-axis**) obtained by flow cytometry. MCF-7 cells were incubated with SLN, SLN-FA, SLN-Mito, SLN-FA-Mito and free Mito at a concentration of 5 µg/mL (**A**) and 50 µg/mL of lipid (**B**) and the FITC Annexin V Apoptosis assay was performed after 24h. The plots represented in A and B are independent experiments obtained in different days…… 163

**Figure S2. Quantification of C6-labelled SLN by flow cytometry in L929 cells**. Cells were incubated with the different SLN and free drug for 1h and 4h. Data expressed as mean ± SD (n = 3). Differences between groups were evaluated using two-way ANOVA followed by Sidak post-hoc test * p<0.05, **** p<0.0001 relatively to the non-functionalized SLN at each time-point.……163

## 4.4. Multifunctional targeted solid lipid nanoparticles for combined photothermal therapy and chemotherapy of breast cancer

**Figure 1. Physicochemical characterization of SLN Au-Mito-FA and corresponding unloaded nanoformulation (SLN Au-FA)**. (**A**) Hydrodynamic size, PDI and zeta potential

determined by DLS and EE%. (**B**) Particle size distribution measured through NTA and corresponding video frames of SLN-Au-FA (left) and SLN Au-Mito-FA (right)…… 177

**Figure 2. NIR light irradiation effect on the temperature variation (∆T) and drug release of the nanoformulations** (**A**) ∆T of SLN Au-FA and SLN Au-FA-Mito at two different concentrations of AuNRs upon irradiation with NIR laser (808 nm, 1.7 W $cm^{-2}$) for 5 min. PBS was used as a control. (**B**) Cumulative release of Mito from SLN Au-Mito-FA with and without NIR laser irradiation for 5 min. Data are expressed as mean ± SD (n = 3)…… 178

**Figure 3. Hemolytic activity of the nanoformulations at different concentrations**. Data represents the average of 3 assays using RBCs from 3 human donors……..…..… 179

**Figure 4. Cytocompatibility of unloaded SLN.** Cell viability was evaluated following incubation with SLN Au-FA at different concentrations in normal (NHDF) and breast cancer cells (MCF-7) after 24 h and 48 h incubation. Data are expressed as mean ± SD (n = 5)**.**……180

**Figure 5. Cellular uptake of C6-labelled SLN in MCF-7 cells using flow cytometry. (A)** Time-dependent uptake of functionalized (SLN C6-FA) and non-functionalized (SLN C6) C6-labelled SLN for 24 h. Values represent mean ± SD; n = 3. Differences between groups were assessed using two-way ANOVA followed by Sidak post-hoc test. *$p$<0.05, **$p$<0.01, ****$p$<0.0001 (**B**) Michaelis-Menten kinetics parameters for SLN C6 and SLN C6-FA…. 181

**Figure 6. CLSM images of SLN uptake in MCF-7 cells**. Cellular uptake of non-functionalized (**A**) and functionalized SLN (**B**) after incubation for 4 h. Blue channel: Hoechst 33342® (nucleus). Green channel: LysoTracker™ Green DND-26. Red channel: Mito.... 182

**Figure 7. Figure 7. Time-lapse CLSM of the MCF-7 cellular uptake of free Mito, SLN-Mito and SLN-Mito-FA**. Cells were incubated with the different conditions at 37 ˚C for 30 min in the confocal incubator chamber and images were acquired every 5 min. (**A**) CLSM images of uptake of free Mito, SLN and SLN-FA in MCF-7 cells for 30 min. (**B**) Normalized fluorescence intensity of Mito relative to the nucleus fluorescence signal for each condition. Blue channel: Hoechst 33342® (nucleus). Red channel: Mito.……..…….183

**Figure 8.** Phototherapeutic and combined PTT-chemotherapy effects of the nanoformulations in MCF-7 cells upon NIR irradiation (808 nm, 1.7 W $cm^{-2}$) for 5 min. Cells were treated for 24 h. Data are expressed as mean ± SD (n = 5). Differences between

groups were assessed using two-way ANOVA followed by Sidak post-hoc test ***$p$<0.001, ****$p$<0.0001…….. 184

**Supplementary data**

**Figure S1**. NMR spectra of mitoxantrone hydrochloride after incubation during 30 min at 20, 30, 40, 50, 60 and 70˚C…….…… 192

**Figure S2. Hemolysis assay.** Image of the samples treated with the highest concentration of nanoformulation tested (40 µg/mL of AuNRs) of SLN-Au-Mito-FA, SLN-Au-FA and controls - negative (saline solution) and positive (TX-100 - 1% v/v) following 1h incubation…… …… 193

**Figure S3. CLSM images of SLN uptake in MCF-7 cells**. Cellular uptake of non-functionalized (**A**) and functionalized SLN (**B**) after incubation for 24 h. Blue channel: Hoechst 33342 (nucleus). Green channel: LysoTracker™ Green DND-26. Red channel: Mito…… 195

## Appendix

**Figure A1.** Study of the influence of pulser laser output power (**A**) and AuNRs concentration (**B**) on the heating behaviour of AuNRs over time…….. 206

**Figure A2.** Study of the influence of the output power of a continuous laser (800 nm) and concentration of AuNRS on the heating behaviour of AuNRs over time…….. 207

**Figure A3.** Maximum temperature reached following pulsed (left) and continuous (right) NIR laser irradiation of the gold nanorods at a concentration of 75 µg/mL at the maximum power for the two laser types measured using a FLIR i7 Infrared Thermal camera. Pulsed laser specifications: Femtosecond Ti:Sapphire amplifier (FemtopowerTM) running with 1kHz repetition rate, pulse duration of 30 fs, wavelength 800 nm. Continuous wave laser: 808 nm with a maximum output power of 2.5W……. 207

**Figure A4.** SLN biodistribution 0h (left) and 1h (right) after retro-orbital injection in healthy wild-type C57BL/6 mice. Left mouse injected with saline solution (control), right mouse injected with the SLN-FA-Cy5 nanoformulation. Data were obtained suing an IVIS Spectrum 200 In vivo Imaging System (Perkin Elmer, MA, USA). Exposure time 20, binning factor 2, excitation filter 620, emission filter 670, f number 1, field of view 10…… 210

# List of Tables

## Chapter 2. Theoretical background

### 2.2. Gold nanostructures as mediators of hyperthermia therapies in breast cancer

**Table 1.** Gold nanorods…….…….. 62

**Table 2.** Gold nanostars…….…….. 63

**Table 3.** Spherical gold nanoparticles…….…… 64

**Table 4**. Gold nanoshells…….…….. 66

**Table 5.** Inorganic hybrid nanostructures……...…... 66

**Table 6.** Organic hybrid nanostructures …… 67

## Chapter 4. Progress Beyond the State of the Art

### 4.1. Mitoxantrone-loaded lipid nanoparticles for breast cancer therapy – Quality-by-design approach and efficacy assessment in 2D and 3D in vitro cancer models

**Table 1**. Regression analysis for the selected responses (size, EE% and LC%) using the quadratic model. Statistically significant values are represented in bold, *p*-value ≤ 0.05 with a 95% confidence interval…… 88

**Table 2.** Predicted versus experimental values obtained for each response (size, EE%, and LC%) of the optimum nanoformulation…….. 88

**Table 3.** Physicochemical characterization of the optimized SLN (SLN-Mito) and corresponding unloaded SLN (SLN): size (determined by DLS), PDI, Zeta potential, EE% and LC%. Data are expressed as mean ± SD (n = 3)…… 88

**Supplementary data**

**Table S1. Lipid screening.** Solubility study of mitoxantrone in different solid lipids…….. 98

**Table S2.** Composition of the 15 formulations produced for the experimental design and correspondent characterization parameters: Size, EE%, and LC%..... 99

**Table S3**. Analysis of variance (ANOVA) for Size. Statistically significant values are represented in bold, *p*-value ≤ 0.05 with a 95% confidence interval……. 100

**Table S4**. Analysis of variance (ANOVA) for EE%. Statistically significant values are represented in bold, *p*-value ≤ 0.05 with a 95% confidence interval……. 100

**Table S5.** Analysis of variance (ANOVA) for LC%. Statistically significant values are represented in bold, p-value ≤ 0.05 with a 95% confidence interval……. 101

**Table S6.** Correlation coefficient ($R^2$) values obtained from fitting of different drug release models for each dissolution medium studied…….. 105

**Table S7.** $IC_{20}$, $IC_{50}$ and $IC_{80}$ values of free Mito and SLN-Mito on 2D cultures of MCF-7. Values were determined using GraphPad Prism Software (v.6.0, GraphPad Software, CA, USA)…….. 108

## 4.2. Hyaluronic acid-decorated lipid nanoparticles for enhanced delivery of mitoxantrone: assessing the influence of the polymer molecular weight on breast cancer cell targeting ability

**Table 1.** Physicochemical characterization of the nanoformulations unloaded (DPPE-HA 20-60 and DPPE-HA 1000-1800) and loaded with Mito (DPPE-HA 20-60-Mito and DPPE-HA 1000-1800-Mito): size, PDI, zeta potential, EE% and LC%. Values represent mean ± SD (n=3)…….. 123

**Supplementary data**

**Table S1.** Physicochemical characterization of C6-loaded SLN……. 136

**4.3. Folate receptor-mediated delivery of mitoxantrone-loaded solid lipid nanoparticles to breast cancer cells**

**Table 1.** Physicochemical characterization of the functionalized versus non-functionalized Mito loaded nanoformulations: size, PDI, zeta potential, EE% and LC%..... 148

**4.4. Multifunctional targeted solid lipid nanoparticles for combined photothermal therapy and chemotherapy of breast cancer**

**Supplementary data**

**Table S1.** Physicochemical characterization of C6-loaded SLN …… 194

# List of abbreviations and symbols

| | |
|---|---|
| **5-FU** | 5-fluorouracil |
| **ALA** | 5-aminolevulinic acid |
| **AMF** | Alternating magnetic field |
| **AuNPs** | Gold nanoparticles |
| **AuNRs** | Gold nanorods |
| **BBB** | Blood-brain barrier |
| **BCRP** | Breast cancer resistance protein |
| **BSA** | Bovine serum albumin |
| **C6** | Coumarin-6 |
| **CIK cells** | Cytokine-induced killer cells |
| **CLSM** | Confocal Laser Scanning Microscopy |
| **CT** | Computed tomography |
| **CTAB** | Cetyltrimethyl ammonium bromide |
| **CXCR4** | C-X-C chemokine receptor type 4 |
| **DALYs** | Disability-adjusted life years |
| **DC** | Dendritic cells |
| **DCC** | Dicyclohexylcarbodiimide |
| **DCIS** | Ductal carcinoma *in situ* |
| **DLS** | Dynamic light scattering |
| **DMSO** | Dimethyl sulfoxide |
| **DPPE** | 1,2-dipalmitoyl-*sn*-glycero-3-phosphoethanolamine |
| **DR5** | Death receptor-5 |
| **DSPE** | 1,2-distearoyl-*sn*-glycero-3-phosphoethanolamine |
| **ECM** | Extracellular matrix |
| **EDC** | Ethyldimethyl-aminopropyl-carbodiimide |

| | |
|---|---|
| **EE%** | Entrapment efficiency |
| **EGFR** | Epidermal Growth Factor Receptor |
| **ELS** | Electrophoretic light scattering |
| **EMA** | European Medicines Agency |
| **EPR** | Enhanced permeability and retention |
| **ER** | Estrogen receptor |
| **FA** | Folic acid |
| **FDA** | Food and Drug Administration |
| **FR** | Folate receptor |
| **GRAS** | Generally recognized as safe |
| **HA** | Hyaluronic acid |
| **HER2** | Human epidermal growth factor receptor 2 |
| **HR** | Hormone receptors |
| **ICG** | Indocyanine green |
| **IFP** | Interstitial fluid pressure |
| **LC%** | Loading capacity |
| **MDR** | Multidrug resistance |
| **MHT** | Magnetic hyperthermia |
| **Mito** | Mitoxantrone |
| **MRI** | Magnetic resonance imaging |
| **MSCs** | Mesenchymal stem cells |
| **NGO** | Nanosized graphene oxide |
| **NHDF** | Normal Human Dermal Fibroblasts |
| **NHS** | N-hydroxysuccinimide |
| **NIR** | Near infrared |
| **NK** | Natural killer |
| **NLC** | Nanostructured lipid carriers |
| **NMR** | Nuclear magnetic resonance |

| | |
|---|---|
| **NTA** | Nanoparticle tracking analysis |
| **P-gp** | P-glyocoprotein |
| **PA** | Photoacoustic |
| **PBS** | Phosphate Buffered Saline |
| **PDI** | Polydispersity index |
| **pdna** | Plasmid DNA |
| **PDT** | Photodynamic therapy |
| **PEG** | Polyethylene glycol |
| **PenStrep** | Penicillin-Streptomycin |
| **PET** | Positron emission tomography |
| **PI** | Propidium iodide |
| **PLGA** | Poly (D, L-lactide-co- glycolic) acid |
| **PR** | Progesterone receptor |
| **PS** | Photosensitizer |
| **PTT** | Photothermal therapy |
| **RBCs** | Red blood cells |
| **RES** | Reticuloendothelial system |
| **RGD** | Arginine-glycine-aspartic acid |
| **SiRNA** | Small interfering RNA |
| **SLN** | Solid lipid nanoparticles |
| **SPR** | Surface plasmon resonance |
| **TDLU** | Terminal duct lobular unit |
| **TEM** | Transmission Electron Microscopy |
| **TNBC** | Triple negative breast cancer |
| **TPGS** | D-α-tocopheryl polyethylene glycol 1000 succinate |

# Chapter 1

## Thesis structure

This thesis is organized into 5 chapters.

### Chapter 1. Thesis structure

In this chapter a description of the thesis organization is given along with an overview of the contents presented in each chapter.

### Chapter 2. Theoretical background

This chapter aims to contextualize the thesis by describing the main aspects of breast cancer, the current treatment, their limitations and opportunities of new nanotechnology-based therapies. In particular, the potential of drug nanodelivery and photothermal therapy in the treatment of this malignancy is highlighted. With that purpose, two sub-chapters were included:

**2.1.** Therapeutic advances in breast cancer using lipid nanoparticles: from targeting strategies to the development of multifunctional nanosystems (To be submitted).

This sub-chapter comprises a literature review describing the main clinical aspects of breast cancer, including its pathophysiology, conventional therapeutics and limitations. The therapeutic potential of nanomedicine in this disease is then highlighted, with a particular emphasis on lipid nanoparticles, focusing on their valuable features and on the most recent advances made in this area, from simple to more complex multifunctional nanosystems.

**2.2.** Gold nanostructures as mediators of hyperthermia therapies in breast cancer (Biochem Pharmacol, 2021. 190, 114639).

In this sub-chapter the molecular and clinical basis of hyperthermia and its role on the management of cancer disease are detailed. The emergent are of nanoparticle-mediated hyperthermia is then described focusing on photototherapy using gold nanostructures, where an overview of the most recent preclinical studies in the context of breast cancer is presented.

## Chapter 3. Motivation and objectives

In this chapter the motivation and the general and specific research aims of this PhD thesis are described.

## Chapter 4. Progress Beyond the State of the Art

In this chapter the progress beyond the state of the art is outlined in the format of four original research articles:

**4.1.** Mitoxantrone-loaded lipid nanoparticles for breast cancer therapy – Quality-by-design approach and efficacy assessment in 2D and 3D in vitro cancer models (Published in International Journal of Pharmaceutics, 2021)

**4.2.** Hyaluronic acid-decorated lipid nanoparticles for enhanced delivery of mitoxantrone: assessing the influence of the polymer molecular weight on breast cancer cell targeting ability (To be submitted)

**4.3.** Folate receptor-mediated delivery of mitoxantrone-loaded solid lipid nanoparticles to breast cancer cells (To be submitted)

**4.4** Multifunctional targeted solid lipid nanoparticles for combined photothermal therapy and chemotherapy of breast cancer (To be submitted)

## Chapter 5. Concluding Remarks and Future Perspectives

This final chapter discusses the main findings and outcomes and outlines the main limitations of the experimental work. In addition, future perspectives are highlighted.

# Chapter 2

## Theoretical background

### Breast cancer

Breast cancer is the deathliest cancer type among women worldwide [1]. This malignancy is highly complex and heterogeneous, being classified based on different parameters, such as histology, expression of specific molecular biomarkers and stage of the disease, with different prognosis and treatment regimens [2, 3]. Conventional therapies, such as chemotherapy, are limited by the lack of precision towards cancer cells, leading to dose-limiting systemic side-effects [4, 5]. Moreover, cancer cells may develop multidrug resistance, which further decreases the efficacy of the therapeutic [6]. The lack of treatment efficacy may result in disease recurrence, metastasis and, ultimately, death [6].

Different therapies and drug combinations can be used, depending on several factors, such as the tumor subtype and stage, patient menopausal status, evidence of metastatic or recurrent disease, among others. Chemotherapy is one of the most common therapeutics, with demonstrated efficacy in all breast cancer subtypes and also in cases of advanced and metastatic disease [4, 7]. Different drug combination can be used in breast cancer chemotherapy, including taxanes, anthracyclines and platinum compounds [8].

### Mitoxantrone

Mitoxantrone (Mito) is a synthetic antineoplastic drug and anthracycline analogue from the class of the anthracenediones, used in chemotherapeutic regimens for advanced breast cancer [9, 10]. Its molecular structure (**Figure 1)** comprises a tricyclic planar chromophore and two basic side chains arranged symmetrically [9]. The polyamine side chains are responsible for the interaction with the phosphate groups of the DNA [9]. Due to this structure, Mito displays natural fluorescence (maximum excitation at 610 and 660 nm and maximum emission at 685 nm), which allows for *in vitro* and *in vivo* studies using fluorescence-based techniques [11, 12]. The emission spectrum is red-shifted when in the presence of DNA [12].

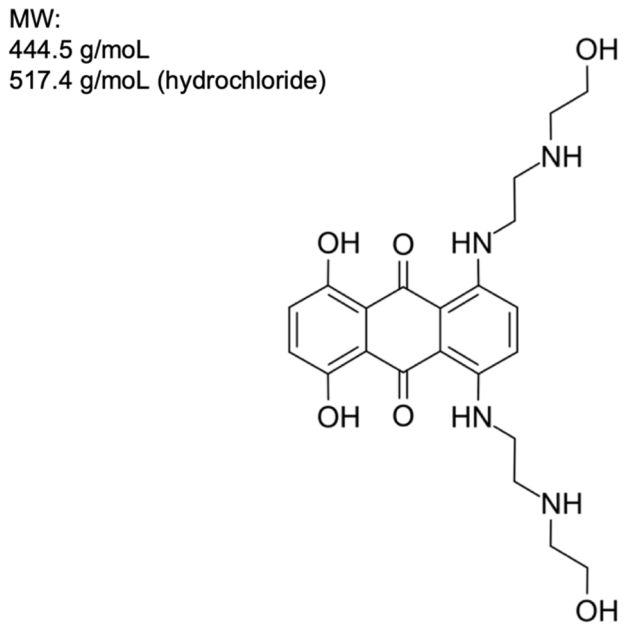



**Figure 1.** Molecular structure and molecular weight (MW) of Mitoxantrone.

Mito was first synthesized in the context of a program in synthetic chemistry at the Medical Research Division of the American Cyanamid Company, whose aim was to develop compounds with a suitable molecular structure for intercalation into the DNA [13]. Among more than 300 synthesized compounds, Mito was the most effective analogue, with high activity *in vitro* and *in vivo* against different tumors, rapidly reaching clinical trial phase [13].

The mechanisms responsible for the anti-cancer effects of Mito are still not entirely understood. Nevertheless, most of its anti-cancer effects are related to the ability of Mito to intercalate into the DNA, leading to disruption of DNA synthesis [9]. Moreover, Mito is also involved in other cellular processes, including formation of DNA cross-links and breaks, inhibition of the enzyme topoisomerase II, prevention of the microtubule assembly and inhibition of protein kinase C activity [14, 15].

In terms of pharmacokinetics, Mito has a very short half-life and rapid plasma clearance (4 to 10 min) in humans, following infusion. The drug is then distributed and sequestered in different tissues and organs, such as liver, heart, lung, kidney and brain. Biliary excretion is the major route of elimination of Mito and its metabolites [16].

Clinically, Mito is used for the treatment of advanced breast and prostate cancer, acute myeloid leukaemia, acute non-lymphocytic leukaemia, ovarian and liver cancer, multiple sclerosis, and non-Hodgkin's lymphoma [16-20]. The drug is commercialised as a

concentrated solution of 2 mg/mL in water (Novantrone®.), which is then reconstituted in 0.9% of sodium chloride or 5% dextrose and administered by intravenous infusion. The recommended dosage for advanced breast cancer is 14 mg/m$^2$ of body surface with 21-day of intervals, as a single agent or 7-12 mg/m$^2$ of body surface in combination regimens [16, 21].

As in most chemotherapeutic drugs, Mitoxantrone binds to the DNA in a nonspecific manner, being able to kill both proliferating and non-proliferating cells [9]. Therefore, different side effects have been reported, such as myelosuppression and cardiotoxicity [22-25]. Nevertheless, Mito has been found to be less cardiotoxic than their anthracycline analogues [9, 26]. Moreover the overexpression of drug efflux transporters in tumor cells, may lead to Mito resistance, which contributes to a diminished efficacy of the drug [27].

Given these limitations, novel therapeutic alternatives have emerged, such as nanotechnology and nanomedicine, as a strategy to ameliorate the systemic side-effects of the drug and improve the accumulation in the tumor region [28, 29]. Moreover, other novel therapeutics may be employed as a combination or a synergistic strategy to improve the anti-tumoral efficacy and desirably reduce the drug dosages. In this context, the combination of Mito with hyperthermia is an appealing therapeutic approach, since different *in vitro* studies have demonstrated that Mito displays an enhanced cytotoxicity against tumoral cells when combined with hyperthermia [30].

**Nanotechnology and Nanomedicine**

Nanotechnology is a multidisciplinary research field working in the manipulation of structures produced at the nanoscale. The concept behind this field of studies was introduced by Richard Feynman in 1959 in a lecture entitled “There’s Plenty of room at the bottom” at Caltech, suggesting the enormous potential of manipulating matter at the atomic and molecular level [31, 32]. Nevertheless, the term “nanotechnology” was only used for the first time by Taniguchi in 1974 to describe semiconductor processes occurring at the nanoscale. The idea and application was expanded and elaborated by Eric Drexler in 1980’s with his book “Engines of Creation: The Coming Era of Nanotechnology” [31, 32]. This field was popularized after several Nobel prize winners, including Heinrich Rohrer with the invention of the scanning tunnelling microscope in 1986, Kroto in 1885 for the discovery of fullerene and Geim and Novoselov for the discovery of graphene [31, 32].

Nowadays, nanotechnology is applied in several areas of science including pharmacy, physics, biology, and materials science. The use of nanotechnology for healthcare

applications is denominated nanomedicine [33]. The potential of nanomedicine in cancer management is well established not only for therapeutic but also for diagnostic purposes. Drug nanodelivery can enhance the therapeutic index of most-anticancer drugs, improve their pharmacokinetics and increase tumor distribution, owing to passive targeting due to the enhanced and permeability retention effect (EPR) [34, 35]. Currently, nanoparticles have already reached clinical stage for breast cancer therapy, being able to ameliorate the efficacy and safety profile of different anti-cancer drugs, such as doxorubicin. Nevertheless, the majority of the clinically available nanoparticles have high manufacture costs and low stability, which hinders their widespread application [35, 36]. Therefore, there is the need to develop novel types of nanoparticles, with improved characteristics and with less associated costs to allow for a large-scale production and subsequently extensive clinical application. In this context, lipid nanoparticles are a promising type of nanoparticle with great potential for the drug delivery in different types of cancer, including breast cancer (**section 2.1**).

**Hyperthermia**

Although one may consider hyperthermia a relatively new treatment modality, its use for therapeutic purposes dates back to ancient times, where heat was applied for the treatment of several diseases, including cancer. An Egyptian papyrus from 3000 BC reports the use of a “fire drill” to treat a breast tumor [37, 38]. In the classical Greece era in the 5$^{th}$ and 4$^{th}$ century BC several Greek scientists have highlighted the importance of heat for cancer healing. The philosopher Parmenides stated that the cure of all diseases, including malignant tumors, could be achieved by the induction of sufficient fever in the patient [37]. Furthermore, the physician Hippocrates used to submerse the patients in the desert sand or in hot baths to cure them, claiming that all the diseases that could not be cured by medicine, surgery or heat were incurable [37, 39]. Between 25 BC and 690 AD several ancient Greek and Roman physicians reported the use of local heat or local cautery with promising results in the remission of tumors [37]. More than 1000 years later, in the 19$^{th}$ and beginning of the 20$^{th}$ centuries, internal local heating such as cauterization and desiccation were commonly employed for the management of bladder, cervical, uterine, oral and other accessible tumors [37, 40]. During these centuries several physicians started to observed tumor regression upon fever induction [37]. In the late 19$^{th}$ century Dr. William B. Coley developed the Coley toxin, a mixture of fever-inducing bacteria (attenuated fluid cultures of *Streptococcus erysipelatis*) containing pyrogenic toxins [41, 42]. This was considered one of the most effective cancer treatment options until the Second World War

[41, 42]. Radiofrequency thermal ablation (RFA) was first described in 1891 and widely applied in several biomedical applications since 1928 [40]. In the 1920's several physicians and scientists have successfully shown that combination of hyperthermia with radiotherapy results in an increased efficacy in cancer treatment [37]. The synergistic combination between heat and chemotherapy was reported for the first time in 1960 [37].

Despite the benefits of hyperthermia in the management of cancer disease, there are still major limitations that hinder its establishment in clinics, namely the necessity of invasive medical procedures, non-uniform tumor heat distribution and lack of precise thermal dosimetry and thermal monitoring in the tumor region [43-46]. In the past few years, efforts have been made to improve the therapeutic outcomes of hyperthermia through the use of nanotechnology, leading to the emergence of novel hyperthermia treatment modalities, such as photothermal therapy (PTT) [47]. (**section 2.2.)**.

## References

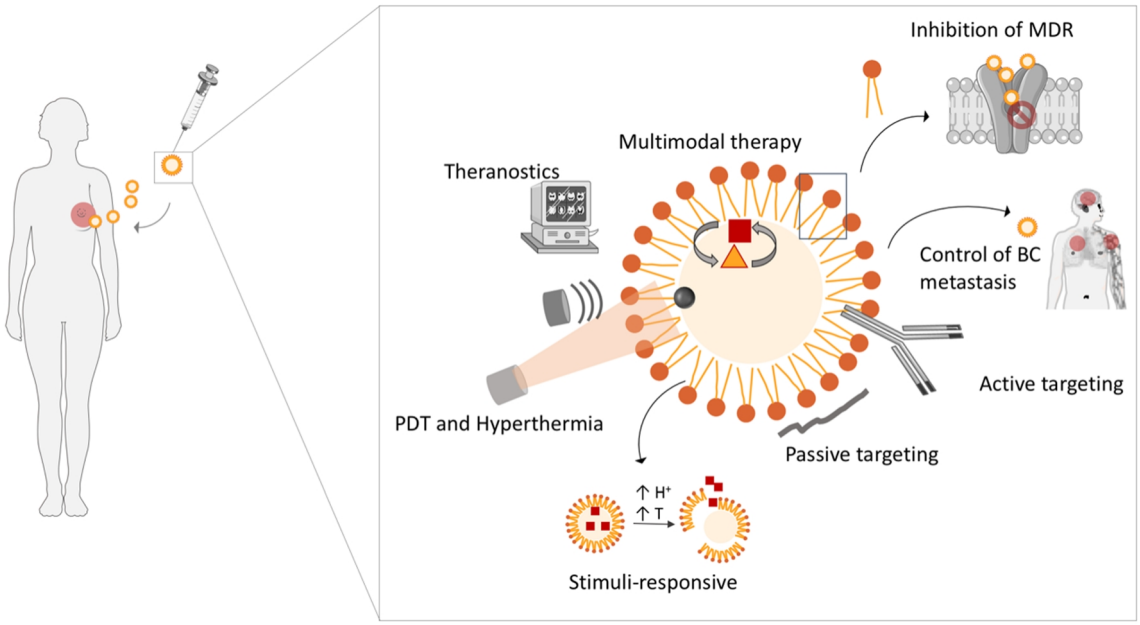

1. Sung, H., J. Ferlay, R.L. Siegel, M. Laversanne, I. Soerjomataram, A. Jemal, and F. Bray, *Global cancer statistics 2020: GLOBOCAN estimates of incidence and mortality worldwide for 36 cancers in 185 countries.* CA: a cancer journal for clinicians, 2021. **71**(3): p. 209-49.
2. DeSantis, C.E., S.A. Fedewa, A. Goding Sauer, J.L. Kramer, R.A. Smith, and A. Jemal, *Breast cancer statistics, 2015: Convergence of incidence rates between black and white women.* CA: a cancer journal for clinicians, 2016. **66**(1): p. 31-42.
3. Dieci, M.V., E. Orvieto, M. Dominici, P.F. Conte, and V. Guarneri, *Rare Breast Cancer Subtypes: Histological, Molecular, and Clinical Peculiarities.* Oncologist, 2014. **19**(8): p. 805-13.
4. Shapiro, C.L. and A. Recht, *Side effects of adjuvant treatment of breast cancer.* New England Journal of Medicine, 2001. **344**(26): p. 1997-2008.
5. Castiglione, M. and M.J. Piccart, *Adjuvant therapy for breast cancer*. Cancer treatment and research,. 2009, New York: Springer. xvi, 490 p.
6. Bai, X., J. Ni, J. Beretov, P. Graham, and Y. Li, *Cancer stem cell in breast cancer therapeutic resistance.* Cancer Treatment Reviews, 2018. **69**: p. 152-63.
7. Amar, S., V. Roy, and E.A. Perez, *Treatment of metastatic breast cancer: looking towards the future.* Breast cancer research and treatment, 2009. **114**(3): p. 413-22.
8. Waks, A.G. and E.P. Winer, *Breast cancer treatment: a review.* Jama, 2019. **321**(3): p. 288-300.
9. Varadwaj, P., K. Misra, A. Sharma, and R. Kumar, *Mitoxantrone: an agent with promises for anticancer therapies.* Electronic Journal of Biology, 2010. **6**(2): p. 36-42.
10. Rossato, L.G., V.M. Costa, P.G. de Pinho, M.D. Arbo, V. de Freitas, L. Vilain, M. de Lourdes Bastos, C. Palmeira, and F. Remiao, *The metabolic profile of mitoxantrone and its relation with mitoxantrone-induced cardiotoxicity.* Archives of toxicology, 2013. **87**(10): p. 1809-20.
11. Bell, D.H., *Characterization of the fluorescence of the antitumor agent, mitoxantrone.* Biochim Biophys Acta, 1988. **949**(1): p. 132-7.
12. Smith, P.J., H.R. Sykes, M.E. Fox, and I.J. Furlong, *Subcellular distribution of the anticancer drug mitoxantrone in human and drug-resistant murine cells analyzed by flow cytometry and confocal microscopy and its relationship to the induction of DNA damage.* Cancer Res, 1992. **52**(14): p. 4000-8.
13. White, R.J. and F.E. Durr, *Development of mitoxantrone.* Investigational new drugs, 1985. **3**(2): p. 85-93.

14. Ho, C.K., S.L. Law, H. Chiang, M.L. Hsu, C.C. Wang, and S.Y. Wang, *Inhibition of microtubule assembly is a possible mechanism of action of mitoxantrone.* Biochem Biophys Res Commun, 1991. **180**(1): p. 118-23.
15. Takeuchi, N., T. Nakamura, F. Takeuchi, E. Hashimoto, and H. Yamamura, *Inhibitory effect of mitoxantrone on activity of protein kinase C and growth of HL60 cells.* J Biochem, 1992. **112**(6): p. 762-7.
16. Ehninger, G., U. Schuler, B. Proksch, K.P. Zeller, and J. Blanz, *Pharmacokinetics and metabolism of mitoxantrone. A review.* Clin Pharmacokinet, 1990. **18**(5): p. 365-80.
17. Enache, M. and E. Volanschi, *Spectral studies on the molecular interaction of anticancer drug mitoxantrone with CTAB micelles.* J Pharm Sci, 2011. **100**(2): p. 558-65.
18. Arlin, Z., D.C. Case, Jr., J. Moore, P. Wiernik, E. Feldman, S. Saletan, P. Desai, L. Sia, and K. Cartwright, *Randomized multicenter trial of cytosine arabinoside with mitoxantrone or daunorubicin in previously untreated adult patients with acute nonlymphocytic leukemia (ANLL). Lederle Cooperative Group.* Leukemia, 1990. **4**(3): p. 177-83.
19. Faulds, D., J.A. Balfour, P. Chrisp, and H.D. Langtry, *Mitoxantrone. A review of its pharmacodynamic and pharmacokinetic properties, and therapeutic potential in the chemotherapy of cancer.* Drugs, 1991. **41**(3): p. 400-49.
20. Sargazi, A., N. Kamali, F. Shiri, and M. Heidari Majd, *Hyaluronic acid/polyethylene glycol nanoparticles for controlled delivery of mitoxantrone.* Artif Cells Nanomed Biotechnol, 2018. **46**(3): p. 500-09.
21. (EMA), E.M.A. *Novantrone EMEA-H-A-30-1399*. [cited 2022 May 4th ]; Available from: https://www.ema.europa.eu/en/about-us/who-we-are.
22. Smith, I., R. Stuart-Harris, N. Pavlidis, and T. Bozek, *Mitoxantrone (novantrone∗) as single agent and in combination chemotherapy in the treatment of advanced breast cancer.* Cancer treatment reviews, 1983. **10**: p. 37-40.
23. Coleman, R., M. Maisey, R. Knight, and R. Rubens, *Mitoxantrone in advanced breast cancer—a phase II study with special attention to cardiotoxicity.* European Journal of Cancer and Clinical Oncology, 1984. **20**(6): p. 771-76.
24. Schell, F., H. Yap, G. Blumenschein, M. Valdivieso, and G. Bodey, *Potential cardiotoxicity with mitoxantrone.* Cancer treatment reports, 1982. **66**(8): p. 1641-43.
25. Guissi, N.E.I., H. Li, Y. Xu, F. Semcheddine, M. Chen, Z. Su, and Q. Ping, *Mitoxantrone-and folate-TPGS2k conjugate hybrid micellar aggregates to circumvent toxicity and enhance efficiency for breast cancer therapy.* Molecular pharmaceutics, 2017. **14**(4): p. 1082-94.
26. Shenkenberg, T.D. and D.D. Von Hoff, *Mitoxantrone: a new anticancer drug with significant clinical activity.* Ann Intern Med, 1986. **105**(1): p. 67-81.
27. Nieth, C. and H. Lage, *Induction of the ABC-Transporters Mdr1/P-gp (Abcb1), Mrp1 (Abcc1), and Bcrp (Abcg2) during establishment of multidrug resistance following exposure to mitoxantrone.* Journal of chemotherapy, 2005. **17**(2): p. 215-23.
28. Wang, L., J. Cao, C. Li, X. Wang, Y. Zhao, T. Li, Y. Du, Z. Tao, W. Peng, and B. Wang, *Efficacy and safety of mitoxantrone hydrochloride liposome injection in Chinese patients with advanced breast cancer: a randomized, open-label, active-controlled, single-center, phase II clinical trial.* Investigational New Drugs, 2021: p. 1-10.
29. Yang, J., Y. Shi, C. Li, L. Gui, X. Zhao, P. Liu, X. Han, Y. Song, N. Li, and P. Du, *Phase I clinical trial of pegylated liposomal mitoxantrone plm60-s: pharmacokinetics, toxicity and preliminary efficacy.* Cancer chemotherapy and pharmacology, 2014. **74**(3): p. 637-46.
30. Herman, T.S., *Effect of Temperature on the Cytotoxicity of Vindesine, Amsacrine, and Mitoxantrone1, 2.* Cancer treatment reports, 1983. **67**(11): p. 1019.
31. Sharon, M., *History of Nanotechnology: From Prehistoric to Modern Times*. 2019: John Wiley & Sons.
32. Hulla, J., S. Sahu, and A. Hayes, *Nanotechnology: History and future.* Human & experimental toxicology, 2015. **34**(12): p. 1318-21.
33. Kammari, R., N.G. Das, and S.K. Das, *Nanoparticulate systems for therapeutic and diagnostic applications.* Emerging Nanotechnologies for Diagnostics, Drug Delivery and Medical Devices, 2017: p. 105-44.
34. Iyer, A.K., G. Khaled, J. Fang, and H. Maeda, *Exploiting the enhanced permeability and retention effect for tumor targeting.* Drug discovery today, 2006. **11**(17-18): p. 812-18.
35. Crommelin, D.J.A., P. van Hoogevest, and G. Storm, *The role of liposomes in clinical nanomedicine development. What now? Now what?* Journal of Controlled Release, 2020. **318**: p. 256-63.

36. Weber, S., A. Zimmer, and J. Pardeike, *Solid Lipid Nanoparticles (SLN) and Nanostructured Lipid Carriers (NLC) for pulmonary application: a review of the state of the art.* European journal of pharmaceutics and biopharmaceutics : official journal of Arbeitsgemeinschaft für Pharmazeutische Verfahrenstechnik e.V, 2014. **86**: p. 7-22.
37. Seegenschmiedt, M. and C. Vernon, *A historical perspective on hyperthermia in oncology*, in *Thermoradiotherapy and thermochemotherapy*. 1995, Springer. p. 3-44.
38. Streffer, C. and D. Van Beuningen, *The biological basis for tumour therapy by hyperthermia and radiation.* Hyperthermia and the Therapy of Malignant Tumors, 1987: p. 24-70.
39. Moyer, H.R. and K.A. Delman, *The role of hyperthermia in optimizing tumor response to regional therapy.* International Journal of Hyperthermia, 2008. **24**(3): p. 251-61.
40. McGahan, J.P. and V.A. van Raalte, *History of Ablation*, in *Tumor Ablation: Principles and Practice*, E. vanSonnenberg, et al., Editors. 2005, Springer New York: New York, NY. p. 3-16.
41. Wiemann, B. and C.O. Starnes, *Coley's toxins, tumor necrosis factor and cancer research: a historical perspective.* Pharmacol Ther, 1994. **64**(3): p. 529-64.
42. Habash, R.W.Y., *Chapter 53 - Therapeutic hyperthermia*, in *Handbook of Clinical Neurology*, A.A. Romanovsky, Editor. 2018, Elsevier. p. 853-68.
43. Jones, E.L., J.R. Oleson, L.R. Prosnitz, T.V. Samulski, Z. Vujaskovic, D. Yu, L.L. Sanders, and M.W. Dewhirst, *Randomized trial of hyperthermia and radiation for superficial tumors.* Journal of Clinical Oncology, 2005. **23**(13): p. 3079-85.
44. Vujaskovic, Z., D.W. Kim, E. Jones, L. Lan, L. McCall, M.W. Dewhirst, O. Craciunescu, P. Stauffer, V. Liotcheva, A. Betof, et al., *A phase I/II study of neoadjuvant liposomal doxorubicin, paclitaxel, and hyperthermia in locally advanced breast cancer.* International journal of hyperthermia : the official journal of European Society for Hyperthermic Oncology, North American Hyperthermia Group, 2010. **26**(5): p. 514-21.
45. Mallory, M., E. Gogineni, G.C. Jones, L. Greer, and C.B. Simone, *Therapeutic hyperthermia: The old, the new, and the upcoming.* Critical Reviews in Oncology/Hematology, 2016. **97**: p. 56-64.
46. Sabel, M.S., *Nonsurgical ablation of breast cancer: future options for small breast tumors.* Surg Oncol Clin N Am, 2014. **23**(3): p. 593-608.
47. Sharma, S., N. Shrivastava, F. Rossi, and N.T.K. Thanh, *Nanoparticles-based magnetic and photo induced hyperthermia for cancer treatment.* Nano Today, 2019: p. 100795.

## 2.1. Therapeutic advances in breast cancer using lipid nanoparticles: from targeting strategies to the development of multifunctional nanosystems

This sub-chapter comprises a literature review (To be submitted) describing breast cancer impact, pathophysiology, classification, standard treatments and current limitations. The role of nanomedicine in surpassing these limitations and improving the clinical outcomes of the conventional therapeutic is then discussed. A particular focus on lipid nanoparticles and their potential for drug delivery in breast cancer is then described by providing an overview of the most recent studies in this area.



# Therapeutic advances in breast cancer using lipid nanoparticles: from targeting strategies to the development of multifunctional nanosystems

Andreia Granja[1], Maria Francisca Bento[1], Célia T. Sousa[2,3] and Salette Reis[1,*]

[1]LAQV, REQUIMTE, Departamento de Ciências Químicas, Faculdade de Farmácia, Universidade do Porto, R. Jorge de Viterbo Ferreira 228, 4050-313, Porto, Portugal.
[2]IFIMUP-IN and Dep. Física e Astronomia, Faculdade de Ciências, Universidade do Porto, Rua Campo Alegre 687, 4169 - 007 Porto, Portugal
[3]Departamento de Física Aplicada, Facultad de Ciencias, Universidad Autónoma de Madrid (UAM), Campus de Cantoblanco, C/ Francisco Tomás y Valiente, 7, M 12 604 - 28049, Madrid, Spain.

[*]corresponding author:

shreis@ff.up.pt

**Abstract**

Breast cancer is the most common malignancy in women worldwide. The conventional drug therapy currently available is far from optimal, due to limited cancer cell-specificity and high systemic toxicity. The need to improve the therapeutic index of most anti-cancer drugs has prompted the application of nanomedicine in this field, leading to very positive outcomes, with some types of nanoparticles being able to reach clinical trial phase or clinical settings. The majority of the clinically approved nanoparticles, however, require expensive manufacturing methods and have limited stability and controlled release properties. Lipid nanoparticles have emerged as a cost-effective, versatile, biocompatible and stable type of nanocarrier, with great potential for drug delivery in numerous applications, including cancer. This review describes the main clinical aspects of breast cancer malignancy, including the standard therapeutics and its limitations, and the nanomedicine approaches currently available in clinics. The potential of lipid nanoparticles as drug delivery vehicles in the management of breast cancer will be outlined and the most recent advances made in this area will be discussed, ranging from passive and active targeting strategies, to the development of multifunctional and multimodal nanosystems.

**Keywords:** Drug delivery, Nanomedicine, Lipid nanoparticles, active targeting, multifunctional nanosystems

# 1. Introduction

Breast cancer is the most prevalent cancer type and the leading cause of cancer deaths in women globally. According to GLOBOCAN 2020 cancer statistics, in 2020, 2.3 million women were diagnosed with the disease and 685 000 deaths occurred worldwide [1]. In addition, breast cancer was found to be the leading cause of disability-adjusted life years (DALYs) in women, with 17.4 million DALYs reported in 2017 [2]. The disease has also a high economic burden. In 2009 breast cancer was reported to have the highest economic costs after lung cancer (€15 billion) and the highest healthcare costs (€6.73 billion) in Europe [3]. Furthermore, according to the National Cancer Institute medical expenditures related with this malignancy in the US were projected to reach $16.5 billion in 2020, being higher that colorectal cancer, lymphoma, lung cancer and prostate cancer [4].

Breast cancer is a highly heterogeneous disease with a complex classification system based on histological and molecular features and also on the stage of the disease, which conditions the treatment regimen employed in each patient [5, 6]. Despite the variety of treatment options available, including surgery, radiotherapy, chemotherapy, endocrine therapy and targeted therapies, most of the drugs have a limited cancer-cell specificity, which causes severe side-effects, reduced response to treatment and eventual disease metastasis or recurrence [7]. In addition, the design of effective and more specific treatment modalities for some breast cancer subtypes, such as triple negative breast cancer (TNBC) remains a challenge [8].

This review provides an overview of breast cancer disease and its standard treatments and limitations, and discusses the therapeutic role of nanomedicine in this malignancy. A particular emphasis on lipid nanoparticles, including solid lipid nanoparticles (SLN) and nanostructured lipid carriers (NLC) will be given and their potential in the management of breast cancer disease will be outlined. In addition, the most recent advances in this area from passive and active targeting strategies to the development of multimodal and multimodal nanosystems will be discussed.

# 2. Breast cancer

The breast is located in the anterior chest wall resting on the pectoralis major muscle and is composed by glandular tissue, adipose tissue and fibrous tissue (stroma) [9, 10]. The glandular tissue contains 15 to 20 structures known as lobes, each of it subdivided into

clusters of 20 to 40 lobules, responsible for milk production. Those are connected to the nipple by thin tubes called ducts [9, 10]. The functional unit of the breast is referred as terminal duct lobular unit (TDLU) and consists of an extralobular terminal duct and a lobule [9]. Breast cancer is caused by an abnormal growth of epithelial cells with predominant origin in the TDLU and is included in the group of solid tumours denominated carcinomas [5, 11]. It is referred as carcinoma *in situ*, when the tumor is limited to the ducts and lobules region, and invasive carcinoma if the overgrowing cells disrupt the basement membrane and invade the stroma [12]. The internal mammary artery is the main responsible for blood supply while the majority of the lymphatic drainage of the breast occurs through the axillary lymph nodes. The study of the lymphatic drainage is of extreme relevance in the context of breast cancer early diagnosis and treatment, as this is the most common route for cancer cell dissemination and metastasis [10].

Breast cancer is highly heterogeneous both at the histological and molecular levels, having different classifications depending on numerous factors, which have been refined over the years [5, 6]. In terms of histological features, breast cancer is referred as ductal or lobular depending of the local where it originated [13]. These categories are then sub-divided into numerous histopathological subtypes based on different features such as type of cell, type and location of secretion and architectural characteristics [13]. The most common histological subtype is invasive ductal carcinoma [14]. The second most common type is invasive lobular carcinoma, comprising almost 15% of all breast cancers. There are other less common subtypes such as ductal carcinoma in situ (DCIS), which is noninvasive and is considered the earliest form of the disease, and inflammatory breast cancer, a rare type that often occurs in younger patients [14, 15].

Concerning its molecular characteristics breast cancer is categorized into four major subtypes: luminal A, luminal B, human epidermal growth factor receptor 2 (HER2) and basal-like, depending on the expression of different molecular targets including hormone receptors (HR) (Estrogen receptor (ER) and Progesterone receptor (PR)) and HER2. The definition of the molecular subtypes has been determinant for the development of more personalized therapies and for the increase of the disease survival, as each molecular subtype is associated with different prognosis, response to treatment and metastatic potential [5]. Luminal A accounts for 50% of all invasive breast cancers and is positive for ER and/or PR and negative for HER2. It has generally a good prognosis and responds well to endocrine therapy such as tamoxifen and aromatase inhibitors [13]. Luminal B is also ER/PR positive and can be positive or negative for HER2. It has a higher proliferative index, a more variable response to endocrine and chemotherapy and a lower prognosis than Luminal A subtype [13, 16]. HER2 subtype is characterized by the overexpression of HER2

and is generally negative for ER and PR. This subtype is associated with a higher proliferative and metastatic potential, however it benefits from the current targeted therapies against HER2, which have shown high efficacy in the inhibition of the disease progression and in the increase of the survival [13, 17, 18]. The basal-like subtype, is negative for ER/PR and HER2, which is why it is also known as triple negative breast cancer (TNBC). Since this subtype does not respond to endocrine and targeted therapies and only 20% respond well to chemotherapy, it has usually a lower prognosis and higher risk of relapse [13, 14]. A considerable part of the ongoing research in breast cancer is focused on the development of molecular therapeutics for TNBC, which include, among others, EGFR inhibitors and JAK kinase inhibitors [5].

Disease prognosis and choice of treatment is also dependent on the stage of the disease. In this context breast cancer is classified using the TNM system. This method is based on the evaluation of the size of the tumor (T), the migration into the regional lymph nodes (N) and the evidence of metastatic disease (M), which can be performed through surgical findings, physical examination, imaging modalities or biopsy [9]. Staging of the disease takes also into account the molecular subtype of the disease and the histological grade of the tumor [9]. Stages vary from stage 0 (carcinoma *in situ*) to stage IV (tumor metastasis in distant organs, such as bone, lung, brain and liver) [9]. A carcinoma *in situ* is confined to the duct or lobule and generally causes no symptoms [19]. Over time, the *in situ* cancer may progress and invade the stroma, becoming an invasive breast cancer, which may eventually reach the adjacent lymph nodes and start a regional metastasis (stage 2–3). When cancer cells migrate from their local of origin and spread to other parts of the body, a distant metastasis is formed, being lung, bone, liver and brain the most frequent sites for breast cancer metastasis (**Figure 1**) [20]. Metastatic disease is responsible for the majority of deaths occurring in breast cancer in women [21].

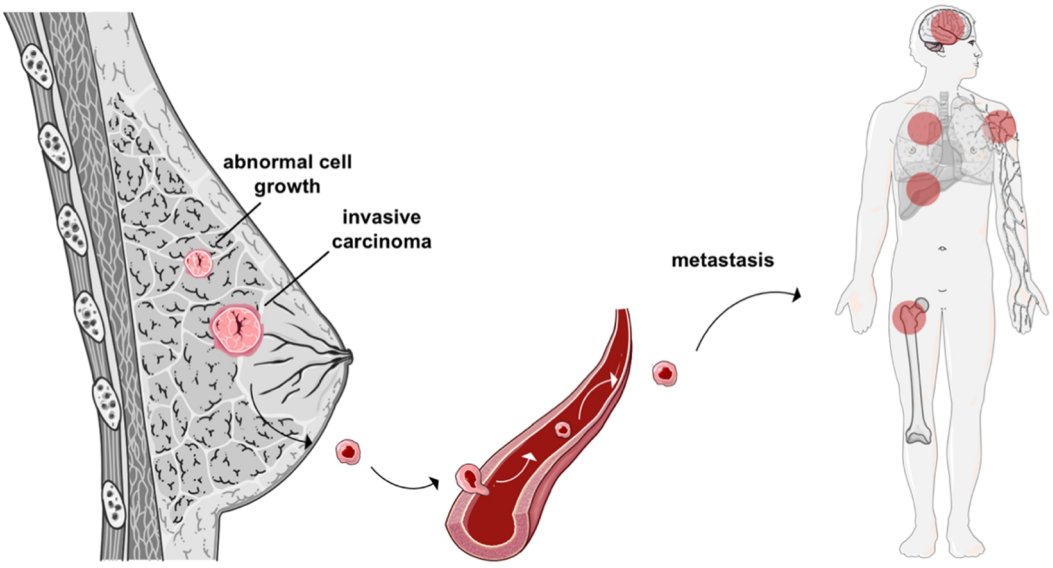



**Figure 1.** Schematic representation of breast cancer development, progression and metastasis.

## 2.1. Breast cancer standard treatments

Currently, patients diagnosed with breast cancer are often given multimodality treatment that includes local and systemic adjuvant therapies. Many different factors are considered when deciding which combination of treatments is the most adequate for the patient, including the age, the menopausal status, the tumor size and location, the molecular subtype, the axillary nodal status and the evidence of metastatic disease, among other factors [14, 22, 23]. Local therapies comprising surgery and radiotherapy are employed for the removal of the primary tumor and, when necessary, the adjacent tissues, and axillary lymph nodes. Adjuvant systemic therapies, include hormonal therapy, targeted therapies and chemotherapy and are used to reduce the tumor size and control cancer metastasis and disease recurrence. They can be employed before (neoadjuvant) or after surgery (adjuvant), or both [14, 24].

Hormonal therapy used to downregulate the ER signalling, is the main systemic therapy for hormone receptor-positive breast cancer, reducing the risk of disease recurrence by nearly half in this subtype [22, 25, 26]. Different types drugs can be used, including tamoxifen, a selective estrogen-receptor modulator, aromatase inhibitors (such as letrozole and anastrozole) or ovarian suppression. The choice of the endocrine therapy depends, among other factors, on the menopausal status of the patient [22, 25].

More recently with the advances in the areas of molecular biology and immunology, targeted therapies have emerged as a novel possibility for the treatment for breast cancer, particularly for the HER2 subtype [22, 25]. This therapeutic relies on the use of small molecules or monoclonal antibodies targeting a specific molecular pathway. The most commonly used targeted therapy for breast cancer is trastuzumab (ie, Herceptin), a humanized anti-HER2 monoclonal antibody. Trastuzumab is generally administered in combination with adjuvant chemotherapy and can substantially increase its clinical outcomes and disease survival in patients with HER2 subtype [22, 25]. Other targeted therapies include HER2 tyrosine kinase inhibitors, such as lapatinib, particularly in metastatic disease [22, 25].

Chemotherapy mainly relies on the use of cytotoxic drugs and, depending on the tumor subtype, it can be administered in combination with endocrine and targeted therapies [22]. In TNBC, chemotherapy is administered alone and is currently the only therapy with demonstrated efficacy in this subtype, being also the main treatment for breast cancer in advanced stage [14]. Chemotherapy regimens comprising anthracyclines (such as doxorubicin) and taxanes (such as paclitaxel) are the preferable regimen choice for treating breast cancer [14]. However, other regimens can also be used, including the docetaxel-cyclophosphamide, doxorubicin-cyclophosphamide and cyclophosphamide-methotrexate-fluorouracil-based polychemotherapy [14, 22]. Additionally, platinum-based chemotherapy is also being investigated for the treatment of TNBC [14].

The treatment of metastatic (also referred as stage IV and advanced) breast cancer disease usually requires different treatment approaches. In this context, the therapeutic is considered palliative aiming to prolong the life time and control and ameliorate the symptoms caused by the disease [27, 28]. If the tumor is HR positive, therapeutic may only comprise endocrine therapy. Patients with HER2-positive tumors receive both chemotherapy and targeted therapies such as trastuzumab, or the tyrosine kinase inhibitor lapatinib, used for trastuzumab refractory tumors [28]. Patients with HR negative tumors, HR positive refractory to endocrine therapy or with severe symptoms caused by the tumor, begin the treatment with chemotherapy [27, 28]. The duration and cycles of chemotherapy is also variable but is generally continuous as long as the patient can tolerate the treatment. Regarding treatment regimens anthracyclines (including doxorubicin, epirubicin and mitoxantrone) and taxanes (such as paclitaxel and docetaxel) are common choices [27, 28]. However, there is a high heterogeneity in the choice of the chemotherapy regimens depending of patients tolerability, existence of prior chemotherapy and the presence of other medical conditions [28]. Other variants such as platinum-based chemotherapy and

nanomedicines aiming to reduce the toxic effects of the free drugs including liposomal doxorubicin and nab-paclitaxel can also be used [27]. Moreover, newer classes of chemotherapeutic agents have been developed including the epothilones and the antiangiogenic agent bevacizumab [28]. In cases of failure of previous chemotherapy regimen, different second or higher line therapies may be employed taking into consideration the risk-benefit ratio for the patient [28].

### 2.1.1. Limitations of the current breast cancer therapeutic

Despite the variety of therapeutics available and the advances made in this area, most of the drugs used in breast cancer therapy have a limited cancer-cell specificity, being unable to distinguish between healthy and cancer cells, which causes severe side-effects, some of them long-term [29]. Those include nausea, fatigue, alopecia, myalgias, myelossupression, ovarian insufficiency and a remarkable decrease on the patients' quality of life [22, 29-31]. Other more severe complications related to specific drugs may also arise. For instance, tamoxifen intake increases the risk of uterine cancer and may induce ischemic cerebrovascular and venous thromboembolic events [22, 32, 33]. Aromatase inhibitors increase the risk of osteoporotic bone fractures [34]. Doxorubicin induces cardiotoxicity, which may progress into cardiomyopathy and congestive heart failure, an effect which is even more accentuated when combined with trastuzumab [31, 35]. Paclitaxel formulations can cause neuropathic pain, nephrotoxicity and neurotoxicity [29-31].

All of the reported systemic side effects limit the drugs maximum tolerated doses, which may result in limited treatment efficacy and in the development of drug resistance or multidrug resistance (MDR). Consequently, a lower response to treatment is expected, which increases the probability of tumor metastasis and disease recurrence [7].

Additionally, some anti-tumoral drugs have limited pharmacokinetics, including quick clearance and short half-life, low solubility and stability in physiological media and reduced capacity to cross biological barriers such as the gastrointestinal tract, the blood-brain barrier and even the tumor tissue itself [36, 37]. Consequently, drugs have to be administered at high dosages, resulting in more accentuated side-effects [36, 37].

Finally, the development of effective treatments for specific types of breast cancer such TNBC and metastatic breast cancer still remains a challenge [8].

These limitations highlight the need to improve the current breast cancer therapy by developing innovative strategies to minimize undesirable side-effects and designing novel approaches and modalities of treatment. In this sense, nanotechnology can have an important contribute.

## 3. The role of nanotechnology in breast cancer treatment

Nanotechnology is a multidisciplinary research field working in the investigation and manipulation of structures produced at the nanoscale. Nowadays, nanotechnology is applied in several areas of science including pharmacy, physics, biology, and materials science. The use of nanotechnology for healthcare purposes is known as nanomedicine [38].

Nanomedicine used in drug delivery plays a vital role in the improvement of cancer treatment, by counteracting several limitations of the standard drug therapies, increasing their therapeutic index and leading to the development of more effective treatment modalities, with less systemic side-effects [39, 40]. This ability to improve conventional drug therapies can be attributed to different characteristics. First, nanoparticles can improve the pharmacokinetic profile of the anti-cancer drugs by increasing their retention time in circulation, improving their stability in different physiological environments, enhancing their solubility in aqueous media, and increasing the transport across specific barriers such as the gastrointestinal tract [39, 40]. The use of nanoparticles also offers the possibility of changing the administration route of the drugs to a more convenient one such as the oral route [41]. Secondly, nanoparticles' small size enables their preferential accumulation in the tumor region due to the enhanced permeability and retention (EPR) effect [42]. This effect is observed in the majority of rapidly growing solid tumors, whose microenvironment is characterized by a disordered and irregular vasculature with large fenestrations between the endothelial cells, with pores varying from 100 nm to 2 μm [42-44]. This event combined with a limited lymphatic drainage, leads to the accumulation of blood-circulating components including drugs, macromolecules and nanoparticles [42]. Different strategies can be employed to enhance the EPR effect and increase the penetration of the nanoparticles, namely vascular permeabilization, vascular disruption and application of hyperthermia, radiotherapy, ultrasound or phototherapy [45].

Nanoparticles' surface properties can be easily modified to further improve the pharmacokinetic properties of the drugs, such as blood circulation time. Surface coating with polyethylene glycol (PEG) is a common strategy to prolong the circulation of the nanocarriers in the bloodstream, by shielding their surface and thereby reducing opsonization and subsequent uptake by macrophages of the reticuloendothelial system (RES). Furthermore, nanoparticles accumulation in tumors can be further enhanced by the use of active targeting strategies directed either to the cancer cells or to other components of the tumor microenvironment, which reduces the likelihood of nonspecific off-target toxicity [46, 47].

Recent advances in drug delivery have enabled the design of more complex and multifunctional nanoparticles. In order to precisely control the release of the drug at the local of interest, stimuli-responsive nanoparticles can be designed. Those are able to release their cargo upon the application of an internal or external stimulus such as pH or heat [48, 49]. Additionally, co-encapsulation of multiple drugs and/or other molecules (such as natural compounds) is also possible through the use of nanoparticles. This can elicit an additive or synergistic effect, thus improving the efficacy of the treatment and limiting drug resistance mechanisms [50].

Apart from the valuable role that nanotechnology plays in the improvement of conventional cancer treatments such as chemotherapy, it can also enhance the efficacy of alternative cancer therapeutics and even facilitate their widespread clinical application, such as in the case of gene therapy, through the encapsulation of genetic material [51]. Photodynamic therapy can also benefit from the use of nanoparticles, which can act either as delivery vehicles to enhance the characteristics of the photosensitizer (PS) or as the PS by themselves [52]. Later on, the design of nanoparticles with specific chemical, optical, magnetic and physical characteristics has enabled the development of novel therapeutics such as hyperthermia (both magnetic hyperthermia and photothermal therapy, PTT) and the simultaneous incorporation of diagnostic and treatment into one single nanovehicle known as theranostics, which enables the visualization and monitorization of the tumor during treatment [53]. Finally, multiple drugs or treatment modalities may be incorporated into one single multimodal nanocarrier to effectively increase cancer cell eradication.

### 3.1. Nanoparticles in clinical stage for breast cancer therapy

Breast cancer is the most common cancer type in women worldwide, however, the current available drug therapy is far from optimal. The need to improve the therapeutic index of chemotherapeutic drugs has prompted the development of different types of nanocarriers for drug delivery [54]. Several nanoparticles have been already approved either by the European Medicines Agency (EMA) and the Food and Drug Administration (FDA) for the treatment of breast cancer and numerous are under development in various clinical stages [38]. The majority of the nanoformulations is liposome-based and often applied in combination with standard chemotherapeutic regimens [54, 55]. Other non-liposomal nanoformulations include albumin-bound paclitaxel (Abraxane), approved by the FDA [56] and Genexol-PM, paclitaxel-loaded polymeric micelles approved by the EMA [57].

Doxil® was the first nanomedicine approved by the FDA for cancer therapy applications. It comprises a PEGylated liposomal formulation loaded with doxorubicin. Doxil® has been shown to attenuate some of the severe side-effects related with free doxorubicin, such as cardiotoxicity, myelossupression, alopecia and nausea [58-60] Over the years, different clinical trials have reported the effectiveness of the combination of Doxil® with standard chemotherapeutic regimens in improving response rates and progression free survival, and limiting toxicity in patients with metastatic breast cancer [61-63]. Despite these favourable results, Doxil® is still not approved for breast cancer treatment [64]. Other liposomal formulations, however, have received FDA and/or EMA approval for the management of breast cancer, including a non-PEGylated (Myocet®) [65], and a PEGylated liposomal doxorubicin formulation (Lipo-Dox®) [66]. Both have demonstrated a significant reduction in the cardiotoxicity associated with free doxorubicin and similar anti-tumoral efficiency. The combination with other chemotherapeutic regimens has also been well tolerated, improving the overall response rate and progression-free survival rate in patients with metastatic breast cancer [65, 66]. Besides doxorubicin, liposomes loaded with other chemotherapeutic drugs, such as paclitaxel [67], docetaxel (clinicaltrials.gov, NCT 01041235), daunorubicin (clinicaltrials.gov, NCT00004207), cisplatin (clinicaltrials.gov, NCT01861496), mitoxantrone (clinicaltrials.gov, NCT04927481) and irinotecan [68] are under different clinical stages for the treatment advanced or metastatic breast cancer.

Liposomal formulations with a higher degree of complexity and multifunctionality have also been developed, with some of them able to reach clinical trial-stage. Those include the thermosensitive liposome ThermoDox®, used for the release of doxorubicin in the tumor site following hyperthermia treatment [69]; the HER2-targeted doxorubicin liposomal formulation MM-302 [70]; 2B3-101, a glutathione PEGylated liposomal doxorubicin for brain

targeting and treatment of breast cancer brain metastasis [71]; and EndoTAG™, a cationic liposome formulation loaded with paclitaxel to target the tumor endothelial cells [72].

Despite their improvement on the safety profile and efficacy of conventional drugs, liposomes have major drawbacks, including low stability and limited controlled release properties [55, 73, 74]. Moreover, they require demanding and expensive manufacturing methods, which restricts their large-scale production and widespread application [55, 73, 74]. To circumvent these limitations, other lipid-based nanoparticles are being explored, such as solid lipid nanoparticles (SLN) and nanostructured lipid carriers (NLC).

## 4. Lipid nanoparticles

Lipid nanoparticles are colloidal carriers containing a lipid matrix solid at body temperature stabilized in an aqueous solution by one or more surfactants [75]. A broad diversity of lipid materials may be used in their composition, including fatty acids, fatty esters, fatty alcohols, triglycerides and waxes, the vast majority being biocompatible, biodegradable and generally recognized as safe (GRAS) [75, 76].

The first generation of lipid nanoparticles, solid lipid nanoparticles (SLN), has emerged in the early 90's as a promising marketable alternative to polymeric, liposomal and emulsion nanoformulations [77]. SLN are composed of solid lipids dispersed in aqueous solution [78]. Their simplicity and versatility have made them popular choices as drug delivery vehicles in different areas, such as cosmetics, food and medical applications [79-82]. Nevertheless, SLN have some drawbacks including limited loading capacity and drug expulsion during storage, following crystalline lipid matrix rearrangement. To overcome these limitations, nanostructured lipid carriers (NLC), the second generation of lipid nanoparticles, were developed in the late 90s. These types of lipid nanoparticles are composed by both solid and liquid lipids, which form a less crystalline and more imperfect lipid matrix, resulting in a higher drug loading [76, 83].

In contrast to liposomes, lipid nanoparticles possess excellent physical stability and tolerability, along with controlled drug release properties [77]. In addition, by requiring less demanding and expensive production methods, their large-scale production is facilitated. Moreover, some of these production methods are entirely free from organic solvents [76]. Depending on the composition and production methods, lipid nanoparticles can accommodate both lipophilic and hydrophilic compounds [84].

Lipid nanoparticles can be produced through a variety of methods, that have been fully detailed elsewhere [85, 86]. The first developed production methods were high pressure homogenization and microemulsion, introduced in the early 2000's [77]. Nowadays, other procedures and variants have been described, such as solvent evaporation, solvent injection and hot homogenization and ultrasonication [85, 86]. More recently, other techniques such as microwave assisted production have also been reported [87].

The choice of the production method depends, among other factors, on the composition and desired properties of the nanoparticles and the characteristics of the molecule to be encapsulated such as thermolability and liposolubility [75].

Through the years, lipid nanoparticles have been explored as delivery vehicles in cosmetics and medical applications and have demonstrated a high versatility. A variety of compounds have been loaded into these nanocarriers ranging from small molecules, to biomacromolecules, nutraceuticals, proteins and genetic material for the treatment of different conditions and pathologies [88-92]. Additionally, different routes have been explored, including the intravenous, oral, pulmonary and topical administration [93-97]. The success of the use of lipid nanoparticles has resulted in the development of numerous patents [98].

The potential of lipid nanoparticles in the management of cancer disease has been investigated in numerous studies. Besides all the advantages of the use of nanomedicine in cancer, elucidated in **section 3**, lipid nanoparticles present specific characteristics that made them particularly promising for drug delivery in cancer, and breast cancer in particular. The potential of lipid nanoparticles in breast cancer pathology and the recent advances made in this area are summarized in **Figure 2** and highlighted in the following sections.

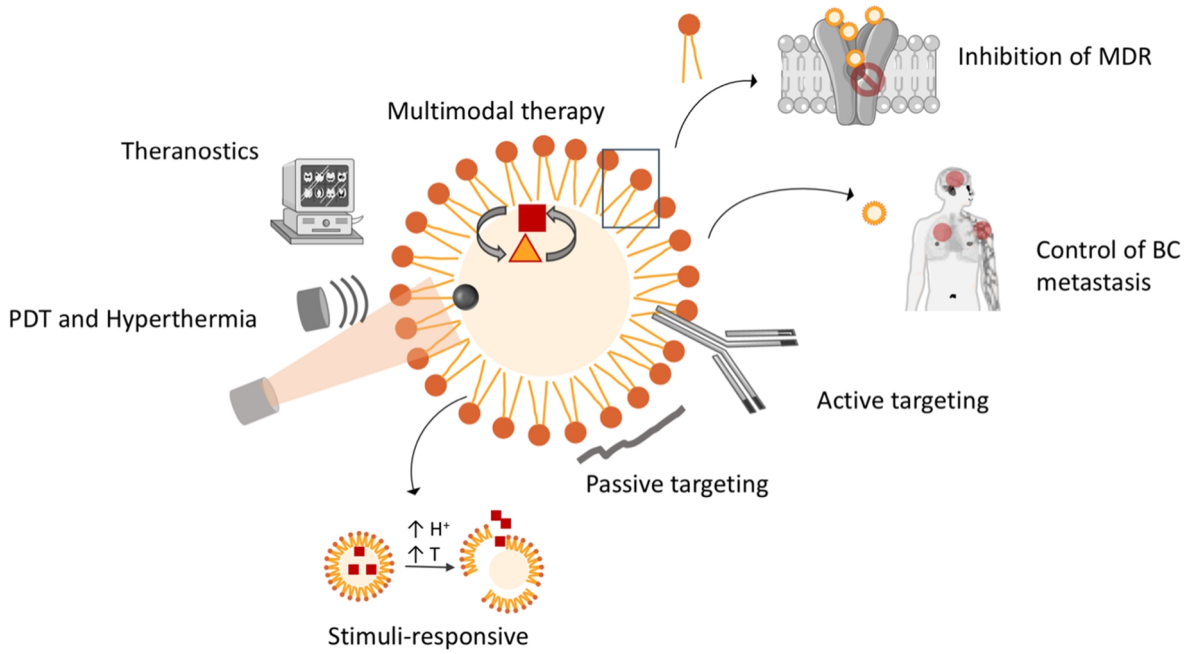



**Figure 2.** Summary of the recent strategies for the management of breast cancer using lipid nanoparticles

## 4.1. Potential and recent advances in the management of breast cancer

### 4.1.1. Enhancement of tumor accumulation using passive and active targeting strategies

#### 4.1.1.1. Passive targeting

The small size of lipid nanoparticles and the EPR effect occurring in most solid tumors facilitates their accumulation in the tumor region, a phenomenon known as passive targeting [99]. Nevertheless, the probability of the nanoparticles reaching the tumor region can be enhanced. A common strategy to do so is to prolong their circulation in the bloodstream through the surface coating with hydrophilic polymers such as PEG. Numerous works have used PEGylated lipid nanoparticles for the management of breast cancer, showing an improved drug circulation time along with higher tumor accumulation [100-107].

Another strategy to enhance nanoparticle tumor penetration is hyperthermia (**detailed in section 4.1.4**.), which increases blood flow, stimulates the opening of the tumor endothelial

barrier and reduces interstitial fluid pressure (IFP) [108]. IFP is an enormous challenge for tumor drug delivery and cancer therapy [109]. Due to the higher vascular permeability, limited lymphatic drainage and dense extracellular matrix (ECM), this pressure is considerably higher in the tumor regions than in normal tissues, as demonstrated in numerous cancer types, including breast cancer [109]. A strategy specifically designed to counteract IFP and improve nanoparticle tumor penetration and drug delivery has been described by Gao et al. [110]. The authors designed cationic NLC decorated with gelatin and co-loaded with imatinib, quercetin and docetaxel. Imatinib is a tyrosine kinase inhibitor that can inhibit cell signalling pathways related with ECM over-production, hence, reducing IFP. The goal of this smart nanosystem was to reach the tumor site where metalloproteinases could degrade the NLC gelatin coating and, subsequently release imatinib, thus decreasing ECM density and IFP. This would lead to an enhanced penetration of the NLC in the tumor. The nanosystem elicited a high cytotoxicity towards 4T1 cells, reducing the value of $IC_{50}$, enhancing apoptosis and inhibiting cell migration comparing with free docetaxel and NLC loaded with docetaxel and quercetin. *In vivo* studies in 4T1-tumor bearing mice showed that the nanoformulation was able to reduce tumor IFP, comparing to the saline solution treatment. Moreover, the nanosystem significantly inhibited tumor growth and pulmonary metastasis comparing with the combination of the free drugs.

#### 4.1.1.2. Active targeting

Despite the potential of nanoparticles to accumulate in the tumor region by means of passive targeting, active cancer cell targeting has a preponderant role in improving the performance of drug delivery systems in breast cancer and limiting off-target toxic effects. Lipid nanoparticles are very versatile nanocarriers and their surface coating can be easily modified with different ligands [81]. Different classes of ligands have been applied for breast cancer targeting, including antibodies, proteins and peptides, polysaccharides and small molecules. The majority of these active targeting strategies is designed to target different receptors overexpressed in breast cancer cells. However, some strategies directed to the tumor vasculature have also been reported.

Surface decoration with antibodies is one of the most common targeting strategies used in cancer [111]. High specificity and selectivity is their most attractive feature [46]. Moreover, some monoclonal antibodies, such as trastuzumab, have already been implemented in clinical settings with very favourable outcomes in breast cancer therapy [22]. Varshosaz and co-workers developed NLC functionalized with trastuzumab for the delivery of

docetaxel to breast cancer cells [100]. Targeted NLC exhibited a greater cytotoxicity in HER2 positive breast cancer cells (BT-474) than in negative breast cancer cells (MDA-MB-468). Additionally, a higher internalization was obtained in the HER2 positive breast cancer cells comparing to the non-functionalized NLC [100]. Siddhartha et al. prepared SLN for the encapsulation of the organosulfur compound with anti-cancer activity diallyl disulfide. The nanoparticles' surface was modified with an antibody anti-RAGE receptor, which is overexpressed in TNBC. A significantly higher internalization in MDA-MB-231 was found along with improved cytotoxic effects when compared to the non-functionalized SLN. Additionally, antibody functionalization resulted in a downregulation of anti-apoptotic proteins and upregulation of pro-apoptotic molecules, suggesting that RAGE is a promising target for the management of TNBC [112]. Recently the same group has developed another strategy for TNBC based on SLN loaded with the γ-secretase inhibitor DAPT and functionalized with an anti-death receptor-5 (DR5) antibody. Since DR5 is a receptor from the tumor necrosis factor family which is overexpressed in TNBC cells, it is considered a promising molecular target. The author found that functionalization of the NLC led to a higher cytotoxicity towards MDA-MB-231 and a selective and improved cancer cell uptake. *In vivo* assays corroborated these results, revealing a greater reduction in tumor growth, when compared to the non-targeted NLC [113].

The use of ligands for nanoparticle surface decoration, including polysaccharides, small molecules or peptides is also a common approach in breast cancer drug delivery. Comparing to antibodies, those are generally less specific, but also less immunogenic, more stable, more economically viable and easier to produce in large-scale [46].

Polysaccharides are often employed as targeting ligands in cancer. In this context, hyaluronic acid (HA) that targets the CD44 receptor, is one of the most common choices [114, 115]. CD44 is a cell transmembrane adhesion glycoprotein abundantly overexpressed in several cancer types such as melanoma, lymphoma, colorectal, breast, and lung [44, 116]. CD44 has two different isoforms, the standard isoform, and the variant isoforms, which are resultant from alternative splicing, all of them with binding affinity to HA. Nevertheless, studies have demonstrated that these isoforms may have distinct roles in cancer pathogenesis. Since variant isoforms present additional binding sites, they can bind to different molecules, such as growth factors and cytokines. In fact, ongoing research suggests that variant isoforms may favour tumor progression and metastasis and lower tumor response to endocrine treatment in breast cancer [117]. Different ligands can bind to CD44, however, due to its abundance, HA, represents the most common CD44 ligand. Their interaction plays a pivotal role in cell adhesion, migration and proliferation and, in the

context of cancer, tumor growth, angiogenesis and metastasis [116, 118]. HA is a high molecular weight negatively charged glycosaminoglycan and one of the main constituents of the ECM, responsible to maintain its integrity, mediate intra and extracellular interactions and mediate cell transduction signals [119, 120]. Due to its high affinity to the CD44 receptor and its biodegradability, non-toxic, non-immunogenic and non-inflammatory properties, HA is popular choice as a targeting moiety in numerous therapeutic applications, including cancer [114, 115, 121]. In fact, HA was found to target the CD44 receptor and internalize into tumor cells via receptor-mediated endocytosis [118, 122]. The binding affinity to CD44 depend, among other factors, on the variety of CD44 distinct isoforms, CD44 spatial distribution and HA molecular weight [122, 123]. Numerous studies have used lipid nanoparticles coated with HA, and very promising results have been highlighted. Overall, HA functionalization resulted in an improved nanoparticle cell uptake and tumor accumulation *in vivo* and an enhanced cytotoxicity towards breast cancer both *in vitro* and *in vivo* in different breast cancer cell lines and breast cancer subtypes. These results demonstrate that HA is an effective ligand for breast cancer active targeting [107, 124-127].

Functionalization with small molecules is also an appealing approach for breast cancer active targeting, due to their low cost, easiness of the conjugation procedure and facility of large-scale production [46]. In this context, folic acid (FA) has been extensively explored as a targeting ligand for breast cancer therapy applications. FA is a water-soluble B vitamin involved in DNA synthesis, methylation and repair. Due to its hydrophilicity, the entrance of FA into the cell has to occur via receptor-mediated endocytosis, mainly through folate receptor (FR). Since cancer cells have an abnormally high rate of proliferation, their demand of FA is much higher than in normal cells, which leads to an overexpression of FR [128, 129]. FR is a membrane glycoprotein with two main isoforms, α and β. FR α is the most abundant FR and the one with the highest binding affinity to FA. This isoform is mostly found in clusters in caveolae and is overexpressed in different types of cancers, including ovarian, endometrial, colorectal, breast and lung. On the other hand, its expression in most normal tissues is negligible, being confined to kidney, lung, choroid plexus and placenta. While the α isoform is generally overexpressed in epithelial tumor cells, β isoform is overexpressed in non-epithelial tumors such as sarcomas and acute myeloid leukemias. Thus, the α isoform has a key role in solid tumor progression and metastasis and is considered a negative prognostic factor for different kinds of cancer, including breast cancer, which makes it a promising therapeutic target. [130, 131]. Different works have developed lipid nanoparticles decorated with FA, showing improved cell internalization and cytotoxicity in different breast cancer cells, such as TNBC and MDR cells [97, 132, 133]. Recently, in a study conducted by Ma et al., FA functionalization was found to have a key role in improving the selectivity

towards breast cancer. The authors produced a multifunctional nanoplatform composed of NLC loaded with gambogic acid and paclitaxel and decorated with acid cleavable-FA and a cell penetrating peptide, dNP2. The functionalization significantly improved the endocytosis of the NLC in different breast cancer cell lines including MDA-MB-231, MCF-7 and 4T1 cells. A higher cytotoxicity was also obtained in 4T1 cells following functionalization with both FA and dNP2, either alone or combined. In addition, *in vivo* biodistribution studies showed than the breast tumor targeting ability of the NLC was significantly improved due to the presence of FA. Following intravenous injection in a 4T1-tumor bearing mice, FA decoration led to an enhanced accumulation of the NLC in the breast tissue. After accumulation in this tissue, the acidic environment induced the cleavage of FA and subsequent cell penetrating actions of dNP2 [134].

Although the majority of the active targeting strategies is designed for breast cancer cell specific receptors, there are also several works focusing on the targeting of the tumor microenvironment, such as the tumor endothelium. The *α*v integrins are adhesion receptors overexpressed at the surface of the tumor vasculature with high affinity to peptides containing the arginine-glycine-aspartic acid (RGD) sequence. Thus, surface decoration with RGD has been shown to enhance tumor vasculature permeability and tumor penetration [46]. Shan et al. decorated SLN with different concentration of cyclic RGD (0 to 10%) and evaluated its influence in integrin binding and breast cancer tumor growth inhibition. The binding affinity of the decorated SLN to the αvβ3 integrin was demonstrated *in vitro*, an effect which increased with increasing concentration of RGD. Moreover, these SLN could inhibit MDA-MB-231 cells invasion and adhesion to fibronection. *In vivo* studies showed that 1% RGD exhibited the highest tumor accumulation retention in an orthotopic MDA-MB-231/EGFP breast tumor mice model [135]. Kebebe et al. [104] prepared NLC loaded with the natural compound gambogic acid and functionalized with monomeric or dimeric cyclic RGD sequence peptides. The nanosystem improved the cell uptake and induced a higher cytotoxicity in 4T1 cells comparing to the non-functionalized NLC. These results were corroborated by the *in vivo* studies which have shown a greater tumor accumulation and tumor growth inhibition in a 4T1Luc- tumor bearing mice, with the dimeric RGD sequence exhibiting the best results [104].

### 4.1.2. Drug resistance inhibition

One major challenge in the treatment of breast cancer is the possibility of single or multidrug resistance, which results in treatment inefficacy and, eventually, disease relapse [136].

Different surfactants routinely used in lipid nanoparticles composition were found to inhibit several drug efflux pumps and, in this way, reverse tumor MDR. In a study conducted by Yamagat et al., common lipid nanoparticles components such as Tween® 20 , Pluronic P85 Span 20 and Brij 30 were able to inhibit Breast cancer resistance protein (BCRP) efflux transporter, while others, including Tween® 20, Pluronic P85, Tween® 80, Span® 20 and Gelucire 44/14 could inhibit P-glyocoprotein (P-gp) efflux pump, enhancing drug uptake into breast cancer cells [137]. These results motivated the work of Wang et al., which developed SLN coated with Pluronic p85 and functionalized with HA for the delivery of paclitaxel against MDR breast cancer cells. The presence of both Pluronic p85 and HA improved the anti-cancer efficacy of the nanosystem towards MCF-7 cells and P-gp overexpressing MCF-7 cells. In addition, an improved pharmacokinetic profile, enhanced tumor accumulation and significant tumor growth inhibition was achieved *in vivo* in a MDR breast cancer xenograft mice model after intravenous injection [124]. Cavaco et al. have also loaded paclitaxel into SLN to evade P-gp efflux. An enhanced anti-cancer effect of paclitaxel-loaded SLN comparing to the free drug was obtained along with a decreased expression of P-gp and MDR1 in the TNBC cell line MDA-MB-436. The authors claimed that the SLN were able to shield paclitaxel against the effects of P-gp and reduce its overexpression in TNBC [102]. Xu and co-workers also incorporated paclitaxel into SLN to enhance its anti-cancer activity and reverse MDR. Paclitaxel-loaded SLN improved the uptake of paclitaxel and exhibited a significantly higher cytotoxicity towards MCF-7/ADR comparing to the free drug and a commercial formulation of paclitaxel [138]. Eskiler et al. reported a SLN-based strategy to fight MDR in TNBC [139]. SLN were loaded with talazoparib, a PolyADP ribose polymerase inhibitor, and evaluated in the HCC193 and HCC193 talazoparib-resistant cell lines. Talazoparib-loaded nanoparticles were able to more effectively inhibit MDR1, BCRP, and MRP1 gene and protein expression than the free drug, demonstrating their potential to counteract MDR in TNBC [139].

Another common nanotherapeutic strategy to fight MDR is the co-encapsulation of anti-cancer drugs and other therapeutics, including chemosensitizers and P-gp inhibitors, as detailed in **section 4.1.7.**

### 4.1.3. Control of metastasis

Metastasis is the main cause of death in breast cancer, which makes its prevention and treatment extremely relevant [21]. Different lipid nanoparticles have been designed for targeting and treatment of breast cancer metastasis in different organs. Besides their efficacy in inhibiting breast cancer metastasis due to an enhanced delivery of the anti-tumoral agents, one of the studies has also reported an intrinsic anti-metastatic activity of the unloaded lipid nanoparticles [140], which highlights their enormous potential in the control of breast cancer metastasis.

The lymphatic system is the primary route for breast cancer metastasis, therefore, lymphatic drug delivery may be a promising therapeutic approach to manage advanced breast cancer. SLN have already been explored for lymph node targeting and lymphatic drug delivery [141, 142]. Lu et al. produced a mitoxantrone delivery vehicle based on SLN to treat breast cancer primary tumor and lymph node metastasis. The authors took advantage of the small size of the SLN (79 nm) for passive targeting of the lymphatic capillaries, which have apertures ranging from 20 to 120 nm. Overall, SLN could improve the retention of mitoxantrone in axillary lymph nodes following subcutaneous local injection. A similar performance in the inhibition of MCF-7 primary tumor and a much higher efficacy in the inhibition of lymph node metastasis was obtained, using a two-fold lower dosage of mitoxantrone comparing to the free drug solution [141]. Shete et al. developed NLC for the oral delivery of tamoxifen to improve its oral bioavailability and simultaneously target the intestinal lymphatic system. NLC substantially improved the accumulation of tamoxifen in the mesenteric lymph nodes and prolonged its circulation in the bloodstream following oral gavage. A dose-dependent anti-tumoral effect was observed in a 4T1 tumor-bearing mice, which was fairly superior comparing to free tamoxifen and a commercial tamoxifen product. Additionally, very limited levels of systemic and hepatotoxicity were observed [142].

Lung is one of the most common organs of breast cancer metastasis and is generally associated with a poor prognosis and a limited life expectancy. The low effectiveness of the treatment options for lung metastasis, highlights the need to address this problematic [143, 144]. Xu et al. designed SLN containing D-α-tocopheryl polyethylene glycol 1000 succinate (TPGS) entrapping sulibinin for the treatment of breast cancer pulmonary metastases. The sulibinin-loaded SLN could downregulate the expression of metastasis-related proteins such as Snail and MMP-9. In addition, SLN decreased the number of metastatic nodules in the lungs by 67% after intraperitoneal injection in a 4T1-luciferase murine spontaneous metastasis model and 39% in a MDA-MB-231 blood vessel metastasis model. The study also demonstrated for the first time that the unloaded SLN presented anti-metastatic

potential [140]. Recently Rocha and co-workers developed SLN for docetaxel delivery to 4T1 cancer cells. SLN exhibited a high anti-tumoral effect and could prevent distant lung metastasis in a 4T1 tumor-bearing mice, with a significantly higher efficacy than the free drug. Nanoparticles were also found to decrease the production of IL-6 serum levels and reduce the expression of ki-67 and BCL-2 in the lung tissues, further supporting the suitability of the nanosystem to inhibit tumor cell proliferation and lung metastasis [145]. NLC have also been produced for the control of lung metastasis. Nordin et al. fabricated NLC loaded with the natural compound citral for oral administration in a 4T1 tumor-bearing mice. NLC could induce a similar anti-tumoral and a higher anti-metastatic effect than the free compound, being able to inhibit both lung and bone-marrow metastasis. These effects were attributed to the downregulation of numerous metastasis and angiogenesis-related genes and proteins, an effect that was significantly higher than that of the free citral [146].

The incidence of brain metastasis in breast cancer is increasing due to earlier diagnosis and improved breast cancer survival, reaching 24% as reported by Rostami et al [147]. The particular characteristics of the blood-brain barrier (BBB), makes the treatment of brain metastasis and other brain malignancies particularly challenging [148]. Lipid nanoparticles are promising candidates for the treatment of breast cancer brain metastasis. In fact, some constituents commonly used in lipid nanoparticle composition, such as the surfactant Tween® 80 can enhance the crossing of the nanoparticles through BBB. Studies suggest that different plasma lipoproteins such as ApoB and ApoE can form a protein corona around the surface of Tween® 80-stabilized nanoparticles, leading to an improved transcytsosis across the BBB [149]. Furthermore, Tween® 80 can also inhibit P-gp efflux pumps present in this barrier [150]. Polymer-lipid hybrid coated with Tween® 80 have been developed by Zhang et al for the treatment of TNBC brain metastasis [151]. Nanoparticles could effectively cross the BBB following intravenous injection and accumulate in the metastatic regions in the brain, inducing a reduction in tumor size and prolonging survival in a MDA-MB-231 tumor bearing mice [151].

### 4.1.4. Introduction of new treatment modalities: Photodynamic therapy and hyperthermia

Photodynamic therapy (PDT) is a minimally invasive therapeutic used for the treatment of several diseases, such numerous skin conditions, infectious diseases, and various types of cancers [152]. This technique relies on the administration of a photosensitizer (PS) followed by irradiation with a laser of a suitable wavelength. The PS is able to absorb this light and

trigger several photochemical and photophysical reactions culminating in the production of reactive oxygen species (ROS), that cause alterations on essential molecules in the cell, affecting its activity, and ultimately, inducing cell death [152, 153]. PDT is an alternative and promising treatment modality for the management of breast cancer, including MDR and TNBC [154, 155] Nevertheless, most PS have major limitations, including poor pharmacokinetic properties, low solubility and reduced tumor accumulation [152]. Lipid nanoparticles have been employed to improve the physicochemical properties of common PS and, desirably, contribute to their establishment in clinical setting either alone or in combination with other therapeutics. Navarro et al. designed SLN for the delivery of the PS temoporfin to breast cancer cell line MCF-7. The authors showed that temoporfin could generate singlet oxygen ($^1O_2$) upon light irradiation, when encapsulated into SLN and that $^1O_2$ could diffuse from inside the SLN to the external media. Moreover, the phototoxicity of the nanoformulation was achieved following irradiation at different light fluences in MCF-7 cells [156]. A nanodelivery system for termeporfin based on SLN was also described by Brezaniova and co-workers. In this work, SLN were able to enhance the phototoxicity of this PS against 4T1 and MDA-MB-231 cells *in vitro* and in a MDA-MB-231 tumor-bearing mice, comparing to a commercial temoporfin formulation [157].

Kamel et al. explored the use of the phytochemical curcumin as a potential PS by formulating it into NLC. Curcumin-loaded NLC led to a significant decrease on MCF-7 cell viability following blue light irradiation, compared to free curcumin. Interestingly the authors found that one of the constituents of the NLC, glyceryl monooleate was more effective in improving the anti-cancer activity of curcumin, which as attributed to its higher curcumin dissolution capacity and also to its ability to inhibit P-gp expression [158].

Oshiro-Junior fabricated FA-coated NLC for the entrapment of a phtalocyanine. NLC-loaded phtalocyanine protected free PS against photobleaching and generated a similar amount of $^1O_2$ than the free PS. Additionally, an increase on MCF-7 cell death was obtained following light irradiation [159]. FA-coated NLC were also designed by Zhang et al. The authors combined PDT and chemotherapy into one single nanoformulation, by encapsulating paclitaxel and functionalising the surface of the NLC with the PS chlorin e6. The developed nanoformulation was able to target MDA-MB-231 cells and generate ROS upon laser illumination, at a higher amount than free chlorin e6. A synergistic effect between chemotherapy and PDT was obtained *in vitro* in the MDA-MB-231 cell line. Additionally, a great tumor targeting ability and anti-tumoral capacity *in vivo* was achieved following multimodal therapy in a MDA-MB-231 tumor xenograft mice model [97].

Hyperthermia consists on the temperature elevation above physiological level (ranging from a few degrees to more than 10ºC) to induce cancer cell death and also improve the performance of other therapeutic, such as chemotherapy [160]. Although its potential in cancer management has been studied since ancient times, the establishment of hyperthermia in clinical settings has been hampered by its limited efficacy and precision [160]. The use of nanotechnology has enabled the development of novel modalities of hyperthermia with higher efficacy and improved performance such as PTT and magnetic hyperthermia.

PTT is a minimally invasive procedure that requires a laser source (generally in the near infrared, NIR) and a PTT agent, which can be either a small molecule or a nanomaterial from different classes including metallic, carbon-based, polymer based and quantum dots. The principle of PTT is based on laser irradiation and subsequent heat release (hyperthermia), which can elicit tumor cell death through different mechanisms [160]. PTT may benefit and improve the current breast cancer therapeutic, either in advances stages of the disease, in combination with other clinical modalities such as chemotherapy or for the thermal ablation of primary tumors, as a less invasive alternative to surgical resection [160]. In this context, a few studies have reported the use of lipid nanoparticles for the delivery of PTT agents, either alone, or combined with chemotherapy, by using multifunctional and multimodal nanosystems that combine dual treatment and laser-triggered drug release.

Li et al. produced NLC for the incorporation of the NIR dye IR780. NLC were functionalized with a chemokine receptor CXCR4 antagonist to control breast cancer metastasis. NLC were able to improve the photothermal effect of IR780 by eliciting a remarkably higher temperature increase upon NIR laser irradiation and protecting the molecule from degradation after repeated cycles of irradiation. A high decrease on 4T1-luc cell viability was obtained following treatment with the nanoformulation and laser irradiation, an effect that was much greater than that of the free dye. *In vivo* studies suggested that NLC could efficiently accumulate in the tumor region after intravenous injection and significantly increase the tumor temperature upon NIR irradiation. Additionally, NLC exhibited a very high anti-tumoral effect after NIR irradiation, being able to fully eradicate the primary tumor in a syngeneic orthotopic mice model of metastatic breast cancer. In addition, the NLC-based PTT treatment was able to inhibit lung metastasis [161]. Zheng et al. combined chemotherapy, PTT and light-triggered drug release into a NLC-based formulation. Nanoparticles were decorated with PEG and HA and loaded with doxorubicin and polyhedral gold nanoparticles, as the PTT agent. NLC could achieve a high temperature

increase upon NIR laser irradiation. Additionally, a doxorubicin burst release was obtained after laser illumination, proving the light-triggered drug release behaviour of the nanosystem. The synergistic effect of chemotherapy and PTT were demonstrated in the breast cancer cell line MDA-MB-231 [107].

Magnetic hyperthermia relies on the use of magnetic nanoparticles that convert the energy from an alternating magnetic field (AMF) into heat [162]. The procedure requires the intratumoral or intravenous injection of the nanoparticles followed by application of an external AMF [162]. The most common nanomaterials used in this technique are iron oxide nanoparticles with diameters ranging from 10 to 100 nm [163, 164]. Magnetic hyperthermia is currently undergoing clinical trials for the treatment of different types of cancer, being considered a valuable tool for the establishment of hyperthermia in clinics, not only due to the tumor specificity and less invasiveness of the technique, but also because it is not limited by the tissue depth penetration [163-165]. Lipid nanoparticles have already been explored for the delivery of magnetic hyperthermia for breast cancer therapy. Ong et al. [166] produced methotrexate and superparamagnetic iron oxide nanoparticles (SPIONs)-loaded NLC for dual chemotherapy and magnetic hyperthermia. The nanoformulation induced a high cytotoxicity towards MDA-MB-231 cells and increased apoptotic cancer cell death upon exposure to an AMF for 20 min [166].

### 4.1.5. Stimuli-responsive drug release

With the advances in nanomedicine over the years, researchers started developing more complex and “smarter” nanoparticles to improve their performance and functionalities. One of these improvements is the design of stimuli-responsive nanocarriers, which can release their cargo upon an internal or external stimuli, such as pH or temperature, leading to a controlled delivery in the local of interest and, in the context of cancer disease, an enhanced anti-cancer performance with limited side-effects [167]. Lipid nanoparticles have been already explored for stimuli-responsive drug release in response to different stimuli.

The potential of SLN for thermoresponsive drug delivery was explored by Rehman et al. [168]. The authors encapsulated the chemotherapeutic drug 5-fluorouracil (5-FU) revealing that the drug was released at a much faster rate at mild hyperthermia conditions (39ºC). Additionally, the nanoformulation showed a higher cytotoxicity towards MDA-MB-231 TNBC cell line at 39ºC than 37ºC, suggesting an enhanced drug release and therapeutic effect upon mild hyperthermia conditions [168]. Zheng et al. constructed pH-sensitive SLN loaded

with doxorubicin to fight breast cancer MDR, taking advantage of the fact that the tumor environment is generally more acidic than the normal tissues. To enhance the uptake and anti-tumoral activity in MCF-7 doxorubicin resistant (MCF-7/ADR) cell line, SLN were conjugated with RGD. Nanoparticles released doxorubicin at a higher rate at pH 5 than pH 7.4, induced a higher tumor reduction in a MCF-7/ADR- tumor bearing mice comparing to the free drug and the non-functionalized SLN. In addition, RGD functionalization resulted in an enhanced tumor accumulation [169].

### 4.1.6. Theranostics

Another functionality that has been receiving considerable attention, with the design of new types of nanoparticles with improved optical, physical and chemical features, is theranostics. This approach provides both therapeutic and imaging properties, enabling simultaneous treatment and diagnosis, contributing to the development of more personalized cancer therapies, through constant monitorization and optimization of the therapeutic [170]. In cancer nanotheranostics, it is possible to encapsulate compounds that provide both therapeutic and imaging properties such as IR780 or temoporfin [157, 161] or use different classes of anti-cancer drugs combined with nanoparticles that offer imaging contrast properties, such as SPIONs [171], gold nanoparticles [172] and quantum dots [134]. Olerile et al. developed an innovative nanotheranostics system using NLC co-loaded with quantum dots and paclitaxel. The nanoformulation was efficiently internalized into MCF-7 cells, demonstrating its potential for breast cancer theranostics [173]. Ahmadifard et al. produced chitosan-coated SLN loaded with letrozole and iron oxide nanoparticles as strategy to enhance tumor drug delivery and as a potential therapeutic and diagnostic tool in the management of breast cancer. An increase in letrozole release was obtained following application of a low frequency pulsed magnetic field. In addition, the combination of letrozole and iron oxide nanoparticles improve the anti-cancer efficacy of the therapy, which was attributed to the antioxidant properties of the iron oxide nanoparticles [174].

### 4.1.7. Co-delivery and multimodal breast cancer therapy

As highlighted in **section 2**, as breast cancer is a highly complex and heterogeneous disease, the current therapeutic usually comprises multimodal and multidrug treatment. Recent studies in nanomedicine have also proposed the combination of several anti-cancer drugs, drugs and chemosensitizers or different therapeutic modalities into one single

nanoplatform to enhance the anti-cancer efficacy, reduce the dosages, limit the drugs associated side-effects and even counteract metastasis and MDR [175]. Despite the expected additive effects of the combination of drugs, synergistic effects were also described in some of the studies, resulting in an improved treatment performance.
Recently Mahoutforoush et al. designed NLC loaded with three anti-cancer drugs, namely, methotrexate, docetaxel and doxorubicin. Methotrexate was used as both anti-cancer and targeting agent due to its affinity to the FR. Targeted NLC exhibited a synergistic anti-cancer cell death in MCF-7 cells and a higher level of apoptosis and autophagy, and inhibited MCF-7 colony formation and cell migration [176].

Tran et al. developed SLN co-loaded with ibuprofen and paclitaxel coated with HA. Ibuprofen was used due to its chemosensitization properties, to enhance the efficacy of paclitaxel. Co-loaded SLN resulted in a synergistic anti-cancer effect in BT-474 and MDA-MB-231 cells and in an enhanced cell uptake into the CD44+ cell line MDA-MB-231 [177].
A synergistic approach for breast cancer management was also proposed by Lages and co-workers [125]. The authors fabricated NLC loaded with doxorubicin, docosahexaenoic acid (DHA) and α-tocopherol succinate (TS). The developed strategy was based on the fact that both DHA and TS are able to enhance the activity of chemotherapeutics. The synergistic effects of the three compounds were observed in the cytotoxicity towards 4T1 cells. Moreover, *in vivo* studies conducted in a tumor-bearing mice model using the same cancer cell line demonstrated an enhancement on tumor growth inhibition following triple therapy, along with prevention of lung metastasis and reduction of doxorubicin-induced cardio and hepatotoxicity [125].

Baek et al. produced SLN decorated with FA co-encapsulating paclitaxel and curcumin to fight breast cancer MDR. The polyphenol curcumin was used as an inhibitor of P-gp, to enhance the therapeutic effect of paclitaxel and overcome MDR into MCF-7/ADR cells. The nanoformulation was able to enhance the accumulation of paclitaxel intro cancer cells comparing to the free drug, either in monotherapy and in combination with curcumin and improve its cytotoxicity towards MCF-7/ADR cells. Additionally, an inhibitory effect on the expression of P-gp following treatment with the SLN was also observed [132]. A co-encapsulation strategy aimed to reverse MDR was also reported by Li et al. [106]. PEG-coated NLC were fabricated for the co-delivery β-lapachone and doxorubicin. β-lapachone was combined with doxorubicin due to its ability to generate ROS and induce NAD(P)H and ATP consumption in tumor cells, limiting the activity of P-gp, which is ATP-dependent. NLC were able to increase doxorubicin accumulation in the nucleus of MCF-7/ADR cells. Additionally, the two molecules were found to have remarkable synergistic effects in the

enhancement of cytotoxicity towards MCF-7/ADR cells. *In vivo* studies in a MCF-7/ADR tumor bearing mice model showed that the nanosystem improved the doxorubicin circulation half-life and tumor accumulation. Moreover, the dual-therapy exhibited a significantly higher anti-tumoral effect in comparison to the individual therapies [106].

A co-delivery nanosystem to improve the anti-cancer efficacy of doxorubicin was also proposed by Borges et al. [178]. NLC were produced for the co-delivery of doxorubicin and the diterpene sclareol, whose anti-cancer effects have been already demonstrated. The combination of the two molecules resulted in a synergistic anticancer effect towards MDA-MB-231 and 4T1 cells. The nanoformulation exhibited a greater anti-tumoral effect in a 4T1-tumor bearing mice, when compared to the free drug. Although the reduction in tumor growth was similar to the one induced by the combination of the free drugs, NLC did not cause body weight reduction and haematological toxicity, in opposite to the free drug therapeutic. This suggests that the NLC were able to improve the tolerability and safety of the treatment [178].

With the increasing scientific knowledge on the molecular and genetic basis of cancer, researches started exploring therapeutic strategies based on concomitant chemotherapy and gene therapy. Gene therapy relies on the administration of plasmid DNA (pDNA) to regulate mutated genes, or small interfering RNA (siRNA), short hairpin RNA and microRNA to modulate the expression of proteins and subsequent cell signalling pathways related with numerous cancer cell factors such as MDR, apoptosis or immune response [179]. The association of gene therapy with chemotherapy has resulted in an enhanced anti-cancer efficacy against breast cancer, as reported in numerous studies [180-182]. Thus, nanotherapeutic strategies based on this combination have been developed over the last few years. Lipid nanoparticles, in particular, are considered efficient nucleic acid delivery vehicles, as their composition can be modulated through the incorporation of cationic lipids, which bind to nuclei acids via electrostatic interaction, forming stable nanocarriers [183]. Yu et al. combined paclitaxel and a pDNA encoding enhanced green fluorescent protein, as a model gene into HA-coated cationic SLN. The nanoformulation induced a remarkable transfection efficiency in MCF-7 cells and limited cancer cell growth with higher efficacy than a commercial paclitaxel formulation. Additionally, HA significantly enhanced SLN internalization in MCF-7 cells. These results were corroborated by the *in vivo* studies in which co-loaded SLN presented a high tumor accumulation and tumor growth inhibition in a MCF-7 mice xenograft model [126]. Liu et al. [184] encapsulated microRNA-200c, which can restore cancer cell sensitivity towards microtubule-targeting drugs, into a cationic SLN and conjugated this nanocarrier with paclitaxel-loaded NLC, as strategy to improve

paclitaxel efficacy against breast cancer stem cells. SLN were able to protect microRNA-200c against degradation and demonstrated a high transfection efficiency. Moreover, they were able to significantly enhance the anti-cancer activity of paclitaxel-loaded NLC in MCF-7 mammospheres [184].

### 4.2. Administration routes

Lipid nanoparticles offer a high versatility in terms of administration routes. Most of the studies here highlighted have focused on the intravenous route of administration with encouraging results, including high tumor targeting ability [97, 104, 106, 124, 126, 134, 161, 169], enhanced drug pharmacokinetic profile [106, 124, 161] and great tumor growth inhibition [97, 104, 106, 124-126, 157, 161, 169]. Despite the promising results obtained with this route, recently, other routes of administration have also been explored.

The oral route of administration is less invasive and preferable in terms of convenience and patient compliance. Lipid nanoparticles have been employed to enhance the oral bioavailability of drugs conventionally given orally in the management of breast cancer therapy, such as most of the hormonal therapies [185, 186]. Moreover, they have also been explored for the oral delivery of conventional chemotherapeutic drugs that are normally administered intravenously [127, 133, 187]. Recently, Moraes et al. produced NLC functionalized with a DSPE-PEG- FA conjugate as a potential delivery vehicle for the oral delivery of doxorubicin. *In vitro* release studies mimicking the gastrointestinal tract revealed that 50% doxorubicin still remained encapsulated in the nanoparticles, demonstrating the suitability of the nanosystem for doxorubicin oral delivery. In addition, a high internalization in MDA-MB-231 induced by the surface functionalization was obtained, along with a high anti-cancer efficacy [133]. Qureshi et al. developed SLN for the oral delivery of docetaxel. SLN induced a sustained release in simulated gastric and intestinal fluids and presented a lower value of $IC_{50}$ in MCF-7 cells than the free drug. Furthermore *in vivo* studies conducted in Sprague-Dawley rats showed that SLN significantly improved the area under the plasma concentration–time comparing with docetaxel-loaded micelles following oral administration [187]. Gao et al. fabricated HA-coated cationic NLC for the delivery of the anti-cancer drug vincristine sulfate. HA functionalization enhanced NLC uptake and cytotoxicity towards MCF-7 cells. *In vivo* studies conducted in Sprague-Dawley rats showed that the functionalized NLC improved the oral bioavailability of vincristine sulfate, comparing with the free drug solution [127]. Different studies have also demonstrated that following oral administration, lipid nanoparticles could avoid the first-pass metabolism and be absorbed via lymphatic system [142, 188]. This fact not only improves the drug bioavailability, but can

also be explored for the treatment of metastatic disease [142]. Baek et al. prepared chitosan-coated SLN loaded with curcumin. A remarkable increase of curcumin oral bioavailability and intestinal lymphatic uptake was obtained after oral administration to Sprague Dawley rats, comparing to the free curcumin solution [188].
Recently, Gadag et al. explored a localized drug delivery system for the breast tissue using the transdermal route of administration. The rational behind this approach is based on the lipophilicity of the NLC, which leads to a high retention in the adipose tissue of the breast, with only limited release in the bloodstream. In order to do so, the authors fabricated NLC loaded with resveratrol and used a microneedle array system for the transdermal delivery of the NLC in Sprague-Dawley rats. The nanosystem combined with microneedle arrays induced a sustained release of resveratrol, improved its pharmacokinetics and significantly enhanced its accumulation in the breast tissue, comparing to orally administered resveratrol. Overall, these results highlight that this novel route of administration associated with lipid nanoparticles is a promising approach to improve drug delivery and therapeutic outcomes in breast cancer [189].

## 5. Conclusions and future perspectives

According to the most recent GLOBOCAN report, breast cancer is the most common malignancy among women [1]. Besides being responsible for a high number of deaths all over the world, breast cancer has also a high impact on patients' DALYs and on economics. The emergence of nanomedicine and its introduction in breast cancer therapy has shown promising results, particularly in reducing the toxic systemic effects of the chemotherapeutic drugs, such as cardiotoxicity. Additionally, their combination with standard chemotherapeutic regimens has improved overall response rates and progression-free survival. However, despite all these advances, the use of these nanoparticles in clinics is still restricted, due to their high manufacturing costs.

Lipid nanoparticles have emerged in the 90's as a cost-effective, stable and versatile type of nanocarrier composed of lipid materials with GRAS status. Their potential in the management of cancer disease and breast cancer in particular is undeniable. Different surfactants commonly used in lipid nanoparticles composition, such as Tween® 80, have shown ability to counteract MDR, one of the major challenges in breast cancer, through the inhibition different efflux transporters such as P-gp and BCRP. Moreover, their potential is the treatment of metastatic breast cancer has been demonstrated in different organs. The targeting of the lymph nodes, the first organ where breast cancer metastasis occurs, using

lipid nanoparticles has been achieved either by local injection or through oral administration, by targeting of the intestinal lymphatic system. Several studies have also shown a high remission of lung metastasis, with one of them showing an intrinsic anti-metastatic potential of the unloaded lipid nanoparticles. Common lipid nanoparticles components such as Tween® 80 have also demonstrate ability to improve the crossing of the BBB, highlighting their potential of the treatment of brain breast cancer metastasis and brain diseases in general.

Lipid nanoparticles are also highly versatile in terms of administration routes. While the intravenous has been the preferred route in most of the studies here highlighted, with encouraging results in terms of tumor targeting and enhanced pharmacokinetic profile, other routes have also been explored. The oral route has been explored either for the delivery drugs commonly administered orally, such as most of the hormonal therapies, or for the delivery of other chemotherapeutic drugs frequently administered intravenously, such as doxorubicin and docetaxel with very interesting outcomes. This is a promising strategy to improve patients' convenience and compliance. Additionally, the oral route has been explored for the treatment of metastatic disease through the targeting of the intestinal lymph nodes. Recently, a localized transdermal administration of the breast tumor has also been proposed though the association with microneedle arrays, with a very high accumulation in the breast tissue and promising therapeutic results.

The size and surface properties of the lipid nanoparticles can also be easily modified to prolong their circulation time, such as through PEGylation. Moreover, the penetration in the tumor region can be further enhanced through the use of specific drugs of using external stimuli such as hyperthermia, which can reduce IFP and increase blood flow and tumor endothelium opening. Additionally, their surface can be easily decorated with numerous targeting ligands ranging from antibodies to small molecules to improve tumor accumulation.

Recent studies in this area have resulted in the introduction of alternative treatment modalities such as gene therapy, PDT and hyperthermia, which have great potential, particularly when associated with other conventional modalities such as chemotherapy. By choosing the most suitable lipid components, those therapies may also be combined with stimuli-responsive smart nanosystems to further improve the anti-tumoral efficacy. Moreover, the possibility of simultaneous tumor imaging and treatment as also started to be explored through the development of nanotheranostics.

Since breast cancer is a highly complex and heterogeneous disease and its current treatment is based on the combination of multiple drugs, and, frequently, multiple therapies, the design of multimodal nanosystems combining different therapeutic alternatives offers a great potential. Those may include chemotherapy, PDT, hyperthermia or gene therapy along with active or passive targeting approaches to enhance the efficacy of the treatment, overcome MDR, reduce drug dosages and limit adverse side-effects. Therefore, it is expected that in the near future, more studies will focus on the development of multifunctional lipid nanosystems.

Nevertheless, despite all the encouraging outcomes here outlined, lipid nanoparticles have still not reached the pharmaceutical market and clinical settings. Future studies should be conducted on the evaluation and optimization of their large-scale production, along with the design of cost-benefit analysis. Taking into account the cost-effective, simple and environmental friendly production methods used in their manufacture, and the low-cost of their main constituents, lipid nanoparticles offer a great alternative to other types of currently clinical available nanocarriers, with a higher chance of widespread clinical application.

## Acknowledgements

This work received financial support from PT national funds (FCT/MCTES, Fundação para a Ciência e Tecnologia and Ministério da Ciência, Tecnologia e Ensino Superior) through the project UIDB/50006/2020 (LAQV-REQUIMTE). Andreia Granja acknowledges FCT (Fundação para a Ciência e Tecnologia) and ESF (European Social Fund) for her PhD grant SFRH/BD/130147/2017. Célia T. Sousa thanks FCT for financial support through the Investigador FCT program (contract no. IF/01159/2015), to the program Atraccion de Talento (CAM), ref. 2020-T1/IND-19889 and the UE's Horizon 2020 research and innovation program under the Marie Sklodowska-Curie grant no. 734801. The authors acknowledge Servier Laboratories for permission for adaptation of figures.

## References


1. Sung, H., J. Ferlay, R.L. Siegel, M. Laversanne, I. Soerjomataram, A. Jemal, and F. Bray, *Global Cancer Statistics 2020: GLOBOCAN Estimates of Incidence and Mortality Worldwide for 36 Cancers in 185 Countries.* CA Cancer J Clin, 2021. **71**(3): p. 209-49.
2. Global Burden of Disease Cancer, C., C. Fitzmaurice, D. Abate, N. Abbasi, H. Abbastabar, F. Abd-Allah, O. Abdel-Rahman, A. Abdelalim, A. Abdoli, I. Abdollahpour, et al., *Global, Regional, and National Cancer Incidence, Mortality, Years of Life Lost, Years Lived With Disability, and Disability-Adjusted Life-Years for 29 Cancer Groups, 1990 to 2017: A Systematic Analysis for the Global Burden of Disease Study.* JAMA oncology, 2019. **5**(12): p. 1749-68.
3. Luengo-Fernandez, R., J. Leal, A. Gray, and R. Sullivan, *Economic burden of cancer across the European Union: a population-based cost analysis.* Lancet Oncol, 2013. **14**(12): p. 1165-74.
4. Mariotto, A.B., K.R. Yabroff, Y. Shao, E.J. Feuer, and M.L. Brown, *Projections of the cost of cancer care in the United States: 2010-2020.* J Natl Cancer Inst, 2011. **103**(2): p. 117-28.
5. Polyak, K., *Heterogeneity in breast cancer.* The Journal of clinical investigation, 2011. **121**(10): p. 3786-88
6. Tan, P.H., I. Ellis, K. Allison, E. Brogi, S.B. Fox, S. Lakhani, A.J. Lazar, E.A. Morris, A. Sahin, and R. Salgado, *The 2019 World Health Organization classification of tumours of the breast.* Histopathology, 2020. **77**(2): p. 181-85.
7. Bai, X., J. Ni, J. Beretov, P. Graham, and Y. Li, *Cancer stem cell in breast cancer therapeutic resistance.* Cancer Treatment Reviews, 2018. **69**: p. 152-63.
8. Collignon, J., L. Lousberg, H. Schroeder, and G. Jerusalem, *Triple-negative breast cancer: treatment challenges and solutions.* Breast Cancer: Targets and Therapy, 2016. **8**: p. 93.
9. Mahul, B.A., E. Stephen, L. Frederick, R. David, K. Robert, K. Mary, E. Jeffrey, C. Carolyn, R. Kenneth, and C. Daniel, *AJCC cancer staging manual*. 2017, Springer New York, NY, USA.
10. Pandya, S. and R.G. Moore, *Breast development and anatomy.* Clinical obstetrics and gynecology, 2011. **54**(1): p. 91-95.
11. Reisner, H., *Pathology: A Modern Case Study*. 2014: McGraw-Hill Education.
12. Kumar, V., A.K. Abbas, N. Fausto, and J.C. Aster, *Robbins and Cotran pathologic basis of disease*. 2014: Elsevier Health Sciences.
13. Makki, J., *Diversity of breast carcinoma: histological subtypes and clinical relevance.* Clinical Medicine Insights: Pathology, 2015. **8**: p. CPath. S31563.
14. Waks, A.G. and E.P. Winer, *Breast Cancer Treatment: A Review.* Jama, 2019. **321**(3): p. 288-300.
15. Sinn, H.P. and H. Kreipe, *A Brief Overview of the WHO Classification of Breast Tumors, 4th Edition, Focusing on Issues and Updates from the 3rd Edition.* Breast Care (Basel), 2013. **8**(2): p. 149-54.
16. Bustreo, S., S. Osella-Abate, P. Cassoni, M. Donadio, M. Airoldi, F. Pedani, M. Papotti, A. Sapino, and I. Castellano, *Optimal Ki67 cut-off for luminal breast cancer prognostic evaluation: a large case series study with a long-term follow-up.* Breast cancer research and treatment, 2016. **157**(2): p. 363-71,10.1007/s10549-016-3817-9.
17. Constantinidou, A. and I. Smith, *Is there a case for anti-HER2 therapy without chemotherapy in early breast cancer?* The Breast, 2011. **20**: p. S158-S61.
18. Geyer, C.E., J. Forster, D. Lindquist, S. Chan, C.G. Romieu, T. Pienkowski, A. Jagiello-Gruszfeld, J. Crown, A. Chan, and B. Kaufman, *Lapatinib plus capecitabine for HER2-positive advanced breast cancer.* New England journal of medicine, 2006. **355**(26): p. 2733-43.
19. DeVita VT, L.T., Lawrence TS, Rosenberg SA, *Devita, Hellman, and Rosenberg's Cancer: Principles and Practice of Oncology*. 11th ed. 2019, Philadelphia.
20. Wang, H., C. Zhang, J. Zhang, L. Kong, H. Zhu, and J. Yu, *The prognosis analysis of different metastasis pattern in patients with different breast cancer subtypes: a SEER based study.* Oncotarget, 2017. **8**(16): p. 26368-79.
21. Redig, A.J. and S.S. McAllister, *Breast cancer as a systemic disease: a view of metastasis.* Journal of internal medicine, 2013. **274**(2): p. 113-26.
22. Castiglione, M. and M.J. Piccart, *Adjuvant therapy for breast cancer*. Cancer treatment and research,. 2009, New York: Springer. xvi, 490 p.

23. Yarnold, J., *Early and locally advanced breast cancer: diagnosis and treatment National Institute for Health and Clinical Excellence guideline 2009.* Clinical Oncology, 2009. **21**(3): p. 159-60.
24. Goldhirsch, A., J.N. Ingle, R.D. Gelber, A.S. Coates, B. Thürlimann, and H.J. Senn, *Thresholds for therapies: highlights of the St Gallen International Expert Consensus on the primary therapy of early breast cancer 2009.* Ann Oncol, 2009. **20**(8): p. 1319-29.
25. Dieci, M.V., E. Orvieto, M. Dominici, P.F. Conte, and V. Guarneri, *Rare Breast Cancer Subtypes: Histological, Molecular, and Clinical Peculiarities.* Oncologist, 2014. **19**(8): p. 805-13.
26. Early Breast Cancer Trialists' Collaborative, G., C. Davies, J. Godwin, R. Gray, M. Clarke, D. Cutter, S. Darby, P. McGale, H.C. Pan, C. Taylor, et al., *Relevance of breast cancer hormone receptors and other factors to the efficacy of adjuvant tamoxifen: patient-level meta-analysis of randomised trials.* Lancet, 2011. **378**(9793): p. 771-84.
27. Mayer, E.L. and H.J. Burstein, *Chemotherapy for metastatic breast cancer.* Hematology/oncology clinics of North America, 2007. **21**(2): p. 257-72.
28. Amar, S., V. Roy, and E.A. Perez, *Treatment of metastatic breast cancer: looking towards the future.* Breast cancer research and treatment, 2009. **114**(3): p. 413-22.
29. Blanco, E. and M. Ferrari, *Emerging nanotherapeutic strategies in breast cancer.* The Breast, 2014. **23**(1): p. 10-18.
30. Pooja, D., H. Kulhari, M. Kuncha, S.S. Rachamalla, D.J. Adams, V. Bansal, and R. Sistla, *Improving Efficacy, Oral Bioavailability, and Delivery of Paclitaxel Using Protein-Grafted Solid Lipid Nanoparticles.* Molecular Pharmaceutics, 2016. **13**(11): p. 3903-12.
31. Shapiro, C.L. and A. Recht, *Side effects of adjuvant treatment of breast cancer.* New England Journal of Medicine, 2001. **344**(26): p. 1997-2008.
32. Chawla, J.S. and M.M. Amiji, *Biodegradable poly (ε-caprolactone) nanoparticles for tumor-targeted delivery of tamoxifen.* International journal of pharmaceutics, 2002. **249**(1): p. 127-38.
33. Mourits, M.J., E.G. De Vries, P.H. Willemse, K.A. Ten Hoor, H. Hollema, and A.G. Van der Zee, *Tamoxifen treatment and gynecologic side effects: a review.* Obstetrics & Gynecology, 2001. **97**(5): p. 855-66.
34. Perez, E.A. and K. Weilbaecher, *Aromatase inhibitors and bone loss.* Oncology (Williston Park, N.Y.), 2006. **20**(9): p. 1029-48.
35. Gianni, L., E. Salvatorelli, and G. Minotti, *Anthracycline cardiotoxicity in breast cancer patients: synergism with trastuzumab and taxanes.* Cardiovasc Toxicol, 2007. **7**(2): p. 67-71.
36. Minchinton, A.I. and I.F. Tannock, *Drug penetration in solid tumours.* Nature Reviews Cancer, 2006. **6**(8): p. 583-92.
37. Mei, L., Z. Zhang, L. Zhao, L. Huang, X.-L. Yang, J. Tang, and S.-S. Feng, *Pharmaceutical nanotechnology for oral delivery of anticancer drugs.* Advanced drug delivery reviews, 2013. **65**(6): p. 880-90.
38. Rajashekar Kammari, N.G.D., Sudip K.Das, *Nanoparticulate Systems for Therapeutic and Diagnostic Applications*, in *Emerging Nanotechnologies for Diagnostics, Drug Delivery and Medical Devices*, K.C.a.A.M. Ashim K. Mitra, Editor. 2017. p. 105-44.
39. Shi, J., P.W. Kantoff, R. Wooster, and O.C. Farokhzad, *Cancer nanomedicine: progress, challenges and opportunities.* Nature reviews. Cancer, 2017. **17**(1): p. 20-37.
40. Wicki, A., D. Witzigmann, V. Balasubramanian, and J. Huwyler, *Nanomedicine in cancer therapy: challenges, opportunities, and clinical applications.* J Control Release, 2015. **200**: p. 138-57.
41. Ghosh, S., S. Ghosh, and P.C. Sil, *Role of nanostructures in improvising oral medicine.* Toxicology reports, 2019. **6**: p. 358-68.
42. Iyer, A.K., G. Khaled, J. Fang, and H. Maeda, *Exploiting the enhanced permeability and retention effect for tumor targeting.* Drug discovery today, 2006. **11**(17-18): p. 812-18.
43. Kalyane, D., N. Raval, R. Maheshwari, V. Tambe, K. Kalia, and R.K. Tekade, *Employment of enhanced permeability and retention effect (EPR): Nanoparticle-based precision tools for targeting of therapeutic and diagnostic agent in cancer.* Materials Science and Engineering: C, 2019. **98**: p. 1252-76.
44. Chang Hyun Kim, S.G.L., Myung Joo Kang, Sangkil Lee & Young Wook Choi, *Surface modification of lipid-based nanocarriers for cancer cell-specific drug targeting.* Journal of Pharmaceutical Investigation, 2017.

45. Ojha, T., V. Pathak, Y. Shi, W.E. Hennink, C.T. Moonen, G. Storm, F. Kiessling, and T. Lammers, *Pharmacological and physical vessel modulation strategies to improve EPR-mediated drug targeting to tumors.* Advanced drug delivery reviews, 2017. **119**: p. 44-60.
46. Pearce, A.K. and R.K. O'Reilly, *Insights into active targeting of nanoparticles in drug delivery: Advances in clinical studies and design considerations for cancer nanomedicine.* Bioconjugate chemistry, 2019. **30**(9): p. 2300-11.
47. Roma-Rodrigues, C., R. Mendes, P.V. Baptista, and A.R. Fernandes, *Targeting Tumor Microenvironment for Cancer Therapy.* International journal of molecular sciences, 2019. **20**(4): p. 840.
48. Lee, Y. and D.H. Thompson, *Stimuli-responsive liposomes for drug delivery.* Wiley interdisciplinary reviews. Nanomedicine and nanobiotechnology, 2017. **9**(5): p. 10.1002/wnan.450.
49. Liu, X., Y. Yang, and M.W. Urban, *Stimuli-Responsive Polymeric Nanoparticles.* Macromol Rapid Commun, 2017. **38**(13).
50. Hu, C.-M.J. and L. Zhang, *Nanoparticle-based combination therapy toward overcoming drug resistance in cancer.* Biochemical Pharmacology, 2012. **83**(8): p. 1104-11.
51. Wang, K., F.M. Kievit, and M. Zhang, *Nanoparticles for cancer gene therapy: Recent advances, challenges, and strategies.* Pharmacological Research, 2016. **114**: p. 56-66,
52. Lucky, S.S., K.C. Soo, and Y. Zhang, *Nanoparticles in photodynamic therapy.* Chemical reviews, 2015. **115**(4): p. 1990-2042,
53. Arranja, A.G., V. Pathak, T. Lammers, and Y. Shi, *Tumor-targeted nanomedicines for cancer theranostics.* Pharmacol Res, 2017. **115**: p. 87-95,
54. Prasad, M., U.P. Lambe, B. Brar, I. Shah, M. J, K. Ranjan, R. Rao, S. Kumar, S. Mahant, S.K. Khurana, et al., *Nanotherapeutics: An insight into healthcare and multi-dimensional applications in medical sector of the modern world.* Biomed Pharmacother, 2018. **97**: p. 1521-37.
55. Crommelin, D.J.A., P. van Hoogevest, and G. Storm, *The role of liposomes in clinical nanomedicine development. What now? Now what?* Journal of Controlled Release, 2020. **318**: p. 256-63.
56. Yardley, D.A., *nab-Paclitaxel mechanisms of action and delivery.* J Control Release, 2013. **170**(3): p. 365-72.
57. Lee, K.S., H.C. Chung, S.A. Im, Y.H. Park, C.S. Kim, S.B. Kim, S.Y. Rha, M.Y. Lee, and J. Ro, *Multicenter phase II trial of Genexol-PM, a Cremophor-free, polymeric micelle formulation of paclitaxel, in patients with metastatic breast cancer.* Breast Cancer Res Treat, 2008. **108**(2): p. 241-50.
58. Anselmo, A.C. and S. Mitragotri, *Nanoparticles in the clinic.* Bioengineering & Translational Medicine, 2016. **1**(1): p. 10-29.
59. Gabizon, A.A., O. Lyass, G.J. Berry, and M. Wildgust, *Cardiac safety of pegylated liposomal doxorubicin (Doxil/Caelyx) demonstrated by endomyocardial biopsy in patients with advanced malignancies.* Cancer Invest, 2004. **22**(5): p. 663-9,10.
60. O'Brien, M.E., N. Wigler, M. Inbar, R. Rosso, E. Grischke, A. Santoro, R. Catane, D.G. Kieback, P. Tomczak, S.P. Ackland, et al., *Reduced cardiotoxicity and comparable efficacy in a phase III trial of pegylated liposomal doxorubicin HCl (CAELYX/Doxil) versus conventional doxorubicin for first-line treatment of metastatic breast cancer.* Ann Oncol, 2004. **15**(3): p. 440-9.
61. Sparano, J.A., A.N. Makhson, V.F. Semiglazov, S.A. Tjulandin, O.I. Balashova, I.N. Bondarenko, N.V. Bogdanova, G.M. Manikhas, G.P. Oliynychenko, V.A. Chatikhine, et al., *Pegylated liposomal doxorubicin plus docetaxel significantly improves time to progression without additive cardiotoxicity compared with docetaxel monotherapy in patients with advanced breast cancer previously treated with neoadjuvant-adjuvant anthracycline therapy: results from a randomized phase III study.* J Clin Oncol, 2009. **27**(27): p. 4522-9,
62. Venturini, M., C. Bighin, F. Puglisi, N. Olmeo, E. Aitini, G. Colucci, O. Garrone, A. Paccagnella, G. Marini, L. Crinò, et al., *A multicentre Phase II study of non-pegylated liposomal doxorubicin in combination with trastuzumab and docetaxel as first-line therapy in metastatic breast cancer.* Breast, 2010. **19**(5): p. 333-8.
63. Wang, L., Y. Hong, J. Ma, M. Han, S. Zhang, B. Shan, and Y. Liu, *Combination of pegylated liposomal doxorubicin and docetaxel as neoadjuvant therapy for breast cancer with axillary lymph node metastasis.* J Int Med Res, 2020. **48**(8): p. 300060520944310.

64. Franco, Y.L., T.R. Vaidya, and S. Ait-Oudhia, *Anticancer and cardio-protective effects of liposomal doxorubicin in the treatment of breast cancer.* Breast cancer (Dove Medical Press), 2018. **10**: p. 131-41.
65. Leonard, R., S. Williams, A. Tulpule, A. Levine, and S. Oliveros, *Improving the therapeutic index of anthracycline chemotherapy: focus on liposomal doxorubicin (Myocet™).* The Breast, 2009. **18**(4): p. 218-24.
66. Rau, K.-M., Y.-C. Lin, Y.-Y. Chen, J.-S. Chen, K.-D. Lee, C.-H. Wang, and H.-K. Chang, *Pegylated liposomal doxorubicin (Lipo-Dox®) combined with cyclophosphamide and 5-fluorouracil is effective and safe as salvage chemotherapy in taxane-treated metastatic breast cancer: an open-label, multi-center, non-comparative phase II study.* BMC cancer, 2015. **15**(1): p. 1-8.
67. Wang, F., M. Porter, A. Konstantopoulos, P. Zhang, and H. Cui, *Preclinical development of drug delivery systems for paclitaxel-based cancer chemotherapy.* Journal of controlled release : official journal of the Controlled Release Society, 2017. **267**: p. 100-18.
68. Sachdev, J.C., P. Munster, D.W. Northfelt, H.S. Han, C. Ma, F. Maxwell, T. Wang, B. Belanger, B. Zhang, Y. Moore, et al., *Phase I study of liposomal irinotecan in patients with metastatic breast cancer: findings from the expansion phase.* Breast Cancer Res Treat, 2021. **185**(3): p. 759-71.
69. de Maar, J.S., B.B.M. Suelmann, M. Braat, P.J. van Diest, H.H.B. Vaessen, A.J. Witkamp, S.C. Linn, C.T.W. Moonen, E. van der Wall, and R. Deckers, *Phase I feasibility study of Magnetic Resonance guided High Intensity Focused Ultrasound-induced hyperthermia, Lyso-Thermosensitive Liposomal Doxorubicin and cyclophosphamide in de novo stage IV breast cancer patients: study protocol of the i-GO study.* BMJ Open, 2020. **10**(11): p. e040162.
70. Munster, P., I.E. Krop, P. LoRusso, C. Ma, B.A. Siegel, A.F. Shields, I. Molnár, T.J. Wickham, J. Reynolds, K. Campbell, et al., *Safety and pharmacokinetics of MM-302, a HER2-targeted antibody-liposomal doxorubicin conjugate, in patients with advanced HER2-positive breast cancer: a phase 1 dose-escalation study.* Br J Cancer, 2018. **119**(9): p. 1086-93.
71. Brandsma, D., B.M. Kerklaan, V. Diéras, S. Altintas, C. Anders, M.A. Ballester, H. Gelderblom, P. Soetekouw, W. Gladdines, and F. Lonnqvist, *Phase 1/2a study of glutathione pegylated liposomal doxorubicin (2b3-101) in patients with brain metastases (BM) from solid tumors or recurrent high grade gliomas (HGG).* Annals of Oncology, 2014. **25**: p. iv157.
72. Awada, A., I. Bondarenko, J. Bonneterre, E. Nowara, J. Ferrero, A. Bakshi, C. Wilke, M. Piccart, and C.S. Group, *A randomized controlled phase II trial of a novel composition of paclitaxel embedded into neutral and cationic lipids targeting tumor endothelial cells in advanced triple-negative breast cancer (TNBC).* Annals of oncology, 2014. **25**(4): p. 824-31.
73. Della Rocca, J., D. Liu, and W. Lin, *Are high drug loading nanoparticles the next step forward for chemotherapy?* Nanomedicine, 2012. **7**(3): p. 303-05.
74. Weber, S., A. Zimmer, and J. Pardeike, *Solid Lipid Nanoparticles (SLN) and Nanostructured Lipid Carriers (NLC) for pulmonary application: a review of the state of the art.* European journal of pharmaceutics and biopharmaceutics : official journal of Arbeitsgemeinschaft für Pharmazeutische Verfahrenstechnik e.V, 2014. **86**: p. 7-22.
75. Shah, R., D. Eldridge, E. Palombo, and I. Harding, *Lipid nanoparticles: Production, characterization and stability*. 2015: Springer.
76. Naseri, N., H. Valizadeh, and P. Zakeri-Milani, *Solid lipid nanoparticles and nanostructured lipid carriers: structure, preparation and application.* Advanced pharmaceutical bulletin, 2015. **5**(3): p. 305.
77. Muller, R., M. Radtke, and S. Wissing, *Solid lipid nanoparticles (SLN) and nanostructured lipid carriers (NLC) in cosmetic and dermatological preparations.* Advanced drug delivery reviews, 2002. **54**(1): p. S131.
78. Beloqui, A., M.Á. Solinís, A. Rodríguez-Gascón, A.J. Almeida, and V. Préat, *Nanostructured lipid carriers: Promising drug delivery systems for future clinics.* Nanomedicine : nanotechnology, biology, and medicine, 2015. **12**: p. 143-61.
79. Wissing, S.A. and R.H. Müller, *Cosmetic applications for solid lipid nanoparticles (SLN).* International Journal of Pharmaceutics, 2003. **254**(1): p. 65-68.
80. Weiss, J., E.A. Decker, D.J. McClements, K. Kristbergsson, T. Helgason, and T. Awad, *Solid lipid nanoparticles as delivery systems for bioactive food components.* Food biophysics, 2008. **3**(2): p. 146-54.

81. Tapeinos, C., M. Battaglini, and G. Ciofani, *Advances in the design of solid lipid nanoparticles and nanostructured lipid carriers for targeting brain diseases.* J Control Release, 2017. **264**: p. 306-32.
82. Rajpoot, K., *Solid Lipid Nanoparticles: A Promising Nanomaterial in Drug Delivery.* Curr Pharm Des, 2019. **25**(37): p. 3943-59.
83. Muller, R.H., R.D. Petersen, A. Hommoss, and J. Pardeike, *Nanostructured lipid carriers (NLC) in cosmetic dermal products.* Adv Drug Deliv Rev, 2007. **59**(6): p. 522-30.
84. Shidhaye, S., R. Vaidya, S. Sutar, A. Patwardhan, and V. Kadam, *Solid lipid nanoparticles and nanostructured lipid carriers-innovative generations of solid lipid carriers.* Current drug delivery, 2008. **5**(4): p. 324-31.
85. Ghasemiyeh, P. and S. Mohammadi-Samani, *Solid lipid nanoparticles and nanostructured lipid carriers as novel drug delivery systems: applications, advantages and disadvantages.* Research in pharmaceutical sciences, 2018. **13**(4): p. 288-303.
86. Hou, D., C. Xie, K. Huang, and C. Zhu, *The production and characteristics of solid lipid nanoparticles (SLNs).* Biomaterials, 2003. **24**(10): p. 1781-85.
87. Aldawsari, H.M. and S. Singh, *Rapid Microwave-Assisted Cisplatin-Loaded Solid Lipid Nanoparticles: Synthesis, Characterization and Anticancer Study.* Nanomaterials (Basel, Switzerland), 2020. **10**(3): p. 510.
88. Nunes, S., A.R. Madureira, D. Campos, B. Sarmento, A.M. Gomes, M. Pintado, and F. Reis, *Solid lipid nanoparticles as oral delivery systems of phenolic compounds: overcoming pharmacokinetic limitations for nutraceutical applications.* Critical reviews in food science and nutrition, 2017. **57**(9): p. 1863-73.
89. Courant, T., E. Bayon, H.L. Reynaud-Dougier, C. Villiers, M. Menneteau, P.N. Marche, and F.P. Navarro, *Tailoring nanostructured lipid carriers for the delivery of protein antigens: Physicochemical properties versus immunogenicity studies.* Biomaterials, 2017. **136**: p. 29-42.
90. Angelova, A., V.M. Garamus, B. Angelov, Z. Tian, Y. Li, and A. Zou, *Advances in structural design of lipid-based nanoparticle carriers for delivery of macromolecular drugs, phytochemicals and anti-tumor agents.* Advances in colloid and interface science, 2017. **249**: p. 331-45.
91. Wang, H., S. Liu, L. Jia, F. Chu, Y. Zhou, Z. He, M. Guo, C. Chen, and L. Xu, *Nanostructured lipid carriers for MicroRNA delivery in tumor gene therapy.* Cancer Cell International, 2018. **18**(1): p. 1-6.
92. Suñé-Pou, M., S. Prieto-Sánchez, Y. El Yousfi, S. Boyero-Corral, A. Nardi-Ricart, I. Nofrerias-Roig, P. Pérez-Lozano, E. García-Montoya, M. Miñarro-Carmona, and J.R. Ticó, *Cholesteryl oleate-loaded cationic solid lipid nanoparticles as carriers for efficient gene-silencing therapy.* International journal of nanomedicine, 2018. **13**: p. 3223.
93. Nasirizadeh, S. and B. Malaekeh-Nikouei, *Solid lipid nanoparticles and nanostructured lipid carriers in oral cancer drug delivery.* Journal of Drug Delivery Science and Technology, 2020. **55**: p. 101458.
94. Passos, J.S., L.C. de Martino, V.F.C. Dartora, G.L. de Araujo, K. Ishida, and L.B. Lopes, *Development, skin targeting and antifungal efficacy of topical lipid nanoparticles containing itraconazole.* European Journal of Pharmaceutical Sciences, 2020. **149**: p. 105296.
95. Zhao, Y., Y.-X. Chang, X. Hu, C.-Y. Liu, L.-H. Quan, and Y.-H. Liao, *Solid lipid nanoparticles for sustained pulmonary delivery of Yuxingcao essential oil: Preparation, characterization and in vivo evaluation.* International journal of pharmaceutics, 2017. **516**(1-2): p. 364-71.
96. Rudhrabatla, V., B. Sudhakar, and K. Reddy, *In vitro and in vivo assessment of designed melphalan loaded stealth solid lipid nanoparticles for parenteral delivery.* Bionanoscience, 2020. **10**(1): p. 168-90.
97. Zhang, Q., J. Zhao, H. Hu, Y. Yan, X. Hu, K. Zhou, S. Xiao, Y. Zhang, and N. Feng, *Construction and in vitro and in vivo evaluation of folic acid-modified nanostructured lipid carriers loaded with paclitaxel and chlorin e6.* International Journal of Pharmaceutics, 2019. **569**: p. 118595.
98. Paliwal, R., S.R. Paliwal, R. Kenwat, B.D. Kurmi, and M.K. Sahu, *Solid lipid nanoparticles: A review on recent perspectives and patents.* Expert opinion on therapeutic patents, 2020. **30**(3): p. 179-94.
99. Rosenblum, D., N. Joshi, W. Tao, J.M. Karp, and D. Peer, *Progress and challenges towards targeted delivery of cancer therapeutics.* Nature communications, 2018. **9**(1): p. 1-12.

100. Varshosaz, J., M.A. Davoudi, and S. Rasoul-Amini, *Docetaxel-loaded nanostructured lipid carriers functionalized with trastuzumab (Herceptin) for HER2-positive breast cancer cells.* Journal of liposome research, 2018. **28**(4): p. 285-95.
101. Sun, S., E. Shang, A. Ju, Y. Li, Q. Wu, Q. Li, Y. Yang, Y. Guo, D. Yang, and S. Lv, *Tumor-targeted hyaluronic acid-mPEG modified nanostructured lipid carriers for cantharidin delivery: An in vivo and in vitro study.* Fitoterapia, 2021: p. 105033.
102. Cavaco, M.C., C. Pereira, B. Kreutzer, L.F. Gouveia, B. Silva-Lima, A.M. Brito, and M. Videira, *Evading P-glycoprotein mediated-efflux chemoresistance using Solid Lipid Nanoparticles.* Eur J Pharm Biopharm, 2017. **110**: p. 76-84.
103. Ramasamy, T., P. Sundaramoorthy, H.B. Ruttala, Y. Choi, W.H. Shin, J.H. Jeong, S.K. Ku, H.G. Choi, H.M. Kim, C.S. Yong, et al., *Polyunsaturated fatty acid-based targeted nanotherapeutics to enhance the therapeutic efficacy of docetaxel.* Drug Deliv, 2017. **24**(1): p. 1262-72.
104. Kebebe, D., Y. Wu, B. Zhang, J. Yang, Y. Liu, X. Li, Z. Ma, P. Lu, Z. Liu, and J. Li, *Dimeric c(RGD) peptide conjugated nanostructured lipid carriers for efficient delivery of Gambogic acid to breast cancer.* International journal of nanomedicine, 2019. **14**: p. 6179-95.
105. Hajipour, H., H. Hamishehkar, S. Nazari Soltan Ahmad, S. Barghi, N.F. Maroufi, and R.A. Taheri, *Improved anticancer effects of epigallocatechin gallate using RGD-containing nanostructured lipid carriers.* Artif Cells Nanomed Biotechnol, 2018. **46**(sup1): p. 283-92.
106. Li, X., X. Jia, and H. Niu, *Nanostructured lipid carriers co-delivering lapachone and doxorubicin for overcoming multidrug resistance in breast cancer therapy.* Int J Nanomedicine, 2018. **13**: p. 4107-19.
107. Zheng, S., V.D. Nguyen, S.Y. Song, J. Han, and J.O. Park, *Combined photothermal-chemotherapy of breast cancer by near infrared light responsive hyaluronic acid-decorated nanostructured lipid carriers.* Nanotechnology, 2017. **28**(43): p. 435102.
108. Grodzinski, P., M. Kircher, M. Goldberg, and A. Gabizon, *Integrating nanotechnology into cancer care*. 2019, ACS Publications.
109. Heldin, C.-H., K. Rubin, K. Pietras, and A. Östman, *High interstitial fluid pressure—an obstacle in cancer therapy.* Nature Reviews Cancer, 2004. **4**(10): p. 806-13.
110. Gao, X., J. Zhang, Z. Huang, T. Zuo, Q. Lu, G. Wu, and Q. Shen, *Reducing interstitial fluid pressure and inhibiting pulmonary metastasis of breast cancer by gelatin modified cationic lipid nanoparticles.* ACS applied materials & interfaces, 2017. **9**(35): p. 29457-68.
111. Ahmad, A., F. Khan, R.K. Mishra, and R. Khan, *Precision cancer nanotherapy: evolving role of multifunctional nanoparticles for cancer active targeting.* Journal of medicinal chemistry, 2019. **62**(23): p. 10475-96.
112. Siddhartha, V.T., S.K.S. Pindiprolu, P.K. Chintamaneni, S. Tummala, and S. Nandha Kumar, *RAGE receptor targeted bioconjuguate lipid nanoparticles of diallyl disulfide for improved apoptotic activity in triple negative breast cancer: in vitro studies.* Artificial cells, nanomedicine, and biotechnology, 2018. **46**(2): p. 387-97.
113. Pindiprolu, S.K.S.S., P.T. Krishnamurthy, C. Dev, and P.K. Chintamaneni, *DR5 antibody conjugated lipid-based nanocarriers of gamma-secretase inhibitor for the treatment of triple negative breast cancer.* Chemistry and Physics of Lipids, 2021. **235**: p. 105033.
114. Yoo, J., C. Park, G. Yi, D. Lee, and H. Koo, *Active targeting strategies using biological ligands for nanoparticle drug delivery systems.* Cancers, 2019. **11**(5): p. 640.
115. Tiwari, S. and P. Bahadur, *Modified hyaluronic acid based materials for biomedical applications.* International journal of biological macromolecules, 2019. **121**: p. 556-71.
116. Xu, H., M. Niu, X. Yuan, K. Wu, and A. Liu, *CD44 as a tumor biomarker and therapeutic target.* Exp Hematol Oncol, 2020. **9**(1): p. 36.
117. Chen, C., S. Zhao, A. Karnad, and J.W. Freeman, *The biology and role of CD44 in cancer progression: therapeutic implications.* Journal of hematology & oncology, 2018. **11**(1): p. 1-23.
118. Sargazi, A., N. Kamali, F. Shiri, and M. Heidari Majd, *Hyaluronic acid/polyethylene glycol nanoparticles for controlled delivery of mitoxantrone.* Artificial cells, nanomedicine, and biotechnology, 2018. **46**(3): p. 500-09.
119. Laurent, T.C. and J.R. Fraser, *Hyaluronan.* Faseb j, 1992. **6**(7): p. 2397-404
120. Stern, R., *Hyaluronidases in cancer biology.* Hyaluronan in Cancer Biology, 2008: p. 207-20.
121. Marinho, A., C. Nunes, and S. Reis, *Hyaluronic Acid: A Key Ingredient in the Therapy of Inflammation.* Biomolecules, 2021. **11**(10): p. 1518.

122. Jordan, A.R., R.R. Racine, M.J. Hennig, and V.B. Lokeshwar, *The role of CD44 in disease pathophysiology and targeted treatment.* Frontiers in immunology, 2015. **6**: p. 182.
123. Tavianatou, A.G., Z. Piperigkou, C. Barbera, R. Beninatto, V. Masola, I. Caon, M. Onisto, M. Franchi, D. Galesso, and N.K. Karamanos, *Molecular size-dependent specificity of hyaluronan on functional properties, morphology and matrix composition of mammary cancer cells.* Matrix Biol Plus, 2019. **3**: p. 100008.
124. Wang, F., L. Li, B. Liu, Z. Chen, and C. Li, *Hyaluronic acid decorated pluronic P85 solid lipid nanoparticles as a potential carrier to overcome multidrug resistance in cervical and breast cancer.* Biomed Pharmacother, 2017. **86**: p. 595-604.
125. Lages, E.B., R.S. Fernandes, J.O. Silva, M. de Souza Â, G.D. Cassali, A.L.B. de Barros, and L.A. Miranda Ferreira, *Co-delivery of doxorubicin, docosahexaenoic acid, and α-tocopherol succinate by nanostructured lipid carriers has a synergistic effect to enhance antitumor activity and reduce toxicity.* Biomed Pharmacother, 2020. **132**: p. 110876.
126. Yu, D., W. Li, Y. Zhang, and B. Zhang, *Anti-tumor efficiency of paclitaxel and DNA when co-delivered by pH responsive ligand modified nanocarriers for breast cancer treatment.* Biomedicine & Pharmacotherapy, 2016. **83**: p. 1428-35.
127. Gao, X., J. Zhang, Q. Xu, Z. Huang, Y. Wang, and Q. Shen, *Hyaluronic acid-coated cationic nanostructured lipid carriers for oral vincristine sulfate delivery.* Drug development and industrial pharmacy, 2017. **43**(4): p. 661-67.
128. Zwicke, G.L., G.A. Mansoori, and C.J. Jeffery, *Utilizing the folate receptor for active targeting of cancer nanotherapeutics.* Nano Reviews & Experiments, 2012. **3**.
129. Kue, C.S., A. Kamkaew, K. Burgess, L.V. Kiew, L.Y. Chung, and H.B. Lee, *Small molecules for active targeting in cancer.* Medicinal research reviews, 2016. **36**(3): p. 494-575.
130. Sudimack, J. and R.J. Lee, *Targeted drug delivery via the folate receptor.* Advanced drug delivery reviews, 2000. **41**(2): p. 147-62.
131. Assaraf, Y.G., C.P. Leamon, and J.A. Reddy, *The folate receptor as a rational therapeutic target for personalized cancer treatment.* Drug Resistance Updates, 2014. **17**(4-6): p. 89-95.
132. Baek, J.-S. and C.-W. Cho, *A multifunctional lipid nanoparticle for co-delivery of paclitaxel and curcumin for targeted delivery and enhanced cytotoxicity in multidrug resistant breast cancer cells.* Oncotarget, 2017. **8**(18): p. 30369-82.
133. Moraes, S., A. Marinho, S. Lima, A. Granja, J. Araújo, S. Reis, C. Sousa, and C. Nunes, *Targeted nanostructured lipid carriers for doxorubicin oral delivery.* International Journal of Pharmaceutics, 2021. **592**: p. 120029.
134. Ma, Z., J. Pi, Y. Zhang, H. Qin, B. Zhang, N. Li, Z. Li, and Z. Liu, *Enhanced Anticancer Efficacy of Dual Drug-Loaded Self-Assembled Nanostructured Lipid Carriers Mediated by pH-Responsive Folic Acid and Human-Derived Cell Penetrating Peptide dNP2.* Pharmaceutics, 2021. **13**(5).
135. Shan, D., J. Li, P. Cai, P. Prasad, F. Liu, A.M. Rauth, and X.Y. Wu, *RGD-conjugated solid lipid nanoparticles inhibit adhesion and invasion of α v β 3 integrin-overexpressing breast cancer cells.* Drug delivery and translational research, 2015. **5**(1): p. 15-26.
136. Ji, X., Y. Lu, H. Tian, X. Meng, M. Wei, and W.C. Cho, *Chemoresistance mechanisms of breast cancer and their countermeasures.* Biomedicine & Pharmacotherapy, 2019. **114**: p. 108800.
137. Yamagata, T., H. Kusuhara, M. Morishita, K. Takayama, H. Benameur, and Y. Sugiyama, *Effect of excipients on breast cancer resistance protein substrate uptake activity.* Journal of controlled release, 2007. **124**(1-2): p. 1-5.
138. Xu, W., E.J. Bae, and M.-K. Lee, *Enhanced anticancer activity and intracellular uptake of paclitaxel-containing solid lipid nanoparticles in multidrug-resistant breast cancer cells.* International journal of nanomedicine, 2018. **13**: p. 7549-63.
139. Guney Eskiler, G., G. Cecener, U. Egeli, and B. Tunca, *Talazoparib nanoparticles for overcoming multidrug resistance in triple‐negative breast cancer.* Journal of cellular physiology, 2020. **235**(9): p. 6230-45.
140. Xu, P., Q. Yin, J. Shen, L. Chen, H. Yu, Z. Zhang, and Y. Li, *Synergistic inhibition of breast cancer metastasis by silibinin-loaded lipid nanoparticles containing TPGS.* International journal of pharmaceutics, 2013. **454**(1): p. 21-30.
141. Lu, B., S.-B. Xiong, H. Yang, X.-D. Yin, and R.-B. Chao, *Solid lipid nanoparticles of mitoxantrone for local injection against breast cancer and its lymph node metastases.* European journal of pharmaceutical sciences, 2006. **28**(1-2): p. 86-95.

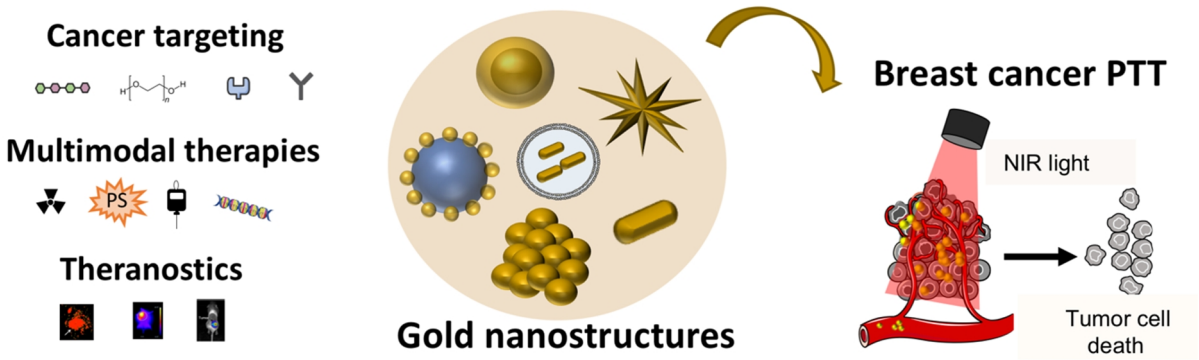
142. Shete, H.K., N. Selkar, G.R. Vanage, and V.B. Patravale, *Tamoxifen nanostructured lipid carriers: enhanced in vivo antitumor efficacy with reduced adverse drug effects.* International journal of pharmaceutics, 2014. **468**(1-2): p. 1-14.
143. Xiao, W., S. Zheng, P. Liu, Y. Zou, X. Xie, P. Yu, H. Tang, and X. Xie, *Risk factors and survival outcomes in patients with breast cancer and lung metastasis: a population-based study.* Cancer medicine, 2018. **7**(3): p. 922-30
144. Jin, L., B. Han, E. Siegel, Y. Cui, A. Giuliano, and X. Cui, *Breast cancer lung metastasis: Molecular biology and therapeutic implications.* Cancer biology & therapy, 2018. **19**(10): p. 858-68.
145. da Rocha, M.C.O., P.B. da Silva, M.A. Radicchi, B.Y.G. Andrade, J.V. de Oliveira, T. Venus, C. Merker, I. Estrela-Lopis, J.P.F. Longo, and S.N. Báo, *Docetaxel-loaded solid lipid nanoparticles prevent tumor growth and lung metastasis of 4T1 murine mammary carcinoma cells.* Journal of nanobiotechnology, 2020. **18**(1): p. 1-20.
146. Nordin, N., S.K. Yeap, H.S. Rahman, N.R. Zamberi, N.E. Mohamad, N. Abu, M.J. Masarudin, R. Abdullah, and N.B. Alitheen, *Antitumor and Anti-Metastatic Effects of Citral-Loaded Nanostructured Lipid Carrier in 4T1-Induced Breast Cancer Mouse Model.* Molecules (Basel, Switzerland), 2020. **25**(11): p. 2670.
147. Rostami, R., S. Mittal, P. Rostami, F. Tavassoli, and B. Jabbari, *Brain metastasis in breast cancer: a comprehensive literature review.* Journal of neuro-oncology, 2016. **127**(3): p. 407-14.
148. Patel, M., E.B. Souto, and K.K. Singh, *Advances in brain drug targeting and delivery: limitations and challenges of solid lipid nanoparticles.* Expert opinion on drug delivery, 2013. **10**(7): p. 889-905.
149. Azhari, H., M. Strauss, S. Hook, B.J. Boyd, and S.B. Rizwan, *Stabilising cubosomes with Tween 80 as a step towards targeting lipid nanocarriers to the blood–brain barrier.* European Journal of Pharmaceutics and Biopharmaceutics, 2016. **104**: p. 148-55.
150. de Mendoza, A.E.-H., V. Préat, F. Mollinedo, and M.J. Blanco-Prieto, *In vitro and in vivo efficacy of edelfosine-loaded lipid nanoparticles against glioma.* Journal of controlled release, 2011. **156**(3): p. 421-26.
151. Zhang, T., H. Lip, C. He, P. Cai, Z. Wang, J.T. Henderson, A.M. Rauth, and X.Y. Wu, *Multitargeted Nanoparticles Deliver Synergistic Drugs across the Blood-Brain Barrier to Brain Metastases of Triple Negative Breast Cancer Cells and Tumor-Associated Macrophages.* Adv Healthc Mater, 2019. **8**(18): p. e1900543.
152. Kwiatkowski, S., B. Knap, D. Przystupski, J. Saczko, E. Kędzierska, K. Knap-Czop, J. Kotlińska, O. Michel, K. Kotowski, and J. Kulbacka, *Photodynamic therapy–mechanisms, photosensitizers and combinations.* Biomedicine & Pharmacotherapy, 2018. **106**: p. 1098-107.
153. Rkein, A.M. and D.M. Ozog, *Photodynamic therapy.* Dermatologic clinics, 2014. **32**(3): p. 415-25.
154. Aniogo, E.C., B. Plackal Adimuriyil George, and H. Abrahamse, *The role of photodynamic therapy on multidrug resistant breast cancer.* Cancer cell international, 2019. **19**: p. 91-91.
155. Medina, M.A., G. Oza, A. Sharma, L.G. Arriaga, J.M. Hernández Hernández, V.M. Rotello, and J.T. Ramirez, *Triple-Negative Breast Cancer: A Review of Conventional and Advanced Therapeutic Strategies.* International journal of environmental research and public health, 2020. **17**(6): p. 2078.
156. Navarro, F.P., G. Creusat, C. Frochot, A. Moussaron, M. Verhille, R. Vanderesse, J.-S. Thomann, P. Boisseau, I. Texier, and A.-C. Couffin, *Preparation and characterization of mTHPC-loaded solid lipid nanoparticles for photodynamic therapy.* Journal of Photochemistry and Photobiology B: Biology, 2014. **130**: p. 161-69.
157. Brezaniova, I., M. Hruby, J. Kralova, V. Kral, Z. Cernochova, P. Cernoch, M. Slouf, J. Kredatusova, and P. Stepanek, *Temoporfin-loaded 1-tetradecanol-based thermoresponsive solid lipid nanoparticles for photodynamic therapy.* Journal of Controlled Release, 2016. **241**: p. 34-44.
158. Kamel, A.E., M. Fadel, and D. Louis, *Curcumin-loaded nanostructured lipid carriers prepared using Peceol™ and olive oil in photodynamic therapy: development and application in breast cancer cell line.* Int J Nanomedicine, 2019. **14**: p. 5073-85.
159. Oshiro-Junior, J.A., M.R. Sato, F.I. Boni, K.L.M. Santos, K.T. de Oliveira, L.M. de Freitas, C.R. Fontana, D. Nicholas, A. McHale, J.F. Callan, et al., *Phthalocyanine-loaded nanostructured lipid carriers functionalized with folic acid for photodynamic therapy.* Materials Science and Engineering: C, 2020. **108**: p. 110462.

160. Granja, A., M. Pinheiro, C.T. Sousa, and S. Reis, *Gold nanostructures as mediators of hyperthermia therapies in breast cancer.* Biochemical Pharmacology, 2021: p. 114639.
161. Li, H., K. Wang, X. Yang, Y. Zhou, Q. Ping, D. Oupicky, and M. Sun, *Dual-function nanostructured lipid carriers to deliver IR780 for breast cancer treatment: Anti-metastatic and photothermal anti-tumor therapy.* Acta Biomater, 2017. **53**: p. 399-413.
162. Dutz, S. and R. Hergt, *Magnetic particle hyperthermia—a promising tumour therapy?* Nanotechnology, 2014. **25**(45): p. 452001.
163. Chang, D., M. Lim, J.A.C.M. Goos, R. Qiao, Y.Y. Ng, F.M. Mansfeld, M. Jackson, T.P. Davis, and M. Kavallaris, *Biologically Targeted Magnetic Hyperthermia: Potential and Limitations.* Frontiers in pharmacology, 2018. **9**: p. 831-31.
164. Sharma, S., N. Shrivastava, F. Rossi, and N.T.K. Thanh, *Nanoparticles-based magnetic and photo induced hyperthermia for cancer treatment.* Nano Today, 2019: p. 100795.
165. Cazares-Cortes, E., S. Cabana, C. Boitard, E. Nehlig, N. Griffete, J. Fresnais, C. Wilhelm, A. Abou-Hassan, and C. Ménager, *Recent insights in magnetic hyperthermia: From the "hot-spot" effect for local delivery to combined magneto-photo-thermia using magneto-plasmonic hybrids.* Advanced Drug Delivery Reviews, 2019. **138**: p. 233-46.
166. Ong, Y.S., M. Bañobre-López, S.A.C. Lima, and S. Reis, *A multifunctional nanomedicine platform for co-delivery of methotrexate and mild hyperthermia towards breast cancer therapy.* Materials Science and Engineering: C, 2020. **116**: p. 111255.
167. Siafaka, P.I., N. Üstündağ Okur, E. Karavas, and D.N. Bikiaris, *Surface modified multifunctional and stimuli responsive nanoparticles for drug targeting: current status and uses.* International journal of molecular sciences, 2016. **17**(9): p. 1440.
168. Rehman, M., A. Ihsan, A. Madni, S.Z. Bajwa, D. Shi, T.J. Webster, and W.S. Khan, *Solid lipid nanoparticles for thermoresponsive targeting: evidence from spectrophotometry, electrochemical, and cytotoxicity studies.* Int J Nanomedicine, 2017. **12**: p. 8325-36.
169. Zheng, G., M. Zheng, B. Yang, H. Fu, and Y. Li, *Improving breast cancer therapy using doxorubicin loaded solid lipid nanoparticles: Synthesis of a novel arginine-glycine-aspartic tripeptide conjugated, pH sensitive lipid and evaluation of the nanomedicine in vitro and in vivo.* Biomedicine & Pharmacotherapy, 2019. **116**: p. 109006.
170. Mohammadpour, Z. and K. Majidzadeh-A, *Applications of two-dimensional nanomaterials in breast cancer theranostics.* ACS Biomaterials Science & Engineering, 2020. **6**(4): p. 1852-73.
171. Huang, Y., K. Mao, B. Zhang, and Y. Zhao, *Superparamagnetic iron oxide nanoparticles conjugated with folic acid for dual target-specific drug delivery and MRI in cancer theranostics.* Materials Science and Engineering: C, 2017. **70**: p. 763-71.
172. Guo, J., K. Rahme, Y. He, L.-L. Li, J.D. Holmes, and C.M. O'Driscoll, *Gold nanoparticles enlighten the future of cancer theranostics.* International journal of nanomedicine, 2017. **12**: p. 6131.
173. Olerile, L.D., *Further Development of Near-Infrared Mediated Quantum Dots and Paclitaxel Co-loaded Nanostructured Lipid Carrier System for Cancer Theragnostic.* Technology in cancer research & treatment, 2020. **19**: p. 1533033820914308-08.
174. Ahmadifard, Z., A. Ahmeda, M. Rasekhian, S. Moradi, and E. Arkan, *Chitosan-coated magnetic solid lipid nanoparticles for controlled release of letrozole.* Journal of Drug Delivery Science and Technology, 2020. **57**: p. 101621.
175. Fan, W., B. Yung, P. Huang, and X. Chen, *Nanotechnology for multimodal synergistic cancer therapy.* Chemical reviews, 2017. **117**(22): p. 13566-638.
176. Mahoutforoush, A., A. Solouk, H. Hamishehkar, M. Haghbin Nazarpak, and S. Abbaspour-Ravasjani, *Novel decorated nanostructured lipid carrier for simultaneous active targeting of three anti-cancer agents.* Life Sci, 2021. **279**: p. 119576.
177. Tran, B.N., H.T. Nguyen, J.O. Kim, C.S. Yong, and C.N. Nguyen, *Combination of a chemopreventive agent and paclitaxel in CD44-targeted hybrid nanoparticles for breast cancer treatment.* Arch Pharm Res, 2017. **40**(12): p. 1420-32.
178. Borges, G.S.M., J.d.O. Silva, R.S. Fernandes, Â.M. de Souza, G.D. Cassali, M.I. Yoshida, E.A. Leite, A.L.B. de Barros, and L.A.M. Ferreira, *Sclareol is a potent enhancer of doxorubicin: Evaluation of the free combination and co-loaded nanostructured lipid carriers against breast cancer.* Life Sciences, 2019. **232**: p. 116678.
179. Teo, P.Y., W. Cheng, J.L. Hedrick, and Y.Y. Yang, *Co-delivery of drugs and plasmid DNA for cancer therapy.* Advanced Drug Delivery Reviews, 2016. **98**: p. 41-63.
180. Lin, T., L. Zhang, J. Davis, J. Gu, M. Nishizaki, L. Ji, J.A. Roth, M. Xiong, and B. Fang, *Combination of TRAIL gene therapy and chemotherapy enhances antitumor and*

*antimetastasis effects in chemosensitive and chemoresistant breast cancers.* Molecular Therapy, 2003. **8**(3): p. 441-48.
181. Tang, T., Y. Cheng, Q. She, Y. Jiang, Y. Chen, W. Yang, and Y. Li, *Long non-coding RNA TUG1 sponges miR-197 to enhance cisplatin sensitivity in triple negative breast cancer.* Biomedicine & Pharmacotherapy, 2018. **107**: p. 338-46.
182. Chen, J., M. Zhu, L. Zou, J. Xia, J. Huang, Q. Deng, and R. Xu, *Long non-coding RNA LINC-PINT attenuates paclitaxel resistance in triple-negative breast cancer cells via targeting the RNA-binding protein NONO.* Acta Biochimica et Biophysica Sinica, 2020. **52**(8): p. 801-09.
183. Kim, H.R., I.K. Kim, K.H. Bae, S.H. Lee, Y. Lee, and T.G. Park, *Cationic solid lipid nanoparticles reconstituted from low density lipoprotein components for delivery of siRNA.* Molecular pharmaceutics, 2008. **5**(4): p. 622-31.
184. Liu, J., T. Meng, M. Yuan, L. Wen, B. Cheng, N. Liu, X. Huang, Y. Hong, H. Yuan, and F. Hu, *MicroRNA-200c delivered by solid lipid nanoparticles enhances the effect of paclitaxel on breast cancer stem cell.* Int J Nanomedicine, 2016. **11**: p. 6713-25.
185. Singh, A., Y.R. Neupane, B. Mangla, and K. Kohli, *Nanostructured Lipid Carriers for Oral Bioavailability Enhancement of Exemestane: Formulation Design, In Vitro, Ex Vivo, and In Vivo Studies.* J Pharm Sci, 2019. **108**(10): p. 3382-95.
186. Dhaundiyal, A., S.K. Jena, S.K. Samal, B. Sonvane, M. Chand, and A.T. Sangamwar, *Alpha-lipoic acid-stearylamine conjugate-based solid lipid nanoparticles for tamoxifen delivery: formulation, optimization, in-vivo pharmacokinetic and hepatotoxicity study.* J Pharm Pharmacol, 2016. **68**(12): p. 1535-50.
187. Qureshi, O.S., H.S. Kim, A. Zeb, J.S. Choi, H.S. Kim, J.E. Kwon, M.S. Kim, J.H. Kang, C. Ryou, J.S. Park, et al., *Sustained release docetaxel-incorporated lipid nanoparticles with improved pharmacokinetics for oral and parenteral administration.* J Microencapsul, 2017. **34**(3): p. 250-61.
188. Baek, J.-S. and C.-W. Cho, *Surface modification of solid lipid nanoparticles for oral delivery of curcumin: Improvement of bioavailability through enhanced cellular uptake, and lymphatic uptake.* European Journal of Pharmaceutics and Biopharmaceutics, 2017. **117**: p. 132-40.
189. Gadag, S., R. Narayan, A.S. Nayak, D.C. Ardila, S. Sant, Y. Nayak, S. Garg, and U.Y. Nayak, *Development and preclinical evaluation of microneedle-assisted resveratrol loaded nanostructured lipid carriers for localized delivery to breast cancer therapy.* International Journal of Pharmaceutics, 2021. **606**: p. 120877.

## 2.2. Gold nanostructures as mediators of hyperthermia therapies in breast cancer

In this sub-chapter, the molecular and clinical basis of hyperthermia in the context of cancer therapy are described along with the current limitations of this therapeutic. The potential of nanotechnology in improving the efficacy and specificity of hyperthermia towards cancer cells is discussed, focusing on a particular type of nanoparticle-mediated hyperthermia, photothermal therapy (PTT). In addition, the valuable characteristics of gold nanostructures as effective promoters of PTT are outlined and the most recent strategies using gold nanostructures for the PTT of breast cancer therapy are critically reviewed. This review paper was published in Biochemical Pharmacology (Elsevier 2021).



Biochemical Pharmacology 190 (2021) 114639

Contents lists available at ScienceDirect

Biochemical Pharmacology

journal homepage: www.elsevier.com/locate/biochempharm

Review

# Gold nanostructures as mediators of hyperthermia therapies in breast cancer

Andreia Granja [a], Marina Pinheiro [a], Célia T. Sousa [b], Salette Reis [a,*]

[a] LAQV, REQUIMTE, Departamento de Ciências Químicas, Faculdade de Farmácia, Universidade do Porto, Rua Jorge de Viterbo Ferreira 228, 4050-313 Porto, Portugal
[b] IFIMUP and Dep. Física e Astronomia, Faculdade de Ciências, Universidade do Porto, Rua Campo Alegre 687, 4169 – 007 Porto, Portugal

ARTICLE INFO

*Keywords:*
Photothermal therapy
Nanotechnology
Gold nanoparticles
Multimodal therapy
NIR laser
Breast cancer

ABSTRACT

Breast cancer is the leading cause of cancer-related deaths among women. Due to the limitations of the current therapeutics, new treatment options are needed. Hyperthermia is a promising approach to improve breast cancer therapy, particularly when combined with chemo and radiotherapy. This area has gained more attention following association with nanotechnology, with the emergence of modalities, such as photothermal therapy (PTT). PTT is a simple, minimally invasive technique that requires a near infrared (NIR) light source and a PTT agent. Gold nanostructures are excellent PTT agents as they offer biocompatibility, versatility, high photothermal conversion efficiency, imaging contrast and an easily-modified surface. In this review, we describe the molecular basis and the current clinical aspects of hyperthermia-based therapies. The emergent area of nanoparticle-induced hyperthermia will be explored, in particular gold nanostructure-mediated PTT, focusing on recent preclinical studies for breast cancer management.

## 1. Introduction

Breast cancer is the most common cancer type and the leading cause of cancer-related deaths among women [1]. In 2018, more than 2 million cases were diagnosed and nearly 627,000 deaths occurred worldwide [1]. This disease comprises at least 21 histologic subtypes classified based on cancer cell morphology and architecture and 4 molecular subtypes according to the expression of specific biological markers, such as estrogen and progesterone receptors (ER and PR) and human epidermal growth factor receptor 2 (HER2) [2,3]. The molecular classification has been determinant for the design of customized therapies, with each subtype associated with distinct risk factors for incidence, treatment responses and clinical outcomes [3]. ER and/or PR-positive HER2-negative is the most common subtype of invasive breast cancer (50% to 65% of all breast tumors) and generally responds well to hormonal therapies [4,5]. HER2-positive account for 20% of all breast cancers and due to the overexpression of HER2, can benefit from the anti-HER2 therapies currently available [4,5]. Tumors lacking hormone receptors and HER2 are known as triple negative breast cancers (TNBC) [4,5]. This subtype accounts for 15% of all breast cancers and is associated with lower prognosis since it cannot benefit from any molecular-based targeted therapy [3]. In addition, these tumors have a high rate of recurrence and only 20% of them respond well to chemotherapy, being one of the most challenging breast cancer subtypes in clinics [5,6].

The survival rates of breast cancer patients vary considerably not only by the stage but also by the molecular subtype of the disease [7–10]. Overall ER and/or PR–positive tumors are associated with the highest survival rates, followed by HER2-positive tumors and, finally, TNBC [7,9,10]. According to the most recent report of the American Cancer Society on breast cancer, the 5-year cancer survival rates in USA patients diagnosed with breast cancer was 92% for ER and/or PR positive-HER2 negative tumors, 89% for ER and/or PR positive-HER2 positive tumors, 83% for HER2-positive tumors, and, finally, 77% for TNBC tumors [11]. The overall 5-year survival rate is also greatly dependent on the stage of the disease, ranging from 98% for stage I to 27% for stage IV [11].

*Abbreviations:* ALA, 5-aminolevulinic acid; AuNPs, gold nanoparticles; CIK, Cytokine-induced killer; DCs, dendritic cells; EE, encapsulation efficiency; EGFR, epidermal growth factor receptor; ER, estrogen receptor; HER2, human epidermal growth factor receptor 2; HGNPs, hollow gold nanoparticles; HSP, heat shock proteins; ICG, indocyanine green; LC, loading capacity; MRI, Magnetic resonance imaging; MSCs, mesenchymal stem cells; NIR, near infrared; NK, natural killer; PA, photoacoustic imaging; PDT, photodynamic therapy; PEG, Poly(ethylene glycol); PET, positron emission tomography; PR, progesterone receptor; PTT, photothermal therapy; ROS, reactive oxygen species; SPR, surface plasmon resonance; TNBC, triple negative breast cancer; ZP, zeta potential.

* Corresponding author.
*E-mail address:* shreis@ff.up.pt (S. Reis).

https://doi.org/10.1016/j.bcp.2021.114639
Received 5 April 2021; Received in revised form 25 May 2021; Accepted 26 May 2021
Available online 30 May 2021
0006-2952/© 2021 Published by Elsevier Inc.

Conventional breast cancer therapies include local treatment (i.e. surgery and radiotherapy) and adjuvant systemic therapies (hormonal therapy, targeted therapy and chemotherapy) [12]. The choice of the adjuvant systemic therapies are based on the molecular subtype of the tumor, the menopausal status of the patient, the tumor size and the axillary nodal status [13]. Hormonal therapies are often used in patients with hormone receptor-positive tumors, either alone or combined with chemotherapy and include the selective estrogen-receptor modulator tamoxifen and aromatase inhibitors. Targeted therapies, such as trastuzumab (a humanized monoclonal antibody that specifically targets the HER2 protein [14]) are indicated for patients whose tumors overexpress the HER2 receptor [12]. This targeted therapy is often administered in combination with chemotherapy regimens increasing substantially its clinical outcomes [3,13]. Another targeted therapy currently used is lapatinib, a HER2 tyrosine kinase inhibitor [13]. Chemotherapy can be administered to patients prior or after surgery and in combination with other adjuvant therapies, such as hormonal and/or targeted therapies [13]. Anthracyclines (*e.g.* doxorubicin) and taxanes (*e.g.* paclitaxel) are two of the most common types of drugs used in chemotherapy regimens [15]. Most of these therapies, however, have major limitations related to their limited cancer cell-specificity [15]. This strongly compromises the therapeutic efficacy of the drugs and causes several adverse side-effects, such as nausea, myalgia, alopecia, ovarian failure, nephrotoxicity, cardiotoxicity, myelosuppression, neurotoxictiy and an overall decrease in the quality of life of the patient [13,15–17]. In addition, several patients develop drug resistance, which favors metastasis and disease recurrence [18]. Other potentially lethal complications regarding specific drugs have also been reported. For instance, tamoxifen administration has been shown to increase the risk of endometrial cancer and induce ischemic cerebrovascular events and venous thromboembolic events [13,19,20]. Doxorubicin can directly damage the myocardium leading to cardiotoxicity which, eventually, may evolve into cardiomyopathy, an effect that can be further enhanced when combined with trastuzumab [17]. Paclitaxel formulations have resulted in neuropathic pain, nephrotoxicity and neurotoxicity, which was attributed to the effects of the drug and the excipient materials [15–17]. Due to these limitations, novel therapeutic alternatives have emerged, including gene therapy, photodynamic therapy (PDT), hyperthermia-based therapies and nanotechnology approaches [21–26].

Hyperthermia-based therapies are promising approaches to improve current breast cancer therapy, particularly when combined with chemo and radiotherapy [27–37]. This area has grown considerably since the emergence of nanoparticle-mediated hyperthermia, as in the case of photothermal therapy (PTT) [38–40]. PTT is a minimally invasive technique that relies on the use of near infrared (NIR) light and a PTT agent that can convert light energy into heat [38–40]. Tumor tissues are then heated and eradicated with great precision and minimal side-effects in the surrounding healthy tissues [38–40]. Gold nanostructures are particularly promising PTT agents due to their biocompatibility, versatility, high NIR absorption and light-to-heat conversion efficiency [38–40]. Additionally, they are also efficient imaging contrast agents contributing to the development of theranostics systems with simultaneous treatment and *in situ* tumor imaging [41].

The aim of this article is to provide a critical review of the most relevant research and current clinical aspects of hyperthermia-based therapies and their applications in breast cancer. The emergent area of nanoparticle-induced hyperthermia will be explored, in particular gold nanostructure-mediated PTT focusing on recent preclinical studies for breast cancer management.

## 2. Hyperthermia-based therapies

The word "hyperthermia" derives from the Greek words "*hyper*" and "*therme*" meaning "excessive" and "heat", respectively, and refers to the artificial induction of localized or systemic heat in the human body [42]. In a more restricted definition, hyperthermia can be regarded as a specific type of thermal therapy based on the elevation of temperature [43]. Thermal therapies can be classified into two major subtypes: hyperthermia (or moderate-temperature hyperthermia) and thermal ablation [44,45]. In hyperthermia, the temperature is raised a few degrees above physiological level (41 °C- 45 °C) usually during 15 to 60 min [43–45]. Thermal ablation is the use of extreme temperatures (above 45 °C) for direct damage or destruction of the tumor tissues [43,44]. A more detailed description of these two thermal therapies is given in the following sections.

### 2.1. Hyperthermia

A range of temperatures between 41 °C to 45 °C is known to trigger different mechanisms that elicit cancer cell death as depicted in Fig. 1.

At the cellular level, hyperthermia can promote the damage of several nuclear proteins leading to the inhibition of different processes related to DNA repair, such as non-homologous end joining, homologous recombination and base excision repair, increasing the number of DNA lesions [46,47]. It can also induce cellular and mitochondrial membrane permeability alterations, along with endoplasmic reticulum stress and mitochondrial dysfunction, which will promote accumulation of intracellular $Ca^{2+}$ and release of reactive oxygen species (ROS) culminating in caspase activation and cell apoptosis [46,48].

In the tumor microenvironment there are also several alterations promoted by hyperthermia. The particular characteristics of this region, such as leaky disorganized vasculature, hypoxia and low pH makes tumor cells more sensitive to heat [49,50]. In fact, a hyperthermia-induced selective cancer cell killing effect has been demonstrated *in vivo* [49,50]. This phenomenon, however, is highly dependent on the exposure time and the temperature achieved in the tumor area [49]. Additionally, hyperthermia promotes the increase of blood flow and perfusion in the tumor region, increasing accumulation of immune cells or even drugs or other therapeutic compounds [51–53]. Hyperthermia has also a significant contribute in the stimulation of the immune system [46,47,53,54]. The heat stimulus induces the release of immunogenic surface ligands, tumor antigens and molecules, such as heat shock proteins (HSP), leading to the activation of natural killer (NK) and dendritic cells (DCs) [46,47,53,54]. DCs will then present the tumor antigens to the cytotoxic $CD8^+$ T cells, leading to their activation and recruitment to the tumor environment [46,47,53,54]. It has also been shown that hyperthermia has a direct effect on the improvement of the activity of NK cells, DCs and $CD8^+$ T cells [53].

Although hyperthermia has demonstrated efficacy in the induction of cancer cell death through different mechanisms, many of them still under study, it is not viable nor efficient to used it alone but rather in combination with other clinical modalities [55]. In fact, hyperthermia is known to act synergistically with both radio and chemotherapy [46,50,56,57]. This enables the achievement of better anti-cancer effects using lower doses of each treatment.

Hyperthermia's complementary effect with X-ray radiation is well documented, being considered one of the most efficient radiation sensitizers [50,56,58]. The susceptibility of cancer cells to radiotherapy is highly dependent on their cell cycle phase, with S phase (synthesis) and G0 phase (quiescence) cells showing a higher resistance to treatment [50,56]. Hyperthermia is able to selectively kill cells in S-phase and G0 phase and inhibit the repair of single-strand breaks and chromosome aberrations caused by radiotherapy [49,50]. Regarding chemotherapy, it is well known that hyperthermia can intensify the effect of several drugs by increasing blood perfusion and oxygenation in the tumor region [51,52], leading to an augmented local concentration and cellular uptake of the drug [49]. Furthermore, hyperthermia inhibits the DNA repair mechanisms triggered by the DNA damage induced by some anti-cancer drugs [57]. This synergistic effect has been demonstrated with several chemotherapeutic drugs, such as alkylating agents, nitrosureas and platinum compounds [49,57,59]. An inhibition of the drug resistance was also observed for the drugs cisplatin, mitomycin C,

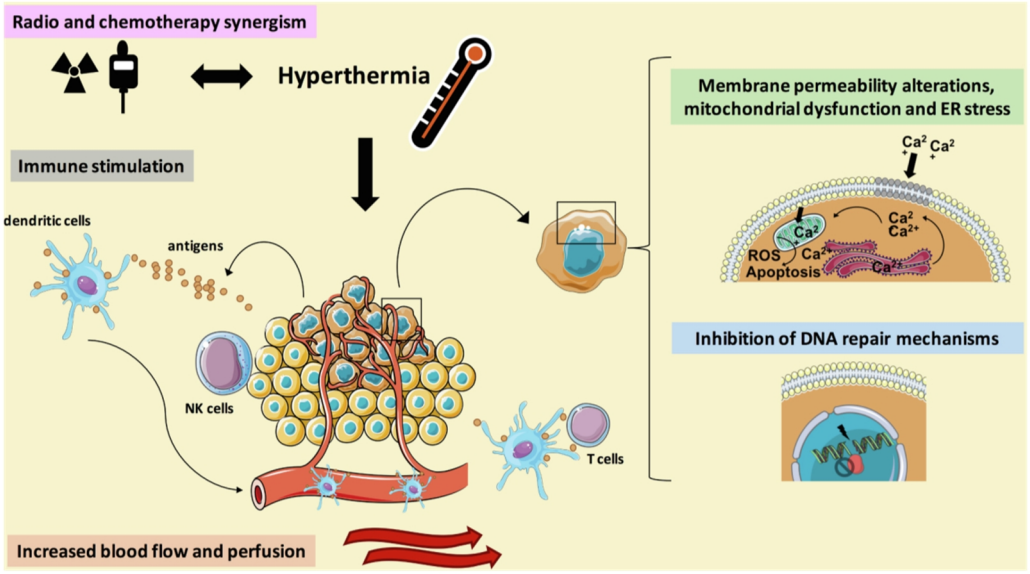



**Fig. 1.** Summary of the effects of hyperthermia at the cellular and tumor microenvironment levels. At the cellular level, hyperthermia can elicit cancer cell death through different mechanisms. Heat induces the denaturation of several nuclear proteins, impairing different mechanisms related to DNA repair. Additionally, hyperthermia compromises the mitochondrial membrane permeability and causes endoplasmic reticulum stress, leading to intracellular $Ca^{2+}$ accumulation and release of ROS, which will culminate in cell apoptosis. In the tumor microenvironment, hyperthermia can improve blood flow and perfusion enhancing the accumulation of drugs and other compounds or even immune cells in the tumor region. Heat can also directly stimulate the immune system and promote the release of immunogenic ligands and tumor antigens, leading to the activation of natural killer (NK) and dendritic cells (DCs) and, subsequently, to the activation and recruitment of cytotoxic $CD8^+$ T cells.

doxorubicin and mitoxantrone [49].

The modalities of hyperthermia currently in clinical settings can be classified into three major categories: whole body, regional and local hyperthermia. Whole body hyperthermia is employed in cases of metastatic disease with the aim of increasing chemotherapeutic drugs efficacy and stimulate the immune response. Regional hyperthermia is suitable for large areas of treatment, such as limbs or for advanced tumors located in deeper tissues [56]. Local hyperthermia is mostly used for solid lesions located superficially or near natural body cavities [56]. Heat can be applied using external methods, with a depth of only a few centimeters or other more invasive procedures, where specific probes are directly inserted into the tumor or in natural body cavities (interstitial and endocavity methods) [49,55,59]. Microwave, radiofrequency, or ultrasounds are the most common sources of energy used in this type of hyperthermia [49].

### 2.2. *Thermal ablation*

In thermal ablation, the tumor is destroyed by the action of extreme temperatures (above 45 °C) [44]. The ablated tissue can be divided into two distinct zones: the central zone, where the ablation tip directly contacts, and the peripheral zone, where the heat is conducted from the central zone, achieving moderate temperature hyperthermia [60,61]. In the central zone, irreversible cell damage occurs, including membrane collapse, protein denaturation and ceasing of the enzyme activity, which leads to tumor apoptosis and coagulative necrosis [60]. This effect is almost immediate for temperatures above 50 °C, while for lower temperatures, a higher exposure time is required [61]. In the peripheral zone the mechanisms reported for hyperthermia detailed in the previous section also occur, one of the most significant being the activation of the immune system due to the accumulation and release of necrotic fragments and intracellular components [60–62].

The major clinical application of thermal ablation is in the removal of small localized tumors in specific types of cancer, such as liver especially in patients that are not eligible for surgery [63]. However, this technique is currently gaining more relevance as an alternative for conventional surgery, as it is more comfortable for the patient and associated with lower risks [63]. Thermal ablation requires the use of ablation applicators that can be inserted percutaneously or during open surgery or laparoscopy [64].

## 3. Nanotechnology as a new strategy for hyperthermia-based therapies

Despite the enormous potential of hyperthermia-based therapies for cancer treatment, there are still major challenges for its establishment in clinical settings. Most of the currently available procedures are invasive and require the use of anesthesia either for the insertion of the electrodes or the catheters to monitor local temperature [28,32]. Additionally, there are major limitations in the uniform heat distribution in the tumor tissues along with lack of rigorous thermal dose administration [56,65]. The imaging techniques for the real-time monitoring of the temperature and location of the tumor are still not precise enough [36,37,56]. This highlights the need of novel therapeutic strategies to circumvent these limitations and make hyperthermia a well-established therapeutic modality in cancer management.

The use of nanotechnology in medicine, known as nanomedicine, has gaining increasing interest over the last decades, especially for biosensing, diagnostics and drug delivery applications, relying on the use of systems produced at the nanoscale [66,67]. Cancer disease, in

particular, has been subject of extensive study in this area with nanomedicine playing an important role in improving cancer therapeutics and diagnostics [67,68]. The small size of the nanoparticles combined with the specific characteristics of the tumor environment, particularly the enhanced permeability and retention effect (EPR), promotes their accumulation in the tumor tissues, a phenomenon known as passive targeting [67,68]. Additionally, an active targeting approach is also possible, where nanoparticles can be functionalized with different types of targeting ligands to increase tumor local concentration [67,69].

Currently with the development of novel nanomaterials with different structural, magnetic, optical and chemical properties and the combined efforts of multidisciplinary research teams, more complex nanosystems are being developed and other applications in cancer are being explored, including tumor imaging and hyperthermia-based therapies [67,68].

Nanotechnology is an appealing approach for the improvement of current hyperthermia therapies, enhancing tumor targeting even in less accessible tumors, promoting a more uniform distribution of heat and offering a minimally invasive therapeutic modality [70,71]. The versatility of the nanoparticles in terms of size, shape, optical and magnetic properties makes them excellent candidates for hyperthermia applications [70,71]. Additionally, some types of nanoparticles, such as metallic are very efficient conductors of heat [70,71]. Nanotechnology applied to hyperthermia led to the introduction of a novel concept denominated as "inside-out hyperthermia". This means that the nanoparticles introduced inside the tumor, become the primary source of heat, absorbing the energy from an external source and releasing heat in response [70]. Therefore, the direction of heat loss is reversed to inside-out, in contrary to what occurs in the more conventional hyperthermia-based therapies that use external heating sources [70]. This increases the heating efficiency in the tumor region and simultaneously limits adverse effects in normal tissues [70].

The combination of treatments, known as multimodal therapy, such as hyperthermia, radio, chemotherapy and photodynamic therapy is also possible through the use of nanotechnology, as one single multifunctional nanoparticle is able to carry multiple therapeutic agents [69,72,73]. Multimodal therapies can increase the efficacy of the treatment, reduce drug dosages and associated side-effects and limit tumor drug resistance [73]. Nanotechnology also enables simultaneous treatment and imaging, a concept known as theranostics, as some nanoparticles are also excellent imaging agents [70].

The application of hyperthermia can also improve the therapeutic outcome of nanomedicines as it can stimulate the opening of the tumor endothelial barrier and reduce the interstitial fluid pressure in the tumor region, enhancing the penetration of the nanoparticles [68]. Additionally, hyperthermia can induce the release of the nanoparticle's content in the tumor, particularly when using thermo-sensitive nanocarriers, such as thermoliposomes, which can release their cargo upon heat-stimulation [74].

Taking into consideration the benefits of combining hyperthermia and nanotechnology nanoparticle-mediated hyperthermia modalities, such PTT have emerged.

## 4. Nanoparticle-based photothermal therapy (PTT)

PTT is a minimally invasive procedure which requires the administration of a PTT agent (either intravenously or intratumorally) followed by irradiation with NIR light [75]. The PTT agent can then convert the energy from the incident NIR light into heat and induce hyperthermia in the tumor region [39]. The principle of PTT is illustrated in Fig. 2.

Laser light in the NIR region (700–1100 nm) is the energy source in PTT due to its higher penetration depth and lower absorption in biological tissues, which limits non-specific heating of healthy tissues [75,76]. Continuous-wave or pulsed-mode laser (nano or femtosecond lasers) can be used [41]. The latter provides a more effective light-to-heat conversion and an instantaneous energy transfer at high intensities inducing high sub-cellular temperatures [41,77]. Short pulsed lasers also cause less heat dissipation, thus inducing less hazards in healthy tissues surrounding the tumor [77]. Continuous lasers, however, induce a higher temperature variation [78].

An ideal PTT agent should be photostable, biocompatible, easily functionalized and have a high NIR absorption cross-section and light-to-heat conversion efficiency [38,41,79]. Numerous types of PTT agents have been developed so far, comprising photoactive small molecules and different classes of nanomaterials, including metallic nanoparticles, carbon-based nanomaterials, polymer-based nanomaterials and quantum dots [38,75,80].

Photoactive small molecules can be used both as PTT and imaging agents due to their fluorescence properties. Different classes of molecules have been applied including cyanines, such as the FDA-approved dye indocyanine green (ICG), phthalocyanines and porphyrins. Most of these molecules are biodegradable and biocompatible and have a high

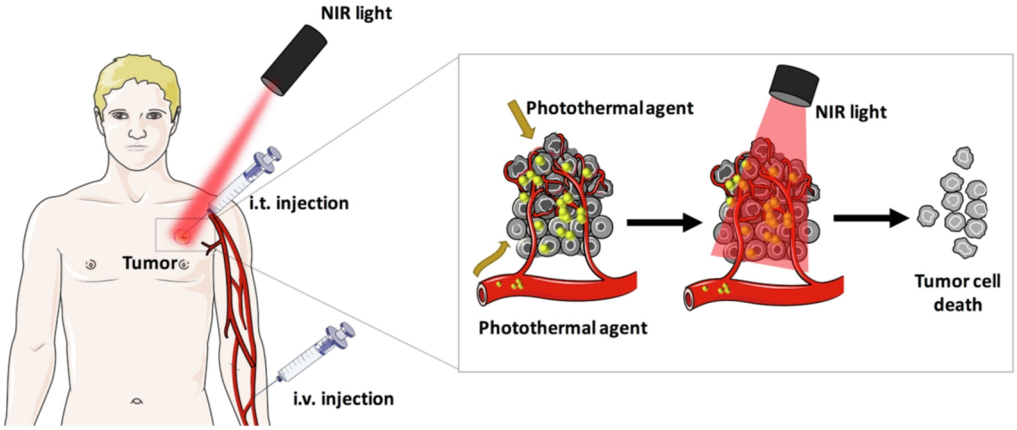



**Fig. 2.** Principle of PTT in cancer management. The photothermal agent is injected either intravenously or intratumorally and accumulates in the tumor tissue via EPR effect or due to active cancer cell-targeting. Tumor is then irradiated with NIR light (using either a continuous or a pulsed laser) with a specific power intensity for a short period of time. The photothermal agent will then release heat upon NIR stimulus, leading to local hyperthermia and tumor cell death.

light-to-heat conversion efficiency. Moreover, some of them can produce ROS upon light irradiation, which enables the combined actions of PTT and PDT in tumor eradication. The widespread application of these small molecules in PTT, however, is limited by their low aqueous solubility, poor stability and photobleaching [81–83]. As a result, many studies have applied nanotechnology to improve the properties of these molecules and potentiate their application in PTT [84,85].

Metal nanoparticles are divided into different categories, the most studied being gold nanostructures (described in detail in section 4.1) and iron oxide nanoparticles. Iron oxide nanoparticles are FDA-approved, small-sized (<30 nm) nanoparticles with good biodegradability and biocompatibility [41,86]. Besides their potential in PTT, iron oxide nanoparticles can also be employed in magnetic hyperthermia (MHT) upon induction of an external magnetic field [86]. Indeed, combined PTT and MHT using iron oxide nanoparticles has already been reported [87]. Due to their magnetic properties, iron oxide nanoparticles can also be used as imaging contrast agents in magnetic resonance imaging (MRI) [86]. Their major limitation is their demand of high irradiation doses, which can be harmful for the patient [86].

Carbon-based nanomaterials contain a c-c backbone with a delocalized electronic structure, which provides them adequate optical and electronic properties for PTT. The most common types of carbon-based nanomaterials applied in PTT are carbon nanotubes and graphene oxide sheets. Carbon nanotubes are tubular structures formed by closed sheets of graphene with diameter at the nanometer scale and length of a few micrometers [88]. Graphene sheets are formed by arrays of carbon atoms extended for hundreds of micrometers with a single atom thickness. Those present a high surface-to-volume–ratio, good mechanical properties and flexibility and an improved light-to-heat conversion efficiency, particularly when used in its reduced form. Carbon-based nanostructures, however, may have some intrinsic toxicity and require surface modification prior to *in vivo* applications [89].

Quantum-dots are small sized nanoparticles (<20 nm) composed of semiconductor materials frequently used as fluorescent probes in several biomedical applications. Although they present a high light-to-heat conversion efficiency, there are still some concerns regarding their biocompatibility and biodegradability in the human body [90–92].

Polymeric-based PTT agents composed of semiconductor nanomaterials have also been widely used in this context with excellent light-to-heat conversion efficiency and imaging properties. Some of the most popular choices in this category include polyanilines and polypyrroles [39,79]. Nevertheless, detailed evaluation regarding their safety is still lacking [39].

### 4.1. Gold-mediated PTT in breast cancer

The use of PTT in breast cancer treatment has been widely reported in the literature with very promising results. The benefits of this technique arise from the easiness of the procedure, the non-requirement of specialized equipment, the use of well-studied biocompatible agents, such as gold nanostructures and the ability to heat the tissue in a more efficient manner minimizing lesions in healthy tissues, due to the phenomenon of "inside-out hyperthermia" [41,70,93].

Among the diversity of available PTT agents described in section 4, gold nanostructures are the most studied agents and the most used in PTT of cancer, including breast cancer. These nanoparticles possess many advantageous characteristics, that make them ideal PTT agents. First, they have a strong absorption cross-section and a high heating efficiency and are extremely versatile in terms of shape and size, which can be modulated to tune the absorption to the NIR region and to maximize the heating efficiency [38–41]. They are also biocompatible and non-immunogenic at clinical relevant concentrations and can accumulate in tumor tissues by passive targeting due to their small size [38–40]. Gold has also the ability to bind to amine and thiol groups, being easily functionalized with targeting ligands or other therapeutic agents, such as chemotherapeutic drugs, facilitating multimodal targeted therapies [38,41]. Moreover, gold nanostructures have a demarked radiosensitization effect due to their high atomic number [94]. Gold can also be used as an imaging agent in photoacoustic (PA), photothermal and X-ray CT imaging, which facilitates the development of theranostic nanoplatforms [41,95]. The temperature achieved by gold-mediated PTT, i.e., moderate-temperature hyperthermia or thermal ablation, can also be modulated according to the intended purpose by manipulating the characteristics of the gold nanostructure and the power source settings.

All these characteristics along with the well-established clinical use of gold nanostructures for years in other diseases, such as rheumatoid arthritis [96], have made gold one of the main mediators of PTT.

The mechanism responsible for laser-induced heat generation in gold nanostructures is well known. Metal nanoparticles, such as gold have a particular characteristic known as surface plasmon resonance (SPR) [39,41]. SPR is caused by the existence of conduction electrons in the metal, which oscillate around the particle's surface [39,41]. When the incident light frequency is coincident with the oscillating electrons, i.e., with the SPR, it induces charge separation and electrons collective oscillation. The relaxation from this high-energy state will then lead to release of heat, a process known as non-radiative relaxation. Finally, the heat is dissipated from the particle to the surrounding environment [39,41]. The oscillation of the electrons depends on their mean free path, which is limited by the particles dimensions, meaning that the SPR frequency is affected by parameters, such as nanoparticle size and shape [40,93]. Due to this fact, numerous complex geometries of gold nanostructures have been developed with the purpose of tuning the SPR to the NIR region [40,93]. Those include, nanorods, nanostars, spherical nanoparticles and nanoshells (Fig. 3.) [39,41]. All of these types of nanostructures have been used for breast cancer treatment either alone or combined with other types of nanoparticles (hybrid nanostructures).

The main implemented strategies including type of gold nanoparticle used, surface modifications, therapy and imaging techniques combinations are schematically represented in Fig. 4. A description of each type of gold nanostructure along with their recent applications as PTT agents in breast cancer, focusing on preclinical studies is given below.

#### 4.1.1. Gold nanorods

Gold nanorods have a strong absorption cross-section at the NIR region corresponding to their longitudinal SPR and present an absorption peak around 500 nm resultant of the transverse SPR [38,41]. They present a high light-to-heat conversion efficiency and their aspect ratio can be easily manipulated through different synthesis methods to modulate the longitudinal SPR band to the NIR region [38,41]. Due to these favourable characteristics, gold nanorods are one of the most popular types of gold nanostructures in PTT.

Many studies have described the use of gold nanorods as effective PTT agents for breast cancer as summarized in Table 1. One of the drawbacks of gold nanorods is the presence of residual amounts of cetyltrimethyl ammonium bromide (CTAB), used in some of the available synthesis protocols, which has high toxicity [97]. Therefore, in most studies, gold nanorods are often coated with polymers such as chitosan or poly(ethylene glycol) (PEG) to improve their biocompatibility [97–100]. The latter is also effective in increasing the circulation time and limit the immunogenicity of the nanorods, as it inhibits serum protein adsorption [101]. Another common coating agent is mesoporous silica, which provides stability and can also enhance drug loading, thus enabling multimodal therapies [99,100,102].

Manivasagan *et al.* produced chitosan oligosaccharide-coated gold nanorods [97]. The nanosystem combined with NIR laser irradiation was extremely effective, achieving complete tumor ablation in MDA-MB-231 tumor-bearing mice after 20 days without recurrence. Biodistribution studies showed a preferential accumulation of the nanorods in the tumor after 24 h and clearence from the body after 5 days, with no organ damage observed, demonstrating the biocompatibility of the nanosystem [97].

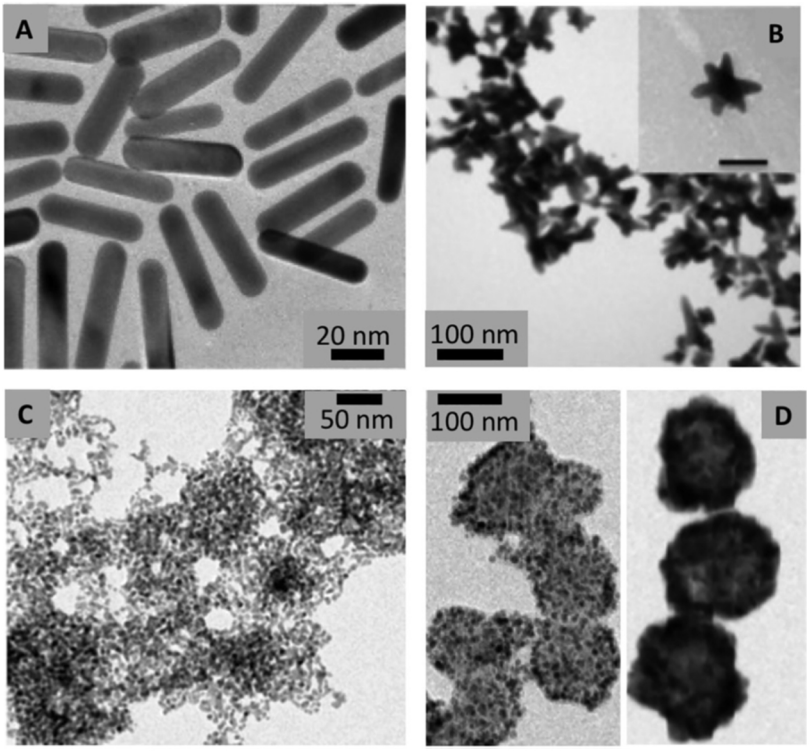



**Fig. 3.** Transmission electron microscopy images of different types of gold nanostructures. (A) Gold nanorods. Adapted from [106],Copyright 2019 with permission from Elsevier. (B) Gold nanostars. Adapted from [112]. (C) Spherical gold nanoparticles. Adapted from [116], Copyright 2018, with permission from Elsevier. (D) Gold nanoshells. Adapted from [77].

Nanorods' surface can also be modified with targeting ligands or specific antibodies to promote an active-cancer cell targeting [6,100,102–106]. Zhang *et al.* developed a therapeutic strategy for TNBC based on gold nanorods functionalized with anti-epidermal growth factor receptor (EGFR), as the targeting of this receptor is considered a promising strategy to fight this breast cancer subtype [6]. PTT with this nanovehicle led to a significant decrease in tumor volume in MDA-MB-231 tumor-bearing mice comparing to the control [6]. Using a similar strategy, these authors took advantage of the optical characteristics of the gold nanorods for PA imaging, which enabled tumor-location and nanoparticle distribution monitoring. The *in vivo* studies showed a selective accumulation in TNBC tumors and almost complete tumor elimination following NIR laser irradiation [103]. Kang *et al.* coated gold nanorods with Trastuzumab for the targeted therapy of HER2-positive breast cancer [104]. The nanosystem also comprised porphyrin for fluorescence tumor imaging. A selective accumulation occurred in BT474 breast cancer xenografted mice that overexpress HER2 [104]. In addition, a significant reduction in tumor volume was obtained following NIR laser irradiation, with no systemic toxicity observed [104].

Although gold nanorod-mediated PTT has demonstrated promising results *in vivo*, in clinical practise hyperthermia is generally not used alone but rather in combination with other modalities such as chemotherapy. Therefore, numerous preclinical studies have explored the combination of PTT with other therapeutic modalities. This allows for a higher efficacy at lower doses of therapeutic compound and, hence, less side-effects [102]. Common therapies combined with gold nanorod-mediated PTT for breast cancer, include chemotherapy, PDT and gene therapy [98–100,102,105–107]. Besides the synergistic effects obtained by the combination of therapies, it is also possible to promote a NIR laser-induced drug release, which further enhances the efficacy of the treatment [99,100,105,107].

Xu *et al.* produced gold nanorods coated with PEG and disulfiram to combine PTT with the anti-cancer activity and tumor targeting ability of disulfiram. The surface coating of the nanorods could increase blood circulation time and tumor accumulation in a MCF-7-xenografted mouse. A high reduction of tumor volume was achieved following NIR irradiation with a decrease of tissue rigidity and angiogenesis in the tumor area comparing to the control [108].

Xu *et al.* reported the use of mesoporous silica and PEG-coated gold nanorods for loading of doxorubicin [99]. To monitor the nanoparticles biodistribution they were labelled with $^{89}$Zr to perform positron emission tomography (PET) imaging. PA imaging was also performed as a complementary technique. The nanosystem could accumulate in the tumor region with high efficiency by passive targeting in 4T1 tumor-bearing mice as a model of TNBC. Furthermore, tumor growth was strongly inhibited following NIR laser irradiation, with a higher efficacy obtained for the bimodality therapy, when compared with the single modalities. Tumors were eliminated at day 21 without recurrences for 6 weeks [99].

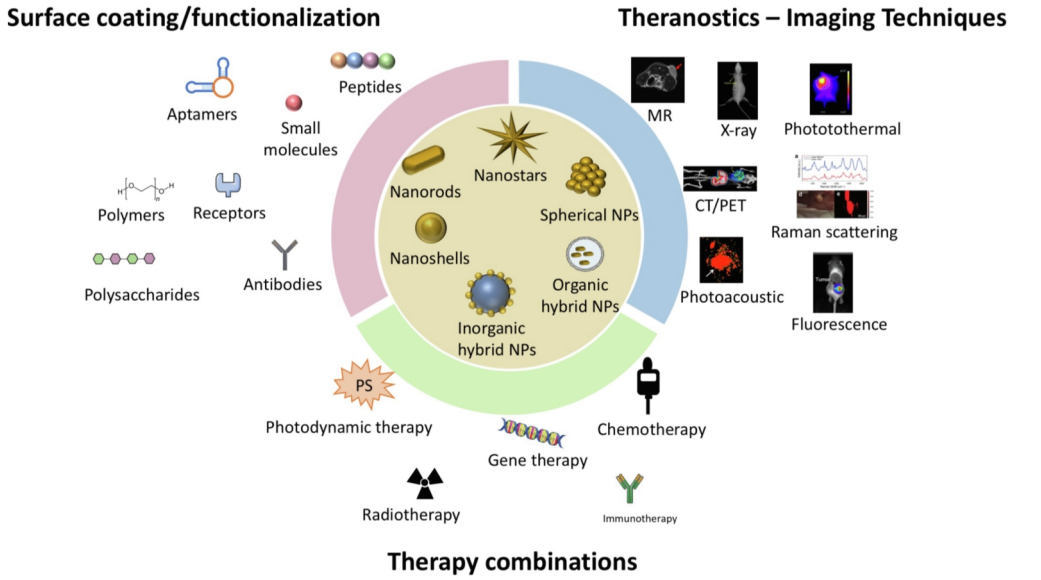



**Fig. 4.** Summary of strategies employed for gold-mediated PTT in breast cancer. Different types of gold nanostructures have been produced including nanorods, nanostars, nanoshells, spherical nanoparticles and hybrid nanostructures comprising two or more types of nanoparticles into one single nanoplatform composed of organic or inorganic materials. Surface modification has been performed to improve the biocompatibility and circulation time of the nanoparticles, the most common being the PEGylation of the nanoparticle surface. Active cancer-cell targeting has been performed through functionalization with specific antibodies, peptides, aptamers or small molecules. Most studies combined PTT with other therapies taking advantage of the synergistic effects between them, including chemotherapy, gene therapy, immunotherapy, photodynamic therapy and radiotherapy. Theranostic nanoplatform have also been designed using several imaging techniques for *in situ* tumor and nanoparticle imaging and thermal monitoring. Imaging techniques figures adapted with permission from [124,135,137], Copyright 2020, 2016, American Chemical Society, from [126,130], Copyright 2018, 2017 with permission from the Royal Society of Chemistry and [94,154], Copyright 2019, 2016 with permission from Elsevier.

Liu *et al.* produced gold nanorods coated with mesoporous silica, PEG and functionalized D-type cell penetrating peptide [100]. The latest was employed to promote breast cancer cell internalization. The photosensitiser chlorin e6 was loaded in the nanosystem for simultaneous PDT [100]. Overall the combination of PTT and PDT was more effective in the remission of breast tumor than the individual treatments in MCF-7 cells xenografted mice [100]. Liu *et al.* also developed a PTT-PDT dual therapy based on gold nanorods coated with mesoporous silica and a charge switchable polymer and loaded with ICG [102]. Additionally, a functionalization with RLA peptide was performed to promote cell internalization and mitochondrial targeting. ICG was able to act both as a photosensitizer for PDT and as a PTT agent, enhancing the effects of gold nanorods. The nanoplatform combined with laser irradiation induced a high decrease in tumor volume comparing to each treatment alone in MCF-7 tumor-bearing mice [102]. Similarly most recently, Cheng *et al.* developed mesoporous silica-coated gold nanorods with simultaneous co-encapsulation of doxorubicin and IR820 for trimodal therapy combining PTT, chemotherapy and PDT. The nanosystem was functionalized with hyaluronic acid for tumor targeting. *In vivo* biodistribution assessed in 4T1 xenografted mice showed a high tumor accumulation over time, however accumulation in other organs such as liver and kidney was also found and kidney excretion of gold nanorods did not occur. Tumor growth suppression following the trimodal treatment was significantly higher than the individual therapies, with almost complete tumor eradication achieved following 5 treatments. Additionally, no signs of doxorubicin-induced cardiotoxicity were observed [109].

Xu *et al.* conducted several studies based on gold nanorods for multimodal therapies [98,105,106]. In the first work the authors have combined PTT with chemotherapy using doxorubicin [105]. A dual active cancer cell targeting was performed by functionalizing the nanorods with folic acid and hyaluronic acid. In addition, the nanoplatform was labelled with Cyanine 7.5 to allow tumor NIR fluorescence imaging [105]. The nanosystem achived high cancer cell internalization promoted by the functionalization. The biodistribution studies showed a long blood circulation and high accumulation in the tumor region in MCF-7 tumor-bearing mice. Furthermore, the multimodal therapy enabled complete tumor remission, without recurrence for 20 days [105]. In a similar work the authors have produced a dual active targeted nanoplatform coated with hyaluronic acid and anti-HER2 antibody for combined PDT and PTT therapies, using 5-aminolevulinic acid (ALA) as a photosensitizer [106]. Similar results were obtained in terms of biodistribution, biocompatibility and tumor eradication, with the highest effectiveness achieved following multimodal therapy. The authors also designed a trimodality therapy comprising PEGylated gold nanorods loaded with ALA and doxorubicin for PTT, PDT and chemotherapy combination. The triple therapy was found to be more effective than the correspondent single therapies and bimodal therapies [98].

Wang *et al.* also described the application of a trimodality therapy comprising PTT, chemotherapy and gene therapy for the treatment of TNBC [107] Gold nanorods were coated with a polycationic co-polymer and loaded with docetaxel and small interfering RNA (siRNA) p-65. The latter was applied to suppress lung metastasis and cancer cell proliferation due to downregulation of genes related with cancer cell invasion, such as matrix metalloproteinase-9. Overall the trimodality induced the highest growth inhibition of the primary tumor and its lung metastasis in

**Table 1**
Gold nanorods.

| Surface coating | Anti-tumor agent | Laser settings | Physicochemical Characterization | Route of Administration | Max Tumor T (°C) | Ref |
|---|---|---|---|---|---|---|
| Chitosan oligosaccharide | – | Wavelength (nm) 808 nm<br>Power density ($Wcm^{-2}$) 2<br>Duration (min) 5 | Size (nm) 26 × 6.8<br>ZP (mV) + 36.83 | Intratumoral | 52.6 | [97] |
| Anti-EGFR antibody | – | Wavelength (nm) 820 nm<br>Power density ($Wcm^{-2}$) 1.5<br>Duration (min) 3 | Size (nm) 40×10 | Intravenous | 43 | [6] |
| Anti-EGFR antibody | – | Wavelength (nm) 820 nm<br>Power density (W $cm^{-2}$) 1.5<br>Duration (min) 3 | Size (nm) 10 × 40 | Intravenous | 43 | [103] |
| Anti-HER2 antibody | – | Wavelength (nm) 808 nm<br>Power density (W $cm^{-2}$) 6.07<br>Duration (min) 5 | Size (nm) 10 × 40 | Intravenous | – | [104] |
| PEG | disulfiram | Wavelength (nm) 808 nm<br>Power density (W $cm^{-2}$) 2<br>Duration (min) 5 | Size (nm) 70 × 20<br>ZP (mV) + 18.9<br>EE (%) 46.4<br>LC (%) 23.2 | Intravenous | 62.8 | [108] |
| Mesoporous silica<br>PEG | Doxorubicin | Wavelength (nm) 808 nm<br>Power density (W $cm^{-2}$) 0.5<br>Duration (min) 5 | Size (nm) 135.9<br>ZP (mV) − 4.3<br>LC (%) 40.9 | Intravenous | 60.2 | [99] |
| Mesoporous silica<br>PEG<br>D-type cell penetrating peptide | chlorin e6 | PTT:<br>Wavelength (nm) 808 nm<br>Power (W) 2<br>Duration (min) 5<br>PDT:<br>Wavelength (nm) 650 nm<br>Power (mW) 50<br>Duration (min) 5 | Size (nm) 171<br>ZP (mV) + 16 | Intravenous | – | [100] |
| Mesoporous silica<br>CS(DMA)-PEG) polymer<br>peptide RLA | ICG | Wavelength (nm) 808 nm<br>Power density (W $cm^{-2}$) 1.5<br>Duration (min) 5 | Size (nm) 57.3 × 16.2,<br>thickness (nm) 21<br>ZP (mV) − 9.4<br>LC (%) 6 | Intravenous | 44.91 | [102] |
| Mesoporous silica<br>Hyaluronic acid | Doxorubicin<br>IR820 | Wavelength (nm) 808 nm<br>Power density (W $cm^{-2}$) 1<br>Duration (min) 5 | Size (nm) 78 × 49<br>ZP (mV) − 4.7<br>LC (%)<br>5 (Dox)<br>3.5 (AuNRs) | intravenous | 54.3 | [109] |
| Folic acid<br>Hyaluronic acid | Doxorubicin | Wavelength (nm) 808 nm<br>Power density ($Wcm^{-2}$) 1.5<br>Duration (min) 5 | Size (nm) 70.9<br>ZP (mV) − 11.4<br>LC (%) 7.1 | Intravenous | 67.5 | [105] |
| Hyaluronic acid<br>Anti-HER2 antibody | ALA | PTT:<br>Wavelength (nm) 808 nm<br>Power density (W $cm^{-2}$) 1<br>Duration (min) 5<br>PDT:<br>Wavelength (nm) 635 nm<br>Power density (W $cm^{-2}$) 0.5<br>Duration (min) 5 | Size (nm) 72.2<br>ZP (mV) − 3.8 | Intravenous | 63.1 | [106] |
| PEG | ALA<br>Doxorubicin | PTT:<br>Wavelength (nm) 808 nm<br>Power density (W $cm^{-2}$) 1<br>Duration (min) 5<br>PDT:<br>Wavelength (nm) 635 nm<br>Power density (W $cm^{-2}$) 0.5<br>Duration (min) 5 | Size (nm) 43<br>ZP (mV) − 6<br>LC (%) 3.6 (dox)<br>LC (%) 8.7 (ALA) | Intravenous | 59 | [98] |
| Cyclodextrin-grafted polyethylenimine | Docetaxel<br>siRNA-p65 | Wavelength (nm) 655 nm<br>Power density ($mcm^{-2}$) 0.2–0.3, 0.4 and 0.5.<br>Duration (min) 3 | ZP (mV) + 20<br>LC (%) 5.6 | Intravenous<br>Intratumoral | 30[a] | [107] |

AlA: 5-aminolevulinic acid, CS(DMA)-PEG): 2,3-dimethylmaleic anhydride-modified chitosan oligosaccharide-block-poly (ethylene glycol), EGFR: Epidermal growth factor receptor, HER2: Human Epidermal growth factor Receptor 2, ICG: Indocyanine green, LC: Loading capacity, Max Tumor T: Maximum Tumor Temperature, PDT: Photodynamic therapy, PEG: Poly(ethylene glycol), PTT: Photothermal therapy, siRNA: Small interfering RNA, ZP: Zeta Potential.

[a] maximum temperature elevation measured in the tumor area

4T1 tumor-bearing mice. The authors claimed that although the laser used was not in the NIR region an effective PTT treatment was achieved when combined with other therapeutic modalities [107].

#### 4.1.2. Gold nanostars

Gold nanostars are anisotropic structures composed of a central spherical core surrounded by several spikes of variable number and size [41]. This aspect is responsible for their high NIR absorption and light-to-heat conversion efficiency and can be easily controlled during the

synthesis process [41,110]. Additionally, their biocompatibility can be enhanced by the use of toxic surfactant-free synthesis methods [110]. Besides their suitability for PTT applications, gold nanostars are considered strong imaging and diagnostic agents and, due to their high surface area, they are also efficient drug delivery vehicles [38,111]. Common therapies combined with gold nanostar-mediated PTT, include chemotherapy, PDT and gene therapy [95,110,112–114]. In most works, surface coating with PEG or functionalization with targeting ligands is a common approach to enhance their biocompatibility and accumulation in tumor tissues, respectively [95,110,112,113]. A summary of applications using gold nanostar-mediated PTT is presented in Table 2.

Li *et al.* have combined PDT and PTT into a single nanoplatorm comprising polydopamine-coated gold nanostars and chlorin e6. The produced nanosystem accumulated in the tumor region at a high extend, however, a higher liver and spleen accumulation was observed. Nevertheless, no signs of toxicity were found. The PTT-PDT combination therapy resulted in a successful tumor eradication, and a higher lung metastasis inhibition comparing to the individual therapies [114].

You *et al.* also reported the production of polydopamine-coated gold nanostars. A surface modification with a PEG-folic acid ligand was performed followed by loading with doxorubicin for multimodal targeted therapy [112]. Polydopamine coating enabled a high doxorubicin loading, improved the photothermal efficiency of gold nanorods and was also responsible for angiogenesis inhibition due to electrostatic interaction with vascular endothelial growth factor. The *in vivo* antitumor efficacy of the nanovehicle was evaluated in multidrug resistant MCF-7/ADR tumor-bearing mice. An enhanced accumulation in tumor region was observed along with NIR-triggered drug release. The nanosystem revealed high efficacy in inhibiting tumor growth and angiogenesis [112]. More recently, in a similar work from the same group, PEGylated gold nanostars were conjugated with doxorubicin, and functionalized with a DNA aptamer for dual active targeting of tumor cells and tumor vasculature [110]. The nanosystem was also tested in a multidrug resistant tumor model demonstrating that the efficacy of the dual therapy in terms of tumor growth inhibition was fairly superior comparing to the monotherapies, even at much lower dosages of doxorubicin [110]. In both studies the nanorods were considered safe although a high accumulation of gold in the liver was reported [110,112]. However, no signs of hepatotoxicity have been identified [110,112].

A gold nanostar-based PTT strategy to fight TNBC was reported by Wang *et al.* Nanostars were coated with hyaluronic acid and loaded with siRNA to inhibit the heat shock protein 72 (Hsp72), a cell chaperone responsible for thermotolerance and tumor cell response to hyperthermia. The goal of the strategy was to sensitize the TNBC cells to PTT and, therefore, enhance the efficacy of the treatment. The nanoplatform exhibit biocompatibility, preferential tumor accumulation and enhanced tumor growth inhibition after intravenous administration and NIR irradiation in a MDA-MB-231/Luc tumor-bearing mice [113].

Recently, Yu *et al.* have also designed a therapy to fight TNBC based on a theranostic nanoplatform comprising gold nanostars loaded with an iridium complex [95]. The nanovehicle was functionalized with a peptide conjugate to target the urokinase-type plasminogen activator receptor, overexpressed in cancer cells. Photothermal, PA and X-ray CT imaging techniques were used to monitor nanoparticles tumor accumulation following intravenous and intratumoral injection, with gold nanorods demonstrating high efficacy as imaging agents in a MDA-MB-231 tumor-bearing mice. A high tumor accumulation and growth inhibition was obtained following administration and NIR laser irradiation, achieving almost complete tumor eradication. Moreover *in vivo* biocompatibility was demonstrated [95].

#### 4.1.3. Spherical gold nanoparticles

Spherical gold nanoparticles were the first type of gold nanostructures studied and have the advantages of being easily synthesized, biocompatible and small [115–117]. This type of nanostructure, however, does not have an absorption cross-section in the NIR region [116]. Instead they absorb preferentially in the range of 500–580 nm, which is not suitable for clinical application due to limited tissue penetration [116]. One way to circumvent this limitation is to cluster the nanoparticles, forming larger aggregates, which shifts their SPR band to the

**Table 2**
Gold nanostars.

| Surface coating | Anti-tumor agent | Laser settings | Physicochemical Characterization | Max Tumor T (°C) | Route of Administration | Ref |
|---|---|---|---|---|---|---|
| Polydopamine | Chlorin e6 | Wavelength (nm) 808 nm<br>Power density (W $cm^{-2}$) 1<br>Duration (min) 5<br>PDT:<br>Wavelength (nm) 635 nm<br>Power density (W $cm^{-2}$) 0.05<br>Duration (min) 5 | Size (nm) 188<br>ZP (mV) − 18.4<br>LC (%) 12.88 | 55 | Intravenous | [114] |
| Polydopamine<br>PEG-Folic acid | Doxorubicin | Wavelength (nm) 808 nm<br>Power density (W $cm^{-2}$) 0.9<br>Duration (min) 3 (3 x) | Size (nm) 149<br>ZP (mV) − 19<br>EE (%) 29.9<br>LC (%) 10.4 | 48 | Intravenous | [112] |
| PEG<br>anti-nucleolin aptamer AS1411 | Doxorubicin | Wavelength (nm) 808 nm<br>Power density (W $cm^{-2}$) 0.9<br>Duration (min) 3 (3 x) | Size (nm) 96.4<br>ZP (mV) − 8<br>EE (%) 90.4 | 60 | Intravenous | [110] |
| Hyaluronic acid | siRNA against Hsp72 | Wavelength (nm) 808 nm<br>Power density (W$cm^{-2}$) 1<br>Duration (min) 5 | Size (nm) 73.2<br>ZP (mV) − 18.3<br>EE (%) 87<br>LC (%) 8.7 | 15[a] | Intravenous | [113] |
| P-AE105 | iridium complex | Wavelength (nm) 808 nm<br>Power density (W $cm^{-2}$) 1.5<br>Duration (min) 15 | Size (nm) 100<br>ZP (mV) + 30 | 67 | Intravenous<br>Intratumoral | [95] |

EE: Encapsulation efficiency, LC: Loading capacity, Hsp72: Heat shock protein 72, Max Tumor T: Maximum Tumor Temperature, P-AE105: polyetherimide-AE105 peptide conjugate, PEG: Poly(ethylene glycol), siRNA: Small interfering RNA, ZP: Zeta Potential.
[a] maximum temperature elevation measured in the tumor area

NIR region [116]. Gold nanoparticles aggregation is generally induced by stabilization or assembly with proteins or organic polymers, which can also increase their biocompatibility [115,116]. The main applications of spherical gold nanoparticles for PTT in breast cancer are shown in Table 3.

Wang *et al.* enhanced the PTT efficiency of positively-charged gold nanoparticles by promoting their-assembly with negatively-charged silk fibroin leading to the formation of silk fibroin nanofibers [118]. The structures presented high NIR absorption and significantly inhibited tumor growth, with almost complete elimination upon NIR illumination in a MCF-7 tumor-bearing mice. These effects contrasted with the bare gold nanoparticles, where PTT was not effective [118].

Lee *et al.* [116] synthesized bovine serum albumin (BSA)-stabilized gold nanoclusters composed of 6 nm gold nanoparticles and strands of the cationic polymer polyallylamine. PA imaging using gold nanoclusters as contrast agents showed a high accumulation in the tumor following intravenous administration via passive targeting in a TNBC 4T1-xenografted mice. Additionally, a demarked tumor volume reduction was achieved after NIR irradiation, comparing to the controls. Biodistribution studies revealed a high kidney and liver accumulation over time. The fraction of gold in the kidney, however could be cleared, as demonstrated by the mice urine analysis. Despite that, no signs of toxicity were found following organ histological analysis [116].

Han *et al.* [115] produced gold nanoclusters assembled with hyaluronic acid and polycaprolactone and loaded with photosensitizer verteporfin for dual PTT-PDT. The production method was based on polymeric nanoassembly and did not require any toxic surfactants such as CTAB. The nanoclusters were tested in a MDA-MB-231 tumor-bearing mice as a TNBC model. Biodistribution studies demonstrated a gradual and prolonged tumor accumulation over 14 days, however accumulation in liver, kidney and spleen was also reported. Dual PTT-PDT laser treatment enabled total tumor elimination and absence of recurrence over 50 days, an effect that was significantly higher comparing to the two individual therapies [115].

Xia *et al.* developed BSA-complexed 20 nm gold nanoparticles forming three dimensional assemblies [119]. The nanosystem was loaded with doxorubicin and functionalized with folic acid. Biodistribution studies showed a high liver accumulation, although tissue damage and body weight alterations were not observed. Upon NIR stimulation an excellent tumor growth inhibition was obtained with complete eradication after 24 days at very low doxorubicin dosages in a MCF-7 tumor-bearing mice. These results demonstrated the efficacy of the synergistic effects between PTT and chemotherapy in breast cancer remission [119].

Gold nanoparticles can also be aggregated after cancer cell internalization. Qian *et al.* constructed a smart nanosystem comprising liposomes loaded with gold nanoparticles that were functionalized with 2 different probes composed of Cyanine 5 (Cy5)-marked molecular beacon, whose loops were complementary to miRNA-21 [117]. The aim of the nanosystem was to hybridize with miRNA-21 upon cancer cell internalization, promoting the opening of the hairpin structure and triggering Cy5-mediated *in situ* tumor fluorescence imaging. Additionally, this would induce the cross-linking between the 2 probes, as their far ends have complementary sequences, causing gold nanoparticles to aggregate and shifting the SPR to the NIR region. This smart nanosystem demonstrated a high retention in the tumor region for at least 48 h and

**Table 3**
Spherical gold nanoparticles.

| Particle description | Surface coating | Anti-tumor agent | Laser settings | Physicochemical Characterization | Route of Administration | Max Tumor T(°C) | Ref |
|---|---|---|---|---|---|---|---|
| AuNPs combined with silk fibroin nanofibers | | | Wavelength (nm) 808 nm<br>Power density (W $cm^{-2}$) 4<br>Duration (min) 6 | Size (nm) (AuNPs) ~ 10<br>ZP (mV) − 10 | Intratumoral | 55 | [118] |
| BSA-stabilized gold nanoclusters | | | Wavelength (nm) 808 nm<br>Power density (W $cm^{-2}$) 1.5<br>Duration (min) 5 | Size (nm)<br><6 (AuNPs)<br>60.3 (nanoclusters)<br>ZP (mV) − 9.6 | Intravenous | 55 | [116] |
| Gold-nanoclustered Hy-PCL nanoassembly | Hyaluronic acid | Verteporfin | PTT:<br>Wavelength (nm) 808 nm<br>Power density (W $cm^{-2}$) 1.5<br>Duration (min) 5<br><br>PDT:<br>Wavelength (nm) 690 nm<br>Power density (W $cm^{-2}$) 0.5<br>Duration (min) 20 | Size (nm) 150<br>ZP (mV) − 16<br>EE (%) 87<br>LC (%) 8.7 | Intravenous | 60 | [115] |
| 3D assemblies of AuNPs complexed with BSA | Folic acid | Doxorubicin | Wavelength (nm) 808 nm<br>Power density (W $cm^{-2}$) 1.5<br>Duration (min) 5 | Size (nm)<br>20 (AuNPs)<br><200 (3D assemblies)<br>ZP (mV) − 12.6<br>LC (%) 0.82 | Intravenous<br><br>Intratumoral | 68 | [119] |
| AuNPs-loaded liposomes | Molecular beacon complementary to miRNA-21 | | Wavelength (nm) 680 nm<br>Power density (W $cm^{-2}$) 0.5<br>Duration (min) 30 | Size (nm)13 (AuNPs) | Intravenous | – | [117] |

AuNPs: gold nanoparticles, BSA: Bovine serum albumin, EE: Encapsulation efficiency, Hy-PCL: hyaluronan-polycaprolactone, LC: Loading capacity, Max Tumor T: Maximum Tumor Temperature, miRNA-21: microRNA-21, PDT: Photodynamic therapy, PEG: Poly(ethylene glycol), PTT: Photothermal therapy, ZP: Zeta Potential.

induced a high tumor volume reduction upon NIR irradiation in a MCF-7 tumor-bearing mice [117].

#### 4.1.4. .Gold nanoshells

Gold nanoshells comprise a core, normally hollow or made of silica, and an outer layer of gold. The shell thickness can me modulated to tune their optical properties, including shifting the SPR to the NIR region for PTT and imaging applications [41]. Gold nanoshells have a high photothermal conversion efficiency and are also commonly used in theranostics [120].

Recently Xu *et al.* synthesized a theranostic nanosystem comprising porous gold nanoshells coated with PEG, trastuzumab and the microtubule-targeted drug derivative of mautansine (DM1). An effective multimodal tumor imaging was obtained combining computed tomography (CT), PA and photothermal imaging. Biodistribution studies revealed an improvement of the targeting ability after functionalization in HER-2 positive SK-BR-3 tumour-bearing mice. However, a higher gold accumulation was found in the liver and spleen. An enhanced tumor growth inhibition was obtained following NIR irradiation comparing to the non-irradiated groups. Additionally, this therapy could enhance of the expression of E-cadherin suggesting a potential anti-metastatic effect [121].

The core of gold nanoshells, which works as a template during the synthesis process, can also be loaded with imaging contrast agents, magnetic nanostructures or drugs giving rise to multi-functional nanostructures [120,122]. Iron oxide nanoparticles are one of the most common types of structures that can be loaded in the core of gold nanoshells as they provide MRI imaging contrast and can also allow for simultaneous magnetic hyperthermia and PTT [77,120,123]. In a study performed by Nunes *et al.* gold nanoshells were produced comprising a core composed of silica and iron oxide [77]. A surface coating with PEG and anti-HER2 antibody was also performed. Nanoshells were administered intravenously in HER2-overexpressing breast tumor xenografted mice once a week for 4 weeks. A detailed biodistribution study was conducted using MRI and other techniques, showing a high tumor accumulation improved by the functionalization in a BT474 xenografted tumor mice. However, gold accumulation in spleen and liver was also observed after 72 h. Tumors were then irradiated with a femtosecond-pulsed laser. A significant tumor growth inhibition and anti-angiogenic effects were obtained, without a macroscopic increase in tumor temperature due to the use of the femtosecond laser. The authors believe that this therapy could be an effective strategy to avoid trastuzumab resistance in HER2-positive breast cancers [77].

Similarly, Zheng *et al.* reported the synthesis of gold nanoshells with a core comprising iron oxide nanoparticles and poly (D, L-lactide-co-glycolide) acid (PLGA) [122]. The nanoplatform was functionalized with trastuzumab for HER2 positive tumor targeting and loaded with doxorubicin for combined PTT and chemotherapy. Nanoparticle tumor accumulation monitored using both PA and MRI revealed that functionalization improved tumor accumulation reaching a peak at 2 h post-injection. Although the histopathology studies and body weight assessments did not indicate signs of toxicity and organ damage, blood biochemical assays revealed a slight acute inflammation in mice 24 h after nanoparticle administration. The nanoparticles comprising the functionalization and dual therapy revealed the highest efficacy in BT474 tumor reduction, particularly upon NIR irradiation, following two treatments with a 10-day difference. It was also found that the nanoplatform associated with NIR could decrease cancer-associated fibroblasts, improving tumor environment remodelling and increasing nanoparticle penetration in the tumor region.

Pang *et al.* have also synthesized a theranostic nanoplatform comprising palladium copper alloy core-gold shell tripods containing radioactive $^{64}$Cu atoms for simultaneous PTT and PET imaging [124]. The nanostructure was conjugated with D-Ala1- peptide T-amide, for the C − C chemokine receptor 5 targeting, which is upregulated in TNBC. Functionalized tripods presented an acceptable blood retention and a superior tumor accumulation comparing to the non-functionalized nanostructures in a 4T1 tumor-bearing mice as a model of TNBC. A tumor temperature of 60.7 °C was achieved and significant tumor reduction was observed after laser irradiation. The nanostructures also revealed high efficiency and stability as contrast agents for *in vivo* PET imaging, which enabled photothermal cancer treatment guidance [124].

Cui *et al.* introduced oxygen-saturated perfluorohexane in the core of gold nanoshells serving simultaneously as an $O_2$ carrier to counteract hypoxia and as an ultrasound contrast agent for tumor visualization. The nanosystem was modified with cisplatin for combined PTT and chemotherapy. The nanoplatform combined with NIR exhibited the highest tumor growth inhibition in a MDA-MB-231 tumor bearing mice compared to other less complex formulations, including gold nanoshells and gold nanoshells + cisplatin alone. Additionally, a lower expression of HIF-1α and lower presence of hypoxic cells in tumor were obtained following chemo/photothermal therapy, demonstrating the ability of the nanosystem to attenuate hypoxic stress [125].

The studies reporting the use of gold nanoshells for breast cancer PTT are summarized in Table 4.

#### 4.1.5. Inorganic hybrid nanostructures

Although gold nanostructures have numerous beneficial characteristics *per se*, the combination with other inorganic nanostructures can be advantageous. They can enhance their PTT efficacy [126,127], work as a platform for drug loading [127,128], enhance their radiosensitization effect [129] and provide other specific imaging properties [129], or novel properties, such as magnetism [94], contributing to the development of multifunctional nanostructures. A summary of the inorganic hybrid nanostructures-containing gold for PTT of breast cancer in presented in Table 5

Yang *et al.* produced a PEGylated nanoplatform comprising two PTT agents: black phosphorus nanosheets and gold nanoparticles, to enhance NIR absorption and PTT efficacy. Gold nanoparticles also worked as imaging agents for surface-enhanced Raman scattering. The nanoplatform was effective in reducing tumor volume following NIR irradiation in a TNBC 4T1-bearing tumor mice. PTT therapy was monitored by Raman scattering which demonstrated marked changes in the characteristic peaks of proteins and DNA in the tumor tissue after PTT [126].

Zhang *et al.* developed folic acid-decorated halloysite nanotubes for loading of gold nanorods and doxorubicin [128]. These nanotubes have a hollow structure which makes them suitable for loading and controlled release of drugs and other therapeutics. The nanosystem was found to be biocompatible an to exhibit efficient tumor targeting. Moreover, it promoted controlled doxorubicin release in the tumor region and significantly inhibited tumor growth under NIR irradiation in a TNBC 4T1 tumor-bearing mice. Additionally, due to the PTT and chemotherapy synergistic effects, an excellent therapeutic effect was obtained with absence of systemic toxicity, in contrast with the free doxorubicin treatment [128].

Wang *et al.* synthesized nanosized graphene oxide (NGO) combined with gold nanostars and doxorubicin as a therapeutic approach for metastatic TNBC [127]. NGO was used along with gold nanostars for combined NIR absorption photothermal effects. Additionally, due to its large surface area, it is also an effective drug carrier. The nanoplatform in combination with laser irradiation could effectively suppress tumor growth and lung metastasis in a metastatic 4T1 breast tumor-bearing mice model. Moreover, the nanoplatform could suppress doxorubicin-mediated cardiotoxicity. In this study, however, a 655 nm laser was used instead of a NIR laser, which may have some limitations for a future clinical applications due to limited tissue penetration [127].

A hybrid nanosystem for combined PTT and radiotherapy was described by Huang *et al.* [129]. In this study, heterogeneous copper selenide-gold nanocrystals coated with radioactive $^{99m}$Tc were produced for combined photothermal and radiosensitization effects. The nanoplatform accumulation in tumor region was monitored via multimodal imaging integrating single photon emission computed tomography

**Table 4**
Gold nanoshells.

| Particle description | Surface coating | Anti-tumor agent | Laser settings | Physicochemical Characterization | Route of Administration | Max Tumor T (°C) | Ref |
|---|---|---|---|---|---|---|---|
| Porous gold nanoshells | mPEG | Trastuzumab | Wavelength (nm) 808 nm<br>Power density (W $cm^{-2}$) 3 | Size (nm)<br>113 | Intravenous | | [121] |
| | | DM1 | Duration (min) 5 | ZP (mV) − 6.9 | | 45 | |
| Silica and iron oxide-core gold shell | PEG<br>Anti-HER2 antibody | | femtosecond-pulsed laser<br>Wavelength (nm): 800 nm (120 fs pulses, maximum energy 1 mJ/pulse, repetition rate 1 kHz).<br>Duration: 30 min | Size (nm)<br>148<br>ZP (mV) − 21 | Intravenous | | [77] |
| Iron oxide -PLGA-core-gold shell | trastuzumab | doxorubicin | Wavelength (nm) 808 nm<br>Power density (W $cm^{-2}$) 1<br>Duration (min) 10 | Size (nm)<br>285.7 | Intravenous | 60 | [122] |
| Palladium copper alloy core-gold shell tripods | PEG<br>DAPTA | | Wavelength (nm) 808 nm<br>Power density (W $cm^{-2}$) 1.2<br>Duration (min) 10 | Size (nm)<br>50 (arm length) | Intravenous | 60.7 | [124] |
| Oxygen-saturated perfluorohexane-core gold shell | PEG | cisplatin | Wavelength (nm) 808 nm<br>Power density (W $cm^{-2}$) 1.5<br>Duration (min) 1 (x 5), 1 min interval | Size (nm)<br>50<br>ZP (mV) − 27.1 | intravenous | 65 | [125] |

DAPTA: D-Ala1- peptide T-amide, DM1: derivative of the microtubule-targeting drug maytansine, HER2: Human Epidermal growth factor Receptor 2, Max Tumor T: Maximum Tumor Temperature, mPEG: methoxy poly(ethylene glycol), PEG: Poly(ethylene glycol), PLGA: Poly (D, L-lactide-co-glycolide) acid, ZP: Zeta Potential.

**Table 5**
Inorganic hybrid nanostructures.

| Particle description | Surface coating | Anti-tumor agent | Laser settings | Physicochemical Characterization | Route of Administration | Max. Tumor T (°C) | Ref |
|---|---|---|---|---|---|---|---|
| Black phosphorus nanosheets functionalized with AuNPs | PEG | | Wavelength (nm) 808 nm<br>Power density (W $cm^{-2}$) 2<br>Duration (min) 2 | Size (nm)<br>26 (AuNPs)<br>485 | Intratumoral | 65 | [126] |
| Gold nanorod-loaded halloysite nanotubes | Folic acid | Doxorubicin | Wavelength (nm) 808 nm<br>Power density (W $cm^{-2}$) 1<br>Duration (min) 8 | Size (nm) 424<br>ZP (mV) − 19.6<br>LC (%) 1.8 | Intravenous | 59 | [128] |
| Gold nanostar-loaded nanosized reduced graphene oxide | Polydopamine<br>PEG | Doxorubicin | Wavelength (nm) 655 nm<br>Power density (W $cm^{-2}$) 4–6<br>Duration (min) 2 | Size (nm) 100<br>LC (%) 67 | Intratumoral | 55* | [127] |
| Heterogeneous copper selenide-gold nanocrystals | PEG labelled with radioactive $^{99m}Tc$ | X-ray radiation 6 Gy | Wavelength (nm) 808 nm<br>Power density (W $cm^{-2}$) 1.5<br>Duration (min) 10 | Size (nm) 37.9<br>ZP (mV) − 0.2 | Intravenous | 60 | [129] |
| α-$Fe_2O_3$ nanoparticles coated with ultrasmall gold nanoseeds | | X-ray radiation 6 Gy | Wavelength (nm) 808 nm<br>Power density (W $cm^{-2}$) 1.5<br>Duration (min) 3 | Size (nm) 49<br>ZP (mV) − 31.7 | Intravenous | 56 | [94] |

AuNPs: gold nanoparticles, LC: Loading capacity, Max Tumor T: Maximum Tumor Temperature, PEG: Poly(ethylene glycol), ZP: Zeta Potential, α-$Fe_2O_3$: cubic alpha-iron(III) oxide.
[a] maximum temperature elevation measured in the tumor area

(SPECT) and PA imaging. A significant tumor growth inhibition was achieved after treatment with the nanoplatform upon NIR irradiation in a TNBC 4T1 tumor-bearing mouse. This effect was even more demarked when combined with radiotherapy, showing a significant enhancement comparing to the radiotherapy alone, thus demonstrating the efficacy of the nanosystem as a radiosensitizer. Additionally, the combination therapy led to 100% survival rate and prevented lung metastasis.

A theranostic hybrid nanosystem for combined PTT and radiosensitization effects was also reported by Zhong *et al.* [94]. The nanosystem comprised cubic alpha-iron(III) oxide nanoparticles (α-$Fe_2O_3$) coated with gold nanoseeds. α-$Fe_2O_3$ nanoparticles were employed as contrast agents for MRI to track nanoparticles tumor accumulation. After NIR irradiation, a high photothermal effect was obtained with a significant tumor growth suppression that was enhanced upon combination with radiotherapy in a TNBC 4T1 tumor-bearing mice. The combination therapy had also an inhibitory effect in lung metastasis [94].

*4.1.6. Organic hybrid nanostructures*

Gold nanostructures are often combined with organic materials that can improve their biocompatibility and biodegradability [130,131], provide novel imaging contrast properties [132,133], enhance drug encapsulation ability for multimodal therapy combinations [134] and increase tumor penetration ability [135–137]. The different types of hybrid nanosystems combining gold nanostructures and organic nanomaterials for breast cancer PTT applications are summarized in Table 6

Ni *et al.* produced gold nanorods embedded in mesoporous organosilica nanoparticles for TNBC therapy [134]. The nanoplatform was loaded with a siRNA against the TNBC therapeutic target PLK1 for dual PTT-gene therapy. Since mesoporous organosilica present a high surface area, they could considerably enhance the siRNA loading capacity. Combination therapy upon NIR irradiation was significantly more effective than individual therapies in the inhibition of tumor growth in a MDA-MB-231/Luc tumor-bearing mice. Moreover, extensive tumor tissue necrosis was achieved with no visible signs of systemic toxicity [134].

A TNBC therapeutic strategy was also reported by Zhang *et al.*, where gold nanostars were loaded in nanoscale metal organic framework (MOFs), forming core–shell nanostructures [132]. MOFs were employed as MRI imaging contrast agents, contributing to the design of a

**Table 6**
Organic hybrid nanostructures.

| Particle description | Surface coating | Anti-tumor agent | Laser settings | Physicochemical Characterization | Route of Administration | Max Tumor T (°C) | Ref |
|---|---|---|---|---|---|---|---|
| AuNRs embedded in mesoporous organosilica nanoparticles | | siRNA against PLK1 | Wavelength (nm) 808 nm<br>Power density (W $cm^{-2}$) 1<br>Duration (min) 6 | Size (nm) 175<br>ZP (mV) + 40 | Intravenous (imaging)<br>Intratumoral (efficacy) | 47 | [134] |
| Gold nanostar-core -metal organic framework-shell nanocomposite | PEG<br>ZD2 peptide | | Wavelength (nm) 808 nm<br>Power density (W $cm^{-2}$) 1.2<br>Duration (min) 5 | Size (nm) 255<br>ZP (mV) − 12 | intravenous | 17[a] | [132] |
| Gold nanostar core-metal-drug coordination shell | | Gemcitabine | Wavelength (nm) 808 nm<br>Power density (W $cm^{-2}$) 0.5<br>Duration (min) 3 | Size (nm) 46<br>EE (%)<br>85.7 (Gem)<br>90 (Gd III) | Intravenous | 53 | [133] |
| AuNPs or HGNPs-loaded thermosensitive liposomes | | Doxorubicin | Wavelength (nm) 808 nm<br>Power density (W $cm^{-2}$) 2<br>Duration (min) 5 | Size (nm) 196<br>23.2 (AuNPs)<br>60.7(HGNPs)<br>ZP (mV) − 29<br>EE (%)<br>10.87 (HGNPs)<br>21.27 (AuNPs)<br>89.3 (dox) | Intravenous | 20[a] | [130] |
| AuNRs-loaded liposomes | Folic acid | Doxorubicin | Wavelength (nm) 808 nm<br>Power (W) 1.5<br>Duration (min) 5 | Size (nm) 154.3<br>7 (AuNRs)<br>ZP (mV) + 25.12<br>EE (%)<br>54.73 (Dox)<br>25.12 (AuNRs) | Intravenous | 43 | [131] |
| Macrophage-phagocytosed liposomes and AuNRs | | Doxorubicin | Wavelength (nm) 808 nm<br>Power density (W) 1.5<br>Duration (min) 5 | Size (nm) 145<br>EE (%)<br>13.3 (AuNRs)<br>35.2 (Doxorubicin | Intravenous<br>Intratumoral | 54.6 | [137] |
| AuNRs-embedded in hollow mesoporous organosilica nanospheres -loaded MSCs | | Paclitaxel | Wavelength (nm) 808 nm<br>Power density (W $cm^{-2}$) 1.3<br>Duration (min) 5 | Size (nm) 227<br>ZP (mV) – 22<br>LC (%) 13.4 | Intratumoral | 16[a] | [135] |
| AuNRs, iron oxide hybrid nanoparticles -loaded MSCs | CXCR4 | Doxorubicin | Wavelength (nm) 808 nm<br>Power density (W $cm^{-2}$) 1.5<br>Duration (min) 10 | Size (nm) 160<br>140 (iron oxide)<br>40x8 (AuNRs)<br>ZP (mV) + 20<br>EE (%) 18.7<br>LC (%) 1.3 | Intravenous<br>Intratumoral | 55 | [136] |
| Gold nanostars-loaded CIK cells | | ICG<br>Trastuzumab | Wavelength (nm) 808 nm<br>(Power density (W $cm^{-2}$)<br>Duration (min) 12 | Size (nm) 135.0.3 ZP (mV) −7.5 LC (%) 14.9 | Intravenous | 41.5 | [155] |

AuNPs: gold nanoparticles, AuNRs: gold nanorods, CXCR4: C-X-C chemokine receptor type 4, CIK cells: Cytokine-induced killer cells, EE: encapsulation efficiency, HGNPs: Hollow gold nanoparticles, LC: Loading capacity, Max Tumor T: Maximum Tumor Temperature, MSCs: Mesenchymal stem cells, PEG: Poly(ethylene glycol), PLK1: Polo Like Kinase 1, siRNA: small interfering RNA ZP: Zeta Potential, α-$Fe_2O_3$: cubic alpha-iron(III) oxide.

[a] maximum temperature elevation measured in the tumor area

theranostics nanosystem. A functionalization with a TNBC-targeted peptide (ZD2) was also performed. The nanosystem proved to be an efficient MRI contrast agent for tumor *in vivo* monitoring, and the targeting ability of the functionalized nanosystem was found to be effective. Moreover, the nanosystem showed an excellent PTT effect upon NIR irradiation in a MDA-MB-231 tumor-bearing mice. Similarly, Li *et al.* [133] have also combined MOFs and gold nanostars in a core–shell nanosystem. MOFs were composed of gadolinium and the drug gemcitabine to allow for simultaneous MRI imaging and chemotherapy, respectively. Nanoparticles could be effectively monitored with MRI and two-photon luminescence imaging techniques *in vivo*. Tumor growth suppression in a 4T1 tumor xenografted mice as a TNBC model was significantly higher for the combined PTT and chemotherapy regimens comparing to the individual therapies.

Liposomes are routinely used as delivery vehicles of drugs and other therapeutic compounds due to their high biocompatibility and stability in physiological environment and their easy accumulation in tumor regions [130,131]. In addition, their composition can be modulated by adding low phase transition lipids leading to the formation of thermosensitive liposomes, that can be disrupted and release their cargo upon heat stimulation [130]. Due to these advantages, liposomes have already reached clinical trials as drug delivery systems of doxorubicin combined with local hyperthermia in breast cancer treatment [32,33] Therefore, the combination of liposomes with gold nanostructures is a promising approach for PTT applications, particularly in combination with other compounds such as chemotherapeutic drugs for the creation of multimodal therapies [130,131].

Li *et al.* designed thermosensitive liposomes for co-delivery of hollow gold nanoparticles (HGNPs) or gold nanoparticles (AuNPs) and doxorubicin for PTT-chemotherapy dual therapy [130]. NIR laser could induce tumor local hyperthermia and simultaneously trigger doxorubicin release in a MCF-7 tumor-bearing mice. Biodistribution studies using NIR imaging showed a preferential accumulation in tumor region, although liver accumulation was also found. In terms of efficacy a synergistic effect between doxorubicin and gold-mediated PTT was obtained particularly when employing HGNPs, which induced the highest tumor growth reduction. Liposomes were also effective in the reduction of doxorubicin-associated systemic toxicity [130]. Similarly, Nguyen *et al.* reported the use of folate-functionalized liposomes for co-loading of gold nanorods and doxorubicin [131]. Efficacy studies in TNBC 4T1 tumor-bearing mice demonstrated a significant tumor growth inhibition that was more demarked in the treatments using functionalized liposomes and in the dual PTT-chemotherapy combination regimen, demonstrating the synergism between the two therapies [131]. These authors have more recently designed a macrophage delivery system based on the phagocytosis of doxorubicin-loaded liposomes and gold nanorods for dual PTT-chemotherapy [137]. The use of macrophages as delivery systems was considered an interesting approach attributed to their biocompatibility, natural nanoparticle-phagocytosis ability and capacity to migrate to the tumor region. The delivery system was evaluated in a TNBC 4T1 tumor-bearing mice after intratumoral injection. The use of macrophages was found to induce the highest tumor growth inhibition comparing to the nanosystem alone and the individual therapies. Biodistribution evaluation was done following intravenous injection showing an effective tumor targeting, with accumulation also occurring in the spleen, lungs and liver. These data demonstrated the feasibility of using cells as effective nanoparticle carriers [137].

Other authors had also reported the benefits of cell-based delivery systems. Wu *et al.* reported the use of mesenchymal stem cells (MSCs) carrying hollow mesoporous organosilica nanospheres for efficient loading of gold nanorods and paclitaxel [135]. MSCs intrinsic ability to migrate and penetrate in the tumor stroma was considered an ideal characteristic to use them as delivery vehicles. PA imaging showed that MSCs retained their tumor migration capacity and contributed to a more homogeneous distribution of the nanoparticles, as compared to the ones without MSCs. Moreover, a higher tumor growth suppression was achieved after NIR irradiation in a MCF-7-xenografted mouse. Synergism between paclitaxel and PTT was also demonstrated [135]. Xu *et al.* had also used MSCs as delivery systems of plasmonic-magnetic hybrid nanoparticles composed of gold nanorods, iron oxide nanoparticles and doxorubicin. MSCs' C-X-C chemokine receptor type 4 (CXCR4) was upregulated in the presence of iron oxide nanoparticles, which enhanced tumor stroma migration. Biodistribution studies using PA imaging showed that MSCs could enhance the tumor migration and penetration of the nanoparticles after both intravenous and intratumoral injection in a MDA-MB-231 tumor bearing mice. However liver, lung and kidney accumulation also occurred following intravenous administration. Significant anti-cancer effects were also found following NIR irradiation, achieving complete tumor eradication and inhibiting tumor recurrence [136]. Recently, Liang *et al.* reported the use of Cytokine-induced killer (CIK) cells for loading of gold nanostars combined with ICG and trastuzumab. Trimodal imaging (PA, CT and fluorescence imaging) and trimodal therapy (PTT, PDT and immunotherapy) could be integrated into this single nanoplatform. CIK cells could enhance tumor penetration due to their tumor-homing ability, as shown by the biodistribution studies, where a preferentially tumor accumulation was observed. Moreover, combination therapy could effectively inhibit tumor growth and prolong survival time of tumor-xenograted mice. CIK cells could also stimulate the immune system, as shown by the increased levels of cytokine secretion following treatment [155].

### *4.2. Bioaccumulation and toxicity assessment of gold nanomaterials*

In the vast majority of the works, the levels of systemic toxicity induced by gold nanostructures were negligible and, in some cases, loading of chemotherapeutic drugs into the nanostucture could suppress their intrinsic toxicity, such as in the case of doxorubicin-induced cardiotoxicity. Despite that, gold accumulation in organs, such as liver, spleen, kidneys and lungs was frequently observed, in some studies at a higher extend than in the tumor region. This should be further evaluated with detailed pharmacokinetics and toxicological studies conducted over longer periods of time and with multiple doses to assess the safety of these nanosystems. It is well known that the pharmacokinetics and toxicity of gold nanostructures is extremely dependent on the size, shape, surface charge and coating, concentration, route of administration and species and, therefore, a detailed study should be conducted for each type of gold nanoparticle developed [138–140]. The blood half-life of gold nanosystems is extremely variable according to the properties mentioned earlier. It is usually higher for smaller particles and it can be significantly enhanced by coating with PEG, as done is most of these studies [138–140]. Accumulation of gold nanostructures occurs preferentially in the liver and spleen [138–140] although it can also occur to a lesser extend in other organs, such as kidney, heart, spleen, brain, lungs, testis and lymph nodes [140,141]. In some long-term studies, bigger gold nanoparticles (at least 100 nm) could persist in several of these organs for more than 6 months, which highlights the need for long term pharmacokinetics studies [140].The dose of the nanoparticle is also a factor that should be taking into account, as there is a dose-dependent accumulation of gold in most of these organs [140]. The excretion of gold nanoparticles should also be further studied and, whenever possible, improved to avoid long-term accumulation and potential toxicity. The excretion of gold nanoparticles occurs mainly via urinary and hepato-biliary pathways but in a relatively low percentage, as there is persistent accumulation in the liver and spleen [140,142,143]. Renal elimination, however, can be enhanced by coating the nanoparticle with chemical compounds, such as glutathione [140].

Following a detailed and long-term evaluation of the safety and biodistribution of gold nanostructures and improvement of some of these pharmacokinetics parameters, clinical translation of this technology could be accelerated.

### 4.3. Gold mediated PTT - clinical prospects

The studies described in section 4.1 highlight the potential of gold-mediated PTT in the treatment of breast cancer, either in the eradication of the primary tumor (tumor ablation modality) or for the treatment of more advanced stages of disease [24,32,60,63,144,145]. In a future clinical application, this therapeutic may be used either as an alternative to surgery for the removal of the tumor or in combination with other treatments such as chemo and radiotherapy for the management of metastatic disease to attenuate the symptoms and prolong the life time of the patient [24,32,60,63,144–146]. It was also highlighted that gold-mediated PTT could effectively eradicate different breast cancer subtypes including HER2–positive, HR-positive and also TNBC, from which there are still no specific therapies available. This suggests that depending on the surface functionalization of the nanostructure, gold-mediated PTT may be a promising therapy for the remission of the most challenging breast cancer subtypes such as TNBC.

When comparing to conventional therapeutics such as surgery, gold-mediated PTT offers a safer and less invasive alternative, with high tumor accumulation and the possibility of reaching regions which are non-surgically accessible [38]. Depending on the temperature achieved, the tumor can be totally ablated without further intervention [63]. As shown by the studies described in the previous sections, by modulating the properties and characteristics of the gold nanostructure it is feasible to reach these temperatures, at least when using rodent tumor models. Other conventional therapeutics such as chemo and radiotherapy induce high levels of systemic toxicity. In contrast, the effects induced by PTT on the surrounding healthy tissues are negligible [40,41,70,93]. In addition, gold-mediated PTT can be used in combination with these modalities to improve their efficacy and, desirably, reduce their dosages [38]. Another important characteristic of this therapeutic is the imaging contrast provided by gold which may allow the visualization of the tumor and lymph node metastasis on mammographies and also help surgeons in defining the surgical resection margins and therefore enhance both the diagnosis and treatment of the disease [25]. Comparing to other conventional hyperthermia treatments already implemented in some clinical centres, where heat is delivered non-specifically into larger areas of the body, PTT offers the possibility of a more localized and precise treatment, without compromising the surrounding healthy tissues [82]. Other types of nanoparticle-mediated hyperthermia such as magnetic hyperthermia are also being studied. PTT however does not require such an expensive and specific equipment as in the case of magnetic hyperthermia [40,41,70,93]. One challenge that gold-mediated PTT faces is the high costs of manufacture and limited homogeneity among batches, particularly when producing more complex types of nanostructures. Nevertheless, if the therapeutic proves to be effective, the reduction of dosages and associated toxicity and the higher cancer remission may counteract or at least attenuate these costs. Nevertheless whenever possible the use of simpler and more affordable materials and molecules is desirable [147].

There are also some limitations regarding the limited tissue penetration depth of the NIR light, which may affect the penetration in the tumor and the efficacy of the treatment. In breast cancer, however, NIR light has been shown to penetrate the breast tissue for at least 10 cm [148]. Additionally the treatment of deeper-located tumors is also possible through the use of optical fibers [80]. Long-term toxicity and organ accumulation, as discussed in section 4.2, may also be a drawback of this therapeutic and further studies should be conducted to assess this effects before clinical translation. Nevertheless, the use of gold in clinics is not new, and its use for the treatment of other pathologies such as rheumatoid arthritis is well documented [96,149,150]. In fact, recently, gold-mediated PTT has reached clinical trials for the treatment of head and neck, lung and prostate cancer (clinicaltrials.gov, NCT 00848042, NCT 01679470, NCT 04,240,639 and NCT 02680535) with the therapy Aurolase®, which comprises the intravenous administration of silica-core gold-nanoshells combined with NIR laser delivered inside the tumor using an optical fiber. It is then expected that in the near future more gold-mediated PTT may reach this phase and also more cancer types, including breast cancer, may benefit from this therapeutic

## 5. Conclusions

Hyperthermia is a promising approach to improve breast cancer current treatment in several stages of disease. Advanced breast cancer and specific subtypes, such as TNBC, that have poor prognosis and less treatment options available, can benefit from the combination of hyperthermia with radio and/or chemotherapy, while primary tumors can be treated with thermal ablation modality as a safer, less invasive alternative to surgery.

The current clinical use of hyperthermia, however, still faces major challenges including non-uniform tissue heat distribution, absence of rigorous thermal dose administration and lack of precise imaging method for tumor thermal monitoring during treatment. Nanotechnology can have a significant impact in the improvement of hyperthermia therapies, enabling the development of minimally invasive techniques with higher tumor-specificity and a more uniform heat distribution. One of these promising techniques is PTT, which requires simple equipment, i.e., a laser light in the NIR region and a PTT agent and can eradicate tumor lesions with high efficacy and few side-effects. Gold nanostructures are excellent PTT agents due to their biocompatibility, strong NIR absorption and high light-to-heat conversion efficiency, Moreover, their surface can be easily functionalized with tumor cell targeting ligands or therapeutic compounds such as drugs, contributing for the development of targeted multimodal therapies. They are also effective imaging agents for PA or photothermal imaging, enabling the design of theranostic nanoplatforms that can provide precise tumor location and local temperature monitoring, overcoming one of the major drawbacks of the current clinical hyperthermia methods.

Numerous preclinical studies have described the application of gold-mediated PTT in breast cancer management. This therapeutic approach has been effective in the remission of different tumours types, such as HER2-positive or TNBC, demonstrating the versatility of the procedure. In most studies the tumor temperature could be monitored in real-time with high precision. The two hyperthermia modalities, i.e., thermal ablation and hyperthermia, were applied, with tumor temperatures varying from 43 °C to 68 °C among studies. It was also noticeable that the irradiation with NIR light *per se* did not induce any significant anti-tumoral effects. This highlights the importance of nanotechnology, particularly gold nanostructures, to improve clinical hyperthermia.

Different types of gold nanostructures have been employed including gold nanorods, gold nanostars, gold nanoshells, spherical gold nanoparticles and hybrid nanostructures. In most cases gold was coated with different types of polymers to increase their biocompatibility and circulation time. In other cases, hybrid nanostructures were developed comprising organic or inorganic nanomaterials. Active cancer cell targeting was a common strategy to enhance tumor accumulation using different types of cell ligands, antibodies and other molecules, which contributed largely to the enhancement of the tumor eradication by increasing the accumulation of the nanoparticles in the tumor regions. Many studies had also reported the use of theranostic nanoplatforms for simultaneous PTT treatment and nanoparticle biodistribution and tumor monitoring, using either gold or other molecules for imaging contrast. Multimodal therapies comprising PTT and chemo, radio, photodynamic, gene or immunotherapy were also described in several studies with very favourable results obtained from the synergism between these therapies. In most cases, complete tumor eradication was obtained along with inhibition of tumor metastasis and reduction of dosages and adverse side-effects. As mentioned earlier, hyperthermia therapy currently applied in clinical practise is not used alone, but combined with other modalities, such as chemotherapy. Therefore, a nanosystem combining gold nanostructures with other therapeutics is particularly promising for a future clinical translation. This enhances the chances of complete tumor

eradication and simultaneously promotes the reduction of drug, nanoparticles and laser doses. In order to increase drug encapsulation and biocompatibility, the nanosystem should comprise a biocompatible component with a high surface area. In this sense, hybrid nanosystems seem to be the most suitable vehicles for this purpose. Cancer cell active targeting should also be performed, as it significantly impacts the tumor eradication rates. Future studies, however, should also take into account the final costs and the scalability of the nanosystems, incorporating less expensive and complex nanomaterials with simple production methods, whenever possible.

Regarding the modality of emission of the NIR laser, in almost all of the reported studies a continuous-wave laser was used. One of the studies, however, reported the use of a femtosecond laser. The use of a pulsed-mode laser can be an advantage. Due to their very high intensity, those can induce high subcellular temperatures and limit the capacity of the cancer cells to activate thermotolerance mechanisms [41,77]. Moreover, pulsed lasers may promote the formation of micro and nanobubbles around the nanoparticles, which can induce physical cancer cell damage [151]. Additionally, they cause less heat dissipation, and therefore, less damage to the surrounding healthy tissues [41,77]. Due to the benefits of pulsed lasers, it is expected than more studies using them may emerge in the near future.

Although in the majority of the studies the level of toxicity of gold nanomaterials was minimum, further studies on pharmacokinetics, long-term toxicity and organ accumulation should be conducted over longer periods of time.

In most of the studies the intravenous was the preferred route of administration. In approximately 25% of the studies, however, the intratumoral administration route was chosen. This is an interesting and promising approach providing a faster and higher tumor cell internalization and hence, higher efficacy, while limiting non-specific organ accumulation and possibly, long-term toxicity effects [140,142,152,153].

Overall, these results highlight the relevance of nanotechnology and, particularly, gold nanomaterials as effective PTT agents for future breast cancer clinical applications. With the first device Aurolase®, under clinical trials for several types of cancer, it is expected that in the near future more gold-based PTT strategies can reach this stage.

## CRediT authorship contribution statement

**Andreia Granja:** Conceptualization, Writing - original draft. **Marina Pinheiro:** Writing - review & editing. **Célia T. Sousa:** Writing - review & editing. **Salette Reis:** Conceptualization, Funding acquisition, Writing - review & editing.

## Declaration of Competing Interest

The authors declare that they have no known competing financial interests or personal relationships that could have appeared to influence the work reported in this paper.

## Acknowledgements

This work received financial support from PT national funds (FCT/MCTES, Fundação para a Ciência e Tecnologia and Ministério da Ciência, Tecnologia e Ensino Superior) through the project UIDB/50006/2020 (LAQV-REQUIMTE). AG thanks FCT for the grant SFRH/BD/130147/2017 and the Programa Operacional Capital Humano (POCH), specifically the BiotechHealth Programme (Doctoral Programme on Cellular and Molecular Biotechnology Applied to Health Sciences). CTS thanks FCT for financial support through the Investigador FCT program (contract no. IF/01159/2015) and the UE's Horizon 2020 research and innovation program under the Marie Sklodowska-Curie grant no. 734801. MP thanks FCT for financial support through program DL 57/2016—Norma transitória (SFRH/BPD/99124/2013).

## References

[1] F. Bray, J. Ferlay, I. Soerjomataram, R.L. Siegel, L.A. Torre, A. Jemal, Global cancer statistics 2018: GLOBOCAN estimates of incidence and mortality worldwide for 36 cancers in 185 countries, CA Cancer J Clin 68 (6) (2018) 394–424.
[2] C.E. DeSantis, S.A. Fedewa, A. Goding Sauer, J.L. Kramer, R.A. Smith, A. Jemal, Breast cancer statistics, 2015: Convergence of incidence rates between black and white women, CA Cancer J. Clin. 66 (1) (2016) 31–42.
[3] M.V. Dieci, E. Orvieto, M. Dominici, P.F. Conte, V. Guarneri, Rare Breast Cancer Subtypes: Histological, Molecular, and Clinical Peculiarities, Oncologist 19 (8) (2014) 805–813.
[4] V. Kumar, A.K. Abbas, N. Fausto, J.C. Aster, Robbins and Cotran pathologic basis of disease, Elsevier Health Sciences (2014).
[5] K. Polyak, Heterogeneity in breast cancer, J. Clin. Investig. 121 (10) (2011) 3786–3788.
[6] M. Zhang, H.S. Kim, T. Jin, W.K. Moon, Near-infrared photothermal therapy using EGFR-targeted gold nanoparticles increases autophagic cell death in breast cancer, Journal of photochemistry and photobiology, B, Biology 170 (2017) 58–64.
[7] A. Weiss, M. Chavez-MacGregor, D.Y. Lichtensztajn, M. Yi, A. Tadros, G.N. Hortobagyi, S.H. Giordano, K.K. Hunt, E.A. Mittendorf, Validation Study of the American Joint Committee on Cancer Eighth Edition Prognostic Stage Compared With the Anatomic Stage in Breast Cancer, JAMA Oncol 4(2) (2018) 203-209.
[8] S. Fallahpour, T. Navaneelan, P. De, A. Borgo, Breast cancer survival by molecular subtype: a population-based analysis of cancer registry data, CMAJ Open 5 (3) (2017) E734–E739.
[9] N. Howlader, K.A. Cronin, A.W. Kurian, R. Andridge, Differences in Breast Cancer Survival by Molecular Subtypes in the United States, Cancer epidemiology, biomarkers & prevention : a publication of the American Association for Cancer Research, cosponsored by the American Society of Preventive, Oncology 27 (6) (2018) 619–626.
[10] R.L. Siegel, K.D. Miller, A. Jemal, Cancer statistics, 2020, CA: A Cancer Journal for Clinicians 70(1) (2020) 7-30.
[11] C.E. DeSantis, J. Ma, M.M. Gaudet, L.A. Newman, K.D. Miller, A. Goding Sauer, A. Jemal, R.L. Siegel, Breast cancer statistics, 2019, CA: a cancer journal for clinicians 69(6) (2019) 438-451.
[12] A. Goldhirsch, J.N. Ingle, R. Gelber, A. Coates, B. Thürlimann, H.-J. Senn, Thresholds for therapies: highlights of the St Gallen International Expert Consensus on the primary therapy of early breast cancer 2009, Ann. Oncol. 20 (8) (2009) 1319–1329.
[13] M. Castiglione, M.J. Piccart, Adjuvant therapy for breast cancer, Springer, New York, 2009.
[14] P.K.H. Morrow, F. Zambrana, F.J. Esteva, Recent advances in systemic therapy: Advances in systemic therapy for HER2-positive metastatic breast cancer, Breast Cancer Res. 11 (4) (2009) 207.
[15] E. Blanco, M. Ferrari, Emerging nanotherapeutic strategies in breast cancer, The Breast 23 (1) (2014) 10–18.
[16] D. Pooja, H. Kulhari, M. Kuncha, S.S. Rachamalla, D.J. Adams, V. Bansal, R. Sistla, Improving Efficacy, Oral Bioavailability, and Delivery of Paclitaxel Using Protein-Grafted Solid Lipid Nanoparticles, Mol. Pharm. 13 (11) (2016) 3903–3912.
[17] C.L. Shapiro, A. Recht, Side effects of adjuvant treatment of breast cancer, N. Engl. J. Med. 344 (26) (2001) 1997–2008.
[18] X. Bai, J. Ni, J. Beretov, P. Graham, Y. Li, Cancer stem cell in breast cancer therapeutic resistance, Cancer Treat. Rev. 69 (2018) 152–163.
[19] J.S. Chawla, M.M. Amiji, Biodegradable poly (ε-caprolactone) nanoparticles for tumor-targeted delivery of tamoxifen, Int. J. Pharm. 249 (1) (2002) 127–138.
[20] M.J. Mourits, E.G. De Vries, P.H. Willemse, K.A. Ten Hoor, H. Hollema, A.G. Van der Zee, Tamoxifen treatment and gynecologic side effects: a review, Obstet. Gynecol. 97 (5) (2001) 855–866.
[21] L.A. Emens, Breast Cancer Immunotherapy: Facts and Hopes, Clinical cancer research : an official journal of the American Association for, Cancer Res. 24 (3) (2018) 511–520.
[22] G. Bottai, M. Truffi, F. Corsi, L. Santarpia, Progress in nonviral gene therapy for breast cancer and what comes next? Expert Opin Biol Ther 17 (5) (2017) 595–611.
[23] S.M. Banerjee, A.J. MacRobert, C.A. Mosse, B. Periera, S.G. Bown, M.R. S. Keshtgar, Photodynamic therapy: Inception to application in breast cancer, Breast (Edinburgh, Scotland) 31 (2017) 105–113.
[24] T.M. Zagar, J.R. Oleson, Z. Vujaskovic, M.W. Dewhirst, O.I. Craciunescu, K. L. Blackwell, L.R. Prosnitz, E.L. Jones, Hyperthermia for locally advanced breast cancer, International journal of hyperthermia : the official journal of European Society for Hyperthermic Oncology, North American Hyperthermia, Group 26 (7) (2010) 618–624.
[25] J. Lee, D.K. Chatterjee, M.H. Lee, S. Krishnan, Gold nanoparticles in breast cancer treatment: promise and potential pitfalls, Cancer Lett 347 (1) (2014) 46–53.
[26] P. Falagan-Lotsch, E.M. Grzincic, C.J. Murphy, New Advances in Nanotechnology-Based Diagnosis and Therapeutics for Breast Cancer: An Assessment of Active-Targeting Inorganic Nanoplatforms, Bioconjug Chem 28 (1) (2017) 135–152.
[27] C.C. Vernon, J.W. Hand, S.B. Field, D. Machin, J.B. Whaley, J. van der Zee, W. L. van Putten, G.C. van Rhoon, J.D. van Dijk, D. Gonzalez Gonzalez, F.F. Liu, P. Goodman, M. Sherar, Radiotherapy with or without hyperthermia in the treatment of superficial localized breast cancer: results from five randomized

controlled trials. International Collaborative Hyperthermia Group, International journal of radiation oncology, biology, physics 35 (4) (1996) 731–744.
[28] E.L. Jones, J.R. Oleson, L.R. Prosnitz, T.V. Samulski, Z. Vujaskovic, D. Yu, L. L. Sanders, M.W. Dewhirst, Randomized trial of hyperthermia and radiation for superficial tumors, J. Clin. Oncol. 23 (13) (2005) 3079–3085.
[29] T. Refaat, S. Sachdev, V. Sathiaseelan, I. Helenowski, S. Abdelmoneim, M. C. Pierce, G. Woloschak, W. Small, B. Mittal, K.D. Kiel, Hyperthermia and radiation therapy for locally advanced or recurrent breast cancer, The Breast 24 (4) (2015) 418–425.
[30] D. Gonzalez Gonzalez, J.D. van Dijk, L.E. Blank, Chestwall recurrences of breast cancer: results of combined treatment with radiation and hyperthermia, Radiotherapy and oncology : journal of the European Society for Therapeutic Radiology and Oncology 12(2) (1988) 95-103.
[31] N.R. Datta, E. Puric, D. Klingbiel, S. Gomez, S. Bodis, Hyperthermia and Radiation Therapy in Locoregional Recurrent Breast Cancers: A Systematic Review and Meta-analysis, International Journal of Radiation Oncology*Biology*Physics 94 (5) (2016) 1073–1087.
[32] Z. Vujaskovic, D.W. Kim, E. Jones, L. Lan, L. McCall, M.W. Dewhirst, O. Craciunescu, P. Stauffer, V. Liotcheva, A. Betof, K. Blackwell, A phase I/II study of neoadjuvant liposomal doxorubicin, paclitaxel, and hyperthermia in locally advanced breast cancer, International journal of hyperthermia : the official journal of European Society for Hyperthermic Oncology, North American Hyperthermia, Group 26 (5) (2010) 514–521.
[33] T.M. Zagar, Z. Vujaskovic, S. Formenti, H. Rugo, F. Muggia, B. O'Connor, R. Myerson, P. Stauffer, I.-C. Hsu, C. Diederich, Two phase I dose-escalation/pharmacokinetics studies of low temperature liposomal doxorubicin (LTLD) and mild local hyperthermia in heavily pretreated patients with local regionally recurrent breast cancer, Int. J. Hyperth. 30 (5) (2014) 285–294.
[34] T. Nguyen, E. Hattery, V.P. Khatri, Radiofrequency ablation and breast cancer: a review, Gland surgery 3 (2) (2014) 128–135.
[35] B.A. Grotenhuis, W.W. Vrijland, T.M.A.L. Klem, Radiofrequency ablation for early-stage breast cancer: Treatment outcomes and practical considerations, European Journal of Surgical Oncology (EJSO) 39 (12) (2013) 1317–1324.
[36] Y. Kerbage, N. Betrouni, P. Collinet, H. Azaïs, S. Mordon, A.-S. Dewalle-Vignion, B. Merlot, Laser interstitial thermotherapy application for breast surgery: Current situation and new trends, The Breast 33 (2017) 145–152.
[37] M.S. Sabel, Nonsurgical ablation of breast cancer: future options for small breast tumors, Surg Oncol Clin N Am 23 (3) (2014) 593–608.
[38] D. Jaque, L.M. Maestro, B. Del Rosal, P. Haro-Gonzalez, A. Benayas, J. Plaza, E. M. Rodriguez, J.G. Sole, Nanoparticles for photothermal therapies, nanoscale 6 (16) (2014) 9494–9530.
[39] E.A. Hussein, M.M. Zagho, G.K. Nasrallah, A.A. Elzatahry, Recent advances in functional nanostructures as cancer photothermal therapy, Int J Nanomedicine 13 (2018) 2897.
[40] N.S. Abadeer, C.J. Murphy, Recent progress in cancer thermal therapy using gold nanoparticles, The Journal of Physical Chemistry C 120 (9) (2016) 4691–4716.
[41] S. Sharma, N. Shrivastava, F. Rossi, N.T.K. Thanh, Nanoparticles-based magnetic and photo induced hyperthermia for cancer treatment, Nano Today 100795 (2019).
[42] M. Seegenschmiedt, C. Vernon, A historical perspective on hyperthermia in oncology, Springer, Thermoradiotherapy and thermochemotherapy, 1995, pp. 3–44.
[43] P.R. Stauffer, Evolving technology for thermal therapy of cancer, Int. J. Hyperth. 21 (8) (2005) 731–744.
[44] R.W. Habash, R. Bansal, D. Krewski, H.T. Alhafid, Thermal therapy, part 1: an introduction to thermal therapy, Critical Reviews™, Biomed. Eng. 34 (6) (2006).
[45] R.W.Y. Habash, Chapter 53 - Therapeutic hyperthermia, in: A.A. Romanovsky (Ed.), Handbook of Clinical Neurology, Elsevier2018, pp. 853-868.
[46] J.C. Peeken, P. Vaupel, S.E. Combs, Integrating Hyperthermia into Modern Radiation Oncology: What Evidence Is Necessary? Front. Oncol. 7 (132) (2017).
[47] A.L. Oei, L.E.M. Vriend, P.M. Krawczyk, M.R. Horsman, N.A.P. Franken, J. Crezee, Targeting therapy-resistant cancer stem cells by hyperthermia, International journal of hyperthermia : the official journal of European Society for Hyperthermic Oncology, North American Hyperthermia, Group 33 (4) (2017) 419–427.
[48] C.-H. Hou, F.-L. Lin, S.-M. Hou, J.-F. Liu, Hyperthermia induces apoptosis through endoplasmic reticulum and reactive oxygen species in human osteosarcoma cells, Int. J. Mol. Sci. 15 (10) (2014) 17380–17395.
[49] J. van der Zee, Heating the patient: a promising approach?, Annals of oncology : official journal of the European Society for, Med. Oncol. 13 (8) (2002) 1173–1184.
[50] E.J. Hall, L. Roizin-Towle, Biological effects of heat, Cancer Res 44 (10 Suppl) (1984) 4708s–4713s.
[51] Z. Vujaskovic, E. Rosen, K. Blackwell, E. Jones, D. Brizel, L. Prosnitz, T. Samulski, M. Dewhirst, Ultrasound guided pO 2 measurement of breast cancer reoxygenation after neoadjuvant chemotherapy and hyperthermia treatment, Int. J. Hyperth. 19 (5) (2003) 498–506.
[52] E.L. Jones, L.R. Prosnitz, M.W. Dewhirst, P.K. Marcom, P.H. Hardenbergh, L. B. Marks, D.M. Brizel, Z. Vujaskovic, Thermochemoradiotherapy improves oxygenation in locally advanced breast cancer, Clinical cancer research : an official journal of the American Association for, Cancer Res. 10 (13) (2004) 4287–4293.
[53] S. Toraya-Brown, S. Fiering, Local tumour hyperthermia as immunotherapy for metastatic cancer, International journal of hyperthermia : the official journal of European Society for Hyperthermic Oncology, North American Hyperthermia, Group 30 (8) (2014) 531–539.
[54] R. Issels, E. Kampmann, R. Kanaar, L.H. Lindner, Hallmarks of hyperthermia in driving the future of clinical hyperthermia as targeted therapy: translation into clinical application, Int. J. Hyperth. 32 (1) (2016) 89–95.
[55] M. Hurwitz, P. Stauffer, Hyperthermia, radiation and chemotherapy: the role of heat in multidisciplinary cancer care, Seminars in oncology, Elsevier (2014) 714–729.
[56] M. Mallory, E. Gogineni, G.C. Jones, L. Greer, C.B. Simone, Therapeutic hyperthermia: The old, the new, and the upcoming, Critical Reviews in Oncology/Hematology 97 (2016) 56–64.
[57] R.D. Issels, Hyperthermia adds to chemotherapy, Eur. J. Cancer 44 (17) (2008) 2546–2554.
[58] M.R. Horsman, J. Overgaard, Hyperthermia: a potent enhancer of radiotherapy, Clinical oncology 19 (6) (2007) 418–426.
[59] P. Wust, B. Hildebrandt, G. Sreenivasa, B. Rau, J. Gellermann, H. Riess, R. Felix, P.M. Schlag, Hyperthermia in combined treatment of cancer, Lancet Oncol. 3 (8) (2002) 487–497.
[60] K.F. Chu, D.E. Dupuy, Thermal ablation of tumours: biological mechanisms and advances in therapy, Nat. Rev. Cancer 14 (3) (2014) 199–208.
[61] A. Mehta, R. Oklu, R.A. Sheth, Thermal Ablative Therapies and Immune Checkpoint Modulation: Can Locoregional Approaches Effect a Systemic Response? Gastroenterol Res Pract 2016 (2016), 9251375-9251375.
[62] H. Takaki, F. Cornelis, Y. Kako, K. Kobayashi, N. Kamikonya, K. Yamakado, Thermal ablation and immunomodulation: From preclinical experiments to clinical trials, Diagn. Interventional Imaging 98 (9) (2017) 651–659.
[63] S.P. Haen, P.L. Pereira, H.R. Salih, H.G. Rammensee, C. Gouttefangeas, More than just tumor destruction: immunomodulation by thermal ablation of cancer, Clin Dev Immunol 2011 (2011), 160250.
[64] P. Prakash, D. Haemmerich, Introduction to microwave tumour ablation special issue, International journal of hyperthermia: the official journal of European Society for Hyperthermic Oncology, North American Hyperthermia Group 33 (1) (2017) 1.
[65] T.M. Zagar, K.A. Higgins, E.F. Miles, Z. Vujaskovic, M.W. Dewhirst, R.W. Clough, L.R. Prosnitz, E.L. Jones, Durable palliation of breast cancer chest wall recurrence with radiation therapy, hyperthermia, and chemotherapy, Radiotherapy and oncology : journal of the European Society for Therapeutic Radiology and Oncology 97 (3) (2010) 535–540.
[66] D.F. Emerich, C.G. Thanos, Nanotechnology and medicine, Expert Opin. Biol. Ther. 3 (4) (2003) 655–663.
[67] A.G. Cuenca, H. Jiang, S.N. Hochwald, M. Delano, W.G. Cance, S.R. Grobmyer, Emerging implications of nanotechnology on cancer diagnostics and therapeutics, Cancer 107 (3) (2006) 459–466.
[68] P. Grodzinski, M. Kircher, M. Goldberg, A. Gabizon, Integrating nanotechnology into cancer care, ACS Publications (2019).
[69] N. Bertrand, J. Wu, X. Xu, N. Kamaly, O.C. Farokhzad, Cancer nanotechnology: the impact of passive and active targeting in the era of modern cancer biology, Adv. Drug Deliv. Rev. 66 (2014) 2–25.
[70] D.K. Chatterjee, P. Diagaradjane, S. Krishnan, Nanoparticle-mediated hyperthermia in cancer therapy, Ther Deliv 2 (8) (2011) 1001–1014.
[71] P. Kaur, M.L. Aliru, A.S. Chadha, A. Asea, S. Krishnan, Hyperthermia using nanoparticles–Promises and pitfalls, International journal of hyperthermia : the official journal of European Society for Hyperthermic Oncology, North American Hyperthermia, Group 32 (1) (2016) 76–88.
[72] M. Zhou, J. Zhao, M. Tian, S. Song, R. Zhang, S. Gupta, D. Tan, H. Shen, M. Ferrari, C. Li, Radio-photothermal therapy mediated by a single compartment nanoplatform depletes tumor initiating cells and reduces lung metastasis in the orthotopic 4T1 breast tumor model, Nanoscale 7 (46) (2015) 19438–19447.
[73] J.A. Kemp, M.S. Shim, C.Y. Heo, Y.J. Kwon, "Combo" nanomedicine: Co-delivery of multi-modal therapeutics for efficient, targeted, and safe cancer therapy, Adv. Drug Deliv. Rev. 98 (2016) 3–18.
[74] G.A. Koning, A.M.M. Eggermont, L.H. Lindner, T.L.M. ten Hagen, Hyperthermia and thermosensitive liposomes for improved delivery of chemotherapeutic drugs to solid tumors, Pharm. Res. 27 (8) (2010) 1750–1754.
[75] Q. Ban, T. Bai, X. Duan, J. Kong, Noninvasive photothermal cancer therapy nanoplatforms via integrating nanomaterials and functional polymers, Biomater. Sci. 5 (2) (2017) 190–210.
[76] A.C.V. Doughty, A.R. Hoover, E. Layton, C.K. Murray, E.W. Howard, W.R. Chen, Nanomaterial Applications in Photothermal Therapy for Cancer, Materials (Basel) 12 (5) (2019) 779.
[77] T. Nunes, T. Pons, X. Hou, K. Van Do, B. Caron, M. Rigal, M. Di Benedetto, B. Palpant, C. Leboeuf, A. Janin, G. Bousquet, Pulsed-laser irradiation of multifunctional gold nanoshells to overcome trastuzumab resistance in HER2-overexpressing breast cancer, J Exp Clin Cancer Res 38 (1) (2019), 306-306.
[78] A. Sahu, M. Kim, J. Ryu, J.-G. Son, E. Lee, G. Tae, Nanographene oxide as a switch for CW/pulsed NIR laser triggered drug release from liposomes, Mater. Sci. Eng., C 82 (2018) 19–24.
[79] Y. Liu, P. Bhattarai, Z. Dai, X. Chen, Photothermal therapy and photoacoustic imaging via nanotheranostics in fighting cancer, Chem. Soc. Rev. 48 (7) (2019) 2053–2108.
[80] E.B. Dickerson, E.C. Dreaden, X. Huang, I.H. El-Sayed, H. Chu, S. Pushpanketh, J. F. McDonald, M.A. El-Sayed, Gold nanorod assisted near-infrared plasmonic photothermal therapy (PPTT) of squamous cell carcinoma in mice, Cancer Lett. 269 (1) (2008) 57–66.
[81] Y. Chen, L. Li, W. Chen, H. Chen, J. Yin, Near-infrared small molecular fluorescent dyes for photothermal therapy, Chin. Chem. Lett. 30 (7) (2019) 1353–1360.

[82] B. Guo, G. Feng, P.N. Manghnani, X. Cai, J. Liu, W. Wu, S. Xu, X. Cheng, C. Teh, B. Liu, A porphyrin-based conjugated polymer for highly efficient in vitro and in vivo photothermal therapy, Small 12 (45) (2016) 6243–6254.

[83] R. Lv, D. Wang, L. Xiao, G. Chen, J. Xia, P.N. Prasad, Stable ICG-loaded upconversion nanoparticles: silica core/shell theranostic nanoplatform for dual-modal upconversion and photoacoustic imaging together with photothermal therapy, Sci. Rep. 7 (1) (2017) 1–11.

[84] F. Wu, L. Chen, L. Yue, K. Wang, K. Cheng, J. Chen, X. Luo, T. Zhang, Small-molecule porphyrin-based organic nanoparticles with remarkable photothermal conversion efficiency for in vivo photoacoustic imaging and photothermal therapy, ACS Appl. Mater. Interfaces 11 (24) (2019) 21408–21416.

[85] X. Zheng, D. Xing, F. Zhou, B. Wu, W.R. Chen, Indocyanine green-containing nanostructure as near infrared dual-functional targeting probes for optical imaging and photothermal therapy, Mol. Pharm. 8 (2) (2011) 447–456.

[86] J. Estelrich, M.A. Busquets, Iron oxide nanoparticles in photothermal therapy, Molecules (Basel, Switzerland) 23 (7) (2018) 1567.

[87] A. Espinosa, R. Di Corato, J. Kolosnjaj-Tabi, P. Flaud, T. Pellegrino, C. Wilhelm, Duality of iron oxide nanoparticles in cancer therapy: amplification of heating efficiency by magnetic hyperthermia and photothermal bimodal treatment, ACS Nano 10 (2) (2016) 2436–2446.

[88] Z.M. Markovic, L.M. Harhaji-Trajkovic, B.M. Todorovic-Markovic, D.P. Kepić, K. M. Arsikin, S.P. Jovanovic, A.C. Pantovic, M.D. Dramicanin, V.S. Trajkovic, In vitro comparison of the photothermal anticancer activity of graphene nanoparticles and carbon nanotubes, Biomaterials 32 (4) (2011) 1121–1129.

[89] A. Sahu, W.I. Choi, J.H. Lee, G. Tae, Graphene oxide mediated delivery of methylene blue for combined photodynamic and photothermal therapy, Biomaterials 34 (26) (2013) 6239–6248.

[90] C.T. Matea, T. Mocan, F. Tabaran, T. Pop, O. Mosteanu, C. Puia, C. Iancu, L. Mocan, Quantum dots in imaging, drug delivery and sensor applications, Int J Nanomedicine 12 (2017) 5421–5431.

[91] S.H. Hu, Y.W. Chen, W.T. Hung, I.W. Chen, S.Y. Chen, Quantum-dot-tagged reduced graphene oxide nanocomposites for bright fluorescence bioimaging and photothermal therapy monitored in situ, Adv. Mater. 24 (13) (2012) 1748–1754.

[92] M. Chu, X. Pan, D. Zhang, Q. Wu, J. Peng, W. Hai, The therapeutic efficacy of CdTe and CdSe quantum dots for photothermal cancer therapy, Biomaterials 33 (29) (2012) 7071–7083.

[93] A. Espinosa, J. Kolosnjaj-Tabi, A. Abou-Hassan, A. Plan Sangnier, A. Curcio, A. K. Silva, R. Di Corato, S. Neveu, T. Pellegrino, L.M. Liz-Marzán, Magnetic (hyper) thermia or photothermia? Progressive comparison of iron oxide and gold nanoparticles heating in water, in cells, and in vivo, Adv. Funct. Mater. 28 (37) (2018) 1803660.

[94] D. Zhong, J. Zhao, Y. Li, Y. Qiao, Q. Wei, J. He, T. Xie, W. Li, M. Zhou, Laser-triggered aggregated cubic alpha-Fe2O3@Au nanocomposites for magnetic resonance imaging and photothermal/enhanced radiation synergistic therapy, Biomaterials 219 (2019), 119369.

[95] S. Yu, G. Huang, R. Yuan, T. Chen, A uPAR targeted nanoplatform with an NIR laser-responsive drug release property for tri-modal imaging and synergistic photothermal-chemotherapy of triple-negative breast cancer, Biomater. Sci. (2020).

[96] G.B. Bluhm, The treatment of rheumatoid arthritis with gold, Semin. Arthritis Rheum. 5 (2) (1975) 147–166.

[97] P. Manivasagan, S. Bharathiraja, M. Santha Moorthy, S. Mondal, T.P. Nguyen, H. Kim, T.T.V. Phan, K.D. Lee, J. Oh, Biocompatible Chitosan Oligosaccharide Modified Gold Nanorods as Highly Effective Photothermal Agents for Ablation of Breast Cancer Cells, Polymers (Basel) 10 (3) (2018) 232.

[98] W. Xu, J. Qian, G. Hou, Y. Wang, J. Wang, T. Sun, L. Ji, A. Suo, Y. Yao, PEGylated hydrazided gold nanorods for pH-triggered chemo/photodynamic/photothermal triple therapy of breast cancer, Acta Biomater. 82 (2018) 171–183.

[99] C. Xu, F. Chen, H.F. Valdovinos, D. Jiang, S. Goel, B. Yu, H. Sun, T.E. Barnhart, J. J. Moon, W. Cai, Bacteria-like mesoporous silica-coated gold nanorods for positron emission tomography and photoacoustic imaging-guided chemo-photothermal combined therapy, Biomaterials 165 (2018) 56–65.

[100] L. Liu, H.-J. Xie, L.-M. Mu, R. Liu, Z.-B. Su, Y.-N. Cui, Y. Xie, W.-L. Lu, Functional chlorin gold nanorods enable to treat breast cancer by photothermal/photodynamic therapy, Int J Nanomedicine 13 (2018) 8119–8135.

[101] J.S. Suk, Q. Xu, N. Kim, J. Hanes, L.M. Ensign, PEGylation as a strategy for improving nanoparticle-based drug and gene delivery, Adv. Drug Deliv. Rev. 99 (Pt A) (2016) 28–51.

[102] J. Liu, H. Liang, M. Li, Z. Luo, J. Zhang, X. Guo, K. Cai, Tumor acidity activating multifunctional nanoplatform for NIR-mediated multiple enhanced photodynamic and photothermal tumor therapy, Biomaterials 157 (2018) 107–124.

[103] M. Zhang, H.S. Kim, T. Jin, J. Woo, Y.J. Piao, W.K. Moon, Near-infrared photothermal therapy using anti-EGFR-gold nanorod conjugates for triple negative breast cancer, Oncotarget 8 (49) (2017) 86566–86575.

[104] X. Kang, X. Guo, X. Niu, W. An, S. Li, Z. Liu, Y. Yang, N. Wang, Q. Jiang, C. Yan, H. Wang, Q. Zhang, Photothermal therapeutic application of gold nanorods-porphyrin-trastuzumab complexes in HER2-positive breast cancer, Sci. Rep. 7 (2017), 42069-42069.

[105] W. Xu, J. Qian, G. Hou, A. Suo, Y. Wang, J. Wang, T. Sun, M. Yang, X. Wan, Y. Yao, Hyaluronic Acid-Functionalized Gold Nanorods with pH/NIR Dual-Responsive Drug Release for Synergetic Targeted Photothermal Chemotherapy of Breast Cancer, ACS Appl Mater Interfaces 9 (42) (2017) 36533–36547.

[106] W. Xu, J. Qian, G. Hou, Y. Wang, J. Wang, T. Sun, L. Ji, A. Suo, Y. Yao, A dual-targeted hyaluronic acid-gold nanorod platform with triple-stimuli responsiveness for photodynamic/photothermal therapy of breast cancer, Acta Biomater 83 (2019) 400–413.

[107] D. Wang, T. Wang, Z. Xu, H. Yu, B. Feng, J. Zhang, C. Guo, Q. Yin, Z. Zhang, Y. Li, Cooperative Treatment of Metastatic Breast Cancer Using Host-Guest Nanoplatform Coloaded with Docetaxel and siRNA, Small 12 (4) (2016) 488–498.

[108] C. Xu, T. Zhang, G. Lu, K. Chen, J. Tao, Y. Zhang, Z. Teng, B. Yang, Disulfiram-gold-nanorod integrate for effective tumor targeting and photothermal-chemical synergistic therapy, Biomater. Sci. 8 (12) (2020) 3310–3319.

[109] D. Cheng, Y. Ji, B. Wang, Y. Wang, Y. Tang, Y. Fu, Y. Xu, X. Qian, W. Zhu, Dual-responsive nanohybrid based on degradable silica-coated gold nanorods for triple-combination therapy for breast cancer, Acta Biomater. (2021).

[110] A.C. del Valle, C.-K. Su, Y.-C. Sun, Y.-F. Huang, NIR-cleavable drug adducts of gold nanostars for overcoming multidrug-resistant tumors, Biomaterials, Science (2020).

[111] Y. Liu, H. Yuan, F.R. Kersey, J.K. Register, M.C. Parrott, T. Vo-Dinh, Plasmonic gold nanostars for multi-modality sensing and diagnostics, Sensors (Basel, Switzerland) 15 (2) (2015) 3706–3720.

[112] Y.-H. You, Y.-F. Lin, B. Nirosha, H.-T. Chang, Y.-F. Huang, Polydopamine-coated gold nanostar for combined antitumor and antiangiogenic therapy in multidrug-resistant breast cancer, Nanotheranostics 3 (3) (2019) 266–283.

[113] S. Wang, Y. Tian, W. Tian, J. Sun, S. Zhao, Y. Liu, C. Wang, Y. Tang, X. Ma, Z. Teng, G. Lu, Selectively Sensitizing Malignant Cells to Photothermal Therapy Using a CD44-Targeting Heat Shock Protein 72 Depletion Nanosystem, ACS Nano 10 (9) (2016) 8578–8590.

[114] Z. Li, F. Yang, D. Wu, Y. Liu, Y. Gao, H. Lian, H. Zhang, Z. Yin, A. Wu, L. Zeng, Ce6-Conjugated and polydopamine-coated gold nanostars with enhanced photoacoustic imaging and photothermal/photodynamic therapy to inhibit lung metastasis of breast cancer, Nanoscale 12 (43) (2020) 22173–22184.

[115] H.S. Han, K.Y. Choi, H. Lee, M. Lee, J.Y. An, S. Shin, S. Kwon, D.S. Lee, J.H. Park, Gold-Nanoclustered Hyaluronan Nano-Assemblies for Photothermally Maneuvered Photodynamic Tumor Ablation, ACS Nano 10 (12) (2016) 10858–10868.

[116] S. Lee, C. Lee, S. Park, K. Lim, S.S. Kim, J.O. Kim, E.S. Lee, K.T. Oh, H.G. Choi, Y. S. Youn, Facile fabrication of highly photothermal-effective albumin-assisted gold nanoclusters for treating breast cancer, Int J Pharm 553 (1–2) (2018) 363–374.

[117] R.C. Qian, Y. Cao, Y.T. Long, Binary System for MicroRNA-Targeted Imaging in Single Cells and Photothermal Cancer Therapy, Anal. Chem. 88 (17) (2016) 8640–8647.

[118] J. Wang, Y. Zhang, N. Jin, C. Mao, M. Yang, Protein-Induced Gold Nanoparticle Assembly for Improving the Photothermal Effect in Cancer Therapy, ACS Appl Mater Interfaces 11 (12) (2019) 11136–11143.

[119] Y. Xia, X. Wu, J. Zhao, J. Zhao, Z. Li, W. Ren, Y. Tian, A. Li, Z. Shen, A. Wu, Three dimensional plasmonic assemblies of AuNPs with an overall size of sub-200 nm for chemo-photothermal synergistic therapy of breast cancer, Nanoscale 8 (44) (2016) 18682–18692.

[120] J. Zhao, M. Wallace, M.P. Melancon, Cancer theranostics with gold nanoshells, Nanomedicine (London, England) 9 (13) (2014) 2041–2057.

[121] P. Xu, R. Wang, W. Yang, Y. Liu, D. He, Z. Ye, D. Chen, Y. Ding, J. Tu, Y. Shen, A DM1-doped porous gold nanoshell system for NIR accelerated redox-responsive release and triple modal imaging guided photothermal synergistic chemotherapy, Journal of nanobiotechnology 19 (1) (2021) 1–19.

[122] D. Zheng, C. Wan, H. Yang, L. Xu, Q. Dong, C. Du, J. Du, F. Li, Her2-Targeted Multifunctional Nano-Theranostic Platform Mediates Tumor Microenvironment Remodeling and Immune Activation for Breast Cancer Treatment, Int J Nanomedicine 15 (2020) 10007.

[123] A. Espinosa, M. Bugnet, G. Radtke, S. Neveu, G.A. Botton, C. Wilhelm, A. Abou-Hassan, Can magneto-plasmonic nanohybrids efficiently combine photothermia with magnetic hyperthermia? Nanoscale 7 (45) (2015) 18872–18877.

[124] B. Pang, Y. Zhao, H. Luehmann, X. Yang, L. Detering, M. You, C. Zhang, L. Zhang, Z.Y. Li, Q. Ren, Y. Liu, Y. Xia, (6)(4)Cu-Doped PdCu@Au Tripods: A Multifunctional Nanomaterial for Positron Emission Tomography and Image-Guided Photothermal Cancer Treatment, ACS Nano 10 (3) (2016) 3121–3131.

[125] G. Cui, P. He, L. Yu, C. Wen, X. Xie, G. Yao, Oxygen self-enriched nanoplatform combined with US imaging and chemo/photothermal therapy for breast cancer, Nanomedicine: Nanotechnology, Biology and Medicine 29 (2020), 102238.

[126] G. Yang, Z. Liu, Y. Li, Y. Hou, X. Fei, C. Su, S. Wang, Z. Zhuang, Z. Guo, Facile synthesis of black phosphorus-Au nanocomposites for enhanced photothermal cancer therapy and surface-enhanced Raman scattering analysis, Biomater Sci 5 (10) (2017) 2048–2055.

[127] F. Wang, Q. Sun, B. Feng, Z. Xu, J. Zhang, J. Xu, L. Lu, H. Yu, M. Wang, Y. Li, W. Zhang, Polydopamine-Functionalized Graphene Oxide Loaded with Gold Nanostars and Doxorubicin for Combined Photothermal and Chemotherapy of Metastatic Breast Cancer, Adv. Healthcare Mater. 5 (17) (2016) 2227–2236.

[128] J. Zhang, X. Luo, Y.P. Wu, F. Wu, Y.F. Li, R.R. He, M. Liu, Rod in Tube: A Novel Nanoplatform for Highly Effective Chemo-Photothermal Combination Therapy toward Breast Cancer, ACS Appl Mater Interfaces 11 (4) (2019) 3690–3703.

[129] Q. Huang, S. Zhang, H. Zhang, Y. Han, H. Liu, F. Ren, Q. Sun, Z. Li, M. Gao, Boosting the Radiosensitizing and Photothermal Performance of Cu2- xSe Nanocrystals for Synergetic Radiophotothermal Therapy of Orthotopic Breast Cancer, ACS Nano 13 (2) (2019) 1342–1353.

[130] Y. Li, D. He, J. Tu, R. Wang, C. Zu, Y. Chen, W. Yang, D. Shi, T.J. Webster, Y. Shen, The comparative effect of wrapping solid gold nanoparticles and hollow gold nanoparticles with doxorubicin-loaded thermosensitive liposomes for cancer thermo-chemotherapy, Nanoscale 10 (18) (2018) 8628–8641.

[131] V.D. Nguyen, H.K. Min, C.S. Kim, J. Han, J.O. Park, E. Choi, Folate receptor-targeted liposomal nanocomplex for effective synergistic photothermal-

chemotherapy of breast cancer in vivo, Colloids Surf B Biointerfaces 173 (2019) 539–548.
[132] L. Zhang, C. Liu, Y. Gao, Z. Li, J. Xing, W. Ren, L. Zhang, A. Li, G. Lu, A. Wu, L. Zeng, ZD2-Engineered Gold Nanostar@Metal-Organic Framework Nanoprobes for T1 -Weighted Magnetic Resonance Imaging and Photothermal Therapy Specifically Toward Triple-Negative Breast Cancer, Adv. Healthcare Mater. 7 (24) (2018), e1801144.
[133] M. Li, L. Li, C. Zhan, D.S. Kohane, Core-Shell Nanostars for Multimodal Therapy and Imaging, Theranostics 6 (13) (2016) 2306–2313.
[134] Q. Ni, Z. Teng, M. Dang, Y. Tian, Y. Zhang, P. Huang, X. Su, N. Lu, Z. Yang, W. Tian, S. Wang, W. Liu, Y. Tang, G. Lu, L. Zhang, Gold nanorod embedded large-pore mesoporous organosilica nanospheres for gene and photothermal cooperative therapy of triple negative breast cancer, Nanoscale 9 (4) (2017) 1466–1474.
[135] J. Wu, Y. Liu, Y. Tang, S. Wang, C. Wang, Y. Li, X. Su, J. Tian, Y. Tian, J. Pan, Y. Su, H. Zhu, Z. Teng, G. Lu, Synergistic Chemo-Photothermal Therapy of Breast Cancer by Mesenchymal Stem Cell-Encapsulated Yolk-Shell GNR@HPMO-PTX Nanospheres, ACS Appl Mater Interfaces 8 (28) (2016) 17927–17935.
[136] C. Xu, Q. Feng, H. Yang, G. Wang, L. Huang, Q. Bai, C. Zhang, Y. Wang, Y. Chen, Q. Cheng, M. Chen, Y. Han, Z. Yu, M.S. Lesniak, Y. Cheng, A Light-Triggered Mesenchymal Stem Cell Delivery System for Photoacoustic Imaging and Chemo-Photothermal Therapy of Triple Negative Breast Cancer, Adv Sci (Weinh) 5 (10) (2018), 1800382-1800382.
[137] V.D. Nguyen, H.-K. Min, D.-H. Kim, C.-S. Kim, J. Han, J.-O. Park, E. Choi, Macrophage-Mediated Delivery of Multifunctional Nanotherapeutics for Synergistic Chemo-photothermal Therapy of Solid Tumors, ACS Appl. Mater. Interfaces (2020).
[138] M. Aborig, P.R.V. Malik, S. Nambiar, P. Chelle, J. Darko, A. Mutsaers, A. N. Edginton, A. Fleck, E. Osei, S. Wettig, Biodistribution and Physiologically-Based Pharmacokinetic Modeling of Gold Nanoparticles in Mice with Interspecies Extrapolation, Pharmaceutics 11 (4) (2019) 179.
[139] J. Wang, Y. Xie, L. Wang, J. Tang, J. Li, D. Kocaefe, Y. Kocaefe, Z. Zhang, Y. Li, C. Chen, In vivo pharmacokinetic features and biodistribution of star and rod shaped gold nanoparticles by multispectral optoacoustic tomography, RSC Adv. 5 (10) (2015) 7529–7538.
[140] Z. Lin, N.A. Monteiro-Riviere, J.E. Riviere, Pharmacokinetics of metallic nanoparticles, Wiley Interdiscip Rev Nanomed Nanobiotechnol 7 (2) (2015) 189–217.
[141] H. Konoeda, H. Takizawa, A. Gower, M. Zhao, O.A. Adeyi, M. Liu, Pharmacokinetics, tissue distribution and safety of gold nanoparticle/PKC Delta inhibitor peptide hybrid in rats, Nanotoxicology 14 (3) (2020) 341–354.
[142] H. Xie, B. Goins, A. Bao, Z.J. Wang, W.T. Phillips, Effect of intratumoral administration on biodistribution of 64Cu-labeled nanoshells, Int J Nanomedicine 7 (2012) 2227.
[143] A.-L. Bailly, F. Correard, A. Popov, G. Tselikov, F. Chaspoul, R. Appay, A. Al-Kattan, A.V. Kabashin, D. Braguer, M.-A. Esteve, In vivo evaluation of safety, biodistribution and pharmacokinetics of laser-synthesized gold nanoparticles, Sci. Rep. 9 (1) (2019) 1–12.
[144] F. Storm, Clinical hyperthermia and chemotherapy, Radiol. Clin. North Am. 27 (3) (1989) 621–627.
[145] L. Zou, H. Wang, B. He, L. Zeng, T. Tan, H. Cao, X. He, Z. Zhang, S. Guo, Y. Li, Current Approaches of Photothermal Therapy in Treating Cancer Metastasis with Nanotherapeutics, Theranostics 6 (6) (2016) 762–772.
[146] T. Okuno, S. Kato, Y. Hatakeyama, J. Okajima, S. Maruyama, M. Sakamoto, S. Mori, T. Kodama, Photothermal therapy of tumors in lymph nodes using gold nanorods and near-infrared laser light, J. Control. Release 172 (3) (2013) 879–884.
[147] Z. Cheng, A. Al Zaki, J.Z. Hui, V.R. Muzykantov, A. Tsourkas, Multifunctional nanoparticles: cost versus benefit of adding targeting and imaging capabilities, Science 338 (6109) (2012) 903–910.
[148] R. Weissleder, A clearer vision for in vivo imaging, Nat. Biotechnol. 19 (4) (2001) 316–317.
[149] M. Chaffman, R. Brogden, R. Heel, T. Speight, G. Avery, Auranofin, Drugs 27 (5) (1984) 378–424.
[150] R. Eisler, Chrysotherapy: a synoptic review, Inflamm. Res. 52 (12) (2003) 487–501.
[151] J. Shao, R.J. Griffin, E.I. Galanzha, J.-W. Kim, N. Koonce, J. Webber, T. Mustafa, A.S. Biris, D.A. Nedosekin, V.P. Zharov, Photothermal nanodrugs: potential of TNF-gold nanospheres for cancer theranostics, Sci. Rep. 3 (2013) 1293.
[152] S. Okarvi, I. Aljammaz, Comparison of intratumoral versus intravenous delivery of 177Lu-labeled bombesin peptide for the targeting of breast carcinoma, J. Nucl. Med. 57 (supplement 2) (2016), 1349-1349.
[153] T. Lammers, P. Peschke, R. Kühnlein, V. Subr, K. Ulbrich, P. Huber, W. Hennink, G. Storm, Effect of intratumoral injection on the biodistribution and the therapeutic potential of HPMA copolymer-based drug delivery systems, Neoplasia 8 (10) (2006) 788–795.
[154] J. Shi, Z. Chen, L. Wang, B. Wang, L. Xu, L. Hou, Z. Zhang, A tumor-specific cleavable nanosystem of PEG-modified C60@Au hybrid aggregates for radio frequency-controlled release, hyperthermia, photodynamic therapy and X-ray imaging, Acta Biomater 29 (2016) 282–297.
[155] S. Liang, M. Sun, Y. Lu, S. Shi, Y. Yang, Y. Lin, C. Feng, J. Liu, C. Dong, Cytokine-induced killer cells-assisted tumor-targeting delivery of Her-2 monoclonal antibody-conjugated gold nanostars with NIR photosensitizer for enhanced therapy of cancer, Journal of Materials Chemistry B 8 (36) (2020) 8368–8382.

# Chapter 3

## Motivation and objectives

Breast cancer is the most prevalent cancer type and the leading cause of cancer-related deaths among women worldwide [1]. The economic impact of breast cancer is also a matter of concern. In 2009, it accounted for the highest economic costs after lung cancer (€15 billion) and the highest healthcare costs (€6.73 billion) among all cancers in Europe [2]. Also, according to the US National Cancer Institute National Cancer Institute, breast cancer-related medical expenditures were expected to reach $16.5 billion in 2020 [3].

Breast cancer is a highly heterogeneous disease, being classified into more than 21 histologic subtypes and at least 4 molecular subtypes, which influence the treatment regimens prescribed to each patient [4, 5]. The standard breast cancer therapies comprise local treatment (*i.e.* surgery and radiotherapy) and adjuvant systemic therapies (hormonal therapy, targeted therapy and chemotherapy) [6]. Currently, chemotherapy is the only adjuvant therapeutic that can be prescribed to every breast cancer molecular subtype and is also the main treatment modality for advanced and metastatic disease [6]. Although its widespread use has resulted in a reduction of breast cancer-associated deaths, chemotherapy has major limitations related to their lack of cancer cell-specificity [7]. This leads to limited therapeutic efficacy and dose-limiting adverse side-effects [7-10]. Moreover, cancer cells may develop multidrug resistance (MDR), which may result in disease recurrence [11]. These limitations highlight the necessity of improving current breast cancer therapy through the design of innovative and economically viable strategies to minimize anti-cancer drugs' undesirable side-effects.

Nanomedicine can have a significant contribute in the improvement of cancer current treatment, by increasing the anti-cancer drugs' therapeutic index, improving their efficacy and limiting systemic side-effects [12, 13]. Their preferential accumulation in the tumor region is facilitated by the enhanced permeability and retention (EPR) effect [14]. In addition, nanoparticles' surface can be decorated to prolong their blood circulation and to improve tumor accumulation, thus limiting nonspecific off-target systemic toxicity [15, 16].

Currently, several nanoparticles, the majority liposome-based, have been approved either by the European Medicines Agency (EMA) and the Food and Drug Administration (FDA) or are under clinical trials for the treatment of breast cancer [17]. Although they have improved

the drugs' safety profiles, most of these nanoparticles require high manufacture costs and have low stability. These facts have hampered their widespread clinical application [18-20]. Therefore, novel economically-affordable types of nanocarriers are needed for the management of breast cancer.

Lipid-based nanoparticles have an enormous potential for healthcare applications. Currently, with the recent COVID-19 pandemic, their impact and clinical success was witnessed all over the world with the development of the COVID-19 mRNA vaccines [21]. Solid matrix lipid nanoparticles, such as solid lipid nanoparticles (SLN) and nanostructured lipid carriers (NLC) have a set of valuable features, including biocompatibility, constituents with generally recognized as safe (GRAS) status and low cost manufacture, which facilitates their production in large-scale [22, 23]. In addition, different lipid nanoparticles' components have demonstrated an inhibitory effect towards several drug efflux pumps, contributing to the reversal of cancer MDR [24].

Therefore, the design of lipid nanoparticle for chemotherapeutic drug delivery in breast cancer may contribute to the enhancement of the current therapeutic, which is the first focus of this thesis. The chemotherapeutic drug Mitoxantrone (Mito), was chosen for this study. Mito is a synthetic chemotherapeutic drug from the anthracenedione class acting through DNA intercalation and subsequent inhibition of DNA replication, with a demonstrated potent anti-cancer activity towards advanced breast cancer [25]. Its administration, however, is limited by several systemic side-effects, the most severe being myelosuppression and cardiotoxicity, which supports the use of nanotechnology to improve its therapeutic index [26-28].

Moreover, since breast cancer is highly heterogeneous and its conventional treatment is based on the combination of multiple drugs, and, often, multiple therapies, the development of multifunctional and multimodal nanosystems combining different therapeutic alternatives offers a great potential.

Hyperthermia is the elevation of temperature of the human body for therapeutic purposes [29]. This modality as demonstrated capacity to induce cancer cell apoptosis by triggering different cellular mechanisms, an effect that is more accentuated into cancer than normal cells. Additionally, hyperthermia can elicit cancer cell death through the stimulation of the immune system and also improve the efficacy of other therapeutics, including radio and chemotherapy [30-32]. Nevertheless, hyperthermia widespread use in clinics is hampered by the high invasiveness of the procedure, necessity of anesthesia, non-uniform heat

distribution, lack of thermal dosimetry and lack of precise tumor temperature monitoring methods [33, 34].

The combination of hyperthermia with nanomedicine can improve the clinical outcomes of hyperthermia, contributing to the development of less invasive, more precise and effective approaches [35, 36]. Hyperthermia, on the other hand, can increase the efficacy of nanomedicines in cancer treatment, by stimulating the opening of the tumor endothelium, reducing interstitial fluid pressure and promoting drug release at the target tissue. With that purpose, different classes of nanoparticle-mediated hyperthermia have emerged, including photothermal therapy (PTT) using plasmonic nanoparticles [37-39].

The combination of chemotherapy with PTT, may, therefore, contribute to the enhancement of breast cancer therapeutic and reduction of drug dosages and associated side-effects [40]. This is the second major goal of this thesis. In addition to the benefits of the combination of these two treatment modalities, the chosen chemotherapeutic drug Mito has demonstrated a higher cytotoxicity along with a reduced cancer cell drug resistance when combined with hyperthermia [32, 41]. Therefore, given these findings, combination of Mito with PTT has a great potential for a future breast cancer clinical application.

Taking into account all of the theoretical aspects, the main goal of this thesis was to develop economically affordable delivery vehicles based on lipid nanoparticles to improve current breast cancer therapy, ultimately combining chemotherapy and PTT. With that purpose, four major objectives were defined:

**1.** Rationale design, production and optimization of SLN for the intravenous delivery of the chemotherapeutic drug Mito using a rationale design.

**2.** Evaluation of the anti-cancer efficacy of the drug-loaded nanosystem in 2D and 3D cancer cell models.

**3.** Improvement of the specificity of the nanosystem towards breast cancer by exploring two different active targeting strategies.

**4.** Development of a targeted multifunctional lipid nanosystems for the combination of chemotherapy and PTT to improve breast cancer therapy.

## References


1. Sung, H., J. Ferlay, R.L. Siegel, M. Laversanne, I. Soerjomataram, A. Jemal, and F. Bray, *Global Cancer Statistics 2020: GLOBOCAN Estimates of Incidence and Mortality Worldwide for 36 Cancers in 185 Countries.* CA Cancer J Clin, 2021. **71**(3): p. 209-49.
2. Luengo-Fernandez, R., J. Leal, A. Gray, and R. Sullivan, *Economic burden of cancer across the European Union: a population-based cost analysis.* Lancet Oncol, 2013. **14**(12): p. 1165-74.
3. Mariotto, A.B., K.R. Yabroff, Y. Shao, E.J. Feuer, and M.L. Brown, *Projections of the cost of cancer care in the United States: 2010-2020.* J Natl Cancer Inst, 2011. **103**(2): p. 117-28.
4. DeSantis, C.E., S.A. Fedewa, A. Goding Sauer, J.L. Kramer, R.A. Smith, and A. Jemal, *Breast cancer statistics, 2015: Convergence of incidence rates between black and white women.* CA: a cancer journal for clinicians, 2016. **66**(1): p. 31-42.
5. Dieci, M.V., E. Orvieto, M. Dominici, P.F. Conte, and V. Guarneri, *Rare Breast Cancer Subtypes: Histological, Molecular, and Clinical Peculiarities.* Oncologist, 2014. **19**(8): p. 805-13.
6. Goldhirsch, A., J.N. Ingle, R. Gelber, A. Coates, B. Thürlimann, and H.-J. Senn, *Thresholds for therapies: highlights of the St Gallen International Expert Consensus on the primary therapy of early breast cancer 2009.* Annals of oncology, 2009. **20**(8): p. 1319-29.
7. Blanco, E. and M. Ferrari, *Emerging nanotherapeutic strategies in breast cancer.* The Breast, 2014. **23**(1): p. 10-18.
8. Pooja, D., H. Kulhari, M. Kuncha, S.S. Rachamalla, D.J. Adams, V. Bansal, and R. Sistla, *Improving Efficacy, Oral Bioavailability, and Delivery of Paclitaxel Using Protein-Grafted Solid Lipid Nanoparticles.* Molecular Pharmaceutics, 2016. **13**(11): p. 3903-12.
9. Shapiro, C.L. and A. Recht, *Side effects of adjuvant treatment of breast cancer.* New England Journal of Medicine, 2001. **344**(26): p. 1997-2008.
10. Castiglione, M. and M.J. Piccart, *Adjuvant therapy for breast cancer*. Cancer treatment and research,. 2009, New York: Springer. xvi, 490 p.
11. Bai, X., J. Ni, J. Beretov, P. Graham, and Y. Li, *Cancer stem cell in breast cancer therapeutic resistance.* Cancer Treatment Reviews, 2018. **69**: p. 152-63.
12. Shi, J., P.W. Kantoff, R. Wooster, and O.C. Farokhzad, *Cancer nanomedicine: progress, challenges and opportunities.* Nature reviews. Cancer, 2017. **17**(1): p. 20-37.
13. Wicki, A., D. Witzigmann, V. Balasubramanian, and J. Huwyler, *Nanomedicine in cancer therapy: challenges, opportunities, and clinical applications.* J Control Release, 2015. **200**: p. 138-57.
14. Iyer, A.K., G. Khaled, J. Fang, and H. Maeda, *Exploiting the enhanced permeability and retention effect for tumor targeting.* Drug discovery today, 2006. **11**(17-18): p. 812-18.
15. Pearce, A.K. and R.K. O'Reilly, *Insights into active targeting of nanoparticles in drug delivery: Advances in clinical studies and design considerations for cancer nanomedicine.* Bioconjugate chemistry, 2019. **30**(9): p. 2300-11.
16. Roma-Rodrigues, C., R. Mendes, P.V. Baptista, and A.R. Fernandes, *Targeting Tumor Microenvironment for Cancer Therapy.* International journal of molecular sciences, 2019. **20**(4): p. 840.
17. Rajashekar Kammari, N.G.D., Sudip K.Das, *Nanoparticulate Systems for Therapeutic and Diagnostic Applications*, in *Emerging Nanotechnologies for Diagnostics, Drug Delivery and Medical Devices*, K.C.a.A.M. Ashim K. Mitra, Editor. 2017. p. 105-44.
18. Della Rocca, J., D. Liu, and W. Lin, *Are high drug loading nanoparticles the next step forward for chemotherapy?* Nanomedicine, 2012. **7**(3): p. 303-05.
19. Crommelin, D.J.A., P. van Hoogevest, and G. Storm, *The role of liposomes in clinical nanomedicine development. What now? Now what?* Journal of Controlled Release, 2020. **318**: p. 256-63.

20. Weber, S., A. Zimmer, and J. Pardeike, *Solid Lipid Nanoparticles (SLN) and Nanostructured Lipid Carriers (NLC) for pulmonary application: a review of the state of the art.* European journal of pharmaceutics and biopharmaceutics : official journal of Arbeitsgemeinschaft für Pharmazeutische Verfahrenstechnik e.V, 2014. **86**: p. 7-22.
21. *Lasting impact of lipid nanoparticles.* Nature Reviews Materials, 2021. **6**(12): p. 1071-71.
22. Shah, R., D. Eldridge, E. Palombo, and I. Harding, *Lipid nanoparticles: Production, characterization and stability*. 2015: Springer.
23. Naseri, N., H. Valizadeh, and P. Zakeri-Milani, *Solid lipid nanoparticles and nanostructured lipid carriers: structure, preparation and application.* Advanced pharmaceutical bulletin, 2015. **5**(3): p. 305.
24. Yamagata, T., H. Kusuhara, M. Morishita, K. Takayama, H. Benameur, and Y. Sugiyama, *Effect of excipients on breast cancer resistance protein substrate uptake activity.* Journal of controlled release, 2007. **124**(1-2): p. 1-5.
25. Varadwaj, P., K. Misra, A. Sharma, and R. Kumar, *Mitoxantrone: an agent with promises for anticancer therapies.* Electronic Journal of Biology, 2010. **6**(2): p. 36-42.
26. Smith, I., R. Stuart-Harris, N. Pavlidis, and T. Bozek, *Mitoxantrone (novantrone®) as single agent and in combination chemotherapy in the treatment of advanced breast cancer.* Cancer treatment reviews, 1983. **10**: p. 37-40.
27. Coleman, R., M. Maisey, R. Knight, and R. Rubens, *Mitoxantrone in advanced breast cancer—a phase II study with special attention to cardiotoxicity.* European Journal of Cancer and Clinical Oncology, 1984. **20**(6): p. 771-76.
28. Guissi, N.E.I., H. Li, Y. Xu, F. Semcheddine, M. Chen, Z. Su, and Q. Ping, *Mitoxantrone-and folate-TPGS2k conjugate hybrid micellar aggregates to circumvent toxicity and enhance efficiency for breast cancer therapy.* Molecular pharmaceutics, 2017. **14**(4): p. 1082-94.
29. Stauffer, P.R., *Evolving technology for thermal therapy of cancer.* International Journal of Hyperthermia, 2005. **21**(8): p. 731-44.
30. Peeken, J.C., P. Vaupel, and S.E. Combs, *Integrating Hyperthermia into Modern Radiation Oncology: What Evidence Is Necessary?* Frontiers in Oncology, 2017. **7**(132).
31. Oei, A.L., L.E.M. Vriend, P.M. Krawczyk, M.R. Horsman, N.A.P. Franken, and J. Crezee, *Targeting therapy-resistant cancer stem cells by hyperthermia.* Int J Hyperthermia, 2017. **33**(4): p. 419-27.
32. van der Zee, J., *Heating the patient: a promising approach?* Ann Oncol, 2002. **13**(8): p. 1173-84.
33. Zagar, T.M., K.A. Higgins, E.F. Miles, Z. Vujaskovic, M.W. Dewhirst, R.W. Clough, L.R. Prosnitz, and E.L. Jones, *Durable palliation of breast cancer chest wall recurrence with radiation therapy, hyperthermia, and chemotherapy.* Radiotherapy and oncology : journal of the European Society for Therapeutic Radiology and Oncology, 2010. **97**(3): p. 535-40.
34. Mallory, M., E. Gogineni, G.C. Jones, L. Greer, and C.B. Simone, *Therapeutic hyperthermia: The old, the new, and the upcoming.* Critical Reviews in Oncology/Hematology, 2016. **97**: p. 56-64.
35. Chatterjee, D.K., P. Diagaradjane, and S. Krishnan, *Nanoparticle-mediated hyperthermia in cancer therapy.* Ther Deliv, 2011. **2**(8): p. 1001-14,10.4155/tde.11.72.
36. Kaur, P., M.L. Aliru, A.S. Chadha, A. Asea, and S. Krishnan, *Hyperthermia using nanoparticles--Promises and pitfalls.* International journal of hyperthermia : the official journal of European Society for Hyperthermic Oncology, North American Hyperthermia Group, 2016. **32**(1): p. 76-88.
37. Jaque, D., L.M. Maestro, B. Del Rosal, P. Haro-Gonzalez, A. Benayas, J. Plaza, E.M. Rodriguez, and J.G. Sole, *Nanoparticles for photothermal therapies.* nanoscale, 2014. **6**(16): p. 9494-530.
38. Hussein, E.A., M.M. Zagho, G.K. Nasrallah, and A.A. Elzatahry, *Recent advances in functional nanostructures as cancer photothermal therapy.* International journal of nanomedicine, 2018. **13**: p. 2897.

39. Abadeer, N.S. and C.J. Murphy, *Recent progress in cancer thermal therapy using gold nanoparticles.* The Journal of Physical Chemistry C, 2016. **120**(9): p. 4691-716.
40. Kemp, J.A., M.S. Shim, C.Y. Heo, and Y.J. Kwon, *"Combo" nanomedicine: Co-delivery of multi-modal therapeutics for efficient, targeted, and safe cancer therapy.* Advanced Drug Delivery Reviews, 2016. **98**: p. 3-18,https://doi.org/10.1016/j.addr.2015.10.019.
41. Herman, T.S., *Effect of Temperature on the Cytotoxicity of Vindesine, Amsacrine, and Mitoxantrone1, 2.* Cancer treatment reports, 1983. **67**(11): p. 1019.

# Chapter 4

## Progress Beyond the State of the Art

This chapter is divided into 4 subchapters according to the manuscripts that the experimental work has originated:

**4.1.** Mitoxantrone-loaded lipid nanoparticles for breast cancer therapy – Quality-by-design approach and efficacy assessment in 2D and 3D in vitro cancer models (International Journal of Pharmaceutics, 2021)

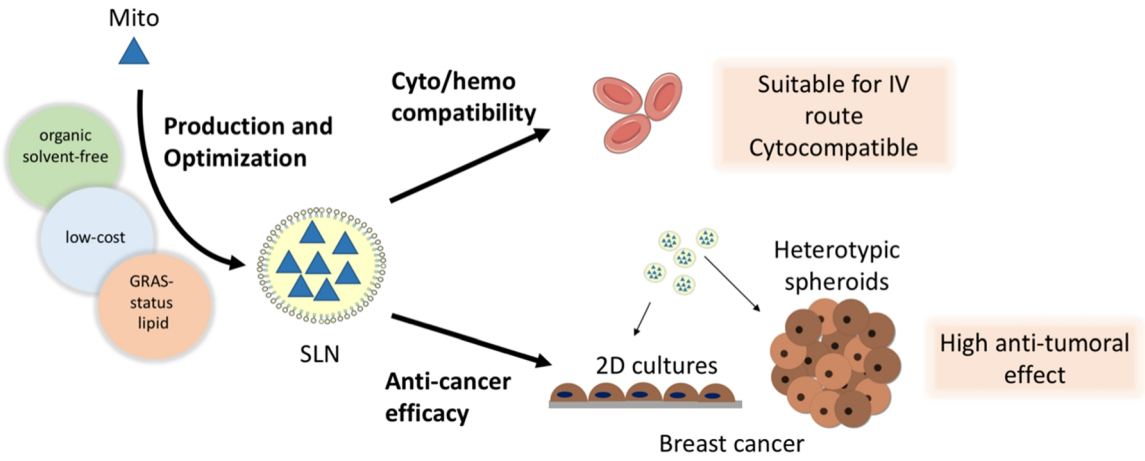
**4.2.** Hyaluronic acid-decorated lipid nanoparticles for enhanced delivery of mitoxantrone: assessing the influence of the polymer molecular weight on breast cancer cell targeting ability (To be submitted)

**4.3.** Folate receptor-mediated delivery of mitoxantrone-loaded solid lipid nanoparticles to breast cancer cells (To be submitted)

**4.4**. Multifunctional targeted solid lipid nanoparticles for combined photothermal therapy and chemotherapy of breast cancer (To be submitted)

## 4.1. Mitoxantrone-loaded lipid nanoparticles for breast cancer therapy – Quality-by-design approach and efficacy assessment in 2D and 3D in vitro cancer models

In this first work, lipid nanoparticles were designed, produced and optimized using a Box-Behnken experimental design for the entrapment of the antineoplastic drug Mitoxantrone (Mito). Nanoparticles were then fully characterized and their hemocompatibility and cytocompatibility was evaluated. Finally, the anti-cancer efficacy was evaluated in *in vitro* 2D and 3D breast cancer models. This work is published in International Journal of Pharmaceutics (Elsevier, 2021).



International Journal of Pharmaceutics 607 (2021) 121044

Contents lists available at ScienceDirect

International Journal of Pharmaceutics

journal homepage: www.elsevier.com/locate/ijpharm

# Mitoxantrone-loaded lipid nanoparticles for breast cancer therapy – Quality-by-design approach and efficacy assessment in 2D and 3D *in vitro* cancer models

Andreia Granja [a], Rita Lima-Sousa [b], Cátia G. Alves [b], Duarte de Melo-Diogo [b], Marina Pinheiro [a], Célia T. Sousa [c], Ilídio J. Correia [b,d,*], Salette Reis [a,*]

[a] LAQV, REQUIMTE, Departamento de Ciências Químicas, Faculdade de Farmácia, Universidade do Porto, 4050-313 Porto, Portugal
[b] CICS-UBI – Centro de Investigação em Ciências da Saúde, Universidade da Beira Interior, 6200-506 Covilhã, Portugal
[c] IFIMUP and Departamento de Física e Astronomia da Faculdade de Ciências da Universidade do Porto, Rua do Campo Alegre 687, 4169-007 Porto, Portugal
[d] CIEPQPF – Departamento de Engenharia Química, Universidade de Coimbra, Rua Sílvio Lima, 3030-790 Coimbra, Portugal

ARTICLE INFO

*Keywords:*
Solid lipid nanoparticles (SLN)
Mitoxantrone
Box-Behnken design
Chemotherapy
Breast cancer
Tumor spheroids

ABSTRACT

Breast cancer is the leading cause of cancer-related deaths among women worldwide. The conventional chemotherapeutic regimens used in the treatment of this disease often lead to severe side-effects and reduced efficacy. In this study, a novel drug delivery system for the chemotherapeutic drug mitoxantrone (Mito) was developed using solid lipid nanoparticles (SLN). The production of the SLN was carried out using an organic-solvent-free, low-cost method and optimized using a Box-Behnken design. SLN presented adequate size for cancer-related applications, more than 90% of EE% and remained stable for at least 6 months. A much higher drug release was obtained at acidic pH (mimicking the endosomal compartment) than plasmatic pH, highlighting the potential of the nanosystem for tumor drug delivery. Additionally, SLN were non-hemolytic and cytocompatible, even at high concentrations of lipid. A significantly higher anti-cancer efficacy was obtained for Mito-loaded SLN comparing to the free drug at different concentrations in MCF-7 2D models. Finally, the nanoformulation was evaluated in heterotypic breast cancer spheroids showing capacity to penetrate the tridimensional structure and ability to induce a high anti-tumoral effect, similarly to the free drug. Overall, these results support that the developed SLN are effective Mito nanocarriers for the treatment of breast cancer.

## 1. Introduction

Breast cancer is the most commonly diagnosed cancer and the leading cause of cancer deaths in women worldwide, with more than 2.2 million new cases and approximately 685,000 deaths reported in 2020 (Sung et al., 2021). The costs associated with this disease are also a matter of concern. In 2009 breast cancer accounted for the second highest total economic costs among all cancers in Europe (€15 billion) and the highest healthcare costs (€6.73 billion) (Luengo-Fernandez et al., 2013). Those rise substantially as the disease progresses, with the healthcare costs of distant breast cancer increasing by 165% compared to local disease (Sun et al., 2018). The conventional treatment for this pathology includes local therapy to remove the tumor and adjacent tissues and adjuvant systemic therapies, such as chemotherapy, hormonal, and targeted therapies. Most of the drugs currently used, however, have a reduced cancer-cell specificity, along with poor pharmacological properties (Mei et al., 2013; Minchinton and Tannock, 2006). This requires administration of higher dosages leading to systemic toxicity and the occurrence of several adverse side-effects with different degrees of severity. These toxic effects compromise the maximum tolerated doses and the efficacy of the drugs (Blanco and Ferrari, 2014). Moreover, cancer cells may develop multidrug resistance, which results in lower responses to treatment and favors metastasis and disease recurrence (Bai et al., 2018). Mitoxantrone (Mito) is a synthetic anticancer agent from the class of anthracenediones with demonstrated efficacy in treating different malignancies such as acute leukemia, lymphomas, melanoma, and advanced breast cancer (Posner et al., 1985; Rossato et al., 2013; Varadwaj et al., 2010). However, as in

* Corresponding authors at: CICS-UBI – Centro de Investigação em Ciências da Saúde, Universidade da Beira Interior, 6200-506 Covilhã, Portugal (I.J. Correia). LAQV, REQUIMTE, Departamento de Ciências Químicas, Faculdade de Farmácia, Universidade do Porto, 4050-313 Porto, Portugal (S. Reis).
*E-mail addresses:* icorreia@ubi.pt (I.J. Correia), shreis@ff.up.pt (S. Reis).

https://doi.org/10.1016/j.ijpharm.2021.121044
Received 18 June 2021; Received in revised form 4 August 2021; Accepted 21 August 2021
Available online 24 August 2021
0378-5173/© 2021 Elsevier B.V. All rights reserved.

most chemotherapeutic drugs, its cell killing effect is not cancer cell-specific, causing diverse side-effects, namely cardiotoxicity and myelosuppression (Posner et al., 1985; Rossato et al., 2013; Varadwaj et al., 2010).

Nanotechnology can have an important contribution in increasing the therapeutic index of chemotherapeutic drugs and developing safer and more effective treatment modalities (Wicki et al., 2015). Different Mito nanodelivery vehicles for breast cancer therapy have been reported in the literature, including liposomes (Mei et al., 2020; Pedrosa et al., 2015), mesoporous silica (Ma et al., 2011), magnetic (Sargazi et al., 2018) and gold (Imanparast et al., 2018) nanoparticles. In particular, lipid nanoparticles, such as solid lipid nanoparticles (SLN) are biodegradable, biocompatible (composed by lipids with generally recognized as safe (GRAS) status) and versatile types of nanocarriers, which makes them attractive for cancer therapy applications (Lasa-Saracibar et al., 2012). Compared to other Mito nanocarriers, such as liposomes, currently under clinical trials (Wang et al., 2020), lipid nanoparticles have several benefits such as high physical stability, the possibility of using cost-effective and green production methods, and easy large-scale production, which highlights their potential for translation into clinics (Feng and Mumper, 2013). A few studies have reported the use of SLN as delivery vehicles of mitoxantrone for breast cancer therapy (Lu et al., 2006; Zhuang et al., 2012). To the best of our knowledge, however, the production of Mito-loaded SLN from green methods has not been reported yet. In addition, the evaluation of the anti-cancer efficacy Mito-loaded SLN in heterotypic breast cancer tumor spheroids has also not been described.

The aim of this work is to develop an affordable and effective Mito delivery system to improve breast cancer therapy and reduce the systemic toxic effects induced by the free drug. SLN were produced using an organic solvent-free, low-cost method. A Box-Behnken design was implemented for a cost-effective and rational optimization of the nanoformulation (Lawrence et al., 2014; Mishra et al., 2018). Detailed characterization was then conducted, the release profile of the drug at physiological and acidic pH was assessed, and the hemocompatibility and cytocompatibility were evaluated. Finally, the efficacy of the nanoformulation was determined in 2D and 3D *in vitro* breast cancer cell models.

## 2. Materials and methods

### 2.1. Materials

Mitoxantrone hydrochloride, Tween® 80, Triton™ X-100 (TX-100), Sodium acetate, Phosphate Buffered Saline (PBS), Dulbecco's modified Eagle's medium F-12 (DMEM-F12), penicillin/streptomycin, trypsin, resazurin and paraformaldehyde were acquired from Sigma-Aldrich® (Sintra, Portugal). Roswell Park Memorial Institute (RPMI-1640) medium was purchased from Gibco (Invitrogen Corporation, Paisley, UK). Cetyl Palmitate was kindly offered by Gatefossé (Nanterre, France). Acetic acid glacial was obtained from VWR International LLC (Radnor PA, USA). Sodium chloride was purchased from Honeywell Fluka™ (NJ, USA). Fetal Bovine Serum (FBS) was purchased from Biochrom AG (Berlin, Germany). Calcein-AM, Propidium Iodide (PI), cell culture plates and T-flasks were purchased from Thermo Fisher Scientific (Porto, Portugal). Agarose was obtained from Grisp (Porto, Portugal). Michigan Cancer Foundation-7 (MCF-7) cell line was acquired from ATCC (Middlesex, UK). Normal Human Dermal Fibroblasts (NHDF) were purchased from Promocell (Heidelberg, Germany). Ultrapure water (18.2 MΩ cm) was obtained from a water purification system (Healforce, Shanghai, China).

### 2.2. Methods

#### 2.2.1. Preparation of solid lipid nanoparticles (SLN)

Solid lipid nanoparticles (SLN were produced by the hot ultrasonication method as previously described (Magalhães et al., 2020). Briefly, a lipid phase comprising the solid lipid (Cetyl palmitate) and the surfactant (Tween® 80) were melted at 70 °C in a water bath (Variomag Electronicrührer, Labortechnik, Munich, Germany). A PBS solution heated at 70 °C (4.4 mL), pH 8.2, was then poured into the lipid phase and the mixture was sonicated (VCX130, Sonics and Material Vibra-CellTM with a CV-18 probe; 115 Newtown CT, USA) at an amplitude frequency of 70% for 5 min. The formed nanoemulsion was then cooled at room temperature and stored at 4 °C. To produce Mito-loaded SLN (SLN-Mito), Mito was dissolved in the PBS solution at the desired amount.

#### 2.2.2. Experimental design

A 15-run, 3-level, 3-factor Box–Behnken design was employed to optimize the SLN nanoformulation, namely, to maximize the Entrapment Efficiency (EE%) and Loading Capacity (LC%) and minimize particle size. The selected independent variables were the amount of Lipid ($X_1$), the amount of Surfactant ($X_2$), and the amount of Mito ($X_3$). For each independent variable, the low (−1), medium (0) and high (+1) levels were chosen according to preliminary SLN production studies. The studied dependent variables were the size ($Y_1$), EE% ($Y_2$), and LC% ($Y_3$). The following equation gives the polynomial equation generated from the experimental design:

$$Y = b_0 + b_1X_1 + b_2X_2 + b_3X_3 + b_{12}X_1X_2 + b_{13}X_1X_3 + b_{23}X_2X_3 + b_{11}X_1^2 + b_{22}X_2^2 + b_{33}X_3^2 \quad (1)$$

where Y is the dependent variable, $b_0$ is the intercept, $X_1$, $X_2$, $X_3$ are the coded levels of independent variables, and $b_1$ to $b_{33}$ are the regression coefficients computed from the observed experimental values of Y. The terms $X_1X_2$ and $X_i^2$ (i = 1, 2 or 3) represent the interaction and quadratic terms, respectively. Data were statistically evaluated by analyzing the statistical significance of coefficients and multiple correlation coefficient ($R^2$) using ANOVA ($p$ values $< 0.05$). The best-fitting experimental model was then selected. All the analyses were performed using the STATISTICA 10 software (Statsoft Power Solutions, Inc., Tulsa, OK, USA). After determining the optimum values for each independent variable, triplicates of the optimum nanoformulation were prepared and characterized and the observed values for each dependent variable were compared with the predicted values given by the Box-Behnken design.

#### 2.2.3. Size, polydispersity index, and zeta potential measurements

The size, polydispersity index (PDI), and zeta potential of the SLN were determined by dynamic light scattering (DLS) and electrophoretic light scattering (ELS) using a ZetaPALS analyzer (Brookhaven Instruments Corporation, Holtsville, NY, USA) operating at a scattering angle of 90° at room temperature, with dust cut-off set to 30. SLN were diluted at a ratio of 1:300. For each sample, 6 runs of 10 cycles each were performed. All measurements were performed in triplicate. Detailed nanoparticle size distribution was also determined using nanoparticle tracking analysis (NTA, NanoSight NS300, Malvern Instruments, Worcestershire, UK) equipped with a 488 nm laser and a high sensitivity scientific CMOS camera. Samples were diluted at a ratio of 1:100,000, injected using a 1 mL sterile syringe in the viewing chamber and measured under constant flow (infusion rate of 50) at 24 °C. Size measurements were obtained based on a 20 s video captured with a camera level of 10 and a detection threshold of 5. For each sample, 5 size measurements were conducted. Data were analyzed using the NTA 3.4. software.

#### 2.2.4. Entrapment efficiency and loading capacity evaluation

EE% and LC% of the nanoformulations were measured using an indirect method of quantification. SLN were diluted (1:65), placed into centrifugal filter units (Amicon® Ultra Centrifugal Filters Ultracell-50 kDa, MERK Millipore, Ltd; Cork, Ireland) and centrifuged at 2851g (Allegra X-15R Centrifuge, Beckman Coulter, Fullerton, California) until

the complete separation of the lipid and aqueous phase. The aqueous phase containing the non-entrapped Mito was recovered and the amount of Mito was quantified by UV–Vis spectrophotometry (Jasco V-660 Spectrophotometer, Software: Spectra Manager v.2, Jasco Corporation, USA) at 610 nm. A calibration curve was previously obtained using PBS pH 8.2 as a solvent.

EE% was determined by calculating the ratio between entrapped Mito (the difference between the total amount of Mito and the non-entrapped Mito) and the total amount of Mito as shown by the following equation:

$$EE\% = \frac{\text{Total amount of Mito} - \text{Non entrapped Mito}}{\text{Total amount of Mito}} \times 100 \quad (2)$$

LC% was obtained by calculating the ratio between the amount of entrapped Mito and the amount of lipid, surfactant, and entrapped Mito, as demonstrated by the following equation:

$$LC\% = \frac{EE\% \times \text{initial amount of Mito}}{\text{Amount of lipid} + \text{surfactant} + EE\% \times \text{initial amount of Mito}} \quad (3)$$

*2.2.5. Transmission electron microscopy analysis*

Morphology of the developed SLN was observed by Transmission Electron Microscopy (TEM). SLN were diluted 100 times in ultrapure water and placed over a cooper-mesh grid for 2 min. Negative staining was then performed using 0.75% (w/v) uranyl acetate for 30 s. Samples were analyzed in TEM (TEM Jeol JEM-1400; JEOL Ltd., Tokyo, Japan) with an accelerating voltage of 80 kV.

*2.2.6. Storage stability*

The storage stability of the SLN was evaluated by performing periodic measurements of the size, PDI, zeta potential and EE% for 6 months. The stability study was conducted in triplicate for each formulation to achieve statistical significance.

*2.2.7. In vitro release assay*

The *in vitro* release of SLN-Mito was performed using a Slide-A-Lyzer dialysis device (Slide-A-Lyzer™ MINI Dialysis Device, MWCO 10 kDa, Thermo Scientific™, MA, USA). The release profile was assessed in PBS at physiological pH (7.4) and in acetate buffer, pH 5.0, simulating the acidic endosomal compartment (Boedtkjer and Pedersen, 2020; Xu et al., 2019). SLN-Mito (0.5 mL) was added into the upper compartment of the dialysis device and 14 mL of the adequate buffer was added to the lower compartment. Devices were then placed in an incubator shaker (ES-60, Lan Technics, USA) at 100 RPM at 37 °C for 24 h. At regular intervals, aliquots of 1 mL were collected from the lower compartment and replaced with 1 mL of fresh buffer heated at 37 °C. Mito content was then analyzed by UV–Vis spectrophotometry, as previously mentioned. Similarly, calibration curves were previously acquired in each buffer.

*2.2.8. Hemolysis assay*

Hemolysis assay was conducted using human blood collected from healthy donors in EDTA-coated tubes. Blood samples were obtained according to the principles of the declaration of Helsinki and were kindly donated by Serviço de Hematologia from Centro Hospitalar Universitário do Porto - Hospital de Santo António. Samples were centrifuged at 955g for 5 min at 4 °C (Allegra X-15R Centrifuge, Beckman Coulter, Fullerton, California) to separate the red blood cells (RBCs) from the remaining blood components. RBCs were then washed 3 times with a 0.85% saline solution and diluted to a 4% (v/v) solution. Nanoformulations were diluted at the desired concentrations in saline solution. A solution of TX-100 (1% v/v) and saline solution were used as positive and negative controls, respectively. RBCs (100 μL) were then incubated with the samples (100 μL) in a 96-well plate at 37 °C for 1 h. After that, the supernatant was removed and the absorbance of hemoglobin was measured at 415 nm by UV–Vis spectroscopy using a plate reader (Biotek Instruments, Winooski, VT, USA). The percentage of hemolysis was calculated as follows:

$$Hemolysis\% = \frac{Abs(sample) - Abs(negative\ control)}{Abs(positive\ control) - Abs(negative\ control)} \times 100 \quad (4)$$

*2.2.9. Cell viability: Cytocompatibility and anti-cancer efficacy assessment in 2D in vitro cancer models*

The effect of the nanoparticles on cell viability was evaluated using the resazurin assay as described previously (Lima-Sousa et al., 2020). The cytocompatibility of the unloaded nanoparticles was assessed both in normal cells (NHDF) and in the breast cancer cell line (MCF-7). The anti-cancer efficacy of SLN-Mito was evaluated in MCF-7 and AU-565 cells. Cells were seeded at a density of 1 x$10^4$ cells per well in 96-well plates and cultured in DMEM-F12 medium (MCF-7) or RPMI Medium 1640 (AU-565) supplemented with 10% (v/v) FBS and 1% (v/v) streptomycin/gentamycin in a humidified incubator (37 °C, 5% $CO_2$) for 24 h. Culture medium was then removed and replaced with different concentrations of each nanoformulation. After the incubation period (24 or 48 h), the medium was removed and replaced by fresh culture medium containing 10% (v/v) of resazurin. After incubation for 4 h in the dark (37 °C, 5% $CO_2$), the fluorescence of resorufin ($\lambda_{ex} = 560$ nm; $\lambda_{em} = 590$ nm) was measured (Spectramax Gemini EM spectrofluorometer). Cells incubated with only culture medium were used as negative ($K^-$) control. The dose–response curves and the values of $IC_{20}$, $IC_{50}$ and $IC_{80}$ of SLN-Mito and free Mito were obtained using GraphPad Prism Software (v.6.0, GraphPad Software, CA, USA).

*2.2.10. Penetration capacity evaluation in 3D in vitro breast cancer models*

Heterotypic breast cancer spheroids were produced as previously described (Costa et al., 2018a; Mó et al., 2020). Briefly, agarose gel (2% w/v) was cast in a micro-mold (3D Petri Dish®, Microtissues Inc., Providence RI, USA) forming spherical micro well-containing structures. These structures were then placed in 12-well culture plates and sterilized by UV radiation for 3 h. After that MCF-7 cells and NHDF, at a 1:1 cell ratio, were seeded at a density of 1 × $10^6$ cells per agarose structure, forming 81 spheroids per structure. Spheroids were grown for 10 days in DMEM-F12 medium supplemented with 10% (v/v) FBS and 1% (v/v) streptomycin/gentamycin (37 °C, 5% $CO_2$), with medium replacement every 2 days. The penetration capacity of the nanoparticles in the heterotypic spheroids was evaluated according to previous studies (Costa et al., 2018b; Mó et al., 2020). Briefly, spheroids were incubated with free Mito and SLN-Mito at a concentration of 10 μM of Mito for 24 h. After that, spheroids were fixed with paraformaldehyde 4% and visualized by Confocal Laser Scanning Microscopy (CSLM) using the fluorescence of Mito for imaging ($\lambda_{ex}/\lambda_{em}$ of 633/656–758 nm) in a Zeiss LSM 710 confocal microscope (Carl Zeiss SMT, Inc., Oberkochen, Germany). Z-stacks were collected with intervals of 30 μm and fluorescence intensity at different penetration depths was determined using ImageJ software.

*2.2.11. Anti-cancer efficacy assessment in 3D in vitro breast cancer models*

To assess the effect on spheroids' viability, different concentrations of SLN-Mito and free Mito diluted in culture medium were added followed by incubation for 48 h. Heterotypic tumor spheroids were produced and maintained as detailed in Section 2.2.10. The resazurin assay was then conducted, as described in Section 2.2.9. Each condition was evaluated in a total of 30 spheroids. The therapeutic effect of the nanoparticles and free drug was also visualized using CLSM. With that purpose, spheroids were incubated with free Mito and SLN-Mito at a concentration of 21 μM of drug equivalents. After 24 h, spheroids were stained with Calcein-AM and PI (according to the manufacturer's protocol) and visualized in CLSM ($\lambda_{ex}/\lambda_{em}$ of 488/493–556 nm (Calcein-AM) and 561/566–719 nm (PI)).

*2.2.12. Statistical analysis*

Statistical analysis was performed using Graphpad Prism6 Software (GraphPad Software Inc., San Diego, CA, USA). Unless stated otherwise,

differences between control and treatment groups were assessed by one-way analysis of variance (ANOVA) using Dunnett's post-hoc test or two-way ANOVA using Tukey's test. A *p*-value lower than 0.05 was considered statistically significant. All data are expressed as mean ± SD.

## 3. Results and discussion

### 3.1. Production optimization – Experimental quality-by-design

Prior to the experimental design, initial studies were conducted to select the most suitable composition of Mito-loaded SLN. A lipid screening was performed by evaluating the solubility of mitoxantrone in different solid lipids at different ratios and solubility was visually estimated taking into account the presence of a clear blue solution and the lowest amount of drug crystals [3, 9] (Table S1). Pilot batches were then produced using the most promising solid lipids and after evaluating the physicochemical properties of the SLN (namely particle size, polydispersity and entrapment efficiency) (data not shown), cetyl palmitate was selected as the solid lipid for the nanoformulation. Additionally, the composition and pH of the aqueous phase was also selected. Other variables such as the speed and time of sonication were defined according to previous studies (Granja et al., 2017). Based on these preliminary studies, three factors (independent variables) were selected as the most relevant for the optimization of the nanoformulation: the amount of Lipid ($X_1$), the amount of Surfactant ($X_2$), and the amount of Mito ($X_3$).

A Box-Behnken design was then applied aiming to evaluate the effect of the selected factors on three different parameters (dependent variables), namely, size, EE%, and LC% and ultimately determine the optimum production conditions according to the desired criteria. The implementation of this type of quality-by-design is a valuable tool in the development of drug delivery systems and in the pharmaceutical industry, enabling the optimization of different process parameters in a systematic, fast, and cost-effective way using a reduced number of experiments (Lawrence et al., 2014; Mishra et al., 2018).

Different combinations of the three factors were defined by the software, resulting in a total of 15 nanoformulations comprising 13 different nanoformulations and three replicates corresponding to the central point. The different combinations of factors and resulting parameters are summarized in Table S2.

The effects of each independent variable were analyzed via regression analysis. Based on the values of the correlation coefficient ($R^2$) between the experimental and the predicted values, the quadratic model was selected to proceed with the analysis (Fig. S1). The significance of the model was statistically validated using ANOVA (Tables S3, S4, and S5). The results of the regression analysis using the quadratic model for each response including the interaction coefficients of each independent variable and the corresponding *p-value* are summarized in Table 1.

**Table 1**
Regression analysis for the selected responses (size, EE% and LC%) using the quadratic model. Statistically significant values are represented in bold, *p*-value ≤ 0.05 with a 95% confidence interval.

| | Size | | EE% | | LC% | |
|---|---|---|---|---|---|---|
| | Coeff. | *p-value* | Coeff. | *p-value* | Coeff. | *p-value* |
| Intercept | **224.250** | **0.000** | **86.665** | **0.000** | **1.496** | **0.000** |
| $X_1$ | 13.600 | 0.068 | 2.850 | 0.090 | **−0.077** | **0.043** |
| $X_1^2$ | 3.462 | 0.315 | 0.230 | 0.754 | 0.012 | 0.405 |
| $X_2$ | **−19.283** | **0.036** | −3.669 | 0.057 | **−0.161** | **0.010** |
| $X_2^2$ | 2.312 | 0.469 | −1.301 | 0.179 | −0.041 | 0.071 |
| $X_3$ | 3.350 | 0.464 | **−10.601** | **0.007** | **0.559** | **0.001** |
| $X_3^2$ | 1.312 | 0.665 | 0.576 | 0.464 | **0.058** | **0.036** |
| $X_1X_2$ | −2.900 | 0.621 | 1.4927 | 0.349 | 0.048 | 0.161 |
| $X_2X_3$ | −2.150 | 0.710 | 0.0004 | 0.100 | −0.063 | 0.104 |
| $X_1X_3$ | −0.600 | 0.916 | 3.6642 | 0.097 | 0.050 | 0.149 |
| $R^2$ | 0.962 | | 0.989 | | 0.999 | |

**Table 2**
Predicted versus experimental values obtained for each response (size, EE%, and LC%) of the optimum nanoformulation.

| | Predicted | Experimental |
|---|---|---|
| Size (nm) | 219 | 230 ± 17 |
| EE% | 99 | 93 ± 6 |
| LC% | 1.6 | 1.5 ± 0.1 |

**Table 3**
Physicochemical characterization of the optimized SLN (SLN-Mito) and corresponding unloaded SLN (SLN): size (determined by DLS), PDI, Zeta potential, EE % and LC%. Data are expressed as mean ± SD (n = 3).

| | Size (nm) | PDI | Zeta potential (mV) | EE% | LC% |
|---|---|---|---|---|---|
| SLN | 226 ± 17 | 0.14 ± 0.02 | −4 ± 1 | – | – |
| SLN-Mito | 230 ± 17 | 0.16 ± 0.01 | −3 ± 1 | 93 ± 6 | 1.5 ± 0.1 |

As shown in Table 1 the values of the coefficients for each factor are either negative or positive, which indicates an antagonist or synergistic effect on the response, respectively. Interaction terms are represented by two factors and quadratic relationships are represented by higher order terms. A visual representation of the statistically significant effects of the factors on each response is depicted in the response contour plots in Fig. S2.

The regression analysis demonstrated that the particle size was significantly affected by the amount of surfactant ($X_2$). The negative sign of the coefficient indicates an inverse relationship, meaning that increasing the amount of surfactant results in a decrease in particle size. This effect may be attributed to a reduction in the interfacial tension between the lipid and the external phase induced by the surfactant, leading to the stabilization and formation of smaller particles, which is in agreement with previous studies (Ferreira et al., 2015; Magalhães et al., 2020).

The amount of drug also had a significant negative effect on EE%. This may occur due to a limited capacity of the lipid matrix to accommodate the drug. This suggests that adding increasing amounts of drug above this capacity increases the amount of non-entrapped drug which reduces the EE% (Gidwani and Vyas, 2016; Joseph et al., 2017).

LC% was significantly affected by the amount of lipid, surfactant, Mito, and the quadratic term of the amount of Mito. Both lipid and surfactant have a significant negative effect on LC%, which is expected as there is an inversely proportional relationship between them, as depicted in Eq. (3). The amount of Mito and the quadratic term of this factor, as expected, had a positive effect on LC%.

As shown in Table 1 and Fig. S1, a good correlation ($R^2$) was obtained for all the regression equations for each response, indicating a good fitting of the quadratic model. The optimum nanoformulation composition was then assessed using the prediction and profiling function on the STATISTICA 10 software. The criteria established for the optimum nanoformulation consisted of maximum EE% and LC% and minimum particle size. To validate the optimization procedure and the prediction ability of the model, the nanoformulation with the optimum composition (210 mg of Solid lipid, 70 mg of surfactant, and 4.5 mg of Mito) was produced in triplicate and characterized. As shown in Table 2 a good agreement between the predicted and observed values was obtained for all the responses, which validates the experimental design and the robustness of the model for the optimization of the nanoformulation.

### 3.2. Nanoparticle physicochemical characterization

After validation of the experimental design, three replicates of the optimal (SLN-Mito) and corresponding unloaded nanoformulations

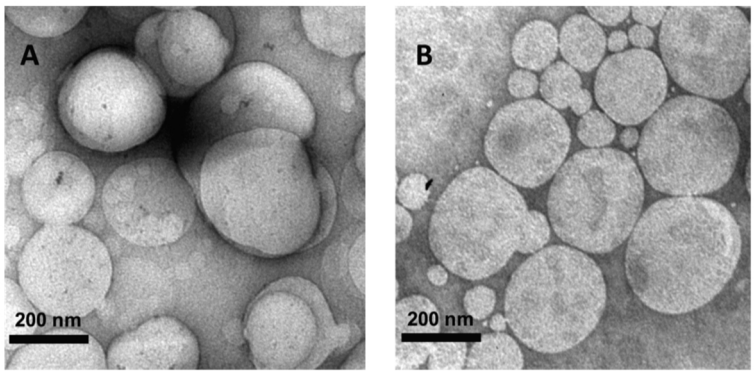



**Fig. 1.** TEM photographs of SLN (**A**) and SLN-Mito (**B**), Magnification 50000X.

(SLN) were produced and characterized in terms of size, PDI, Zeta potential, EE% and LC% (Table 3). The results of particle size performed using DLS suggest that the entrapment of Mito did not significantly affect the hydrodynamic diameter of the nanoparticles, which remained around 230 nm. A more detailed size distribution analysis was performed using NTA (Fig. S3), which is a relatively recent technique that can complement the results obtained by DLS (Filipe et al., 2010). A mean particle size of 155 ± 2 and 153 ± 3 nm, for SLN and SLN-Mito, respectively, were obtained by NTA, which are lower than the values obtained using DLS. This difference can be explained by the fact that DLS measurements are frequently biased towards the presence of larger nanoparticles, even at a very small number, as the light scattering intensity is more affected by the size than by the number of nanoparticles (Amaro-Gahete et al., 2019). NTA, in contrast, measures the hydrodynamic diameter by tracking each nanoparticle individually through image analysis, providing a more detailed characterization of size distribution (Amaro-Gahete et al., 2019; Fan et al., 2015). DLS, on the other hand, is a less time-consuming and non-destructive technique (Amaro-Gahete et al., 2019).

Overall, these results suggest that the nanoparticles have a suitable

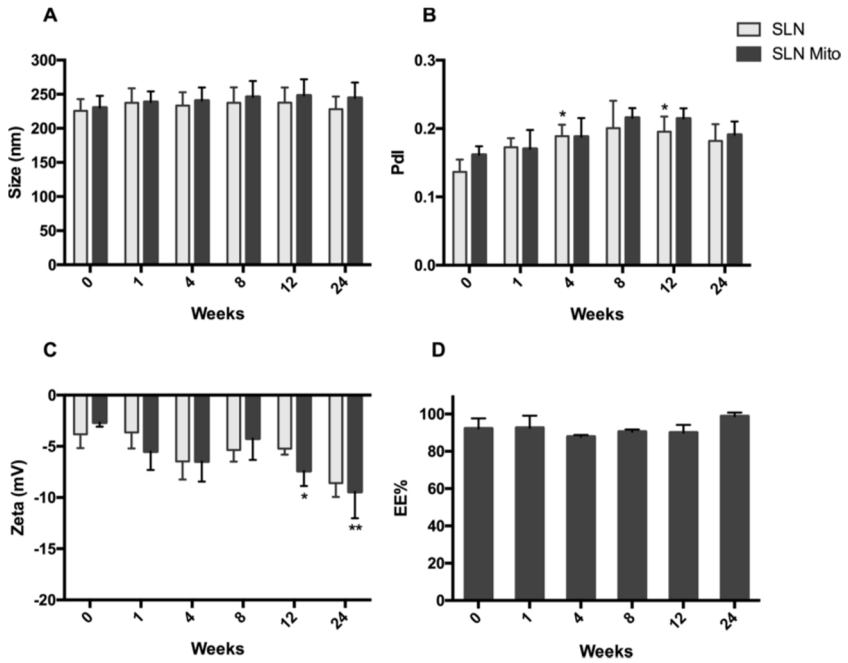



**Fig. 2.** Storage stability of (**A**) particle size, (**B**) PDI, (**C**) zeta potential and (**D**) EE% over 24 weeks at 4 °C. Data are expressed as mean ± SD (n = 3). Differences between control (time point 0) and other time points were performed using One-way ANOVA followed by Dunnett's test (*) denotes statistically significant differences relative to the correspondent week 0. $*p < 0.05$, $**p < 0.01$.

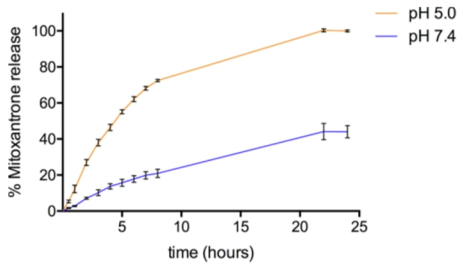



**Fig. 3.** Cumulative release of Mito at physiological (7.4) and acidic (5.0) pH. Data are expressed as mean ± SD (n = 3).

size for intravenous administration and tumor passive accumulation through the enhanced permeability and retention (EPR) effect (Attia et al., 2019; Huang et al., 2021; Singh and Lillard Jr, 2009). The values of PDI were below 0.2, which indicates the presence of an homogeneous population for lipid-based nanocarriers (Danaei et al., 2018). Zeta potential for both SLN and SLN-Mito were close to neutral (−3 ± 1 mV), which is expected due to the use of a dispersion media of physiologic ionic strength (PBS), which is higher than double deionized water (Brown et al., 2016). Similar results have been reported elsewhere (Goutayer et al., 2010; Rajapaksa et al., 2010). This can be an advantage in cancer therapy applications since neutral or slightly negative surface charges are associated with a limited uptake by the reticuloendothelial system, longer circulation half-lives, and higher tumor accumulation following intravenous administration (Blanco et al., 2015; Ernsting et al., 2013). Finally, a high value of EE% (93%) was obtained, corroborating the predicted results from the Box-Behnken design.

Nanoparticle morphology and size distribution were also evaluated using TEM (Fig. 1). Both nanoformulations present spherical morphology, absence of particle aggregation, and particle size in agreement with the DLS and NTA measurements.

### 3.3. Storage stability

Storage stability was evaluated over a period of 24 weeks (6 months). Nanoformulations were kept at 4 °C, and periodic assessments of their physiochemical properties were performed. As shown in Fig. 2**A**, particle size remained stable during the 6 months of the study, which suggests the absence of aggregate formation during storage. Fig. 2**B** shows the variation of PDI and corroborates these results, showing that, although a slight increase can be observed, the values of this parameter remained below 0.2 after 6 months of storage, which is an indicator of a homogeneous population for lipid-based nanocarriers (Danaei et al., 2018). An increase in the zeta potential absolute values occurred in the last two time-points of the study. Nevertheless, all the values remained slightly negative, below −10 mV (Fig. 2**C**). Encapsulation efficiency remained above 90% for at least 6 months, demonstrating the absence of drug leaking during storage (Fig. 2**D**). These results support that the developed nanoformulations are stable in suspension for at least 6 months.

### 3.4. In vitro release study

The release of Mito from the SLN was assessed using the dialysis method at pH 7.4 and 5.0 to simulate the physiological environment and the endosomal compartment, respectively (Kim et al., 2014). The cumulative percentages of Mito release are presented in Fig. 3 where a pH-dependency can be observed. At pH 7.4, SLN releases Mito in a controlled manner, with more than 60% of drug remaining encapsulated after 24 h, suggesting that only a limited amount of drug will be released in physiological environment such as the bloodstream and other normal

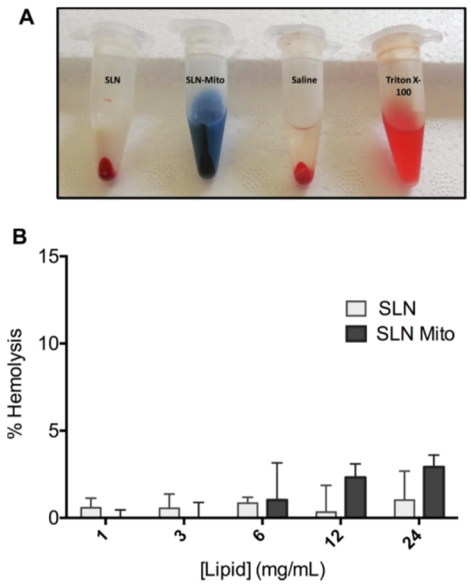



**Fig. 4.** *In vitro* hemolysis assay of SLN and SLN-Mito. (**A**) Image of the samples treated with the highest concentration (24 mg/mL) tested of SLN and SLN-Mito and controls - negative (saline solution) and positive (TX-100–1% v/v) following 1 h incubation. (**B**) Graphic representation of the concentration-dependent hemolysis induced by SLN and SLN-Mito. Data are expressed as mean ± SD (n = 3).

tissues. A much faster release is observed at pH 5.0, characteristic of the acidic endosomal compartment. To evaluate the mechanism of drug release from the SLN at the two pH, data were fitted to different drug release models including zero order, first order, Higuchi, Hixson-Crowell and Korsmeyer-Peppas. The correlation coefficients ($R^2$) and the release rate constants (k) obtained for each model is presented in Table S6. Based on these values, the Higuchi model was found to be the model that best described the release kinetics of the drug at both pH conditions. This suggests that the release of Mito occurs mainly by a diffusion-controlled process [1]. The release rate constant ($k_H$) obtained for the two studied pH also clearly demonstrates a higher drug release rate at pH 5.0 than at pH 7.4.

Overall, these data show that SLN can release Mito at a much faster rate at acidic than at physiological pH. This suggests that once in the human body, SLN will presumably have a controlled drug release in the bloodstream and normal healthy tissues, which can reduce the systemic toxic effects of the free drug. Additionally, a much faster release will occur in acidic environments such as the tumor tissue and endosomal compartment, where the free drug can exert its effect. These findings support that the developed nanoformulations are suitable carriers for the delivery of Mito to tumor tissues.

### 3.5. Hemolysis assay

The hemocompatibility of the SLN was assessed through a hemolysis assay using human RBCs collected from 3 healthy donors. Hemolysis was assessed in a concentration range from 1 to 24 mg/mL of lipid after incubation for 1 h. As shown in Fig. 4, all values of hemolysis were lower than 5% even at very high concentrations of lipid, with the maximum of hemolysis reaching only 3%. These findings support that the developed SLN are non-toxic according to ISO 10993–4 (ISO10993-4, 2017) and,

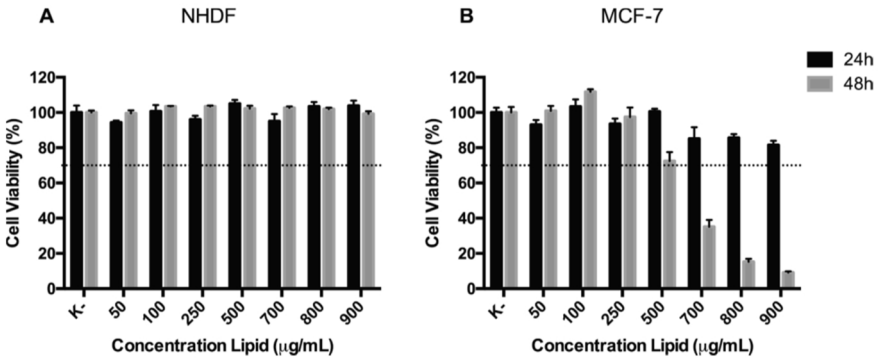



**Fig. 5.** Effect of unloaded SLN on the viability of NHDF (**A**) and breast cancer cell line MCF-7 (**B**) at different lipid concentrations after 24 and 48 h of incubation. Data are expressed as mean ± SD (n = 5).

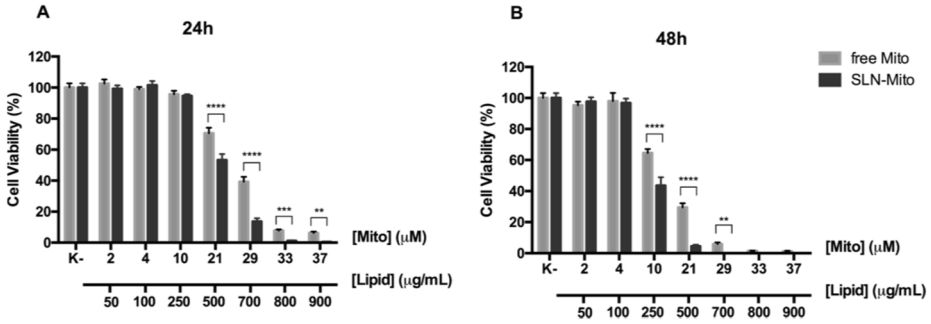



**Fig. 6.** Anti-cancer activity of SLN-Mito versus free Mito on MCF-7 cells at increasing concentrations of Mito (and corresponding lipid concentrations) after 24 h (**A**) and 48 h (**B**) of incubation. Differences between groups were determined using two-way ANOVA with Tukey's test. Data are expressed as mean ± SD (n = 5). $^{**}p < 0.01$, $^{***}p < 0.001$, $^{****}p < 0.0001$.

therefore, safe for intravenous administration.

### 3.6. Cytocompatibility assessment

The safety of the SLN was further evaluated through the assessment of their cytocompatibility for both normal and cancer cells. As depicted in Fig. 5**A**, unloaded SLN did not induce any reduction in cell viability up to 900 μg/mL of lipid after incubation for 24 and 48 h in human fibroblasts. These results are in agreement with previous studies where concentrations up to 1000 μg/mL of similar types of nanoparticles were found to be cytocompatible for NHDF cells after 24 h and 48 h incubation (Doktorovova et al., 2014; Ruktanonchai et al., 2009). In the MCF-7 breast cancer cell line (Fig. 5**B**), SLN were found to be cytocompatible for 24 h at the highest concentration tested. After 48 h of incubation, however, SLN were cytocompatible up to a concentration of 500 μg/mL of lipid. An $IC_{50}$ of 605 μg/mL of lipid was determined for this incubation period (Fig. S4). This value is comparable or higher than others reported in the literature for similar types of nanoparticles in MCF-7 cells following 48 h incubation, demonstrating the high cytocompatibility of the produced SLN (Abbasalipourkabir et al., 2011; Miao et al., 2013; Ying et al., 2011).

### 3.7. Anti-cancer efficacy on 2D in vitro breast cancer models

The anti-cancer efficacy was evaluated in MCF-7 cell lines for 24 and 48 h (Fig. 6A and 6B). As expected, a decrease in breast cancer cell viability is observed with increasing Mito concentrations. It is noteworthy that SLN-Mito have a significantly higher anti-tumoral effect comparing to the free drug. After 24 h of incubation, SLN-Mito elicit a significantly higher cancer cell death when compared with free Mito at concentrations of 21 μM (corresponding to 500 μg/mL of lipid) or higher, with only 14% of cell viability at a concentration of 29 μM and almost full eradication at the highest concentrations tested. This effect cannot be attributed to any intrinsic toxicity of the lipid matrix, as in this range of concentrations, all the corresponding unloaded SLN were found to be cytocompatible, as highlighted in Fig. 5. After 48 h of incubation, a similar trend was observed with SLN-Mito significantly improving MCF-7 cells' death at concentrations of 10 μM or higher, achieving almost full eradication at a concentration of 21 μM, corresponding to a lipid concentration of 500 μg/mL, which was found to be cytocompatible (Fig. 6**B**). To further demonstrate the anti-cancer efficacy of the nanosystem, the effects of the nanoformulation on cell viability were also evaluated in the HER-2-positive breast cancer cell line Au-565 (Figs. S5 and S6). A similar trend can be observed, with comparable or higher anti-cancer activity induced by SLN-Mito comparing to the free drug.

Based on the results obtained in MCF-7 cells, dose–response curves were plotted (Fig. S7) and values of $IC_{50}$, $IC_{20}$, and $IC_{80}$ were calculated (Table S7). $IC_{50}$ values for free Mito and SLN-Mito were found to be 25 and 21 μM after 24 h incubation and 13 μM and 10 μM after 48 h incubation, which further supports the higher anti-cancer activity of SLN-

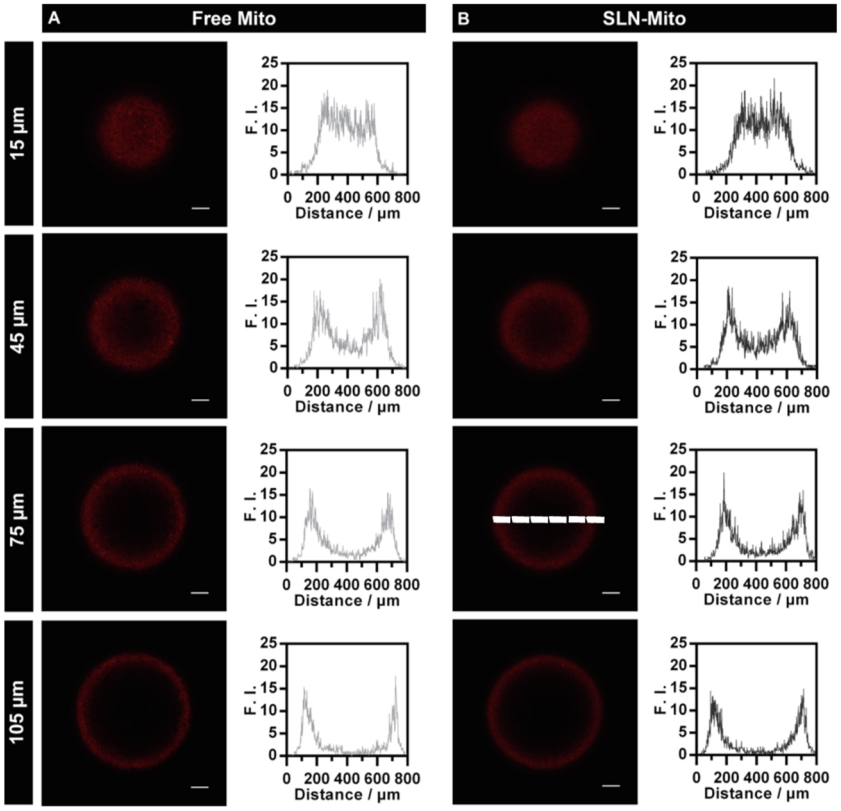



**Fig. 7.** CLSM z-stacks free drug (**A**) *vs.* SLN-Mito (**B**) at a concentration of 10 µM of Mito in heterotypic spheroids at a penetration depth of 15, 45, 75 and 105 µm, and respective plots of the fluorescence intensity (F. I.) across the spheroid's diameter. Red channel: Mito. Scale bars correspond to 100 µm.

Mito comparing to the free drug.

Comparing to other mitoxantrone nanodelivery vehicles reported in the literature, the SLN developed in this study demonstrated a higher capacity to improve the anti-cancer efficacy of Mito (Ma et al., 2011; Sargazi et al., 2018). For instance, Sargazi *et al.* developed hyaluronan PEGylated magnetic nanoparticles conjugated with Mito and showed that after 48 h and 72 h the nanosystem could not inhibit MCF-7 cell viability, in contrast to what occurred with the free drug at a concentration range of 25–400 µM (Sargazi et al., 2018). Ma *et al.* showed a similar or lower anti-tumor efficacy of Mito-loaded mesoporous silica nanoparticles comparing to free Mito up to 10 µg/mL (22 µM) after 24 h incubation (Ma et al., 2011). Other works have developed Mito nanodelivery systems reporting values of $IC_{50}$ relatively lower than the ones described in our study (Pedrosa et al., 2015; Wang et al., 2018). Nevertheless, in one of these studies the nanosystem comprising nanoliposomes could not improve the efficacy of the free drug (Pedrosa et al., 2015), while in another work, chitosan/hyaluronate polyelectrolyte nanoparticles did not induce full eradication of MCF-7 cells even after treatment with high concentrations of Mito (45 µM) (Wang et al., 2018).

Overall, our results clearly demonstrate the capacity of the developed SLN to improve the anti-tumoral activity of Mito in 2D *in vitro* breast cancer models.

### *3.8. Penetration and therapeutic efficacy on 3D in vitro breast cancer models*

Although 2D cell monolayers offer a quick and relatively easy way to assess the toxicity and anti-cancer efficacy of nanomedicines, the complexity of the solid tumor microenvironment cannot be replicated using these models (Costa et al., 2016; Lu and Stenzel, 2018; Nath and Devi, 2016). In contrast, 3D *in vitro* cancer models, such as spheroids, can replicate several features of the *in vivo* solid tumors in terms of heterogeneity, cell and extracellular matrix interactions, pH, nutrient access, and drug permeability. For these reasons, spheroids are considered valuable tools for drug and nanomedicine screening and prediction of their outcomes *in vivo* (Costa et al., 2016; Lu and Stenzel, 2018; Nath and Devi, 2016).

First, the penetration of the nanoparticles was evaluated through CLSM using the fluorescence of Mito for visualization. As shown in Fig. 7, fluorescence signals were found at different penetration depths, demonstrating that the nanoparticles are able to cross the physical barrier created by the spheroid. The plots of fluorescence intensity showed that the vast majority of the SLN could effectively penetrate at the outer layers of the spheroid, with some of them being able to reach the core, as shown by the weak fluorescence signal obtained from the inner sections. These results are in agreement with other works where it was demonstrated that the inner layer of the spheroid is less affected by

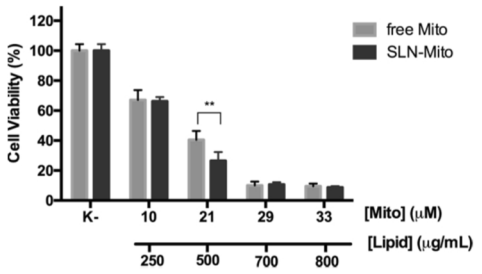



**Fig. 8.** Anti-cancer activity of SLN-Mito versus free Mito on heterotypic spheroids. Data are expressed as mean ± SD (n = 30). Differences between groups were determined using two-way ANOVA with Tukey's test. $^{**}p < 0.01$.

the effect of nanomedicines (Lee et al., 2009). Such is a consequence of the higher resistance of spheroids to nanomedicines' penetration (*e.g.* due to increased cell–cell interactions) (Lee et al., 2009).

Overall, SLN-Mito showed a similar capacity to the free drug to penetrate the spheroid.

To evaluate the anti-cancer efficacy, different concentrations of SLN-Mito and corresponding free drug were tested in the heterotypic breast cancer spheroids (Fig. 8). A dose-dependent response was obtained with similar effects induced by the free drug and SLN-Mito (approximately 66% of viability) at the lowest concentration tested (10 μM). At a concentration of 21 μM, SLN-Mito elicited a significantly higher cell death with only 27% viable cells remaining compared to 41% induced by the free drug. For the highest concentrations tested, anti-cancer effects were similar for both treatments with approximately 9% of cell viability obtained at the highest concentration tested. These results contrast to what occurred in the 2D cultures (Fig. 6**B**), where SLN-Mito reduced cell viability to 44% compared to 65% of the free drug at a concentration of 10 μM, and at 21 μM or higher concentrations almost full eradication (4% cell viability) was achieved after treatment with SLN-Mito. This can be attributed to the high complexity of the 3D model, which makes it less susceptible to anti-cancer therapeutics when compared to cells cultured in monolayer. For instance, the limited amount of oxygen and nutrients in the tumor spheroid may lead to an enhanced number of quiescent cells, which have a higher therapeutic resistance. Moreover, heterotypic spheroids were used in this study to better mimic the heterogeneity of the tumor tissue. This may further increase the therapeutic resistance of the spheroid due to increased secretion of cytokines and proliferation factors resultant from the interaction between fibroblasts and MCF-7 cells (Nunes et al., 2019).

The effect of 21 μM of both free Mito and SLN-Mito (of Mito equivalents) was further evaluated by staining with Calcein-AM/PI and visualization using CLSM. As shown in Fig. 9, in the negative control spheroids present a regular spherical morphology and are composed by an outer layer with living proliferating cells (stained with Calcein-AM) and a necrotic core, as predicted for these types of spheroids (Wallace and Guo, 2013). A much higher amount of PI-stained cells is visible following both treatments when compared to the control. When comparing the two treatments it is possible to observe that SLN-Mito induced a higher amount of PI-stained cells than the free drug, which is in agreement with the anti-cancer activity results shown in Fig. 8.

Overall, these results highlight the efficacy of the developed nanosystem for the management of breast cancer demonstrating its capacity to penetrate the breast cancer tumor spheroid and to induce a high antitumoral effect, comparable to the free drug.

## 4. Conclusion

In the present work, SLN were produced for the entrapment of the chemotherapeutic drug Mito, using an organic-solvent free and low-cost

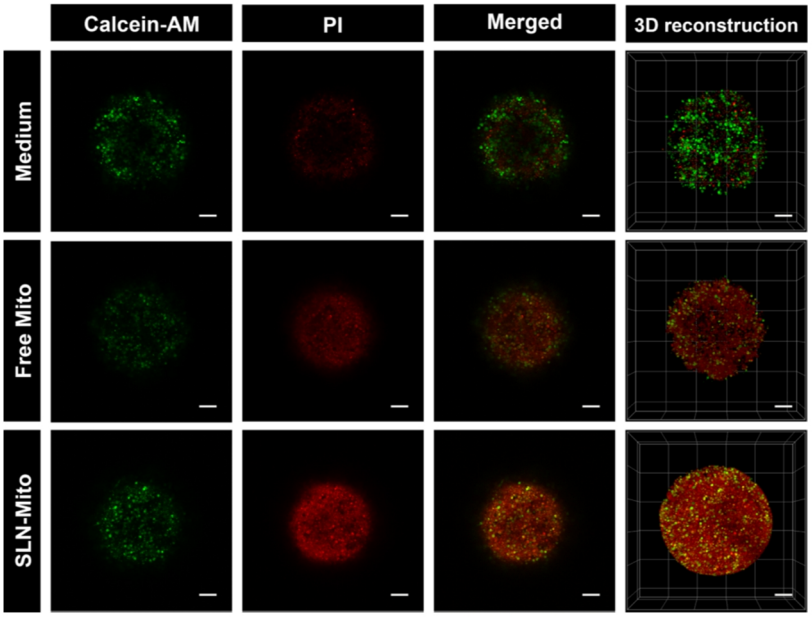



**Fig. 9.** CLSM images of heterotypic spheroids after incubation with culture medium and free drug and SLN-Mito at a concentration of 21 μM of Mito following Calcein-AM/PI staining. Green channel: Calcein-AM; Red channel: PI. Scale bars correspond to 100 μm.

production method. Particle size, EE%, and LC% were then optimized in a cost-effective way through the application of a Box-Behnken quality-by-design. Overall, SLN presented an adequate size for intravenous administration and tumor passive targeting and an EE% higher than 90% and remained stable for at least 6 months. The *in vitro* release studies suggest that following 24 h after intravenous administration, a controlled release of Mito will occur at physiological pH such as the bloodstream and normal tissues, which may limit the drugs' systemic toxicity. On the other hand, a much faster release occurs at acidic pH, such as the tumor environment and the cell endosomal compartment, where the free drug can exert its effects. Hemolysis assay conducted using human RBCs revealed that the nanoformulation in non-hemolytic even at high concentrations, further supporting its suitability for intravenous administration. Additionally, the biocompatibility of the lipid vehicle was assessed in both normal (NHDF) and cancer cells (MCF-7) showing very high tolerability even after treatment with high concentrations of lipid. The therapeutic efficacy of the nanoformulation was then evaluated in MCF-7 cells, where it was found that SLN could effectively increase the therapeutic efficacy of Mito, as shown by the values of $IC_{50}$ of the free drug versus SLN-Mito following 24 h and 48 h incubation. Finally, to better mimic the complexity of the tumor microenvironment, heterotypic spheroids were developed and the antitumoral effect of the nanoformulation was assessed. The results demonstrated that the nanoformulation was able to elicit a high antitumoral effect and effectively cross the physical barrier created by the tumor spheroid.

Overall, the results presented in this work highlight that the developed SLN are promising Mito nanocarriers for the treatment of breast cancer. Their simple and low-cost production methods and their higher stability in comparison to other clinical available nanocarriers, such as liposomes, may benefit their clinical translation in the near future.

## CRediT authorship contribution statement

**Andreia Granja:** Conceptualization, Investigation, Data curation, Formal analysis, Writing – original draft. **Rita Lima-Sousa:** Investigation, Formal analysis, Writing – review & editing. **Cátia G. Alves:** Investigation, Formal analysis, Writing – review & editing. **Duarte Melo-Diogo:** Conceptualization, Supervision, Writing – review & editing. **Marina Pinheiro:** Supervision, Writing – review & editing. **Célia T. Sousa:** Supervision, Writing – review & editing. **Ilídio J. Correia:** Resources, Supervision, Writing – review & editing. **Salette Reis:** Conceptualization, Resources, Supervision, Writing – review & editing.

## Declaration of Competing Interest

The authors declare that they have no known competing financial interests or personal relationships that could have appeared to influence the work reported in this paper.

## Acknowledgments

This work received financial support from PT national funds (FCT/MCTES, Fundação para a Ciência e Tecnologia and Ministério da Ciência, Tecnologia e Ensino Superior) through the project UIDB/50006/2020 (LAQV-REQUIMTE). This work was also financed by CENTRO-01-0145-FEDER-028989 and POCI-01-0145-FEDER-031462. Andreia Granja acknowledges FCT (Fundação para a Ciência e Tecnologia) and ESF (European Social Fund) for her PhD grant SFRH/BD/130147/2017. Rita Lima-Sousa and Cátia G. Alves acknowledge funding from individual PhD fellowships from FCT (SFRH/BD/144922/2019 and SFRH/BD/145386/2019). Duarte de Melo-Diogo acknowledges CENTRO-01-0145-FEDER-028989 for the funding given in the form of a research contract. Marina Pinheiro thanks FCT for financial support through program DL 57/2016-Norma transitória (SFRH/BPD/99124/2013). Célia T. Sousa thanks FCT for financial support through the Investigador FCT program (contract no. IF/01159/2015) and the UE's Horizon 2020 research and innovation program under the Marie Sklodowska-Curie grant no. 734801. The authors are also grateful to Dr. Rui Fernandes (Histology and Electron Microscopy Service – Instituto de Investigação e Inovação em Saúde, Universidade do Porto) for expertise and technical assistance with transmission electron microscopy.

## Appendix A. Supplementary material

Supplementary data to this article can be found online at https://doi.org/10.1016/j.ijpharm.2021.121044.

## References

Abbasalipo, R., Salehzadeh, A., Abdullah, R., 2011. Cytotoxicity effect of solid lipid nanoparticles on human breast cancer cell lines. Biotechnology 10 (6), 528–533.
Amaro-Gahete, J., Benítez, A., Otero, R., Esquivel, D., Jiménez-Sanchidrián, C., Morales, J., Caballero, Á., Romero-Salguero, F., 2019. A comparative study of particle size distribution of graphene nanosheets synthesized by an ultrasound-assisted method. Nanomaterials 9 (2), 152. https://doi.org/10.3390/nano9020152.
Attia, M.F., Anton, N., Wallyn, J., Omran, Z., Vandamme, T.F., 2019. An overview of active and passive targeting strategies to improve the nanocarriers efficiency to tumour sites. J. Pharmacy Pharmacology 71, 1185-1198.
Bai, X., Ni, J., Beretov, J., Graham, P., Li, Y., 2018. Cancer stem cell in breast cancer therapeutic resistance. Cancer Treat. Rev. 69, 152–163.
Blanco, E., Ferrari, M., 2014. Emerging nanotherapeutic strategies in breast cancer. The Breast 23 (1), 10–18.
Blanco, E., Shen, H., Ferrari, M., 2015. Principles of nanoparticle design for overcoming biological barriers to drug delivery. Nat. Biotechnol. 33 (9), 941–951.
Boedtkjer, E., Pedersen, S.F., 2020. The acidic tumor microenvironment as a driver of cancer. Annu. Rev. Physiol. 82 (1), 103–126.
Brown, M.A., Goel, A., Abbas, Z., 2016. Effect of electrolyte concentration on the stern layer thickness at a charged interface. Angew. Chem. 128 (11), 3854–3858.
Costa, E.C., Moreira, A.F., de Melo-Diogo, D., Correia, I.J., 2018a. ClearT immersion optical clearing method for intact 3D spheroids imaging through confocal laser scanning microscopy. Opt. Laser Technol. 106, 94–99.
Costa, E.C., Moreira, A.F., de Melo-Diogo, D., Correia, I.J., 2018b. Polyethylene glycol molecular weight influences the Clear T2 optical clearing method for spheroids imaging by confocal laser scanning microscopy. J. Biomed. Opt. 23, 055003.
Costa, E.C., Moreira, A.F., de Melo-Diogo, D., Gaspar, V.M., Carvalho, M.P., Correia, I.J., 2016. 3D tumor spheroids: an overview on the tools and techniques used for their analysis. Biotechnol. Adv. 34 (8), 1427–1441.
Danaei, M., Dehghankhold, M., Ataei, S., Hasanzadeh Davarani, F., Javanmard, R., Dokhani, A., Khorasani, S., Mozafari, M., 2018. Impact of particle size and polydispersity index on the clinical applications of lipidic nanocarrier systems. Pharmaceutics 10 (2), 57. https://doi.org/10.3390/pharmaceutics10020057.
Doktorovova, S., Souto, E.B., Silva, A.M., 2014. Nanotoxicology applied to solid lipid nanoparticles and nanostructured lipid carriers–a systematic review of in vitro data. Eur. J. Pharm. Biopharm. 87 (1), 1–18.
Ernsting, M.J., Murakami, M., Roy, A., Li, S.-D., 2013. Factors controlling the pharmacokinetics, biodistribution and intratumoral penetration of nanoparticles. J. Controlled Release : Official J. Controlled Release Soc. 172 (3), 782–794.
Fan, Y., Sahdev, P., Ochyl, L.J., J. Akerberg, J., Moon, J.J., 2015. Cationic liposome–hyaluronic acid hybrid nanoparticles for intranasal vaccination with subunit antigens. J. Control. Release 208, 121–129.
Feng, L., Mumper, R.J., 2013. A critical review of lipid-based nanoparticles for taxane delivery. Cancer Lett. 334 (2), 157–175.
Ferreira, M., Chaves, L.L., Lima, S.A.C., Reis, S., 2015. Optimization of nanostructured lipid carriers loaded with methotrexate: a tool for inflammatory and cancer therapy. Int. J. Pharm. 492 (1-2), 65–72.
Filipe, V., Hawe, A., Jiskoot, W., 2010. Critical evaluation of Nanoparticle Tracking Analysis (NTA) by NanoSight for the measurement of nanoparticles and protein aggregates. Pharm. Res. 27 (5), 796–810.
Gidwani, B., Vyas, A., 2016. Preparation, characterization, and optimization of altretamine-loaded solid lipid nanoparticles using Box-Behnken design and response surface methodology. Artif. Cells Nanomed. Biotechnol. 44 (2), 571–580.
Goutayer, M., Dufort, S., Josserand, V., Royère, A., Heinrich, E., Vinet, F., Bibette, J., Coll, J.-L., Texier, I., 2010. Tumor targeting of functionalized lipid nanoparticles: assessment by in vivo fluorescence imaging. Eur. J. Pharm. Biopharm. 75 (2), 137–147.
Granja, A., Vieira, A.C., Chaves, L.L., Nunes, C., Neves, A.R., Pinheiro, M., Reis, S., 2017. Folate-targeted nanostructured lipid carriers for enhanced oral delivery of epigallocatechin-3-gallate. Food Chem. 237, 803–810.
Huang, D., Sun, L., Huang, L., Chen, Y., 2021. Nanodrug delivery systems modulate tumor vessels to increase the enhanced permeability and retention effect. J. Personalized Med. 11 (2), 124. https://doi.org/10.3390/jpm11020124.
Imanparast, A., Bakhshizadeh, M., Salek, R., Sazgarnia, A., 2018. Pegylated hollow gold-mitoxantrone nanoparticles combining photodynamic therapy and chemotherapy of cancer cells. Photodiagn. Photodyn. Ther. 23, 295–305.
ISO10993-4, 2017. Biological Evaluation of Medical Devices Part 4. Selection of Tests for Interactions with Blood. International Organization for Standardization, Geneva, Switzerland.

Joseph, E., Reddi, S., Rinwa, V., Balwani, G., Saha, R., 2017. Design and in vivo evaluation of solid lipid nanoparticulate systems of Olanzapine for acute phase schizophrenia treatment: Investigations on antipsychotic potential and adverse effects. Eur. J. Pharm. Sci. 104, 315–325.
Kim, S.W., Oh, K.T., Youn, Y.S., Lee, E.S., 2014. Hyaluronated nanoparticles with pH-and enzyme-responsive drug release properties. Colloids Surf., B 116, 359–364.
Lasa-Saracibar, B., Estella-Hermoso de Mendoza, A., Guada, M., Dios-Vieitez, C., Blanco-Prieto, M.J., 2012. Lipid nanoparticles for cancer therapy: state of the art and future prospects. Expert Opinion on Drug Delivery 9 (10), 1245–1261.
Yu, L.X., Amidon, G., Khan, M.A., Hoag, S.W., Polli, J., Raju, G.K., Woodcock, J., 2014. Understanding pharmaceutical quality by design. The AAPS J. 16 (4), 771–783.
Lee, J., Lilly, G.D., Doty, R.C., Podsiadlo, P., Kotov, N.A., 2009. In vitro toxicity testing of nanoparticles in 3D cell culture. Small 5, 1213–1221.
Lima-Sousa, R., de Melo-Diogo, D., Alves, C.G., Cabral, C.S.D., Miguel, S.P., Mendonça, A.G., Correia, I.J., 2020. Injectable in situ forming thermo-responsive graphene based hydrogels for cancer chemo-photothermal therapy and NIR light-enhanced antibacterial applications. Mater. Sci. Eng., C 117, 111294. https://doi.org/10.1016/j.msec.2020.111294.
Lu, B., Xiong, S.-B., Yang, H., Yin, X.-D., Chao, R.-B., 2006. Solid lipid nanoparticles of mitoxantrone for local injection against breast cancer and its lymph node metastases. Eur. J. Pharm. Sci. 28 (1-2), 86–95.
Lu, H., Stenzel, M.H., 2018. Multicellular tumor spheroids (MCTS) as a 3D in vitro evaluation tool of nanoparticles. Small 14 (13), 1702858. https://doi.org/10.1002/smll.v14.1310.1002/smll.201702858.
Luengo-Fernandez, R., Leal, J., Gray, A., Sullivan, R., 2013. Economic burden of cancer across the European Union: a population-based cost analysis. Lancet Oncol. 14 (12), 1165–1174.
Ma, Y., Zhou, L., Zheng, H., Xing, L., Li, C., Cui, J., Che, S., 2011. pH-responsive mitoxantrone (MX) delivery using mesoporous silica nanoparticles (MSN). J. Mater. Chem. 21 (26), 9483. https://doi.org/10.1039/c1jm10750j.
Magalhães, J., L. Chaves, L., C. Vieira, A., G. Santos, S., Pinheiro, M., Reis, S., 2020. Optimization of rifapentine-loaded lipid nanoparticles using a quality-by-design strategy. Pharmaceutics 12 (1), 75. https://doi.org/10.3390/pharmaceutics12010075.
Mei, K.-C., Liao, Y.-P., Jiang, J., Chiang, M., Khazaieli, M., Liu, X., Wang, X., Liu, Q.i., Chang, C.H., Zhang, X., Li, J., Ji, Y., Melano, B., Telesca, D., Xia, T., Meng, H., Nel, A. E., 2020. Liposomal delivery of mitoxantrone and a cholesteryl indoximod prodrug provides effective chemo-immunotherapy in multiple solid tumors. ACS Nano 14 (10), 13343–13366.
Mei, L., Zhang, Z., Zhao, L., Huang, L., Yang, X.-L., Tang, J., Feng, S.-S., 2013. Pharmaceutical nanotechnology for oral delivery of anticancer drugs. Adv. Drug Deliv. Rev. 65 (6), 880–890.
Miao, J., Du, Y.-Z., Yuan, H., Zhang, X.-G., Hu, F.-Q., 2013. Drug resistance reversal activity of anticancer drug loaded solid lipid nanoparticles in multi-drug resistant cancer cells. Colloids Surf., B 110, 74–80.
Minchinton, A.I., Tannock, I.F., 2006. Drug penetration in solid tumours. Nat. Rev. Cancer 6 (8), 583–592.
Mishra, V., Thakur, S., Patil, A., Shukla, A., 2018. Quality by design (QbD) approaches in current pharmaceutical set-up. Expert Opinion on Drug Delivery 15 (8), 737–758.
Mó, I., Alves, C.G., de Melo-Diogo, D., Lima-Sousa, R., Correia, I.J., 2020. Assessing the combinatorial chemo-photothermal therapy mediated by sulfobetaine methacrylate-functionalized nanoparticles in 2D and 3D in vitro cancer models. Biotechnol. J. 15 (12), 2000219. https://doi.org/10.1002/biot.v15.1210.1002/biot.202000219.
Nath, S., Devi, G.R., 2016. Three-dimensional culture systems in cancer research: Focus on tumor spheroid model. Pharmacol. Ther. 163, 94–108.
Nunes, A.S., Barros, A.S., Costa, E.C., Moreira, A.F., Correia, I.J., 2019. 3D tumor spheroids as in vitro models to mimic in vivo human solid tumors resistance to therapeutic drugs. Biotechnol. Bioeng. 116 (1), 206–226.
Pedrosa, L.R.C., ten Hagen, T.L.M., Süss, R., van Hell, A., Eggermont, A.M.M., Verheij, M., Koning, G.A., 2015. Short-chain glycoceramides promote intracellular mitoxantrone delivery from novel nanoliposomes into breast cancer cells. Pharm. Res. 32 (4), 1354–1367.
Posner, L.E., Dukart, G., Goldberg, J., Bernstein, T., Cartwright, K., 1985. Mitoxantrone: an overview of safety and toxicity. Invest. New Drugs 3, 123–132.
Rajapaksa, T.E., Bennett, K.M., Hamer, M., Lytle, C., Rodgers, V.G.J., Lo, D.D., 2010. Intranasal M cell uptake of nanoparticles is independently influenced by targeting ligands and buffer ionic strength. J. Biol. Chem. 285 (31), 23739–23746.
Rossato, L.G., Costa, V.M., de Pinho, P.G., Arbo, M.D., de Freitas, V., Vilain, L., de Lourdes Bastos, M., Palmeira, C., Remião, F., 2013. The metabolic profile of mitoxantrone and its relation with mitoxantrone-induced cardiotoxicity. Arch. Toxicol. 87 (10), 1809–1820.
Ruktanonchai, U., Sakulkhu, U., Bejrapha, P., Opanasopit, P., Bunyapraphatsara, N., Junyaprasert, V., Puttipipatkhachorn, S., 2009. Effect of lipid types on physicochemical characteristics, stability and antioxidant activity of gamma-oryzanol-loaded lipid nanoparticles. J. Microencapsul. 26 (7), 614–626.
Sargazi, A., Shiri, F., Keikha, S., Majd, M.H., 2018. Hyaluronan magnetic nanoparticle for mitoxantrone delivery toward CD44-positive cancer cells. Colloids Surf., B 171, 150–158.
Singh, R., Lillard, J.W., 2009. Nanoparticle-based targeted drug delivery. Exp. Mol. Pathol. 86 (3), 215–223.
Sun, L.i., Legood, R., dos-Santos-Silva, I., Gaiha, S.M., Sadique, Z., Diaby, V., 2018. Global treatment costs of breast cancer by stage: a systematic review. PLoS ONE 13 (11), e0207993.
Sung, H., Ferlay, J., Siegel, R.L., Laversanne, M., Soerjomataram, I., Jemal, A., Bray, F., 2021. Global cancer statistics 2020: GLOBOCAN estimates of incidence and mortality worldwide for 36 cancers in 185 countries. CA Cancer J. Clin. 71 (3), 209–249.
Varadwaj, P., Misra, K., Sharma, A., Kumar, R., 2010. Mitoxantrone: an agent with promises for anticancer therapies. Electron. J. Biol. 6, 36–42.
Wallace, D.I., Guo, X., 2013. Properties of tumor spheroid growth exhibited by simple mathematical models. Front. Oncol. 3, 51.
Wang, J., Asghar, S., Jin, X., Chen, Z., Huang, L., Ping, Q., Zong, L.i., Xiao, Y., 2018. Mitoxantrone-loaded chitosan/hyaluronate polyelectrolyte nanoparticles decorated with amphiphilic PEG derivates for long-circulating effect. Colloids Surf., B 171, 468–477.
Wang, L., Zhao, Y., Li, T., Cao, J., Du, Y., Tao, Z., Peng, W., Wang, B., Zhang, J., Wang, Z., 2020. Efficacy and safety of liposomal mitoxantrone (Lipo-MIT) in advanced breast cancer (ABC): A randomized, open label, active-controlled, single-center, phase II clinical trial. American Society of Clinical Oncology.
Wicki, A., Witzigmann, D., Balasubramanian, V., Huwyler, J., 2015. Nanomedicine in cancer therapy: challenges, opportunities, and clinical applications. J. Controlled Release: Official J. Controlled Release Soc. 200, 138–157.
Xu, Y., Shan, Y., Zhang, Y., Yu, B., Shen, Y., Cong, H., 2019. Multifunctional Fe3O4@ C-based nanoparticles coupling optical/MRI imaging and pH/photothermal controllable drug release as efficient anti-cancer drug delivery platforms. Nanotechnology 30 (42), 425102. https://doi.org/10.1088/1361-6528/ab2e40.
Ying, X.-Y., Cui, D., Yu, L., Du, Y.-Z., 2011. Solid lipid nanoparticles modified with chitosan oligosaccharides for the controlled release of doxorubicin. Carbohydr. Polym. 84 (4), 1357–1364.
Zhuang, Y.-G., Xu, B., Huang, F., Wu, J.-J., Chen, S., 2012. Solid lipid nanoparticles of anticancer drugs against MCF-7 cell line and a murine breast cancer model. Die Pharmazie-An Int. J. Pharm. Sci. 67, 925–929.

# Supplementary data

## Mitoxantrone-loaded lipid nanoparticles for breast cancer therapy – quality-by-design approach and efficacy assessment in 2D and 3D *in vitro* cancer models.

Andreia Granja[1], Rita Lima-Sousa[2], Cátia G. Alves[2], Duarte de Melo-Diogo[2], Marina Pinheiro[1], Célia T. Sousa[3], Ilídio J. Correia[2,4] and Salette Reis[1]

[1]LAQV, REQUIMTE, Departamento de Ciências Químicas, Faculdade de Farmácia, Universidade do Porto,
4050-313 Porto, Portugal
[2]CICS-UBI – Centro de Investigação em Ciências da Saúde, Universidade da Beira Interior, 6200-506 Covilhã, Portugal
[3]IFIMUP-IN and Departamento de Física e Astronomia da Faculdade de Ciências da Universidade do Porto, Rua do Campo Alegre 687, 4169-007, Porto, Portugal
[4]CIEPQPF – Departamento de Engenharia Química, Universidade de Coimbra, Rua Sílvio Lima, 3030-790 Coimbra, Portugal

*corresponding authors: Ilídio J. Correia: icorreia@ubi.pt; Salette Reis: shreis@ff.up.pt;

**Table S1. Lipid screening.** Solubility study of mitoxantrone in different solid lipids

| | **Ratio (Mito:Lipid)** | |
|---|---|---|
| **Lipid** | **1:6** | **1:10** |
| Compritol 888 ATO | - | + |
| Precirol ATO5 | + | ++ |
| Monosteol | - | - |
| Cetyl Palmitate | + | ++ |
| Gelucire 43/01 | + | + |
| Labrafil M 2130 CS | + | ++ |
| Softisan 649 | - | - |
| Softisan 100 | - | - |
| Dynasan 114 | - | - |
| Dynasan 118 | - | - |
| Witepsol S51 | - | - |
| Witepsol E76 | - | - |
| Witepsol E85 | - | - |

$^{-}$ not soluble $^{+}$slightly soluble $^{++}$soluble

**Table S2.** Composition of the 15 formulations produced for the experimental design and correspondent characterization parameters: Size, EE%, and LC%.

| | Factors | | | Responses | | |
|---|---|---|---|---|---|---|
| Formulation | **Solid lipid (mg) ($X_1$)** | **Surfactant (mg) ($X_2$)** | **Mito (mg) ($X_3$)** | **Size (nm)** | **EE %** | **LC %** |
| 1 | 210 | 70 | 6 | 223.7 | 91.2 | 1.92 |
| 2 | 270 | 70 | 6 | 256.9 | 93.3 | 1.62 |
| 3 | 210 | 110 | 6 | 193.2 | 80.0 | 1.48 |
| 4 | 270 | 110 | 6 | 214.8 | 88.1 | 1.37 |
| 5 | 210 | 90 | 3 | 205.7 | 96.9 | 0.96 |
| 6 | 270 | 90 | 3 | 233.7 | 96.5 | 0.80 |
| 7 | 210 | 90 | 9 | 215.8 | 65.0 | 1.91 |
| 8 | 270 | 90 | 9 | 241.4 | 79.2 | 1.94 |
| 9 | 240 | 70 | 3 | 244.7 | 97.5 | 0.93 |
| 10 | 240 | 110 | 3 | 205.9 | 91.7 | 0.78 |
| 11 | 240 | 70 | 9 | 251.3 | 83.2 | 2.35 |
| 12 | 240 | 110 | 9 | 203.9 | 77.4 | 1.95 |
| 13 | 240 | 90 | 6 | 241.5 | 83.3 | 1.49 |
| 14 | 240 | 90 | 6 | 222.4 | 86.5 | 1.55 |
| 15 | 240 | 90 | 6 | 237.2 | 88.2 | 1.58 |

**Table S3**. Analysis of variance (ANOVA) for Size. Statistically significant values are represented in bold, *p*-value ≤ 0.05 with a 95% confidence interval.

| Factor | SS | Df | MS | F | p |
|---|---|---|---|---|---|
| **(1)Solid lipid (L)** | 1331.712 | 1 | 1331.712 | 13.26538 | 0.067807 |
| **Solid lipid (Q)** | 177.067 | 1 | 177.067 | 1.76379 | 0.315441 |
| **(2)Surfactant (L)** | **2677.298** | **1** | **2677.298** | **26.66897** | **0.035511** |
| **Surfactant (Q)** | 78.981 | 1 | 78.981 | 0.78674 | 0.468666 |
| **(3)Mitoxantrone (L)** | 80.802 | 1 | 80.802 | 0.80488 | 0.464316 |
| **Mitoxantrone (Q)** | 25.442 | 1 | 25.442 | 0.25343 | 0.664641 |
| **1L by 2L** | 33.640 | 1 | 33.640 | 0.33509 | 0.621182 |
| **1L by 2Q** | 0.180 | 1 | 0.180 | 0.00179 | 0.970072 |
| **1Q by 2L** | 23.120 | 1 | 23.120 | 0.23030 | 0.678658 |
| **1L by 3L** | 1.440 | 1 | 1.440 | 0.01434 | 0.915614 |
| **1Q by 3L** | 21.780 | 1 | 21.780 | 0.21695 | 0.687172 |
| **2L by 3L** | 18.490 | 1 | 18.490 | 0.18418 | 0.709612 |
| **Error** | 200.780 | 2 | 100.390 | | |
| **Total SS** | 5234.516 | 14 | | | |

**Table S4**. Analysis of variance (ANOVA) for EE%. Statistically significant values are represented in bold, *p*-value ≤ 0.05 with a 95% confidence interval.

| Factor | SS | df | MS | F | P |
|---|---|---|---|---|---|
| **(1)Solid lipid (L)** | 58.496 | 1 | 58.4960 | 9.6506 | 0.089871 |
| **Solid lipid Q)** | 0.778 | 1 | 0.7783 | 0.1284 | 0.754381 |
| **(2)Surfactant (L)** | 96.906 | 1 | 96.9059 | 15.9874 | 0.057232 |
| **Surfactant (Q)** | 25.001 | 1 | 25.0013 | 4.1247 | 0.179359 |
| **(3)Mitoxantrone(L)** | **809.188** | **1** | **809.1883** | **133.4988** | **0.007408** |
| **Mitoxantrone (Q)** | 4.896 | 1 | 4.8957 | 0.8077 | 0.463651 |
| **1L by 2L** | 8.912 | 1 | 8.9120 | 1.4703 | 0.349093 |
| **1L by 2Q** | 1.630 | 1 | 1.6304 | 0.2690 | 0.655695 |
| **1Q by 2L** | 2.813 | 1 | 2.8134 | 0.4641 | 0.565997 |
| **1L by 3L** | 53.704 | 1 | 53.7044 | 8.8601 | 0.096762 |
| **1Q by 3L** | 53.495 | 1 | 53.4954 | 8.8256 | 0.097087 |
| **2L by 3L** | 0.000 | 1 | 0.0000 | 0.0000 | 0.999797 |
| **Error** | 12.123 | 2 | 6.0614 | | |
| **Total SS** | 1092.904 | 14 | | | |

**Table S5.** Analysis of variance (ANOVA) for LC%. Statistically significant values are represented in bold, p-value ≤ 0.05 with a 95% confidence interval

| Factor | SS | df | MS | F | P |
|---|---|---|---|---|---|
| **(1)Solid lipid(L)** | **0.042246** | **1** | **0.042246** | **21.857** | **0.042834** |
| **Solid lipid (Q)** | 0.002121 | 1 | 0.002121 | 1.097 | 0.404774 |
| **(2)Surfactant (L)** | **0.187019** | **1** | **0.187019** | **96.759** | **0.010177** |
| **Surfactant (Q)** | 0.024433 | 1 | 0.024433 | 12.641 | 0.070809 |
| **(3)Mitoxantrone (L)** | **2.248183** | **1** | **2.248183** | **1163.149** | **0.000859** |
| **Mitoxantrone (Q)** | **0.050297** | **1** | **0.050297** | **26.023** | **0.036346** |
| **1L by 2L** | 0.009182 | 1 | 0.009182 | 4.750 | 0.161122 |
| **1L by 2Q** | 0.009501 | 1 | 0.009501 | 4.916 | 0.156911 |
| **1Q by 2L** | 0.001990 | 1 | 0.001990 | 1.029 | 0.417075 |
| **1L by 3L** | 0.010167 | 1 | 0.010167 | 5.260 | 0.148810 |
| **1Q by 3L** | 0.032249 | 1 | 0.032249 | 16.685 | 0.055034 |
| **2L by 3L** | 0.015745 | 1 | 0.015745 | 8.146 | 0.103966 |
| **Error** | 0.003866 | 2 | 0.001933 | | |
| **Total SS** | 3.084178 | 14 | | | |

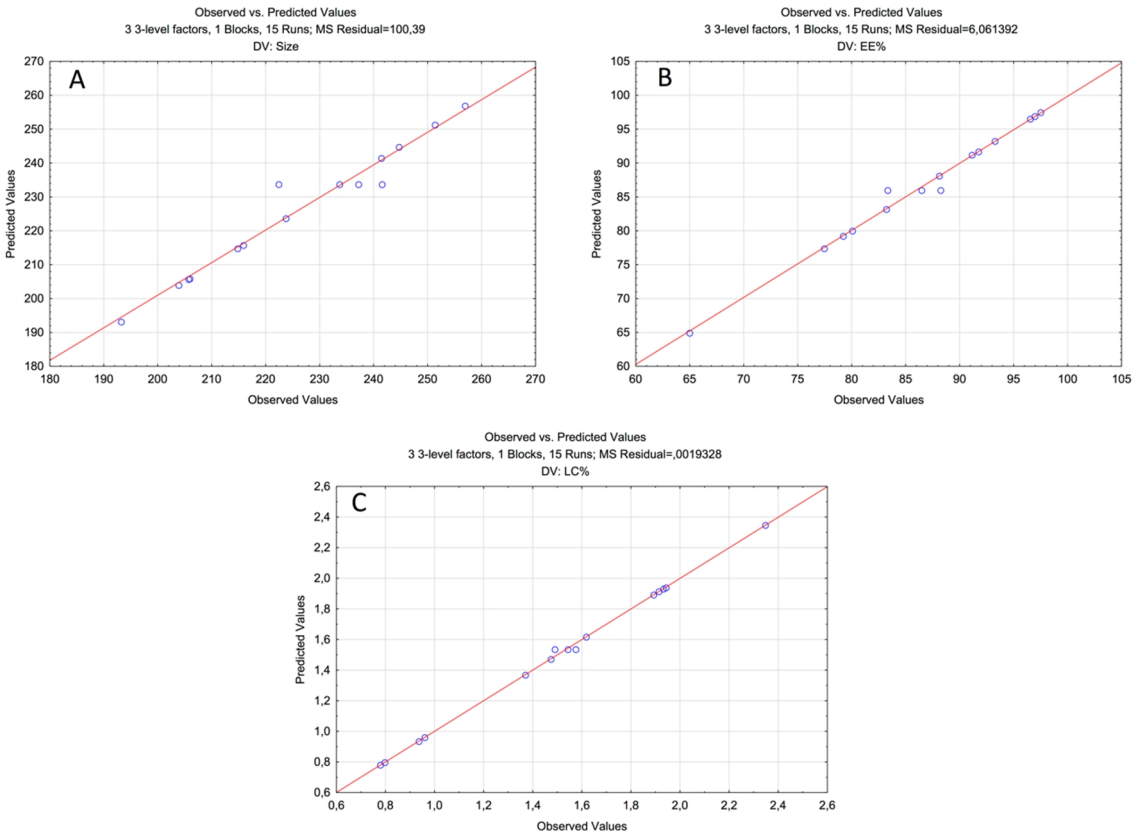



**Figure S1.** Correlation of the measured vs. predicted values of the dependent variables after fitting using the quadratic model. (**A**) Size (**B**) EE% (**C**) LC%

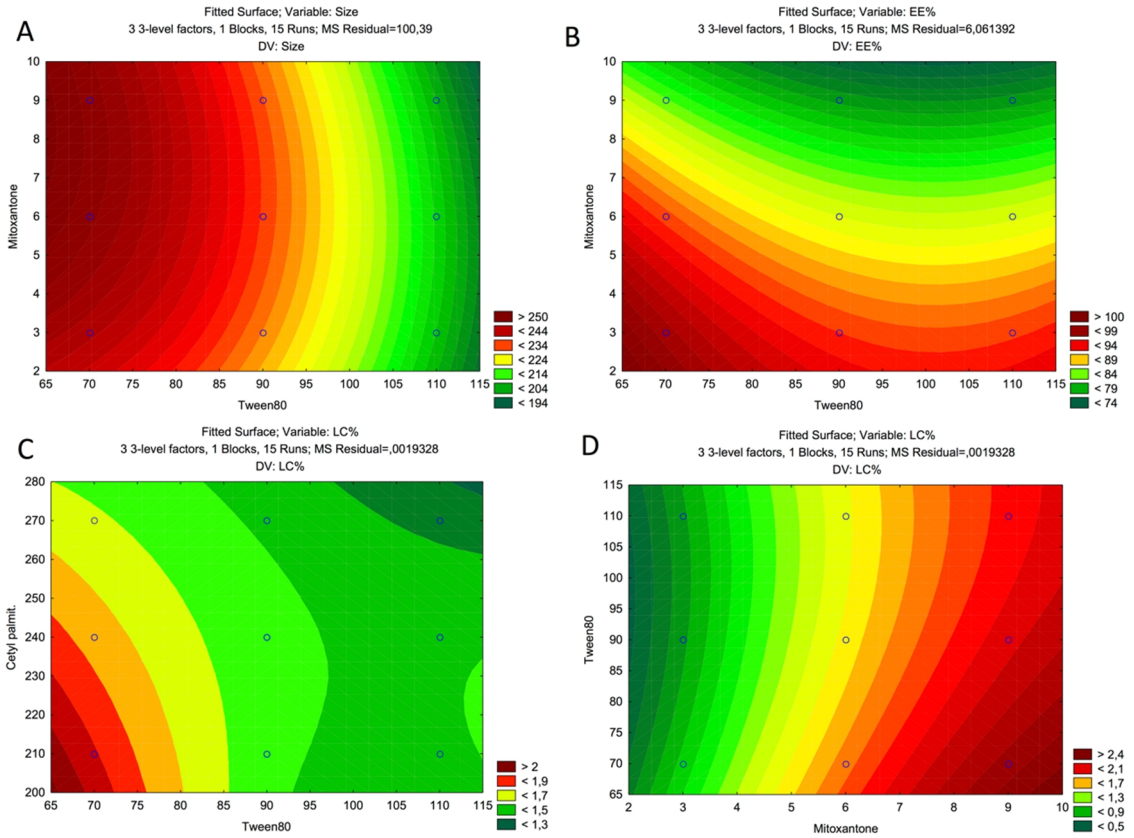



**Figure S2.** Response contour plots in two-dimensions representing the statistically significant effects (*p*-value<0.05) for each dependent variable. (**A**) Effect of the amount of Mitoxantrone and surfactant on particle size. (**B**) Effect of the amount of Mitoxantrone and surfactant on EE%. (**C**) Effect of the amount of lipid and Mitoxantrone on LC%. (**D**) Effect of the amount of lipid and surfactant on LC%.

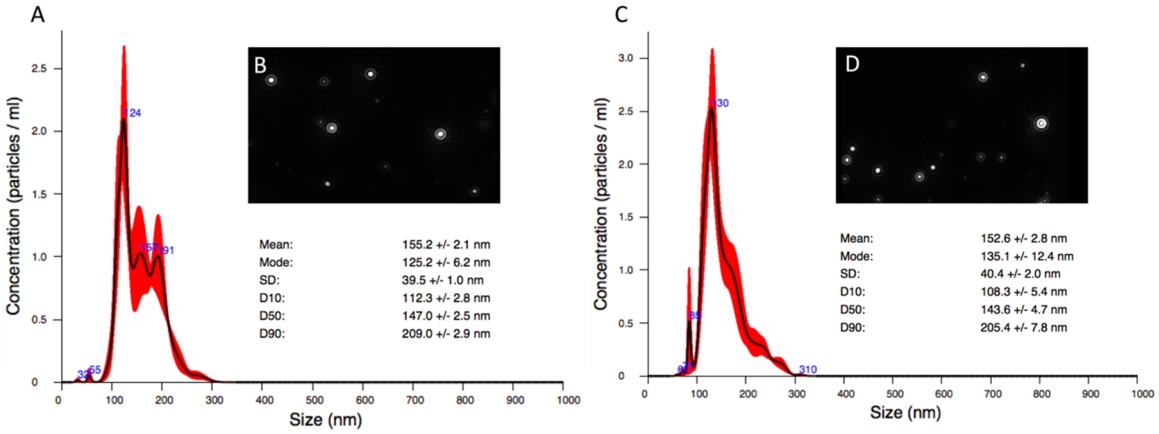



**Figure S3.** Particle size determination of SLN (A and B) and SLN-Mito (C and D) using NTA. (A) and (C) Average size distribution following 5 measurements. (B) and (D) NTA video frames

**Table S6.** Correlation coefficient ($R^2$) values obtained from fitting of different drug release models for each dissolution medium studied.

| Dissolution medium pH | Zero order | | First order | | Higuchi | | Hixson-Crowell | | Korsmeyer-Peppas | |
|---|---|---|---|---|---|---|---|---|---|---|
| | $R^2$ | $K_0$ | $R^2$ | $K_1$ | $R^2$ | $K_H$ | $R^2$ | $K_{Hc}$ | $R^2$ | $K_{KP}$ |
| **5.0** | 0.801 | 0.001 | 0.482 | 0.034 | **0.941** | 0.007 | 0.801 | -3.527 | 0.922 | 0.741 |
| **7.4** | 0.96 | 0.001 | 0.636 | 0.044 | **0.995** | 0.002 | 0.968 | -1.762 | 0.981 | 0.857 |

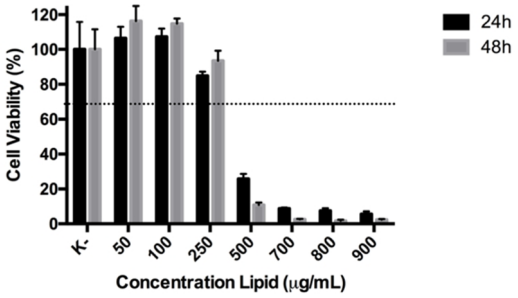



**Figure S4** Effect of unloaded SLN on the viability of HER-2 positive breast cancer cell line AU-565 (**B**) at different lipid concentrations after 24 and 48h of incubation. Data are expressed as mean ± SD (n = 5).

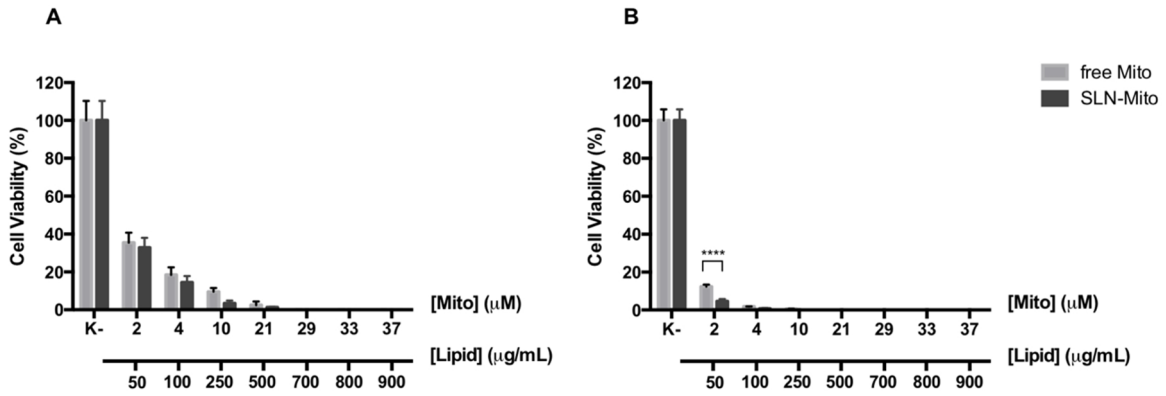



**Figure S5** Anti-cancer activity of SLN-Mito versus free Mito on AU-565 cells at increasing concentrations of Mito (and corresponding lipid concentrations) after 24h (**A**) and 48h (**B**) of incubation. Differences between groups were determined using two-way ANOVA using Tukey's test. Data are expressed as mean ± SD (n = 5). ****$p$<0.0001.

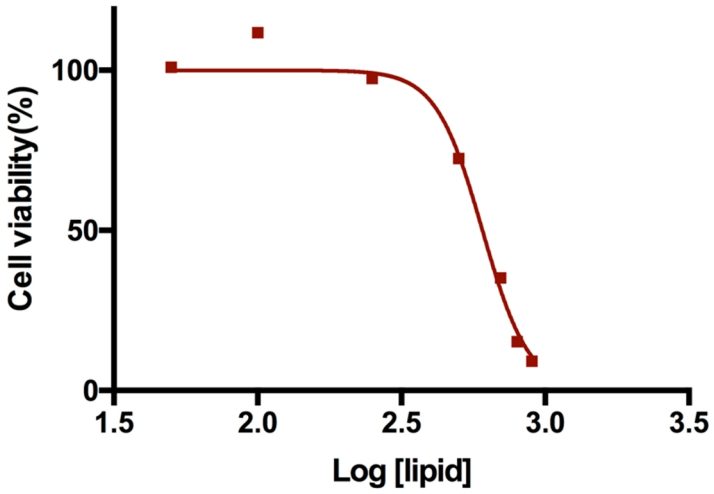



**Figure S6.** Dose-response curve of MCF-7 cells after 48h incubation with unloaded SLN.

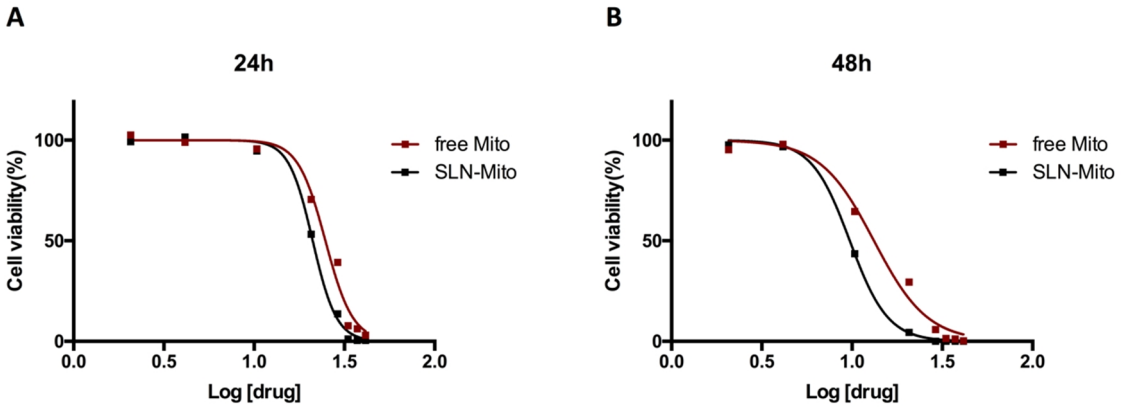


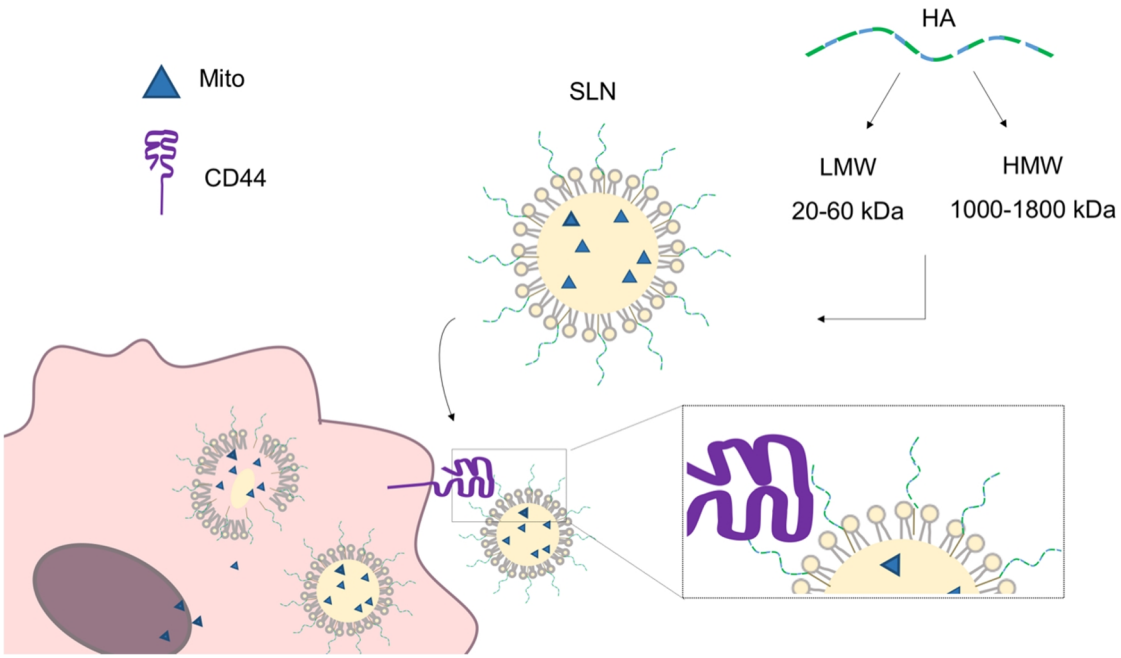

**Figure S7.** Dose-response curves of MCF-7 cells after 24h (**A**) and 48h (**B**) incubation with free mitoxantrone and SLN-Mito.

**Table S7.** $IC_{20}$, $IC_{50}$ and $IC_{80}$ values of free Mito and SLN-Mito on 2D cultures of MCF-7. Values were determined using GraphPad Prism Software (v.6.0, GraphPad Software, CA, USA).

| | **$IC_{20}$ (µM)** | **$IC_{50}$ (µM)** | **$IC_{80}$ (µM)** |
|---|---|---|---|
| **Free Mito (24h)** | 20 | 25 | 32 |
| **SLN-Mito (24h)** | 17 | 21 | 26 |
| **Free Mito (48h)** | 8 | 13 | 21 |
| **SLN-Mito (48h)** | 7 | 10 | 14 |

## 4.2. Hyaluronic acid-decorated lipid nanoparticles for enhanced delivery of mitoxantrone: assessing the influence of the polymer molecular weight on breast cancer cell targeting ability

The aim of this chapter was to improve the selectivity of the previously optimized SLN by developing an affordable active targeting strategy based on hyaluronic acid (HA). Here, SLN were functionalized with a low molecular weight (LMW) and a high molecular weight (HMW) HA. Nanoparticles were characterized to ensure that the functionalization did not substantially affect their main characteristics and the influence of the HA MW on breast cancer cell internalization was studied.



# Hyaluronic acid-decorated lipid nanoparticles for enhanced delivery of mitoxantrone: assessing the influence of the polymer molecular weight on breast cancer cell targeting ability

Andreia Granja[1,‡], Maria Francisca Bento[1,‡], Tânia Moniz[1], Cláudia Nunes[1], Célia T. Sousa[2,3] and Salette Reis[1,*]

[1]LAQV, REQUIMTE, Departamento de Ciências Químicas, Faculdade de Farmácia, Universidade do Porto, R. Jorge de Viterbo Ferreira 228, 4050-313, Porto, Portugal.
[2]IFIMUP-IN and Dep. Física e Astronomia, Faculdade de Ciências, Universidade do Porto, Rua Campo Alegre 687, 4169 - 007 Porto, Portugal
[3]Departamento de Física Aplicada, Facultad de Ciencias, Universidad Autónoma de Madrid (UAM), Campus de Cantoblanco, C/ Francisco Tomás y Valiente, 7, M 12 604 - 28049, Madrid, Spain.

‡ These authors contributed equally to this work
*corresponding author: shreis@ff.up.pt

## Abstract

Mitoxantrone (Mito) is a potent antineoplastic drug used in the treatment of advanced breast cancer. Nevertheless, issues related with lack of tumor-specificity lead to dose-limiting side-effects. In this work, a Mito delivery system based on solid lipid nanoparticles (SLN) targeting $CD44^+$ breast cancer cells is proposed. SLN were surface decorated with a conjugate containing hyaluronic acid (HA) of low (20-60 kDa) and high (1000-1800 kDa) molecular weight to evaluate the influence of this parameter on breast cancer cell targeting ability. Nanoparticles presented suitable characteristics for intravenous administration and were non-hemolytic to human RBCs. Moreover, SLN were found to be stable for at least 16 weeks. Cell viability studies conducted in MCF-7 cells demonstrated that SLN could maintain the high anti-tumoral efficacy of the free drug. Additionally, the values of $IC_{50}$ suggest that SLN functionalized with HA of a high molecular weight (SLN-HA1000) elicit a higher cytotoxicity than the low molecular weight HA- functionalized SLN. Finally, cellular uptake studies using flow cytometry and confocal microscopy pointed to an enhanced internalization of SLN-HA1000 in breast cancer cells. Overall, the resulting data suggest that the use of a high molecular weight HA for nanoparticle functionalization results in an improved breast cancer cellular uptake.

**Keywords:** Hyaluronic acid, CD44 receptor, Solid lipid nanoparticles (SLN), MCF-7 cells, cellular uptake,

# 1. Introduction

Breast cancer is the deadliest cancer type in women worldwide [1]. Chemotherapy is the main treatment for most breast cancers in advanced stage and is often included in the therapeutic regimen for different breast cancer subtypes [2]. The efficacy of this treatment modality, however, is hindered by its non-specific tissue distribution, leading to the occurrence of severe systemic side-effects. Mitoxantrone (Mito) is a DNA intercalating antineoplastic agent from the anthracenediones class with proved clinical effectiveness in the treatment different cancers, including advanced breast cancer [3, 4]. Nevertheless, several dose-limiting adverse events restrict the efficacy and clinical application of the drug, the most severe being myelosuppression and cardiotoxicity [5-8].

Nanomedicine has been explored for chemotherapy drug delivery aiming to reduce the associated adverse side-effects, improve tumor drug distribution and overcome drug multidrug resistance [9, 10]. Liposomes, in particular have already demonstrated benefits in reducing drugs' toxic effects, namely cardiotoxicity and improving response rates and progression free survival in different clinical studies [11, 12]. Nevertheless, their demanding manufacture methods, difficult scalability and high formulation costs have restricted their commercialisation and the expansion of its clinical application [13-16]. Lipid nanoparticles, such as solid lipid nanoparticles (SLN) offer a safe, economically affordable and physical stable alternative for the delivery of anti-cancer drugs [17, 18]. Despite the advantage of the EPR effect, active cancer cell targeting strategies can further enhance nanoparticles accumulation in the tumor region, while limiting non-specific tissue drug distribution. Hyaluronic acid (HA) is a glycosaminoglycan responsible to maintain the extracellular matrix integrity and mediate intra and extracellular interactions [19]. Given its biodegradability, non-immunogenic and non-toxic properties and its high affinity towards CD44 receptor, a cell transmembrane adhesion glycoprotein overexpressed in several cancers, HA is commonly used as a targeting moiety for nanoparticle surface decoration [20-22]. The binding of HA with CD44 is responsible for cell adhesion, migration and proliferation and is influenced by different factors, including the CD44 isoform and spatial distribution and HA molecular weight [23, 24]. Several biophysical studies have demonstrated that HA molecular weight is one of the determinant factors affecting the affinity of the molecule towards CD44 receptor, revealing that higher molecular weight HA has in general a stronger affinity with CD44 [25-27]. Nevertheless, the influence of this parameter on cancer cell targeting remains to be fully elucidated and is still a matter of discussion. In fact, several studies performed in cancer lines have corroborated the biophysical studies results, showing that the use of HA of a higher molecular weight results in an improved cancer cell

targeting efficiency [28-30]. In contrast, other works have shown an opposite tendency [31, 32]. Also, both high and low molecular weight HA have been explored for nanoparticle functionalization and cancer targeting [30]. In our previous work, an SLN-based Mito delivery system has been developed, demonstrating a high anti-cancer efficacy against breast cancer 2D and 3D *in vitro* models [33]. Here, HA-functionalized SLN were produced to further improve Mito breast cancer cell selectivity. Moreover, to shed light on the role of HA molecular in CD44 binding affinity, two HA targeting ligands have been synthesized containing a high and a low molecular weight HA, respectively. Breast cancer cell internalization was then studied to evaluate the influence of this parameter on breast cancer cell internalization.

# 2. Materials and methods

## 2.1. Materials

Cetyl Palmitate was kindly supplied by Gatefossé (Nanterre, France). Hyaluronic acid (HA, 20-60 kDa and 1000-1800 kDa) was kindly provided by Freshine Chemicals Company (Las Vegas, USA). Mitoxantrone hydrochloride, Tween® 80, Deuterium oxide ($D_2O$), N-hydroxysuccinimide (NHS), Ethyldimethyl-aminopropyl-carbodiimide (EDC), Hydrochloric acid (HCl), Sodium chloride, Sodium acetate solution, Dimethyl sulfoxide (DMSO), Triton™ X-100, Trypan Blue powder, Resazurin sodium salt, Dulbecco's Phosphate Buffered Saline 10X (PBS), Coumarin-6 (C6) (98%), Propidium iodide (PI) solution and Formalin solution neutral buffered 10% were obtained from Sigma-Aldrich® (St Louis, MO, USA). 1,2-dipalmitoyl-*sn*-glycero-3-phosphoethanolamine (DPPE) was obtained from Avanti Polar lipids (Merck, Darmstadt, Germany). Sodium hydroxide was acquired from VWR International (Radnor, PA, USA). Dulbecco's Modified Eagle's Medium (DMEM), 0.25% Trypsin-EDTA (1X), Penicillin-Streptomycin (PenStrep) and Heat Inactivated Fetal Bovine Serum (FBS) were purchased from Gibco® by Life Technologies™ (UK). Hoechst 33342®, Trihydrochloride, Trihydrate and LysoTracker™ Green DND-26 were obtained from Invitrogen (Invitrogen, Thermo Fisher Scientific, MA, USA). MCF-7 cell line was purchased from ATCC (Middlesex, UK). Ultrapure water was purified by an Ultra-pure water system (18.2 MΩ cm, Healforce, Shanghai, China) by a reverse osmosis process.

## 2.2. Synthesis of 1,2-dipalmitoyl-*sn*-glycero-3-phosphoethanolamine-hyaluronic acid (DPPE-HA) conjugates

Two distinct DPPE-HA conjugates were synthesized using a low (20-60 kDa) and a high HA molecular weight (1000-1800 kDa). The synthesis was performed based on a protocol previously established in our lab, with slight modifications [34]. Briefly, 0.1 g of HA were dissolved in ultrapure water (to achieve a final concentration of 2 mg/mL) followed by addition of 0.5 g of EDC and 0.52 g of NHS. After adjusting the pH to 4, the obtained solution was incubated for 2 h at 37˚C (ES-60 incubator, Lan Technics, USA). Subsequently, 0.1 g of DPPE were added to the solution and the pH was adjusted to 8.6 using borate buffer (0.1 M), followed by incubation for 24 h at 37˚C. The resulting solution was then centrifuged at 4500 RPM at 4˚C for 50 minutes (Allegra X-15R Centrifuge, Beckman Coulter, Fullerton, California) and washed three times with PBS buffer. Next, the conjugate solution was dialysed (6-8 kDa dialysis membrane, Spectrum Labs, CA, USA) against 500 mL of ultrapure water to remove reaction by-products. After 48 h, the HA-DPPE conjugate was

lyophilized for 72 h using a freeze dryer (LyoQuest −85 plus v.407, Telstar). The obtained white dry powder was stored at -20˚C until further use.

### 2.3. Nuclear magnetic resonance (NMR) analysis

To evaluate the efficacy of the synthesis, the two DPPE-HA conjugates (DPPE-HA 20 and DPPE-HA 1000) were characterized by NMR. HA, DPPE and the conjugates were dissolved in deuterium oxide ($D_2O$) in a microtube and transferred to NMR tubes. The $^1H$ spectrum of HA was obtained on a Bruker Avance III 400, operating at 400.15 MHz for $^1H$ atoms, equipped with pulse gradient units, capable of producing magnetic field pulsed gradients in the z-direction of 50.0 G/cm. NMR spectra of DPPE and conjugates were recorded on a Bruker Avance III 600 HD spectrometer, operating at 600.13 MHz for $^1H$, equipped with 5 mm CryoProbe Prodigy and pulse gradient units, capable of producing magnetic field pulsed gradients in the z-direction of 50 G/cm. The NMR measurements of DPPE and conjugates were carried out at 30 °C and with water suppression using excitation sculpting with gradients [35]. Spectra were then acquired and analysed regarding the presence of resonance signals characteristic of each component (HA20, HA1000 and DPPE) by using the standard Bruker software (version 4.01). NMR analyses were performed at Laboratory of Structural Analysis, “Centro de Materiais da Universidade do Porto” (CEMUP) (Portugal).

### 2.4. Preparation of the SLN

SLN were produced using the hot ultra-sonication method and the nanoformulation composition was established based on one of our recent studies [33]. In brief, 210 mg of cetyl palmitate and 70 mg of Tween® 80 were melted at 70˚C in a water bath. After that, 4.4 mL of pre-heated PBS were added to the lipid phase and quickly stirred for partial homogenization before sonication at 70% for 5 min (VCX130, Sonics and Material Vibra-CellTM with a CV-18 probe; 115 Newtown CT, USA). The produced nanoemulsion was cooled at room temperature and stored at 4˚C until further use. Functionalized nanoparticles were obtained by adding the DPPE-HA conjugate to the lipid phase in a ratio of 1% w/w of the total lipid mass after lipid melting. For the production of Milo-loaded SLN, 4.5 mg of Mito were dissolved in the aqueous phase and added to the lipid phase. For the cellular uptake studies using flow cytometry, C6-loaded SLN were produced by adding C6 to the lipid melt at a ratio of 0.025% of the total mass of lipid+surfactant.

### 2.5. Size, polydispersity index (PDI) and zeta potential determination

The mean particle size, PDI and zeta potential of the different nanoformulations was assessed using dynamic light scattering (DLS) and electrophoretic light scattering (ELS) in a ZetaPALS Analyzer (Brookhaven Instruments Corporation; Software: Particle Sizing v.5 Brookhaven Instruments; Holtsville, NY, USA) operating at a scattering angle of 90°, with dust cut-off set to 30 and refractive index of 1.33 at room temperature. For each determination, 3 runs of 2 min each were performed. Prior to the measurements, nanoformulations were diluted in a ratio of 1:400. Nanoparticle size distribution was also evaluated by nanoparticle tracking analysis (NTA) technique using a NanoSight NS300 (Malvern Instruments, Worcestershire, UK) equipped with a 488 nm laser and a high sensitivity scientific CMOS camera. Nanoformulations were diluted at a ratio of 1:100,000 in distilled water, injected in the viewing chamber and measured at an infusion rate of 50 at 24˚C. Size measurements were determined based on 5 independent 20s video captured with a camera level of 10 and a detection threshold of 5. Data were analyzed by using the NTA 3.4. software.

### 2.6. Entrapment Efficiency and Loading Capacity

The determination of Mito entrapment efficiency (EE%) and loading capacity (LC%) was performed by UV-vis spectrophotometry, by measuring the amount of non-entrapped drug. In brief, nanoformulations were diluted at a ratio of 1:65 and centrifuged (Allegra X-15R Centrifuge, Beckman Coulter, Fullerton, California) in centrifugal filter units (Amicon® Ultra Centrifugal Filters Ultracell-50 kDa, MERK Milipore, Ltd; Cork, Ireland) at 3900 RPM until complete separation of SLN and the aqueous phase containing the free Mito. The amount of non-entrapped Mito present in the supernatant was quantified by UV-vis spectroscopy (Jasco V-660 Spectrophotometer, Software: Spectra Manager v.2, Jasco Corportation, USA) at 610 nm.

The EE% was calculated based on the following equation:

$$EE\% = \frac{\text{Total amount of Mito-Amount of Mito in the supernatant}}{\text{Total amount of Mito}} \qquad \text{(Equation 1)}$$

The LC% was calculated per mass of lipid,surfactant and entrapped Mito as follows:

$$LC\% = \frac{\text{Total amount of Mito-Amount of Mito in the supernatant}}{\text{Amount of lipid+surfactant+EE\% } \times \text{ initial amount of Mito}} \qquad \text{(Equation 2)}$$

### 2.7. Storage stability

To evaluate the storage stability of the formulations over time, regular measurements of size, PDI, zeta potential and EE% were performed over a period of 4 months. Formulations were stored at 4˚C over this period of time. For each nanoformulation, the study was performed in triplicate.

### 2.8. *In vitro* drug release

The *in vitro* release of Mito from the two functionalized SLN (SLN-HA20 and SLN-HA1000) was investigated using a dialysis technique under sink conditions using a Slide-A-Lyzer dialysis device (Slide-A-Lyzer™ MINI Dialysis Device, MWCO 10kDa, Thermo Scientific™, MA, USA). The study was conducted at pH 7.4 (PBS), simulating the physiological environment and at pH 5.0 (acetate buffer), simulating the endosomal/lysosomal compartment. Briefly, 500 µL of each drug-loaded SLN formulation were added in the upper container of the dialysis device and the lower compartment was filled with 14 mL of the correspondent buffer media. The dialysis tubes were subsequently placed at 37˚C in an incubator shaker (ES-60, Lan Technics, USA) under agitation (100 RPM). At pre-determined time-points, aliquots (1mL) were collected from the lower compartment and replaced by an equal amount of fresh media. Finally, the amount of Mito in the release media was quantified by UV-vis spectroscopy (Jasco V-660 Spectrophotometer, Software: Spectra Manager v.2, Jasco Corporation, USA) at 610 nm. Prior to this assay, calibration curves of Mito in PBS pH 7.4 and acetate buffer pH 5.0 were obtained.

### 2.9. Hemolysis assay

A hemolysis assay was performed to evaluate the hemolytic effects of the SLN by analysing the release of hemoglobin, as an indicator of red blood cells (RBCs) lysis following NP exposure [36]. For this assay, human blood samples from three distinct donors were obtained according to the principles of the declaration of Helsinki and were kindly donated by Serviço de Hematologia from Centro Hospitalar Universitário do Porto - Hospital de Santo António. (Porto, Portugal). Blood samples were collected in tubes containing EDTA and were centrifuged at 955 × g for 5 min at 4˚C (Allegra X-15R Centrifuge, Beckman Coulter, Fullerton, California). The resulting plasma fraction (supernatant) was discarded

and the RBCs were then washed three times with physiological sterile saline solution (0.85%). After the last washing step, the resulting samples were diluted in saline solution to yield an RBCs concentration of 4% (v/v). The nanoformulations were diluted in saline solution, with final concentrations ranging from 3 to 24 mg/mL of lipid. The positive and negative controls selected for the experiment were Triton™ X-100 1% (v/v) and saline solution 0.85%, respectively. Samples were then incubated with the RBCs (at a 1:1 ratio) in 96-well plate and incubated for 1 h at 37˚C. After that, the supernatant was recovered and the release of hemoglobin was assessed by measuring the absorbance of each sample at 415 nm in a microplate reader (Biotek Instruments, Winooski, VT, USA). The percentage of hemolysis was determined according to the following equation:

$$\text{Hemolysis } \% = \frac{\text{Abs (sample)} - \text{Abs (negative control)}}{\text{Abs (positive control)} - \text{Abs (negative control)}} \qquad \text{(Equation 3)}$$

### 2.10. MCF-7 cell viability

MCF-7 cell viability following treatment with the produced SLN was measured by the resazurin assay. MCF-7 cells were seeded onto 96-well tissue culture plates (Falcon®, Becton Dickson; England)) at a density of $1x10^4$cells per well in DMEM supplemented with 10% (v/v) FBS and 1% (v/v) PenStrep and incubated for 24 h at 37˚C, 5% $CO_2$. After that, the different nanoformulations (SLN, SLN-HA20, SLN-HA1000 unloaded and loaded with Mito) and free Mito were diluted in DMEM to reach specific concentrations, which were incubated with the cells for 24 h at 37˚C, 5% $CO_2$. Positive control consisted of cells treated with only DMEM. A control media containing only DMEM was also included to correct for background fluorescence. After the incubation period, media was removed and replaced with resazurin solution (10%v/v in DMEM) followed by incubation in the dark for 4 h at 37˚C, 5% $CO_2$. The fluorescence of resorufin in the supernatant was then measured using a fluorometer (Biotek Instruments, Winooski, VT, USA) ($\lambda_{ex}$ = 560 nm; $\lambda_{em}$ = 590 nm). The dose-response curves and the values of $IC_{50}$ of free drug and drug-loaded nanoformulations were determined using GraphPad Prism Software (v.6.0, GraphPad Software, CA, USA).

### 2.11. Cellular uptake studies

The cellular uptake of the nanoformulation was studied by confocal laser scanning microscopy (CLSM) and flow cytometry.

### 2.11.1. Confocal microscopy

For the studies conducted in CLSM, MCF-7 cells were seeded in µ-slide 8-well imaging plates (Ibitreat, Ibidi GmbH, Munich, Germany) at a density of 1 x $10^4$ cells per well and grown for 24 h at 37˚C, 5% $CO_2$. Subsequently, cells were treated with the different Mito-loaded nanoformulations (SLN, SLN-HA20, SLN-HA1000) at a concentration of 0.21 µM of Mito and incubated for 4 h and 24 h at 37˚C, 5% $CO_2$. After that, medium was removed and cells were washed three times with PBS followed by staining with Lysotracker (60 nM in DMEM). After incubation for 30 min at 37˚C, 5% $CO_2$, cells were rinsed three times with PBS and fixed with formalin solution for 30 min at room temperature. After a three-step washing with PBS, cells' nucleus were stained with Hoechst (8 µM in PBS) and incubated for 10 min at room temperature protected from light followed by another three step-washing with PBS. Images were recorded on a Leica Stellaris 8 confocal microscope (LeicaMicrosystems, Wetzlar, Germany) equipped with the Leica Application Suite X package (LAS X) using a $\lambda_{ex}/\lambda_{em}$ of 350⁄461 nm (Hoechst 33342®), $\lambda_{ex}/\lambda_{em}$ of 504⁄511 nm (LysoTracker™ Green) and $\lambda_{ex}/\lambda_{em}$ of 610/630 nm (Mito) with a resolution of 1024×1024 using a 63X/1.4 oil immersion objective. CLSM images were analysed using Fiji ImageJ software (version 2.0, National Institutes of Health).

CLSM studies were performed at the Imaging by confocal and fluorescence lifetime laboratory, CEMUP (Portugal).

### 2.11.2. Flow cytometry

Flow cytometry was performed to quantify the uptake of the different SLN over-time, as previously reported [37]. To do so, C6-labeled SLN functionalized with the two DPPE-HA conjugates and without any functionalization were produced as described in **section 2.4**. MCF-7 cells were seeded in 24-well plates at a density of 2 × $10^5$ cells per well and grown for 24 h at 37˚C, 5% $CO_2$. Cells were then incubated with the different C6-labeled nanoformulations at a concentration of 250 µg/mL of lipid for 1 h, 4 h and 24 h. After the different incubation times, cells were washed twice with PBS, recovered with trypsin-EDTA 0.25% (w/v), and resuspended in PBS. Cells were then analysed in a BD Accuri C6 flow cytometer (BD Biosciences, Erembodegem, Belgium). Dead cells were excluded through PI staining (0.01 mg/mL). Trypan blue (0.004%) was added to quench the C6 signal from the non-internalized SLN. At least 10,000 events were recorded for each sample. Data analysis was performed using the BD Accuri™ C6 software (BD Biosciences, Belgium).

### 2.12. Statistical analysis

Statistical analysis was performed using Graphpad Prism6 Software (GraphPad Software Inc., CA, USA). Data were analyzed by one-way analysis of variance (ANOVA) or two-way ANOVA with a *p*-value < 0.05 considered statistically significant. All data are expressed as mean ± SD.

# 3. Results

## 3.1. $^{1}$H NMR characterization

HA of two different molecular weight (20-60 and 1000-1800 kDa) was chosen for the functionalization of the SLN to improve the targeting ability towards $CD44^{+}$ cancer cells. To this end, conjugates of the phospholipid DPPE with low MW (20-60 kDa) and high MW (1000-1800 kDa) HA were synthesized to evaluate the influence of the HA molecular weight on breast cancer cell internalization. $^{1}$H NMR spectroscopy was used to verify whether the covalent bond between DPPE and HA had been established, prior to its coupling to the SLN. For this aim, firstly the $^{1}$H NMR spectra of each component, HA and DPPE, have been recorded for the identification of the most characteristic resonance signals, as depicted in **Figure 1B and 1C**. In the $^{1}$H NMR spectrum of HA20, it was possible to register three sets of signals: a, b and c (**Figure 1A and B**), at 4.6-4.5, 3.8-3.4 and 2.0 ppm as previously reported [34]. The spectra of DPPE revealed the characteristic signals at 1.6-1.2, 0.9 and 2.3-2.1 ppm, respectively assigned as d, e and f (**Figure 1A and B**). The spectra of the resultant conjugate DPPE-HA20 showed the signals correspondent to the DPPE component at 1.6-1.2, 0.9 and 2.2-2.1 ppm, as well as those from the polymer unit, particularly the singlet at 2.0 and the low field peaks appearing between 3.8 and 3.8 ppm (**Figure 1 A and B**). The present of the two set of signals confirmed the conjugation of both components.

Regarding conjugate DPPE-HA1000, its precursor HA1000 presented signals in the $^{1}$H NMR spectrum in the same chemical shift described above for polymer HA20 (**Figure 1 A and C**). The analysis of the spectrum of the conjugate confirmed the functionalization since both sets of peaks from the polymer and the lipid were present. It was possible to detect the signals from the HA1000 at 2.0 and 4.2-3.6 ppm as well as those remaining from the lipid component (d, e and f) appearing at 1.6-1.2, 0.9 and 2.3-2.1 ppm, respectively (**Figure 1 A and C**). The results obtained are in agreement with those reported previously [34].
Globally, the NMR studies confirmed that the conjugation of HA and DPPE has been established, proving the suitability of the selected synthesis method.

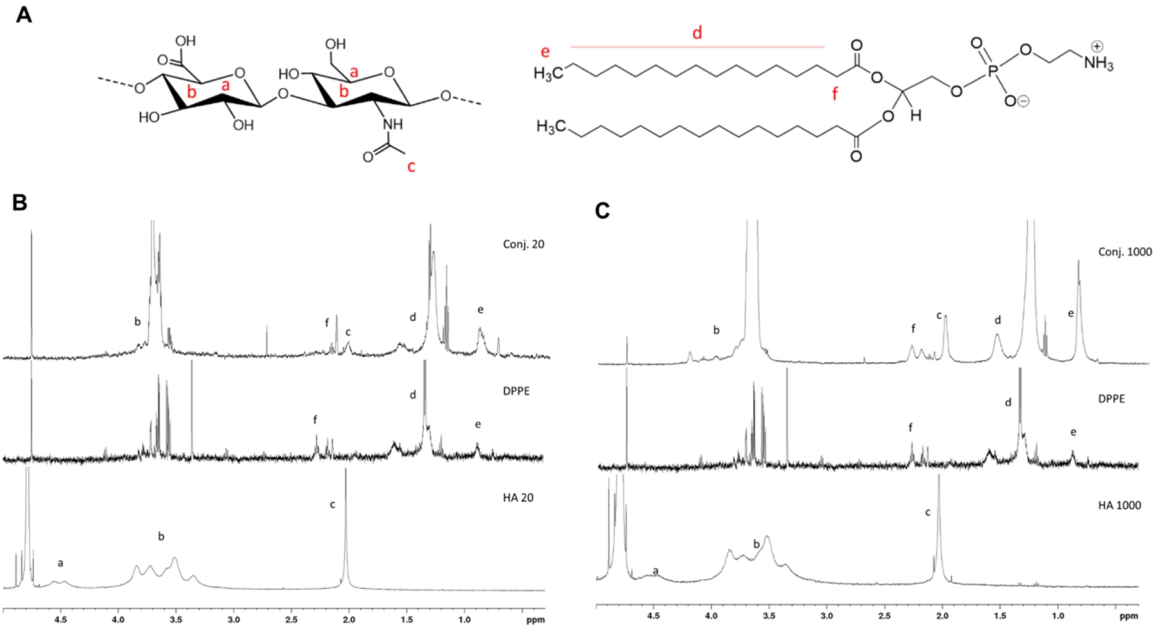



**Figure 1**. **NMR characterization of the DPPE-HA conjugates** (**A**) Chemical structure of HA (left) and DPPE (right) (**B**) NMR spectra of the DPPE-HA20 conjugate and their precursors DPPE (middle) and HA20 (bottom). (**C**) NMR spectra of the DPPE-HA1000 and their precursors DPPE (middle) and HA1000 (bottom).

### 3.2. Physicochemical characterization

A cost-effective organic-solvent free method was chosen for the production of the SLN, as reported previously [33]. Mito-loaded and unloaded nanoparticles functionalized with the two DPPE-HA conjugates were prepared and subsequently characterized in terms of size, PDI, EE% and LC% (**Table 1**). The particle size obtained ranged from 198 to 220 nm, which is adequate for intravenous administration and may also benefit from the EPR effect, leading to passive tumor targeting [38-40]. PDI values remained at values of 0.2 or lower, pointing to the presence of a homogeneous population, with acceptable monodispersity [41]. Moreover, SLN exhibited close to-neutral values of zeta potential, which is expected given the salt complexity of the solvent used [42, 43]. It is also noticeable that the loading of Mito did not have a significant influence on the particles' hydrodynamic diameter. Also, there were no significant differences in the sizes of the SLN functionalized with the two conjugates. As a complement, the SLN were also analysed by the NTA technique (**Figure S1**). The average particle size measurements using DLS and NTA were found to be relatively different, with values of 190 and 220 nm measured by DLS in contrast with the particle size of around 144 nm measured by NTA. As a single particle analysis method with

high resolution, NTA is able to detect both large and small particles providing a more accurate particle distribution. On the contrary, since large particles scatter more light than smaller ones, the DLS technique may underestimate the proportion of smaller particles in the system [44], which explains the differences found using the two methods. Finally, high values of EE% (>88%) were obtained for both nanoformulations, with no statistically significant differences between them, suggesting that the HA molecular weight had no interference on the ability of NPs to internalize the drug.

**Table 1.** Physicochemical characterization of the nanoformulations unloaded (DPPE-HA 20-60 and DPPE-HA 1000-1800) and loaded with Mito (DPPE-HA 20-60-Mito and DPPE-HA 1000-1800-Mito): size, PDI, zeta potential, EE% and LC%. Values represent mean ± SD (n=3)

| | SLN-HA20 | SLN-HA1000 | SLN-HA20-Mito | SLN-HA1000-Mito |
|---|---|---|---|---|
| **Size (nm)** | 198 ± 6 | 211 ± 8 | 198 ± 5 | 220 ± 12 |
| **PDI** | 0.16 ± 0.02 | 0.19 ± 0.02 | 0.16 ± 0.02 | 0.21 ± 0.04 |
| **Zeta potential (mV)** | -6 ± 6 | 2 ± 14 | -3 ± 13 | -3 ± 6 |
| **EE%** | N/A | N/A | 100 ± 1 | 88 ± 10 |
| **LC%** | N/A | N/A | 2.14 ± 0.02 | 1.90 ± 0.22 |

### 3.3. *In vitro* drug release

The release of Mito from the two SLN was performed using the dialysis technique at pH 7.4 and 5, simulating the physiological environment and endosomal compartment, respectively [45]. The cumulative percentages of Mito released during 24 h, is presented in **Figure 2**. It is possible to observe that at pH 7.4, only 20% of Mito was released after 8h and roughly 50% of the drug remained entrapped in the SLN at the end of the 24 h. In contrast, at pH 5.0, a much faster release occurred, with 40% release after 8h and almost complete drug release measured at the end of the study. Moreover, a similar release pattern is observed for the two nanoformulations, suggesting that the HA MW did not influence the mechanism of drug release from the nanoparticles. Overall, these results point to a controlled release profile of the SLN at physiological environment and a higher release at acidic pH, characteristic of the endosomal compartment. Therefore, this data support the suitability of the SLN for the intravenous delivery of Mito, that will presumably sustain the release of Mito while in the bloodstream, minimizing systemic side-effects, and subsequently, release the drug at a faster rate after internalization in $CD44^+$ cancer cells.

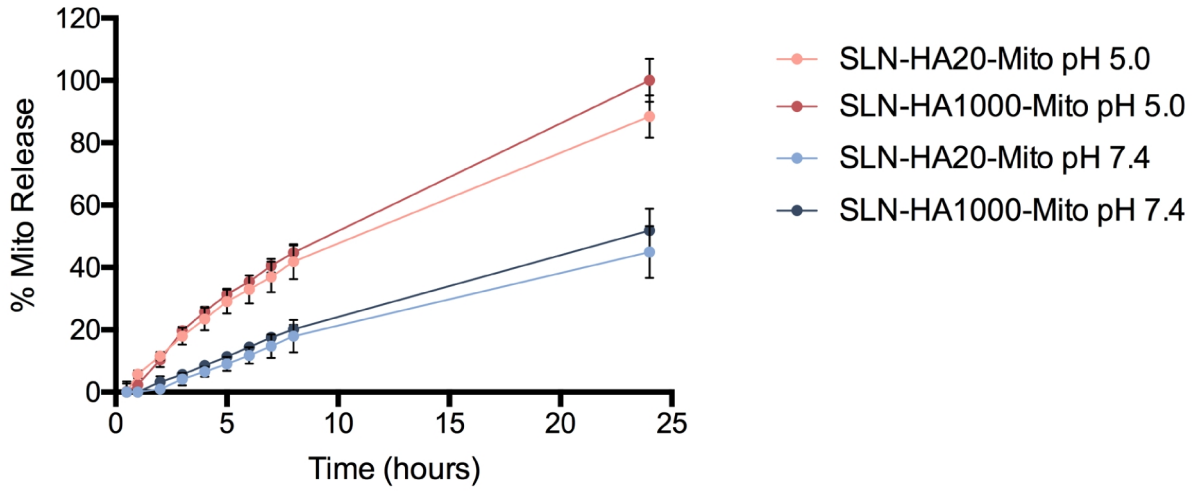



**Figure 2. *In vitro* drug release assay.** Cumulative drug release of Mito from SLN HA and SLN HA1000 at pH 7.4 and pH 5.0. Values represent mean ± SD (n=3)

### 3.4. Storage stability

The physical stability of the nanoformulations upon storage was evaluated over a period of 4 months. SLN were stored at 4˚C and periodic assessments of the nanoparticles' size, PDI, zeta potential and EE% were performed (**Figure 3**). As shown in **Figure 3A**, particle size remained stable, with only slight variations during the 4 months of study, with values remaining compatible with intravenous injection and tumor passive targeting at the end of the study. In terms of PDI, a slight increase occurred over time, nevertheless values remained below 0.3, pointing to the presence of a homogeneous population for at least 4 months (**Figure 3B**) [41]. The zeta potential values remained neutral over the course of the assay, as expected, with no statistical significant differences observed (**Figure 3C**). The EE% was also determined over time to verify the occurrence of drug expulsion during storage. As shown in **Figure 3D,** there were no statistically significant differences in EE% compared to day. Overall, these data suggest that the nanoformulations are stable for at least 4 months stored at 4˚C.

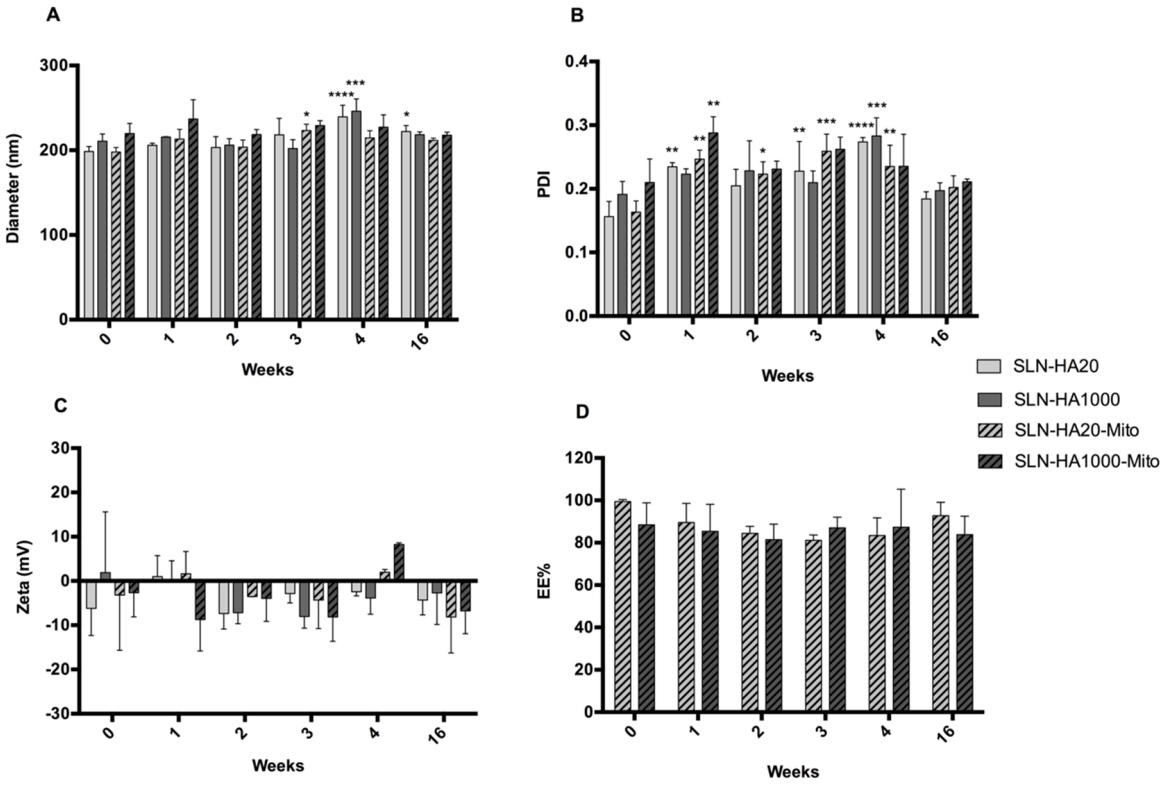



**Figure 3. Storage stability study**. Effect of the time of storage on size (A), PDI (B), zeta potential (C) and EE& (D) of SLN DPPE-HA nanoformulations unloaded (DPPE-HA) and loaded (DPPE-HA-Mito). Values represent the mean ± SD (n=3). Differences between groups were assessed using two-way ANOVA followed by Dunnet post-hoc test *p<0.05, **p<0.01, ***p<0.001, ****<0.0001 relatively to the correspondent nanoformulation at week 0.

### 3.5. Hemolysis assay

The hemocompatibility of the nanoformulations was assessed *in vitro* using human RBCs collected from 3 volunteers. As shown in **Figure 4**, no hemolytic activity was found for all the concentrations tested of each nanoformulation. These findings support that the developed formulations are non-toxic according to ISO 10993-4 [46] and, hence not hazardous as drug carrier administered intravenously.

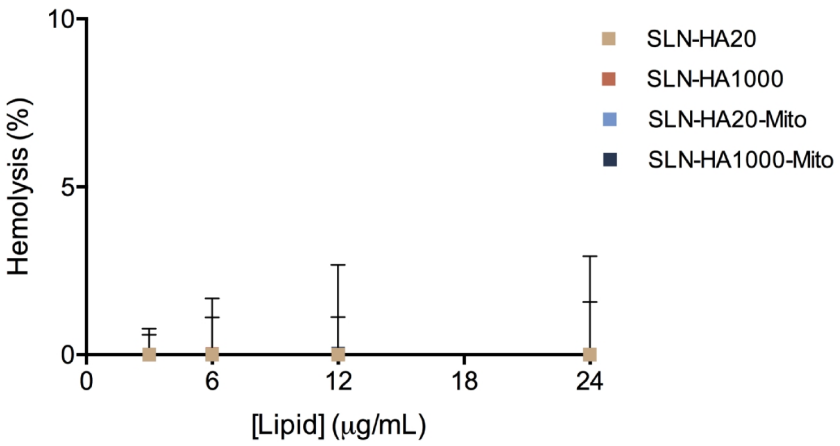



**Figure 4. *In vitro* hemolysis assay**. RBCs from three human donors were incubated with increasing concentrations of loaded and unloaded nanoformulations. Values represent mean ± SD (n=3)

### 3.6. *C*ell viability evaluation

The effects of the nanoformulation on cancer cell viability was assessed in the $CD44^+$ cell line MCF-7. First, the cytocompatibility of the unloaded nanoformulations was analysed. As shown in **Figure 5**, unloaded lipid nanocarriers were well tolerated up to a concentration of 500 µg/mL of lipid after 24 h of exposure. No statistically significant differences were observed in terms of cell viability reduction caused by functionalization of SLN, which suggests that both the lipid vehicle and the HA conjugates have a high cytocompatibility. The viability of MCF-7 cells incubated with the drug-loaded nanoparticles is presented in **Figure 6A**. The presented data show a reduction in cancer cell viability comparable to that of the free drug, proving the anti-cancer efficacy of the nanoformulation. This could be observed for concentrations as low as 2.10 µM of drug (corresponding to 50 µg/mL of lipid). The results of cell viability were then used to plot dose-response curves (**Figure S2**) and determine the values of $IC_{50}$ (**Figure 6B**). These results further support that the nanoparticles induced similar anti-cancer effects than the free drug. It is also suggested that SLN functionalized with the HA of higher MW (SLN HA1000-1800-Mito) elicit a higher cytotoxicity towards MCF-7 cells when compared to SLN functionalized with the lower HA MW (SLN HA20-60-Mito).

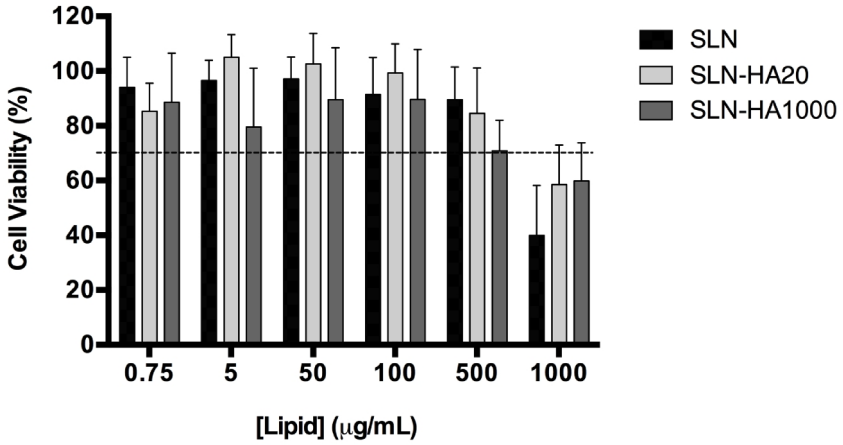
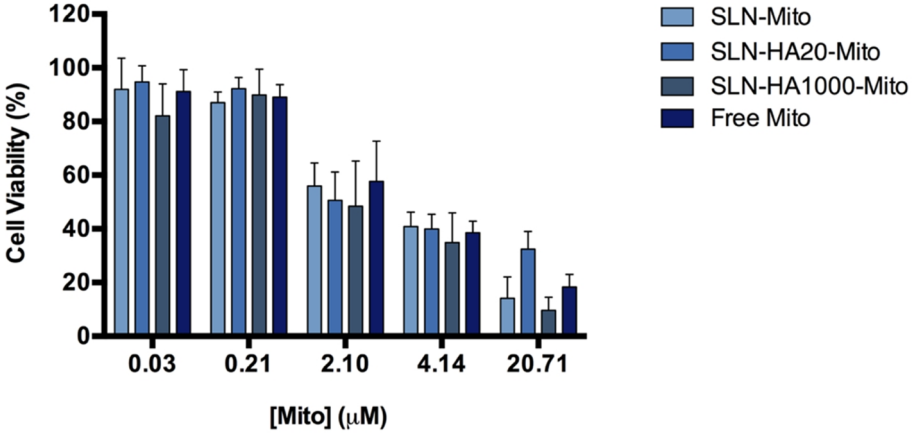



**Figure 5. Effects of the unloaded SLN on MCF-7 cell viability.** Cell viability was assessed by the resazurin assay after 24 h of exposure to the different unloaded nanoformulations at increasing concentrations of lipid. Values represent the mean ± SD (n=3).

A




B

| | SLN-Mito | SLN HA20-60-Mito | SLN HA1000-1800-Mito | Free Mito |
|---|---|---|---|---|
| $IC_{50}$ (μM) | 2.55 | 3.10 | 1.85 | 2.68 |

**Figure 6. Effects of drug-loaded SLN on MCF-7 cell viability**. (A) Cell viability was assessed by the resazurin assay after 24 h of exposure to the different drug-loaded nanoformulations at increasing concentrations of Mito. Values represent the mean ± SD (n=3). (B) Values of $IC_{50}$ determined for each drug-loaded nanoformulation

### 3.7. Cellular uptake visualization using CLSM

CLSM was used to assess and visualize the internalization of the nanoparticles into MCF-7 cells after 4 h and 24 h of incubation. As shown in **Figure 7**, at 4 h of incubation Mito-loaded SLN seem to mostly accumulate in the cytoplasm, including in the lysosomes, as

seen by the merge of the green and red signals. In addition, a higher fluorescence intensity could be observed in the cells incubated with both SLN-HA20-Mito and SLN-HA1000-Mito, comparing with SLN-Mito, suggesting that HA could improve cancer cell internalization. It is also noticeable that after incubation with SLN-HA1000-Mito, a higher signal of Mito fluorescence is present in the cytoplasm and nuclear region, when comparing with SLN-HA20-Mito. After 24 h, a higher fluorescence intensity was observed in the cytoplasm for all the conditions tested, as shown by the color intensity in the red channel. Additionally, a higher red fluorescence in the cell nucleus could be visualized, which suggests that at least part of the drug was released and translocated to the nuclear region, which is the drug cellular target. Since at least 40% of the drug was already released at this time point (according to the *in vitro* drug release studies presented in **section 3.3**, the differences between each condition were less evident. Overall, the CLSM images provide evidence for the preferential uptake of SLN-HA1000 into cancer cells after incubation for 4 h and a translocation of the drug to the nuclear region after incubation for 24 h.

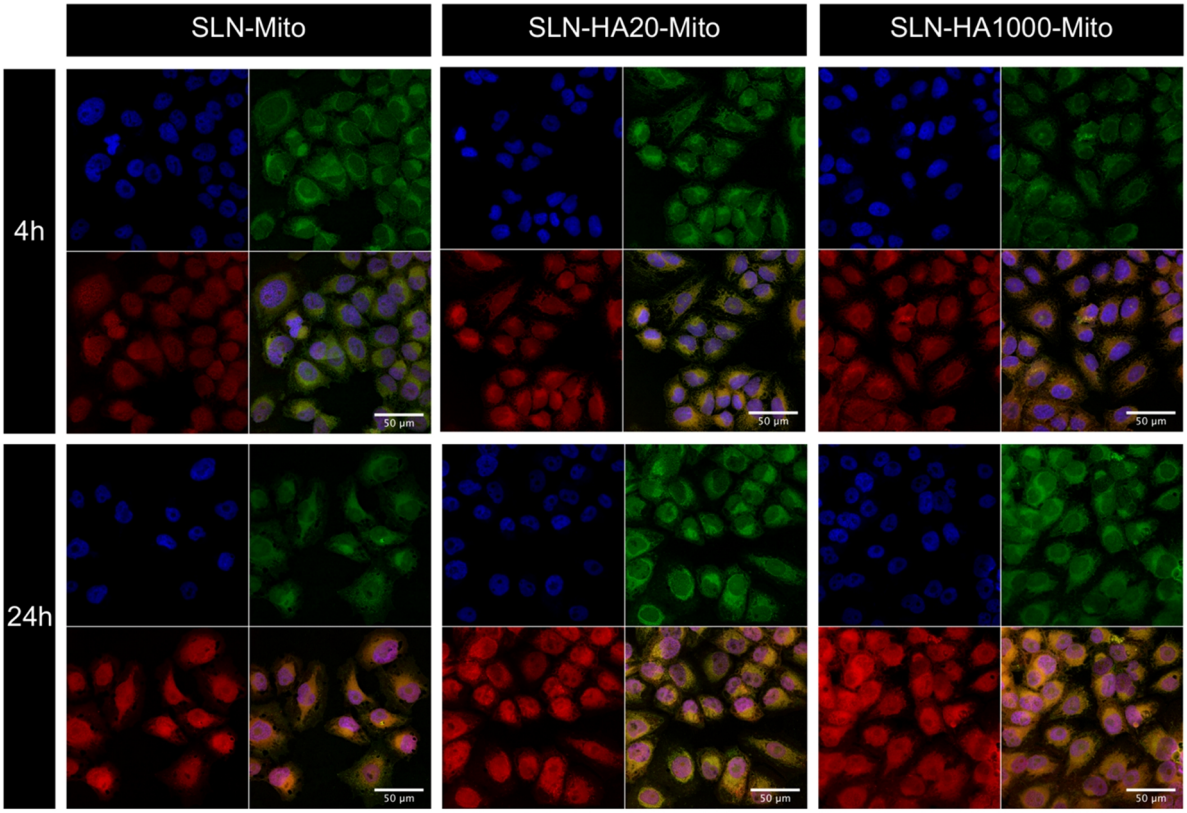



**Figure 7. CLSM images of the MCF-7 cellular uptake**. Cells were incubated with the different Mito-loaded SLN (SLN, SLN-HA20, SLN-HA1000) for 4 h and 24 h. Blue channel: Hoechst 33342 (nucleus). Green channel: LysoTracker™ Green DND-26. Red channel: Mito.

### 3.8. Cellular uptake quantification by flow cytometry

In addition to the cellular uptake imaging obtained through CLSM, a quantitative analysis was performed by flow cytometry. With that purpose, non-functionalized and HA functionalized C6-labelled SLN were produced and characterized to ensure that their physicochemical characteristics were not considerably affected (**Table S1**). The mean cell fluorescence after incubation at different time-points is shown in **Figure 8.** It is possible to observe an increase in fluorescence over time, suggesting a time-dependent uptake. A significantly higher internalization was achieved for SLN HA1000 compared to both SLN and SLN-HA20 after 1 h, 4 h and 24 h of incubation. These findings corroborate the results obtained with CLSM, where a higher internalization was visually detected after incubation with SLN-HA1000-Mito, in particular after incubation for 4 h. In addition, these data are consistent with the cell viability assay, which demonstrated that SLN-HA1000 induced a slightly higher cytotoxicity in MCF-7 cells, as assessed by the value of $IC_{50}$, which may be a result of a higher cellular internalization. Overall, cellular uptake results point to an enhanced cancer cell internalization after SLN functionalization with HA of a higher MW. This outcome is also in agreement with several biophysical-based approaches reported in the literature that demonstrated that HA of a high molecular weight has a higher binding affinity to CD44 receptor [25-27].

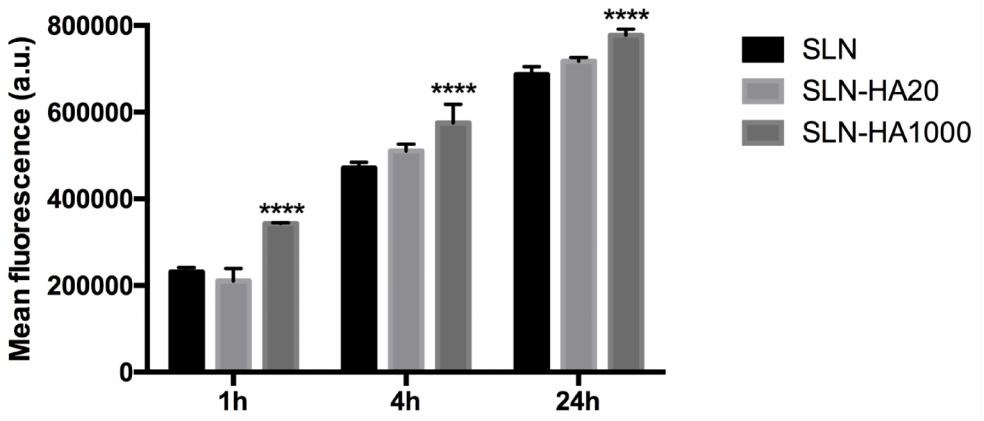



**Figure 8. MCF-7 cellular uptake of C6-loaded SLN measured by flow cytometry.** Cells were incubated with the different nanoformulations for 1 h, 4 h and 24 h. Data expressed as mean ± SD (n = 3). Differences between groups were assessed using two-way ANOVA followed by Dunnet post-hoc test **** $p<0.0001$ relatively to the non-functionalized SLN.

## 4. Conclusion

In this study, HA-functionalized SLN were developed to improve the delivery of Mito to breast cancer $CD44^+$ cells, aiming to enhance the tumor accumulation of the drug and limit its adverse side-effects. Moreover, the role of the HA MW on breast cancer cell targeting ability was also studied, by functionalizing the SLN with two HA of low and high MW, respectively (20-60 kDa and HA 1000-1800 kDa). SLN were produced using an organic-solvent free, and economically affordable production method, which may facilitate their large-scale production. Nanoparticles showed adequate characteristics for intravenous administration, as shown by their physicochemical characteristics, drug release behaviour and limited haemolytic activity. The cell viability of MCF-7 after 24 h exposure to the developed nanoformulations, revealed a high therapeutic efficacy for concentrations as low as 2.41 μM of drug (corresponding to 50 μg/mL of lipid). The values of $IC_{50}$ showed that SLN maintain the high anti-cancer effects of the free drug, with SLN-HA1000-Mito inducing a slightly higher cytotoxicity as compared with SLN-HA20-Mito. Finally, SLN uptake was evaluated in MCF-7 cells, showing a time-dependent internalization and a translocation of the drug to the nuclear region after 24 h. A preferential uptake occurred for HA1000 functionalized SLN, a fact that was demonstrated using both confocal microscopy and flow cytometry.

Overall, the strategy proposed in this work proved to be successful, leading to an improvement of the accumulation of the SLN into breast cancer cells, and desirably, a reduction of non-specific tissue accumulation, limiting the adverse side-effects of the drug. Moreover, the results here highlighted point to a preferential cancer cell internalization following functionalization with HA of 1000-1800 kDa, suggesting that the use of HA of a higher MW may be beneficial for future HA-based cancer active targeting strategies. Nevertheless, future studies should be conducted by including other breast cancer cell lines to corroborate these results and should also be validated *in vivo* in clinically relevant models.

## Acknowledgments

This work received financial support from PT national funds (FCT/MCTES, Fundação para a Ciência e Tecnologia and Ministério da Ciência, Tecnologia e Ensino Superior) through the project UIDB/50006/2020 (LAQV-REQUIMTE) and HEALTH-UNORTE I&D&I project (NORTE-01-0145-FEDER-000039) co-financed by European Regional Development Fund

(ERDF), through the NORTE 2020 (Programa Operacional Regional do Norte 2014/2020). Andreia Granja acknowledges FCT (Fundação para a Ciência e Tecnologia) and ESF (European Social Fund) for her PhD grant SFRH/BD/130147/2017. Cláudia Nunes is thankful to FCT for the investigator Grant (IF/00293/2015). Célia T. Sousa thanks FCT for financial support through the Investigador FCT program (contract no. IF/01159/2015), to the program Atraccion de Talento (CAM), ref. 2020-T1/IND-19889 and the UE's Horizon 2020 research and innovation program under the Marie Sklodowska-Curie grant no. 734801. The authors are also grateful for the technical support from the Laboratory of Structural Analysis and the Imaging by confocal and fluorescence lifetime laboratory at CEMUP, Portugal, for the NMR and CLSM studies, respectively.

## References


1. Sung, H., J. Ferlay, R.L. Siegel, M. Laversanne, I. Soerjomataram, A. Jemal, and F. Bray, *Global Cancer Statistics 2020: GLOBOCAN Estimates of Incidence and Mortality Worldwide for 36 Cancers in 185 Countries.* CA Cancer J Clin, 2021. **71**(3): p. 209-249.
2. Waks, A.G. and E.P. Winer, *Breast Cancer Treatment: A Review.* Jama, 2019. **321**(3): p. 288-300.
3. Varadwaj, P., K. Misra, A. Sharma, and R. Kumar, *Mitoxantrone: an agent with promises for anticancer therapies.* Electronic Journal of Biology, 2010. **6**(2): p. 36-42.
4. Rossato, L.G., V.M. Costa, P.G. de Pinho, M.D. Arbo, V. de Freitas, L. Vilain, M. de Lourdes Bastos, C. Palmeira, and F. Remiao, *The metabolic profile of mitoxantrone and its relation with mitoxantrone-induced cardiotoxicity.* Archives of toxicology, 2013. **87**(10): p. 1809-1820.
5. Smith, I., R. Stuart-Harris, N. Pavlidis, and T. Bozek, *Mitoxantrone (novantrone®) as single agent and in combination chemotherapy in the treatment of advanced breast cancer.* Cancer treatment reviews, 1983. **10**: p. 37-40.
6. Coleman, R., M. Maisey, R. Knight, and R. Rubens, *Mitoxantrone in advanced breast cancer—a phase II study with special attention to cardiotoxicity.* European Journal of Cancer and Clinical Oncology, 1984. **20**(6): p. 771-776.
7. Schell, F., H. Yap, G. Blumenschein, M. Valdivieso, and G. Bodey, *Potential cardiotoxicity with mitoxantrone.* Cancer treatment reports, 1982. **66**(8): p. 1641-1643.
8. Guissi, N.E.I., H. Li, Y. Xu, F. Semcheddine, M. Chen, Z. Su, and Q. Ping, *Mitoxantrone-and folate-TPGS2k conjugate hybrid micellar aggregates to circumvent toxicity and enhance efficiency for breast cancer therapy.* Molecular pharmaceutics, 2017. **14**(4): p. 1082-1094.
9. Shi, J., P.W. Kantoff, R. Wooster, and O.C. Farokhzad, *Cancer nanomedicine: progress, challenges and opportunities.* Nature reviews. Cancer, 2017. **17**(1): p. 20-37.
10. Su, Z., S. Dong, S.-C. Zhao, K. Liu, Y. Tan, X. Jiang, Y.G. Assaraf, B. Qin, Z.-S. Chen, and C. Zou, *Novel nanomedicines to overcome cancer multidrug resistance.* Drug Resistance Updates, 2021. **58**: p. 100777.
11. O'Brien, M.E., N. Wigler, M. Inbar, R. Rosso, E. Grischke, A. Santoro, R. Catane, D.G. Kieback, P. Tomczak, S.P. Ackland, et al., *Reduced cardiotoxicity and comparable efficacy in a phase III trial of pegylated liposomal doxorubicin HCl (CAELYX/Doxil) versus conventional doxorubicin for first-line treatment of metastatic breast cancer.* Ann Oncol, 2004. **15**(3): p. 440-9.
12. Wang, L., Y. Hong, J. Ma, M. Han, S. Zhang, B. Shan, and Y. Liu, *Combination of pegylated liposomal doxorubicin and docetaxel as neoadjuvant therapy for breast cancer with axillary lymph node metastasis.* J Int Med Res, 2020. **48**(8): p. 300060520944310.
13. Della Rocca, J., D. Liu, and W. Lin, *Are high drug loading nanoparticles the next step forward for chemotherapy?* Nanomedicine, 2012. **7**(3): p. 303-305.
14. Crommelin, D.J.A., P. van Hoogevest, and G. Storm, *The role of liposomes in clinical nanomedicine development. What now? Now what?* Journal of Controlled Release, 2020. **318**: p. 256-263.
15. Weber, S., A. Zimmer, and J. Pardeike, *Solid Lipid Nanoparticles (SLN) and Nanostructured Lipid Carriers (NLC) for pulmonary application: a review of the state of the art.* European journal of pharmaceutics and biopharmaceutics : official journal of Arbeitsgemeinschaft für Pharmazeutische Verfahrenstechnik e.V, 2014. **86**: p. 7-22.
16. Bunjes, H. and B. Siekmann, *Manufacture, characterization, and applications of solid lipid nanoparticles as drug delivery systems.* Microencapsulation-Methods and Industrial Applications, 2006. **213**: p. 268.
17. Bayón-Cordero, L., I. Alkorta, and L. Arana, *Application of solid lipid nanoparticles to improve the efficiency of anticancer drugs.* Nanomaterials, 2019. **9**(3): p. 474.
18. Joshi, M.D. and R.H. Müller, *Lipid nanoparticles for parenteral delivery of actives.* European journal of pharmaceutics and biopharmaceutics, 2009. **71**(2): p. 161-172.
19. Stern, R., *Hyaluronidases in cancer biology.* Hyaluronan in Cancer Biology, 2008: p. 207-220.
20. Xu, H., M. Niu, X. Yuan, K. Wu, and A. Liu, *CD44 as a tumor biomarker and therapeutic target.* Exp Hematol Oncol, 2020. **9**(1): p. 36.
21. Tiwari, S. and P. Bahadur, *Modified hyaluronic acid based materials for biomedical applications.* International journal of biological macromolecules, 2019. **121**: p. 556-571.
22. Yoo, J., C. Park, G. Yi, D. Lee, and H. Koo, *Active targeting strategies using biological ligands for nanoparticle drug delivery systems.* Cancers, 2019. **11**(5): p. 640.

23. Jordan, A.R., R.R. Racine, M.J. Hennig, and V.B. Lokeshwar, *The role of CD44 in disease pathophysiology and targeted treatment.* Frontiers in immunology, 2015. **6**: p. 182.
24. Wang, W., D. Chen, and K. Zhu, *SOX2OT variant 7 contributes to the synergistic interaction between EGCG and Doxorubicin to kill osteosarcoma via autophagy and stemness inhibition.* J Exp Clin Cancer Res, 2018. **37**(1): p. 37.
25. Wolny, P.M., S. Banerji, C. Gounou, A.R. Brisson, A.J. Day, D.G. Jackson, and R.P. Richter, *Analysis of CD44-hyaluronan interactions in an artificial membrane system: insights into the distinct binding properties of high and low molecular weight hyaluronan.* Journal of Biological Chemistry, 2010. **285**(39): p. 30170-30180.
26. Yang, C., M. Cao, H. Liu, Y. He, J. Xu, Y. Du, Y. Liu, W. Wang, L. Cui, and J. Hu, *The high and low molecular weight forms of hyaluronan have distinct effects on CD44 clustering.* Journal of Biological Chemistry, 2012. **287**(51): p. 43094-43107.
27. Jiang, L., G. Liu, H. Liu, J. Han, Z. Liu, and H. Ma, *Molecular weight impact on the mechanical forces between hyaluronan and its receptor.* Carbohydrate polymers, 2018. **197**: p. 326-336.
28. Tavianatou, A.G., Z. Piperigkou, C. Barbera, R. Beninatto, V. Masola, I. Caon, M. Onisto, M. Franchi, D. Galesso, and N.K. Karamanos, *Molecular size-dependent specificity of hyaluronan on functional properties, morphology and matrix composition of mammary cancer cells.* Matrix Biol Plus, 2019. **3**: p. 100008.
29. Qhattal, H.S.S. and X. Liu, *Characterization of CD44-mediated cancer cell uptake and intracellular distribution of hyaluronan-grafted liposomes.* Molecular pharmaceutics, 2011. **8**(4): p. 1233-1246.
30. Arpicco, S., C. Lerda, E. Dalla Pozza, C. Costanzo, N. Tsapis, B. Stella, M. Donadelli, I. Dando, E. Fattal, and L. Cattel, *Hyaluronic acid-coated liposomes for active targeting of gemcitabine.* European Journal of Pharmaceutics and Biopharmaceutics, 2013. **85**(3): p. 373-380.
31. Zhong, L., Y. Liu, L. Xu, Q. Li, D. Zhao, Z. Li, H. Zhang, H. Zhang, Q. Kan, and J. Sun, *Exploring the relationship of hyaluronic acid molecular weight and active targeting efficiency for designing hyaluronic acid-modified nanoparticles.* Asian journal of pharmaceutical sciences, 2019. **14**(5): p. 521-530.
32. Li, W., C. Zheng, Z. Pan, C. Chen, D. Hu, G. Gao, S. Kang, H. Cui, P. Gong, and L. Cai, *Smart hyaluronidase-actived theranostic micelles for dual-modal imaging guided photodynamic therapy.* Biomaterials, 2016. **101**: p. 10-19.
33. Granja, A., R. Lima-Sousa, C.G. Alves, D. de Melo-Diogo, M. Pinheiro, C.T. Sousa, I.J. Correia, and S. Reis, *Mitoxantrone-loaded lipid nanoparticles for breast cancer therapy–quality-by-design approach and efficacy assessment in 2D and 3D in vitro cancer models.* International Journal of Pharmaceutics, 2021: p. 121044.
34. Gouveia, V.M., J. Lopes-de-Araújo, S.A. Costa Lima, C. Nunes, and S. Reis, *Hyaluronic acid-conjugated pH-sensitive liposomes for targeted delivery of prednisolone on rheumatoid arthritis therapy.* Nanomedicine, 2018. **13**(9): p. 1037-1049.
35. Hwang T.L., S.A.J., *Water Suppression That Works. Excitation Sculpting Using Arbitrary Wave-Forms and Pulsed-Field Gradients.* Journal of Magnetic Resonance, Series A, 1995. **112**(2): p. 275-279.
36. Greco, I., N. Molchanova, E. Holmedal, H. Jenssen, B.D. Hummel, J.L. Watts, J. Håkansson, P.R. Hansen, and J. Svenson, *Correlation between hemolytic activity, cytotoxicity and systemic in vivo toxicity of synthetic antimicrobial peptides.* Sci Rep, 2020. **10**(1): p. 13206.
37. Silva, M.I., A.I. Barbosa, S.A. Costa Lima, P. Costa, T. Torres, and S. Reis, *Freeze-dried Softisan® 649-based lipid nanoparticles for enhanced skin delivery of cyclosporine A.* Nanomaterials, 2020. **10**(5): p. 986.
38. Attia, M.F., N. Anton, J. Wallyn, Z. Omran, and T.F. Vandamme, *An overview of active and passive targeting strategies to improve the nanocarriers efficiency to tumour sites.* J Pharm Pharmacol, 2019. **71**(8): p. 1185-1198.
39. Huang, D., L. Sun, L. Huang, and Y. Chen, *Nanodrug Delivery Systems Modulate Tumor Vessels to Increase the Enhanced Permeability and Retention Effect.* J Pers Med, 2021. **11**(2).
40. Singh, R. and J.W. Lillard, Jr., *Nanoparticle-based targeted drug delivery.* Exp Mol Pathol, 2009. **86**(3): p. 215-23.
41. Danaei, M., M. Dehghankhold, S. Ataei, F. Hasanzadeh Davarani, R. Javanmard, A. Dokhani, S. Khorasani, and M.R. Mozafari, *Impact of Particle Size and Polydispersity Index on the Clinical Applications of Lipidic Nanocarrier Systems.* Pharmaceutics, 2018. **10**(2).

42. Fatisson, J., I.R. Quevedo, K.J. Wilkinson, and N. Tufenkji, *Physicochemical characterization of engineered nanoparticles under physiological conditions: effect of culture media components and particle surface coating.* Colloids Surf B Biointerfaces, 2012. **91**: p. 198-204.
43. Li, Y., A. Yediler, Z. Ou, I. Conrad, and A. Kettrup, *Effects of a non-ionic surfactant (Tween-80) on the mineralization, metabolism and uptake of phenanthrene in wheat-solution-lava microcosm.* Chemosphere, 2001. **45**(1): p. 67-75.
44. Hou, J., H. Ci, P. Wang, C. Wang, B. Lv, L. Miao, and G. You, *Nanoparticle tracking analysis versus dynamic light scattering: Case study on the effect of Ca(2+) and alginate on the aggregation of cerium oxide nanoparticles.* J Hazard Mater, 2018. **360**: p. 319-328.
45. Kim, S.W., K.T. Oh, Y.S. Youn, and E.S. Lee, *Hyaluronated nanoparticles with pH- and enzyme-responsive drug release properties.* Colloids Surf B Biointerfaces, 2014. **116**: p. 359-64.
46. ISO10993-4, *Biological Evaluation of Medical Devices Part 4. Selection of Tests for Interactions with Blood*. 2017.

## Supplementary data

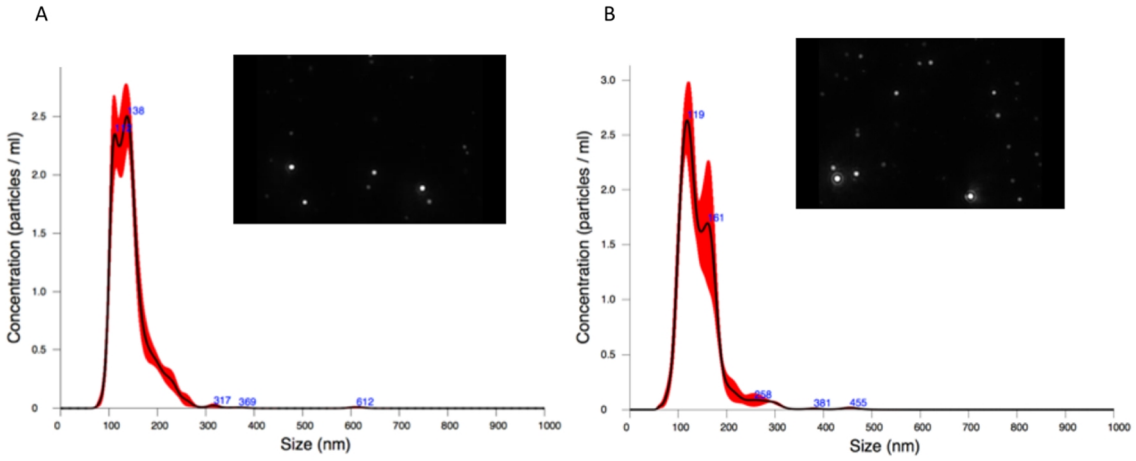



**Figure S1.** NTA analysis of SLN-HA20-Mito (A) and SLN-HA1000-Mito (B). Size distribution and NTA video frames.

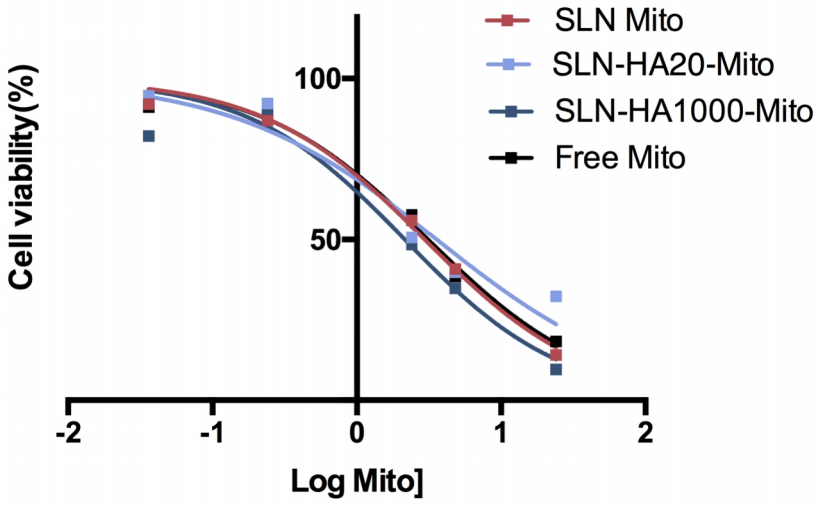


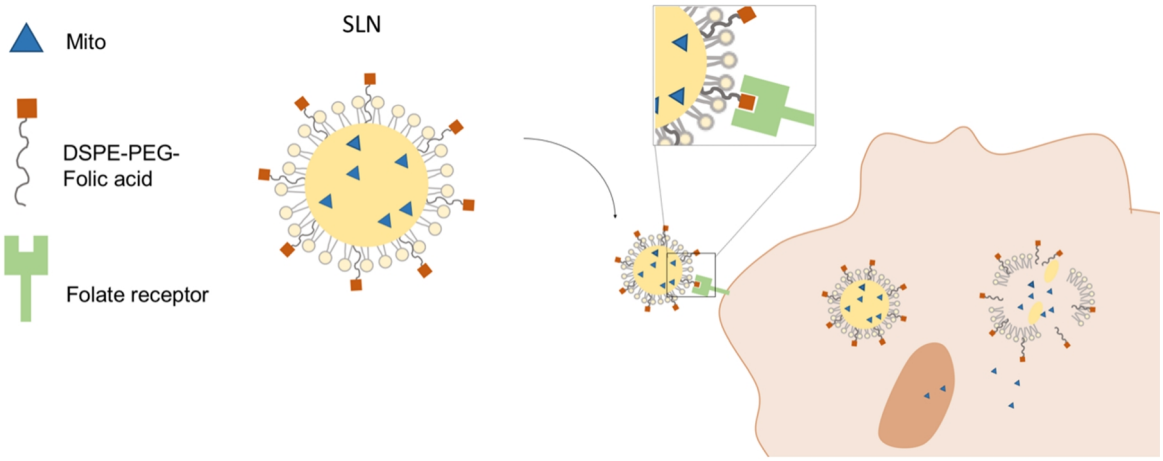

**Figure S2.** Dose-response curves of MCF-7 cells following incubation with free drug, HA-functionalized and non-functionalized Mito-loaded SLN for 24 h.

**Table S1.** Physicochemical characterization of C6-loaded SLN

| | **Size** | **PDI** | **ζ-potential** |
|---|---|---|---|
| **SLN C6** | 214 ± 1 | 0.136 ± 0.004 | -13 ± 13 |
| **SLN C6 HA20** | 200 ± 2 | 0.199 ± 0.003 | -10 ± 10 |
| **SLN C6 HA1000** | 197 ± 2 | 0.183 ± 0.02 | -5 ± 7 |

## 4.3. Folate receptor-mediated delivery of mitoxantrone-loaded solid lipid nanoparticles to breast cancer cells

In this chapter, a different economically-affordable cancer active targeting strategy was developed and studied. A DSPE-PEG-Folic acid conjugate was synthesized and used for the surface decoration of the SLN. Nanoparticles were characterized, their anti-cancer effect was evaluated by performing cell viability and apoptosis studies and the efficacy of the functionalization was evaluated by performing cellular uptake studies. In addition, the preferential routes of nanoparticle internalization were evaluated. This work was submitted to Pharmacological research, Elsevier.



# Folate receptor-mediated delivery of mitoxantrone-loaded solid lipid nanoparticles to breast cancer cells

Andreia Granja[1,], Cláudia Nunes[1], Célia T. Sousa[2,3] and Salette Reis[1,*]

[1]LAQV, REQUIMTE, Departamento de Ciências Químicas, Faculdade de Farmácia, Universidade do Porto, R. Jorge de Viterbo Ferreira 228, 4050-313, Porto, Portugal.

[2]IFIMUP-IN and Dep. Física e Astronomia, Faculdade de Ciências, Universidade do Porto, Rua Campo Alegre 687, 4169 - 007 Porto, Portugal

[3]Departamento de Física Aplicada, Facultad de Ciencias, Universidad Autónoma de Madrid (UAM), Campus de Cantoblanco, C/ Francisco Tomás y Valiente, 7, M 12 604 - 28049, Madrid, Spain.

[*]corresponding author:

shreis@ff.up.pt

## Abstract

The standard breast cancer therapy still faces major challenges due to non-specific tumor distribution and occurrence of dose-limiting adverse side-effects. Nanomedicine constitutes an appealing approach to improve the therapeutic index of different anti-cancer drugs. Given their biocompatibility, low-cost manufacture and easy surface modification, lipid nanoparticles, such as solid lipid nanoparticles (SLN), have a great potential for drug delivery in cancer therapy. In this work, SLN entrapping the antineoplastic drug Mitoxantrone (Mito) were developed and functionalized with Disteroylphosphatidylethanolamine-poly(ethylene glycol)-folic acid (DSPE-PEG-FA) ligand to improve blood circulation and tumor selectivity and limit the drug systemic side-effects. Nanoparticles presented adequate size and size distribution for intravenous injection and were stable for at least 6 months. Additionally, their hemocompatibility was demonstrated. Moreover, functionalized nanoparticles were able to improve the anti-cancer effect of the free drug, as assessed by the values of $IC_{50}$ and the apoptotic effects in MCF-7 cells. Moreover, an enhanced cellular internalization of the functionalized SLN was demonstrated by confocal microscopy and flow cytometry studies. Finally, the cellular uptake of the SLN was found to occur via macropinocytosis and clathrin-mediated endocytosis, suggesting the involvement of (folate receptor) (FR)-mediated endocytosis. Overall these findings highlight that the developed SLN are efficient nanocarriers for the selective delivery of Mito to breast cancer cells.

**Keywords:** Active targeting, Folic acid, Folate receptor, MCF-7 cells, Cellular uptake pathways

# 1. Introduction

Breast cancer is the main cause of cancer deaths in women, being responsible for 685 000 deaths globally in 2020 [1]. Different modalities are currently employed for the treatment of this malignancy, including surgery, radiotherapy, chemotherapy, hormonal and targeted therapies, which are chosen according to different factors, such as the patients' breast cancer subtype, [2]. Nevertheless, treatment efficacy is often compromised by the heterogeneity of the tumor, possibility of multidrug resistance and lack of tumor specificity, leading to dose-limiting off-target toxic effects [3, 4]. Mitoxantrone (Mito) is an anthracenedione acting through DNA intercalation and subsequent inhibition of DNA replication, with a demonstrated high anti-cancer activity towards different malignancies, including advanced breast cancer [5]. However, its administration is restricted by several systemic side-effects including myelosuppression and cardiotoxicity [6-8]. Moreover, drug multidrug resistance (MDR) associated with the overexpression of different drug efflux transporters can also occur following exposure to Mito, further limiting its therapeutic efficacy [9].

Nanomedicine constitutes an effective alternative treatment modality for cancer therapy, being able to overcome some limitations of conventional cancer therapeutics. Nanoparticles used as drug delivery vehicles can increase the therapeutic index of the drugs, improve tumor accumulation due to the enhanced permeability and retention (EPR) effect and limit cancer MDR [10-12]. Moreover, their pharmacokinetics can be improved through surface modification, for instance nanoparticle circulation in the bloodstream can be prolonged through surface coating with hydrophilic polymers, such as polyethylene glycol (PEG), which limit opsonisation and recognition by the reticuloendothelial system [13]. A broad diversity of nanoparticles can be used for drug delivery including polymeric, metallic, liposomes and lipid nanoparticles [14, 15]. Lipid nanoparticles, such as solid lipid nanoparticles (SLN) are colloidal nanocarriers with a solid lipid matrix with numerous advantages for drug delivery applications, including biocompatibility, biodegradability, high stability, low cost, and simple production methods, which can facilitate their large-scale production [16-18].

To improve the selectivity towards cancer cells and minimize non-specific tissue distribution, active cancer cell targeting strategies can be developed. To do so, nanoparticles can be functionalized with different ligands, including antibodies, proteins, polysaccharides and small molecules [19]. Surface decoration with small molecules, such as folic acid (FA) is an attractive strategy for cancer active targeting given their low cost, easy nanoparticle conjugation, limited immune system stimulation and negligible

interference on the pharmacokinetics of the nanocarrier [13]. FA is a water-soluble vitamin B required for DNA synthesis and repair, which is delivered intracellularly via folate receptor (FR)-mediated endocytosis. FR, particularly the α isoform is overexpressed in most solid tumors, including breast, while having negligible expression in normal tissues, which makes nanoparticles decoration with FA a promising therapeutic strategy [20-22].

In this work Mito-loaded SLN were functionalized with a 1,2-distearoyl-*sn*-glycero-3-phosphorylethanolamine-poly(ethylene glycol)-folic acid (DSPE-PEG-FA) conjugate to enhance its selectivity towards breast cancer cells and limit the systemic side-effects of the free drug. SLN were produced and fully characterized to ensure that their properties were adequate for intravenous administration. The nanoparticles anti-tumoral and apoptotic effects and targeting efficiency were assessed in the $FR^+$ MCF-7 cell line. In addition, the cellular pathway involved in the internalization of the nanoparticles was investigated. Although, there are two studies reported in the literature focusing on the development of lipid nanoparticles for the entrapment of mitoxantrone targeting the folate receptors, to the best of our knowledge, this is the first study reporting the production of Mito-loaded SLN using a sustainable green method. Additionally, we also provide a detailed investigation of the nanoparticles cellular uptake, uptake pathways and apoptotic effects, which has not yet been elucidated in previous works.

# 2. Materials and methods

## 2.1. Materials

Folic Acid (FA), Trimethylamine, Dicyclohexylcarbodiimide (DCC), N-hydroxysuccinimide (NHS), Dimethyl sulfoxide (DMSO) ≥ 99.9%, Mitoxantrone hydrochloride, Tween® 80, Hydrochloric acid (HCl), Sodium chloride, Sodium acetate solution, Dimethyl sulfoxide (DMSO), Triton™ X-100, Trypan Blue powder, Resazurin sodium salt, Dulbecco's Phosphate Buffered Saline 10X (PBS), Coumarin-6 (C6) (98%), Propidium iodide (PI) solution, Formalin solution neutral buffered 10%, Chlorpromazine, Filipin, Cytochalasin D and Sodium azide were purchased from Sigma-Aldrich® (St Louis, MO, USA). Cetyl Palmitate was kindly provided by Gatefossé (Lyon, France). DSPE-$PEG_{2000}$-$NH_2$ (1,2-distearoyl-*sn*-glycero-3-phosphoethanolamine-N-[amino(polyethylene glycol)-2000 (ammonium salt) was purchased from Avanti® Polar Lipids (Merck, Darmstadt, Germany). Dulbecco's Modified Eagle's Medium (DMEM), 0.25% Trypsin-EDTA (1X), Penicillin-Streptomycin (PenStrep) and Heat Inactivated Fetal Bovine Serum (FBS) were obtained from Gibco® by Life Technologies™ (UK). Hoechst 33342®, Trihydrochloride Trihydrate and LysoTracker™ Green DND-26 were acquired from (Invitrogen, Thermo Fisher Scientific, MA, USA). MCF-7 cell line was obtained from ATCC (Middlesex, UK). L929 cell line was purchased from Cell Lines Service (CLS, Eppelheim, Germany). Ultrapure water was purified by an Ultra-pure water system (18.2 MΩ cm, Healforce, Shanghai, China).

## 2.2. Synthesis of the Disteroylphosphatidylethanolamine-poly(ethylene glycol) - folic acid (DSPE-PEG-FA) conjugate

The DSPE-PEG-FA conjugate was synthesized as previously described in our lab [23]. Briefly, 1 g of FA was dissolved in a mixture of DMSO (40 mL) and triethylamine (0.5 mL) under anhydrous conditions in the dark overnight. The resulting solution was mixed with 0.5 g of DCC and 0.52 g of NHS followed by overnight stirring in the dark overnight. After that, the mixture was filtered using a 0.45 μM filter and solvents were evaporated under vacuum. The coupling of DSPE-PEG-$NH_2$ to FA-NHS was performed by adding 50 mg of DSPE-$PEG_{2000}$-$NH_2$ dissolved into 1 mL of DMSO to 2 mL of the FA-NHS solution, followed by overnight stirring in the dark under anhydrous conditions. DMSO was then evaporated under vacuum and 6 mL of water were added to the solution. To remove unconjugated FA, the conjugate was dialyzed against 1 L of ultrapure water for 48 h. Finally, the conjugate solution was lyophilized using a freeze dryer (LyoQuest −85 plus v.407, Telstar).

### 2.3. Solid lipid nanoparticles (SLN) production

SLN production method and composition were defined according to our recent work [24]. Briefly, lipid phase comprising Cetyl palmitate and Tween® 80 were melted in a water bath at 70˚C. Subsequently 4.4 mL of PBS solution at pH 8.2 pre-heated at 70˚C, were added to the lipid phase followed by ultrasonication at 70% for 5 min (VCX130, Sonics and Material Vibra-CellTM with a CV-18 probe; 115 Newtown CT, USA). The nanoformulation was allowed to cooled to room temperature and then stored at 4˚C until further use. For the preparation of functionalized SLN, DSPE-PEG-FA conjugate was added to the lipid melt at 1% of the lipid mass in the formulation. Mito-loaded SLN were obtained by dissolving 4.5 mg of the drug in the aqueous phase before its addition to the lipid melt. For the cellular uptake assays conducted in flow cytometry, SLN were labelled with C6 by adding an equivalent of 0.025% of the total mass of lipid and surfactant (corresponding to 68 μg of C6) to the lipid phase after lipid melting.

### 2.4. Size and zeta potential determination

The determination of nanoparticle size, size distribution and zeta potential was performed by dynamic light scattering and electrophoretic light scattering, respectively, using a ZetaPALS Analyzer (Brookhaven Instruments Corporation; Software: Particle Sizing v.5 Brookhaven Instruments; Holtsville, NY, USA). Prior to each measurement, nanoformulations were diluted at a ratio of 1:200 and measured at 25˚C with a light incidence angle of 90˚. For each measurement 6 runs of 2 min each were performed.

### 2.5. Entrapment efficiency (EE%) and Loading capacity (LC%)

The encapsulation efficiency was determined using an indirect method of quantification. Briefly, nanoformulations were diluted at a ratio of 1:65, placed in centrifugal filter units (Amicon® Ultra Centrifugal Filters Ultracell-50 kDa, MERK Milipore, Ltd; Cork, Ireland) and centrifuged at 3900 RPM (Allegra X-15R Centrifuge, Beckman Coulter, Fullerton, California) until separation of the lipid and aqueous phase. The amount of non-entrapped drug present in the supernatant was quantified by UV-vis spectrophotometry ((Jasco V-660 Spectrophotometer, Software: Spectra Manager v.2, Jasco Corporation, USA) by measuring the absorbance at 610 nm. The EE% and was determined according to the following equation:

$$EE\% = \frac{\text{Total amount of Mito-Amount of Mito in the supernatant}}{\text{Total amount of Mito}} \quad \text{(Equation 1)}$$

The LC% was calculated as follows:

$$LC\% = \frac{\text{Total amount of Mito-Amount of Mito in the supernatant}}{\text{Amount of lipid+surfactant+EE\% × initial amount of Mito}} \quad \text{(Equation 2)}$$

### 2.6. Storage stability

The storage stability was evaluated during 6 months by performing periodic assessments of the nanoparticles' size, PDI, zeta potencial and EE%. During this period, nanoformulations were stored at 4˚C.

### 2.7. *In vitro* drug release

The drug release was evaluated in physiological (PBS, pH 7.4) and acidic pH (acetate buffer, pH 5.0) to simulate the blood circulation and normal tissues and the acidic tumor environment and endosomal compartments, respectively. This study was carried out using the dialysis technique under sink conditions. Briefly, Mito-loaded SLN (500 µL) were added to the upper compartment of a dialysis device (Slide-A-Lyzer™ MINI Dialysis Device, MWCO 10kDa, Thermo Scientific™, MA, USA) and the lower compartment was filled with 14 mL of the adequate buffer. After that, the devices were placed in an incubator shaker (ES-60, Lan Technics, USA) at 37˚C under agitation (100 RPM). At defined time-points aliquots of 1 mL were collected from the lower compartment and replaced by the same volume of pre-heated buffer. The amount of Mito released was then quantified by UV-vis spectrophotometry, as previously described. Data were obtained using the average of the triplicates.

### 2.8. Hemolysis assay

To evaluate the hemolytic potential of the nanoformulations and their suitability for an intravenous administration, a hemolysis assay was performed. Human blood from 3 healthy donors was collected in EDTA-coated tubes, centrifuged at 955 × g for 5 min at 4˚C (Allegra X-15R Centrifuge, Beckman Coulter, Fullerton, California) to separate the red blood cells

(RBCs) from the remaining blood components and washed three times with physiological saline solution (0.85%). Nanoformulation was then diluted in saline solution and incubated with the RBCs (4% v/v in saline solution) in a 96-well plate at 37˚C for 1 h. Saline solution and Triton™ X-100 (1%) were used as negative and positive control, respectively. After the incubation period, the supernatant was collected and the amount of released hemoglobin was quantified by UV-vis spectrophotometry at 415 nm in a microplate reader (Biotek Instruments, Winooski, VT, USA). The percentage of hemolysis was calculated as follows:

$$\text{Hemolysis } \% = \frac{\text{Abs (sample)} - \text{Abs (negative control)}}{\text{Abs (positive control)} - \text{Abs (negative control)}} \qquad \text{(Equation 3)}$$

All the procedures were carried out according to the principles of the declaration of Helsinki. Blood samples were kindly donated by Serviço de Hematologia from Centro Hospitalar Universitário do Porto - Hospital de Santo António. (Porto, Portugal).

### 2.9. Cell viability assessment

The anti-cancer activity of the nanoformulations was assessed in MCF-7 cells by performing the resazurin assay. In brief, MCF-7 cells were seeded in 96-well plates ($1\times10^4$ cells per well) in DMEM supplemented with 10% (v/v) FBS and 1% (v/v) PenStrep and incubated at 37˚C, 5% $CO_2$. After 24 h, the nanoparticles were diluted at the desired concentrations in supplemented DMEM and incubated with the cells for 24 h at 37˚C, 5% $CO_2$. The nanoparticle-containing media was then removed and replaced by a 10% v/v (in DMEM) resazurin solution, which was incubated in the dark for 4h at 37˚C, 5% $CO_2$. Cell viability was then determined by quantifying the fluorescence of resorufin in the cells' supernatant using a fluorometer (Biotek Instruments, Winooski, VT, USA) ($\lambda_{ex}$ = 560 nm; $\lambda_{em}$ = 590 nm). After that, dose-response curves were plotted and the values of $IC_{50}$ of the free drug and the drug-loaded SLN were assessed using GraphPad Prism Software (v.6.0, GraphPad Software, CA, USA).

### 2.10. Apoptosis assay

Apoptosis in MCF-7 cells induced by the nanoformulations was evaluated using the FITC Annexin V Apoptosis Detection Kit with 7-AAD (Biolegend®, California, USA), according to the manufacturer's instructions. Briefly, MCF-7 cells were seeded in 24-well

plates at a density of $2\times10^5$ cells per well and incubated for 24 h in supplemented DMEM. Subsequently, cells were incubated with the different nanoformulations at two different concentrations (5 and 50 µg/mL of lipid). After 24 h, cells were washed twice with PBS, detached with trypsin-EDTA 0.25% (w/v), centrifuged for 5 min at 300 g and washed twice with cold PBS. Cells were then resuspended into Annexin V binding buffer, followed by staining with FITC Annexin V and 7-AAD viability staining solution and incubated in the dark for 15 min at room temperature. Apoptosis was evaluated in a BD Accuri C6 flow cytometer (BD Biosciences, Erembodegem, Belgium) with at least 10,000 events acquired for each sample. Data were analysed using the BD Accuri™ C6 software (BD Biosciences, Belgium).

### 2.11. Cellular uptake

#### 2.11.1. Confocal laser scanning microscopy (CLSM)

Nanoparticle internalization in MCF-7 cells was visualized in CLSM. MCF-7 cells were seeded at a density of $1\times10^4$ cells per well in 8 well-µ-slides (Ibitreat, Ibidi GmbH, Munich, Germany) and grown in supplemented DMEM at 37˚C, 5% $CO_2$. After 24 h, cells were incubated with the functionalized and non-functionalized Mito-loaded SLN (0.21 µM of Mito) for 4h at 37˚C, 5% $CO_2$. Cells were then washed three times with PBS, stained with Lysotracker (60 nM in DMEM) and incubated for 30 min at 37˚C, 5% $CO_2$. After that, cells were rinsed three times with PBS and fixed with formalin solution for 30 min at room temperature followed by another three-step washing with PBS. Finally, cells were stained with Hoechst (8 µM in PBS) and incubated for 10 min at room temperature in the dark before a three-step washing with PBS. Images of cancer cell internalization were acquired on a Leica Stellaris 8 confocal microscope (LeicaMicrosystems, Wetzlar, Germany) equipped with the Leica Application Suite X package (LAS X) using a $\lambda_{ex}/\lambda_{em}$ of 350⁄461 nm (Hoechst 33342®), $\lambda_{ex}/\lambda_{em}$ of 504⁄511 nm (LysoTracker™ Green) and $\lambda_{ex}/\lambda_{em}$ of 610/630 nm (Mito) with a resolution of 1024×1024 using a 63X/1.4 oil immersion objective. Images were analysed using Fiji ImageJ software (version 2.0, National Institutes of Health). CLSM studies were performed at the Imaging by confocal and fluorescence lifetime laboratory, CEMUP, Portugal.

#### 2.11.2. Flow cytometry

The quantification of the nanoparticle cellular uptake in MCF-7 cells was carried out using flow cytometry. With that purpose, C6-labelled SLN were previously produced as described in **section 2.3**. Cells were seeded in 24-well plates ($2\times10^5$ cells per well) and grown in supplemented DMEM for 24 h at 37˚C, 5% $CO_2$. Functionalized and non-functionalized C6-labelled SLN (250 µg/mL of lipid) were then added to the cells and incubated for 1 h, 4 h and 24 h. After the incubation periods, cells were washed twice with PBS, detached with trypsin-EDTA 0.25% (w/v), resuspended in PBS and stained with PI (0.01 mg/mL) to exclude dead cells and trypan blue (0.004%) to quench the C6 signal from the nanoparticles adsorbed at the cell surface [25]. Cellular uptake was then measured in a BD Accuri C6 flow cytometer (BD Biosciences, Erembodegem, Belgium) with at least 10,000 events acquired per sample. The same protocol was followed using the mouse fibroblast L929 cell line, used as a negative control.

Data analysis was performed using the BD Accuri™ C6 software (BD Biosciences, Belgium).

### 2.11.3. Cellular uptake pathways

To study the different cellular pathways involved in the uptake of the SLN, cells were treated with specific cellular uptake pathway inhibitors and the resultant nanoparticle uptake was then assessed by flow cytometry [26]. Briefly, MCF-7 cells were seeded in 24-well plates ($2\times10^5$ cells per well) in supplemented DMEM and grown at 37˚C, 5% $CO_2$ for 24 h. After that, cells were incubated with DMEM-containing the different cellular uptake pathway inhibitors (sodium azide 1 mg/m, chlorpromazine, 10 µg/mL, filipin 1 µg/mL and cytochalasin D 5 µg/mL) at 37˚C, 5% $CO_2$ or incubated with fresh DMEM at 4˚C for 30 min. Subsequently, functionalized and non-functionalized C6-labelled nanoparticles were added (250 µg/mL of lipid) in the presence of the different inhibitors and incubated for 1 h, 37˚C, 5% $CO_2$. Cellular uptake was then determined in a BD Accuri C6 flow cytometer, as described in the previous section.

## 2.12. Statistical analysis

Statistical analysis was performed using Graphpad Prism6 Software (GraphPad Software Inc., CA, USA). Data were analyzed by one-way analysis of variance (ANOVA) or two-way ANOVA with a $p$-value < 0.05 considered statistically significant. All data are expressed as mean ± SD.

# 3. Results

## 3.1. Physicochemical characterization and storage stability

Functionalized SLN were produced and their physicochemical characteristics were evaluated and compared with that of non-functionalized SLN. As shown in **Table 1**, there were non-significant differences between the two nanoformulations, which suggests that the addition of the DSPE-PEG-FA ligand had no interference on the particles size, size distribution, surface charge and ability to internalize the drug.

**Table 1**. Physicochemical characterization of the functionalized versus non-functionalized Mito loaded nanoformulations: size, PDI, zeta potential, EE% and LC%.

| | Size | PdI | Zeta potential (mV) | EE% | LC% |
|---|---|---|---|---|---|
| **SLN-Mito** | 230 ± 17 | 0.16 ± 0.01 | -3 ± 1 | 93 ± 6 | 1.5 ± 0.1 |
| **SLN-FA-Mito** | 228 ± 4 | 0.15 ± 0.01 | -8 ± 7 | 97 ± 4 | 1.5 ± 0.1 |

The storage stability of the functionalized nanoparticles during 6 months was assessed by performing periodic measurements of their physicochemical characteristics as presented in **Figure 1**. The presented data indicate that particle size did not change considerably after 6 months, suggesting that the nanoparticles did not form aggregates over time and remains with an adequate value for intravenous administration and tumor accumulation [27-29]. The same conclusion is suggested by the analysis of the values of PdI, which remain below 0.2 after 6 months, suggesting the presence of an homogenenous population [30]. In addition, there were no significant differences in the values of zeta potential, which remain slightly negative during the period of study, due to the ionic strength of the solvent used for the SLN production [31, 32]. Finally, the EE% of Mito remain high without statistically significant alterations during the period of study, suggesting the absence of drug release during storage. Overall, the results suggest that after functionalization the nanoparticles properties are still adequate for an intravenous administration and tumor accumulation via EPR effect with a high entrapment efficiency of the drug and an acceptable loading capacity.

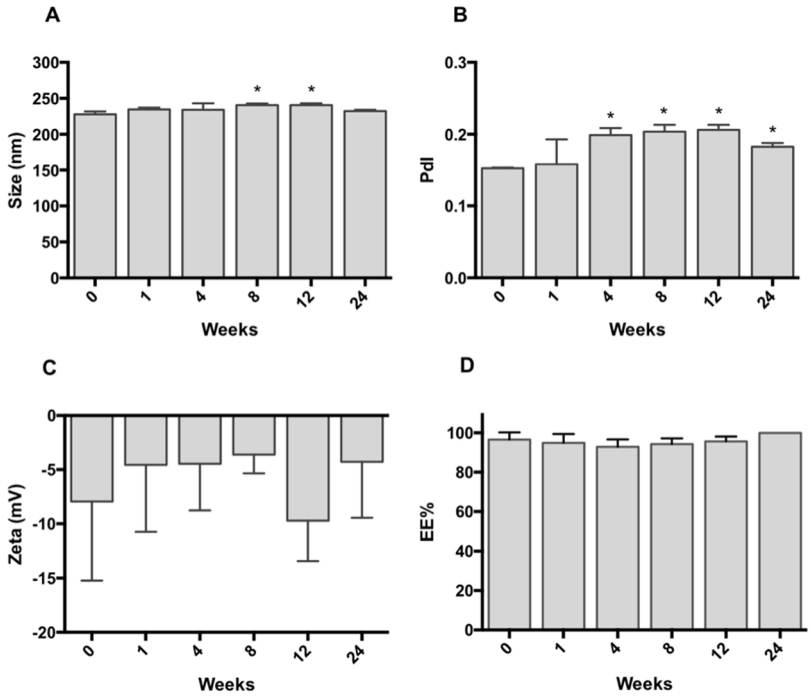



**Figure 1. Storage stability of SLN-FA-Mito during 6 months stored at 4˚C**: Size (**A**), PdI (**B**), Zeta potencial (**C**) and EE% (**D**). Data expressed as mean ± SD (n = 3). Differences between groups were assessed using two-way ANOVA followed by Dunnet post-hoc test *p<0.05, relatively to week 0.

### 3.2. *In vitro* drug release

An *in vitro* drug release study was conducted to evaluate the release behaviour of Mito at physiological and acidic pH [33, 34]. The cumulative drug release is presented in **Figure 2**. The presented data indicate a higher and faster drug release at acidic pH, characteristic of the tumor microenvironment and the endosomal compartment, with 56% released after 8h and 82% released after 24h. On the other hand, at physiological pH (7.4) a sustained Mito release occured, with only 12% released after 8h and 32% after 24h. This data suggest that the developed SLN are suitable for loading of Mito and subsequent intravenous administration, enabling a high release in acidic environment, characteristic of the tumor regions and the cell endosomal compartment, while limiting drug release in more neutral pH values, thus preventing release in the blood circulation and healthy tissues.

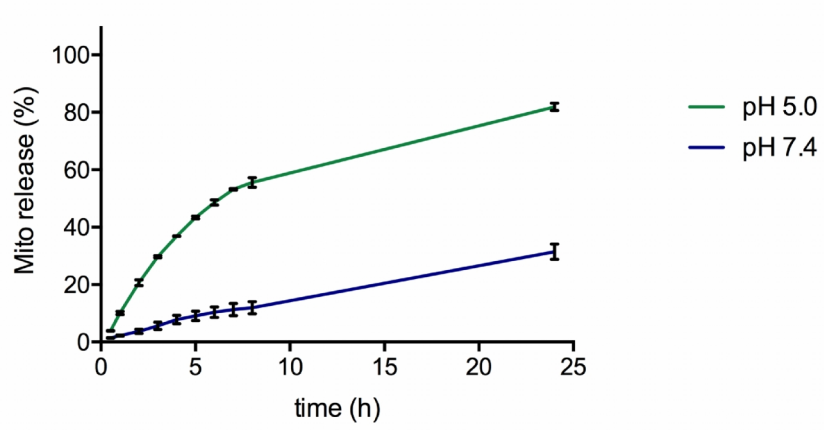



**Figure 2. *In vitro* drug release.** Cumulative drug release of SLN-FA-Mito at pH 5.0 and 7.4. Data expressed as mean ± SD (n = 3).

### 3.3. Hemolysis assay

A hemolysis assay was carried out to evaluate the haemolytic potential of the SLN in human RBCs. As shown in **Figure 3**, nanoparticles were non-hemolytic up a high concentration of lipid of 24 mg/mL, inducing less than 5% of hemolysis [35]. These results suggest that the nanoformulations are hemocompatibility and hence, safe for intravenous administration.

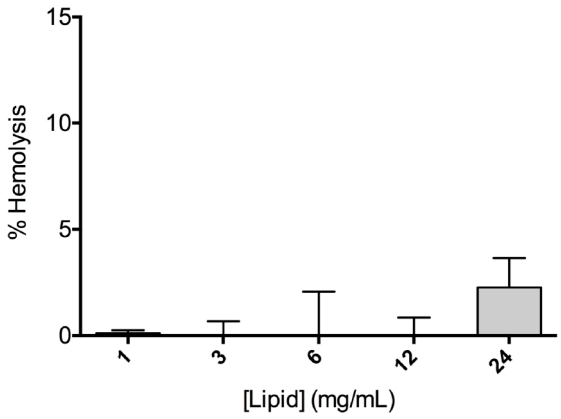



**Figure 3. *In vitro* hemolysis assay.** Human RBCs were exposed to increasing concentrations of SLN-FA-Mito and incubated at 37°C for 1h. Data expressed as mean ± SD using RBCs from 3 healthy donors (n=3).

### 3.4. Cellular viability

The cellular viability of the SLN, its correspondent functionalized SLN and free drug were evaluated in the breast cancer cell line MCF-7. As shown in **Figure 4A**, unloaded SLN were found to be well-tolerated, demonstrating a high cytocompatibility in MCF-7 cells, even at high concentrations of lipid, and comparable to others reported in the literature [36, 37]. The highest concentration tolerated by MCF-7 cells (500 µg/mL of lipid) was then selected as

the maximum concentration to evaluate the anti-cancer activity of the Mito-loaded SLN (**Figure 4B**). These results indicate that both SLN and SLN-FA could preserve the high anti-cancer activity of Mito towards breast cancer. Moreover, the results point to a higher capacity of SLN-FA-Mito to elicit a reduction in MCF-7 cell viability in comparison to the non-functionalized SLN and the free drug. To gather more information about the anti-cancer effects of each condition, dose-response curves were plotted and the values of $IC_{50}$ were calculated. The values obtained were 2.68 μM for the free drug, 2.55 μM for SLN-Mito and 1.06 μM for SLN-FA-Mito, which suggests that the latter could in fact improve the anti-tumoral activity compared with the free drug. Similar findings were reported by Xu et al., which demonstrated that Mito-loaded polysaccharide nanoparticles could elicit higher cytotoxicity than free Mito towards MCF-7 cells [38]. This fact can be attributed to an enhanced intracellular delivery of the drug associated with the active cancer cell targeting of the FR+ cell line MCF-7 [39]. Moreover, the internalization of the free drug and drug-loaded nanoparticles may occur through different cellular uptake pathways. Mito can enter cells by passive diffusion [40] or through flip-flop diffusion [41], the latter occurring at a slower rate than other analogous anthracyclines, which makes it more susceptible to P-glycoprotein (P-gp)-mediated efflux [41]. Nanoparticles, on the other hand, may enter cells through endocytosis, which can enhance the intracellular delivery of the drug and simultaneous evade the efflux mediated by P-gp and other transporters, as reported previously for the analogous drug doxorubicin [42, 43].

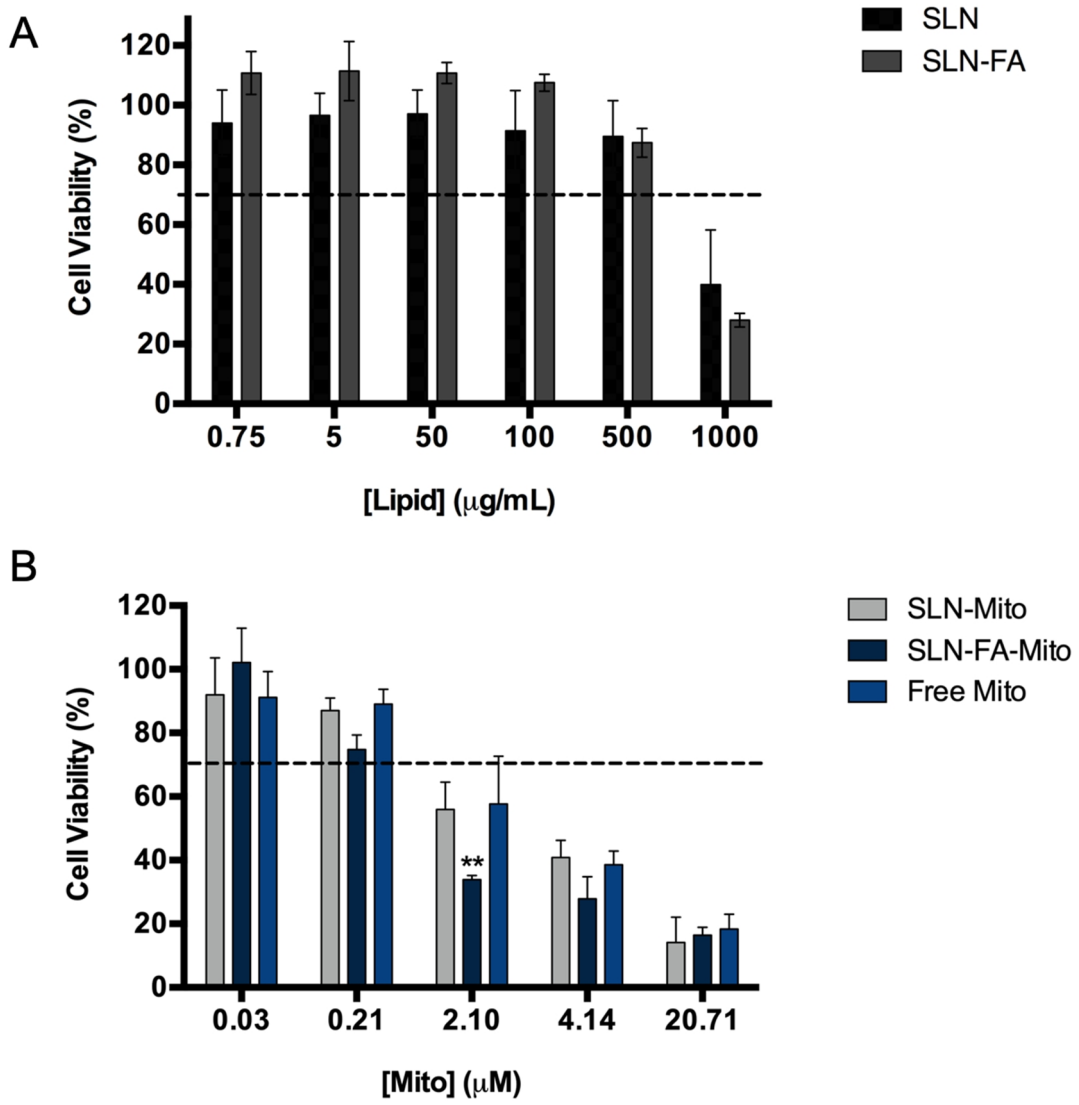



**Figure 4. Effect of the unloaded (A) and Mito-loaded (B) nanoformulations on MCF-7 cell viability.** MCF-7 cells were treated with the different nanoformulations for 24 h and cell viability was determined by the resazurin assay. Data expressed as mean ± SD (n = 3). Differences between groups were assessed using two-way ANOVA followed by Dunnet post-hoc test **p<0.01 relatively to the free drug.

### 3.5. Induction of apoptosis

The induction of apoptosis following treatment with each nanoformulation and free drug was investigated using FITC Annexin V Apoptosis assay with 7-AAD. Mito is an anthracenedione that inhibits cancer cell growth through DNA intercalation and subsequent disruption of DNA synthesis and repair. Moreover, it has also demonstrated ability to induce apoptosis in breast cancer cells [44]. Therefore, in this assay, the inherent ability of Mito to induce apoptosis in MCF-7 cells was evaluated either free or encapsulated into SLN, as shown in **Figure 5** and representative scatter plots in **Figure S1.** A dose-dependent induction of apoptosis was observed after cell incubation with Mito-loaded nanoformulations and free

Mito. At the lowest concentration tested (**Figure 5A**), a significantly higher degree of apoptosis was observed for SLN-Mito, SLN-FA-Mito and free Mito, comparing to the control. Nevertheless, apoptosis was not higher than 15% for each treatment, the majority of it being related to early apoptotic events. The percentage of viable cells obtained were 85, 89 and 88%, for SLN-Mito, SLN-FA-Mito and free Mito, respectively, which is consistent with the cell viability assays.

In contrast, at the highest concentration tested (**Figure 5B**) a higher amount of apoptosis, in particular late apoptosis and necrosis states, was observed after treatment with drug-loaded SLN and free drug. In this context, 18.4, 17.4 and 12.7% of the cells were found in late apoptosis and 10.0, 18.2 and 11.9 % in necrosis, following treatment with SLN-Mito, SLN-FA-Mito and free Mito, respectively. A significant difference in the percentage of late apoptotic cells was found following treatment with both SLN-Mito and SLN-FA-Mito comparing to the control group, suggesting the efficiency of the nanoparticles in maintaining the apoptotic effects of the drug. Finally, a significantly higher percentage of necrosis was found following treatment with SLN-FA-Mito, suggesting that treatment with this nanoformulation could improve cancer cell death, thus corroborating the cell viability assays. For the two concentrations tested, unloaded SLN did not induce apoptosis, presenting effects similar to the control group, which is in agreement the cellular viability assays and further supports the high cytocompatibility of the lipid nanovehicle.

Overall, the apoptosis assay suggests that Mito could retain or even slightly improve its apoptotic effect towards MCF-7 cells after incorporation into SLN.

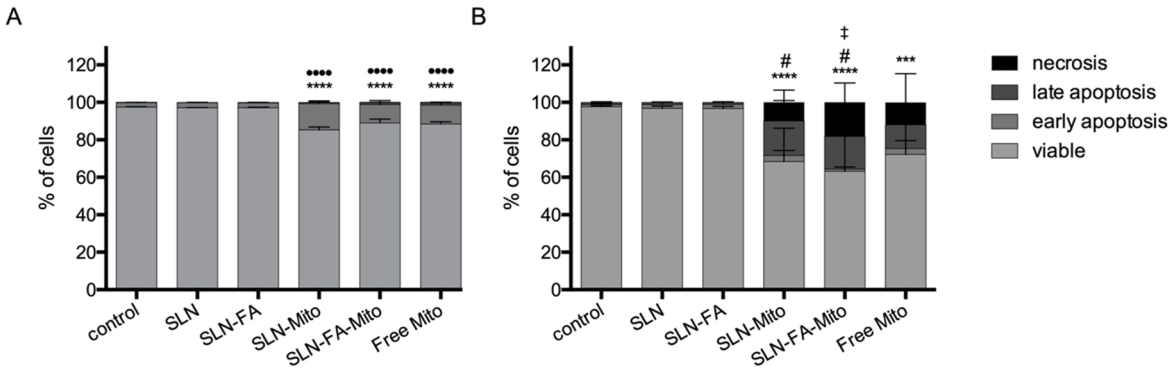



**Figure 5. Apoptosis of MCF-7 cells following incubation with the nanoformulations using the FITC Annexin V Apoptosis assay.** Cells were incubated for 24 h with the different nanoformulations and free drug at a concentration of 5 µg/mL (**A**) and 50 µg/mL of lipid (**B**), corresponding to 0.21 µM and 2.1 µM of Mito. Data expressed as mean ± SD (n = 3). Differences between each treatment and control group were assessed using two-way ANOVA followed by Dunnet post-hoc test. viable: **** $p<0.0001$, *** $p<0.001$; early apoptosis: •••• $p<0.0001$; late apoptosis # $p<0.05$; necrosis: ‡ $p<0.05$.

### 3.6. Cellular uptake visualization by Confocal microscopy

To evaluate the efficiency of the active targeting strategy CLSM was used to visualize the uptake of functionalized and non-functionalized SLN after incubation with MCF-7 cells for 4 h. As presented in **Figure 5,** after 4 h incubation, Mito-loaded SLN are mostly located in the cytoplasm region and, specifically, in the lysosomes, as seen by the red and green fluorescence overlay. Moreover, a Mito translocation to the nucleus can be observed, as shown by the purple/pink color of the nuclear region due to overlay of the blue and red signals. This suggests that both SLN are able to effectively deliver Mito to MCF-7 cells and, specifically to the nucleus, which is the cellular target of the drug. Moreover, a stronger red fluorescence intensity was observed after incubation with SLN-FA-Mito when comparing to SLN-Mito, which is observed both in the cytoplasm and in the nuclear region, as seen by the enhanced pink coloration of the nucleus. The overall CLSM data indicate that both SLN could deliver Mito to MCF-7 cells and mediate its translocation to the nucleus. Moreover, an enhanced uptake and nuclear translocation occurred in FA-surface decorated SLN, possibly mediated by the folate receptor.

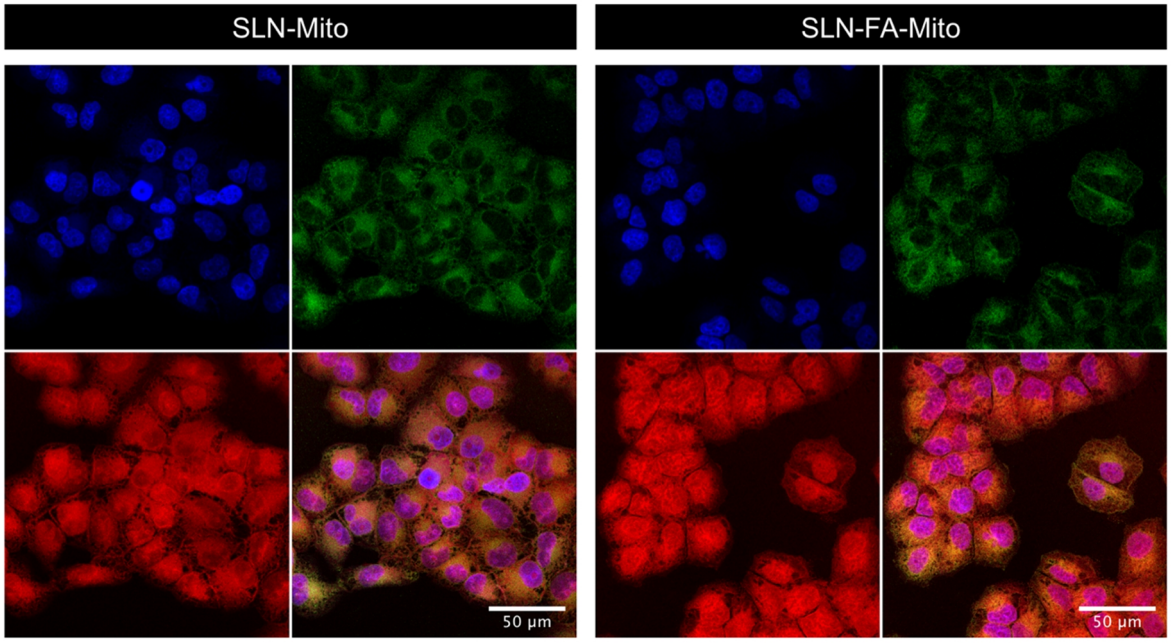



**Figure 6. CLSM images of the MCF-7 cellular uptake of non-functionalized and functionalized Mito-loaded SLN.** Cells were incubated with the nanoformulation for 4h. Blue channel: Hoechst 33342 (nucleus). Green channel: LysoTracker™ Green DND-26. Red channel: Mito.

### 3.7. Cellular uptake quantification using flow cytometry

To quantify the cellular uptake of the nanoparticles, flow cytometry studies were conducted. To perform this assay, C6-labelled SLN were previously produced, as described in **section**

**2.3** and characterized to ensure that their physicochemical characteristics were similar to that of Mito-loaded SLN (SLN, size: 214 ± 1 nm, PDI: 0.14 ± 0.01, zeta potential: -13 ± 13 mV; SLN-FA, size: 227 ± 2 nm, PDI 0.14 ± 0.01, zeta potential -6 ± 1 mV). MCF-7 cells were then incubated with non-fictionalized and FA-functionalized SLN for 1, 4 and 24 h and the cellular fluorescence was then quantified (**Figure 6**). The data show an enhanced cellular fluorescence measured after incubation with SLN-FA for all the time-points studied. This suggests that SLN-FA were internalized at a faster rate and a higher amount than SLN, suggesting that the functionalization improved the nanoparticle cellular uptake mediated by the folate receptor. These data are consistent with the CLSM results, as well as with the cell viability studies, where functionalized SLN elicited higher cytotoxicity that non-functionalized SLN towards MCF-7 cells, which can be related to a higher internalization. A similar study was conducted in the L929 cell line, which, in contrast to MCF-7, is a normal cell line with a neglible expression of the folate receptors [45, 46]. The results (**Figure S2**) demonstrated no differences in L929 cellular uptake between folic functionalized and non-functionalized SLN after 1h and 4h of incubation. This suggests that the SLN entrance into this normal cell line was non-mediated by the folate receptor, and, more importantly, that folic acid functionalization did not contribute to an enhanced uptake in normal cells.

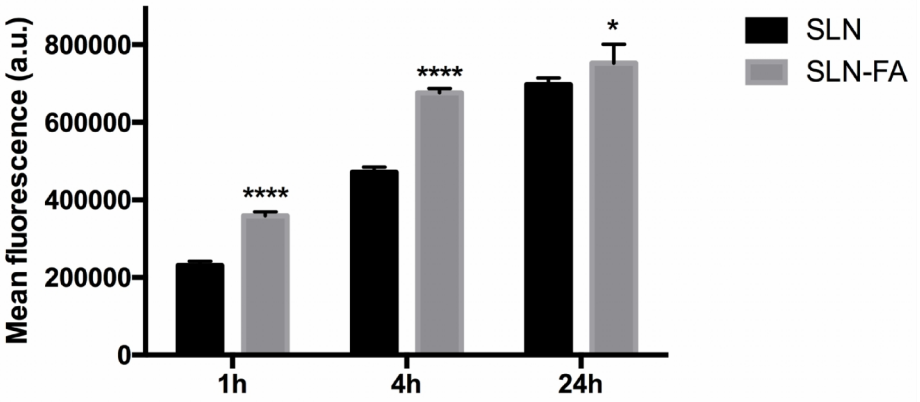



**Figure 7. Quantification of MCF-7 cellular uptake of C6-labelled SLN by flow cytometry**. Cells were incubated with the different nanoformulations for 1h, 4h and 24h. Data expressed as mean ± SD (n = 3). Differences between groups were assessed using two-way ANOVA followed by Sidak post-hoc test * $p<0.05$, **** $p<0.0001$ relatively to the non-functionalized SLN at each time-point.

### 3.8. Cellular uptake pathways

To investigate the cellular uptake pathway of the nanoparticles, MCF-7 cells were incubated with different inhibitors (sodium azide 1 mg/m, chlorpromazine, 10 µg/mL, filipin 1 µg/mL and cytochalasin D 5 µg/mL) and subsequently exposed to SLN and SLN-FA in the presence of each inhibitor. The results of nanoparticle cellular uptake for each condition are presented in **Figure 7**.

Since nanoparticles internalization can occur via endocytosis or through an energy-independent non-endocytic pathway, first the energy-dependency of the SLN uptake was investigated. In order to do so, cells were incubated at 4˚C and the resulting SLN cellular uptake was then analysed and compared to that at 37˚C. A statistically significant reduction in cellular uptake occurred for the two types of SLN when incubated at 4˚C (**Figure 7**), suggesting that their uptake occurred through an active energy-dependent process. Low temperatures are associated with increased membrane rigidity, thus compromising both passive diffusion and active energy-dependent uptake [25]. Additionally, cells were incubated with sodium azide, an active transport inhibitor [47]. A significant reduction in cell internalization occurred for SLN-FA-Mito in this condition, although to a less extent than incubation at 4˚C. Similar findings have been described elsewhere [48, 49]. In fact, sodium azide is able to inhibit ATP production by blocking the electron transport chain. Nevertheless, cells can compensate the reduction of intracellular ATP by using exogenous ATP, thus allowing nanoparticle endocytosis [48, 49]. Overall these results suggest that the uptake of the nanoparticles is energy-dependent and that functionalized SLN may be internalized via active transport.

Next, to evaluate the mechanisms of energy-dependent endocytosis responsible for nanoparticle uptake, cells were incubated with specific endocytic inhibitors. Chlorpromazine was used due to its inhibitory effect on clathrin-mediated endocytosis, filipin is able to inhibit caveolae-mediated endocytosis and cytochalasin D can inhibit macropinocytosis and also caveolae-mediated endocytosis [50]. As seen in **Figure 7**, consistent with the results of incubation with sodium azide, which did not seem to affect the internalization of non-functionalized SLN, none of the endocytic inhibitors influenced their uptake, suggesting that the entrance of non-functionalized SLN may occur mainly through a non-endocytic mechanism, such as passive diffusion. On the other hand, a statistically significant reduction in the cellular uptake of SLN-FA was found following incubation with cytochalasin D and chlorpromazine. Similar outcomes have been reported for lipid-based nanoparticles [26, 51]. Cytochalasin D prevents the depolymerization of the actin cytoskeleton, inhibiting macropinocytosis [50]. The influence of macropinocytosis in the nanoparticles uptake is likely to occur, as this is a common route for small molecules, amino acids and nanoparticles uptake in different cancer cells [52, 53]. Chlorpromazine inhibits clathrin-mediated endocytosis, which is one of the main pathways for nanoparticle internalization, in particular with particle sizes ranging from 100 to 200 nm [54]. Moreover, different studies have reported that clathrin-mediated endocytosis is one of the major pathways through which FR and FR-targeted nanoparticles are internalized [55-57], which suggests that SLN-FA internalization occurs through a FR-mediated endocytosis.

Overall these data suggest the involvement of both clathrin-mediated endocytosis and macropinocytosis in the internalization of the SLN-FA. These findings are in agreement with the CLSM studies, which suggested a possible localization of the nanoparticles in the lysosomes, since both macropinocytosis and clathrin-mediated endocytosis culminate in the lysosomal compartment, in contrast to what occurs in caveolae-mediated endocytosis [58].

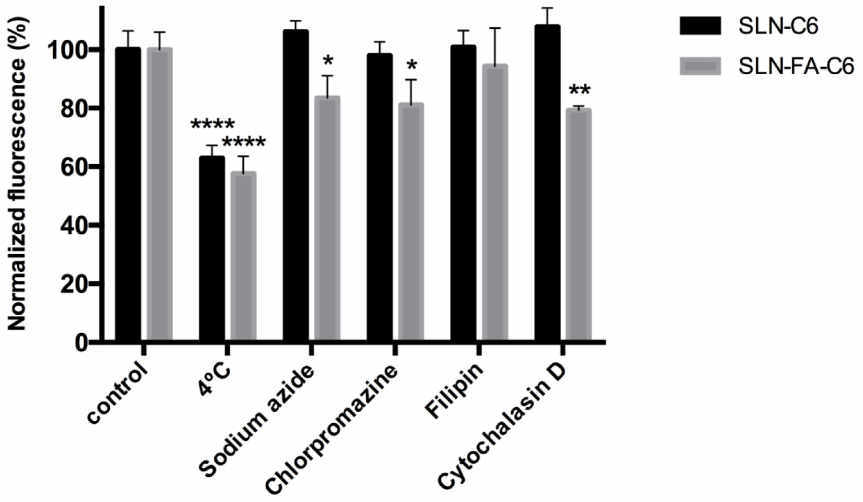



**Figure 8. Effect of energy and different cellular uptake pathway inhibitors on MCF-7 internalization of SLN-C6 and SLN-FA-C6**. Cells were incubated with the different pathway inhibitors for 30 min prior to incubation with the nanoparticles for 1h. Fluorescence values were normalized with the values of the cells incubated at 37˚C without any inhibitor. Data expressed as mean ± SD (n = 3). Differences between groups were assessed using two-way ANOVA followed by Dunnet post-hoc test *p<0.05, **p<0.01,****p<0.0001 relatively to corresponding control SLN.

## 4. Conclusion

In this work, Mito-loaded SLN functionalized with a DSPE-PEG-FA conjugate were produced to prolong drug circulation in the bloodstream and improve drug delivery in $FR^+$ breast cancer cells. SLN presented adequate release properties for intravenous injection with Mito being released at a fast rate at acidic pH, and in a sustained manner at physiological pH. Moreover, nanoparticles were non-hemolytic to human RBCs. Therefore, the developed nanoparticles presented adequate characteristics for an intravenous administration and tumor accumulation through EPR effect and remain stable for at least 6 months. Cellular viability studies demonstrated that SLN were able to preserve the high anti-cancer activity of Mito and even improve its cytotoxicity towards MCF-7 cells, as suggested by the lower value of $IC_{50}$ and by the high apoptotic effects of the

nanoformulation. This fact can be attributed to different cellular uptake mechanisms. Nanoparticles are generally internalized by endocytosis, while the free drug enters cells by passive or flip-flop diffusion. In addition, intracellular drug delivery can be further enhanced due to FR-mediated endocytosis, leading to a higher intracellular accumulation of Mito, and, hence a higher cytotoxicity. These findings were corroborated by the cellular uptake assays conducted using CLSM and flow cytometry, were FA-functionalized SLN showed a higher internalization in MCF-7 than their non-functionalized counterparts. Moreover, the cellular uptake of SLN-FA was found to be energy-dependent with the involvement of macropinocytosis and clathrin-coated pits, the latter being associated with FR-mediated endocytosis. Overall, these data suggest that DSPE-PEG-FA-functionalized SLN are an effective Mito delivery system, being able to selectively deliver the drug towards FR+ cancer cells and desirably limit non-specific tissue distribution and systemic toxic effects.

## Acknowledgments

This work received financial support from PT national funds (FCT/MCTES, Fundação para a Ciência e Tecnologia and Ministério da Ciência, Tecnologia e Ensino Superior) through the project UIDB/50006/2020 and HEALTH-UNORTE I&D&I project (NORTE-01-0145-FEDER-000039) co-financed by European Regional Development Fund (ERDF), through the NORTE 2020 (Programa Operacional Regional do Norte 2014/2020). Andreia Granja acknowledges FCT (Fundação para a Ciência e Tecnologia) and ESF (European Social Fund) for the PhD grant SFRH/BD/130147/2017. Cláudia Nunes is thankful to FCT for the investigator Grant (IF/00293/2015). Célia T. Sousa thanks FCT for financial support through the Investigador FCT program (contract no. IF/01159/2015), to the program Atraccion de Talento (CAM), ref. 2020-T1/IND-19889 and the UE's Horizon 2020 research and innovation program under the Marie Sklodowska-Curie grant no. 734801

## References


1. Sung, H., J. Ferlay, R.L. Siegel, M. Laversanne, I. Soerjomataram, A. Jemal, and F. Bray, *Global Cancer Statistics 2020: GLOBOCAN Estimates of Incidence and Mortality Worldwide for 36 Cancers in 185 Countries.* CA Cancer J Clin, 2021. **71**(3): p. 209-49.
2. Waks, A.G. and E.P. Winer, *Breast Cancer Treatment: A Review.* Jama, 2019. **321**(3): p. 288-300.
3. Blanco, E. and M. Ferrari, *Emerging nanotherapeutic strategies in breast cancer.* The Breast, 2014. **23**(1): p. 10-18.
4. Bai, X., J. Ni, J. Beretov, P. Graham, and Y. Li, *Cancer stem cell in breast cancer therapeutic resistance.* Cancer Treatment Reviews, 2018. **69**: p. 152-63.
5. Varadwaj, P., K. Misra, A. Sharma, and R. Kumar, *Mitoxantrone: an agent with promises for anticancer therapies.* Electronic Journal of Biology, 2010. **6**(2): p. 36-42.
6. Smith, I., R. Stuart-Harris, N. Pavlidis, and T. Bozek, *Mitoxantrone (novantrone∗) as single agent and in combination chemotherapy in the treatment of advanced breast cancer.* Cancer treatment reviews, 1983. **10**: p. 37-40.
7. Coleman, R., M. Maisey, R. Knight, and R. Rubens, *Mitoxantrone in advanced breast cancer—a phase II study with special attention to cardiotoxicity.* European Journal of Cancer and Clinical Oncology, 1984. **20**(6): p. 771-76.
8. Guissi, N.E.I., H. Li, Y. Xu, F. Semcheddine, M. Chen, Z. Su, and Q. Ping, *Mitoxantrone-and folate-TPGS2k conjugate hybrid micellar aggregates to circumvent toxicity and enhance efficiency for breast cancer therapy.* Molecular pharmaceutics, 2017. **14**(4): p. 1082-94.
9. Nieth, C. and H. Lage, *Induction of the ABC-Transporters Mdr1/P-gp (Abcb1), Mrp1 (Abcc1), and Bcrp (Abcg2) during establishment of multidrug resistance following exposure to mitoxantrone.* Journal of chemotherapy, 2005. **17**(2): p. 215-23.
10. Shi, J., P.W. Kantoff, R. Wooster, and O.C. Farokhzad, *Cancer nanomedicine: progress, challenges and opportunities.* Nature reviews. Cancer, 2017. **17**(1): p. 20-37.
11. Wicki, A., D. Witzigmann, V. Balasubramanian, and J. Huwyler, *Nanomedicine in cancer therapy: challenges, opportunities, and clinical applications.* J Control Release, 2015. **200**: p. 138-57.
12. Su, Z., S. Dong, S.-C. Zhao, K. Liu, Y. Tan, X. Jiang, Y.G. Assaraf, B. Qin, Z.-S. Chen, and C. Zou, *Novel nanomedicines to overcome cancer multidrug resistance.* Drug Resistance Updates, 2021. **58**: p. 100777.
13. Pearce, A.K. and R.K. O'Reilly, *Insights into active targeting of nanoparticles in drug delivery: Advances in clinical studies and design considerations for cancer nanomedicine.* Bioconjugate chemistry, 2019. **30**(9): p. 2300-11.
14. Cho, K., X.U. Wang, S. Nie, and D.M. Shin, *Therapeutic nanoparticles for drug delivery in cancer.* Clinical cancer research, 2008. **14**(5): p. 1310-16.
15. Nasirizadeh, S. and B. Malaekeh-Nikouei, *Solid lipid nanoparticles and nanostructured lipid carriers in oral cancer drug delivery.* Journal of Drug Delivery Science and Technology, 2020. **55**: p. 101458.
16. Shah, R., D. Eldridge, E. Palombo, and I. Harding, *Lipid nanoparticles: Production, characterization and stability*. 2015: Springer.
17. Muller, R., M. Radtke, and S. Wissing, *Solid lipid nanoparticles (SLN) and nanostructured lipid carriers (NLC) in cosmetic and dermatological preparations.* Advanced drug delivery reviews, 2002. **54**(1): p. S131.
18. Naseri, N., H. Valizadeh, and P. Zakeri-Milani, *Solid lipid nanoparticles and nanostructured lipid carriers: structure, preparation and application.* Advanced pharmaceutical bulletin, 2015. **5**(3): p. 305.
19. Tapeinos, C., M. Battaglini, and G. Ciofani, *Advances in the design of solid lipid nanoparticles and nanostructured lipid carriers for targeting brain diseases.* J Control Release, 2017. **264**: p. 306-32.
20. Zwicke, G.L., G.A. Mansoori, and C.J. Jeffery, *Utilizing the folate receptor for active targeting of cancer nanotherapeutics.* Nano Reviews & Experiments, 2012. **3**.
21. Kue, C.S., A. Kamkaew, K. Burgess, L.V. Kiew, L.Y. Chung, and H.B. Lee, *Small molecules for active targeting in cancer.* Medicinal research reviews, 2016. **36**(3): p. 494-575.
22. Assaraf, Y.G., C.P. Leamon, and J.A. Reddy, *The folate receptor as a rational therapeutic target for personalized cancer treatment.* Drug Resistance Updates, 2014. **17**(4-6): p. 89-95.

23. Lopes-de-Araújo, J., A.R. Neves, V.M. Gouveia, C.C. Moura, C. Nunes, and S. Reis, *Oxaprozin-Loaded Lipid Nanoparticles towards Overcoming NSAIDs Side-Effects.* Pharmaceutical research, 2016. **33**(2): p. 301-14.
24. Granja, A., R. Lima-Sousa, C.G. Alves, D. de Melo-Diogo, M. Pinheiro, C.T. Sousa, I.J. Correia, and S. Reis, *Mitoxantrone-loaded lipid nanoparticles for breast cancer therapy–quality-by-design approach and efficacy assessment in 2D and 3D in vitro cancer models.* International Journal of Pharmaceutics, 2021: p. 121044.
25. Silva, M.I., A.I. Barbosa, S.A. Costa Lima, P. Costa, T. Torres, and S. Reis, *Freeze-dried Softisan® 649-based lipid nanoparticles for enhanced skin delivery of cyclosporine A.* Nanomaterials, 2020. **10**(5): p. 986.
26. Moraes, S., A. Marinho, S. Lima, A. Granja, J. Araújo, S. Reis, C. Sousa, and C. Nunes, *Targeted nanostructured lipid carriers for doxorubicin oral delivery.* International Journal of Pharmaceutics, 2021. **592**: p. 120029.
27. Attia, M.F., N. Anton, J. Wallyn, Z. Omran, and T.F. Vandamme, *An overview of active and passive targeting strategies to improve the nanocarriers efficiency to tumour sites.* J Pharm Pharmacol, 2019. **71**(8): p. 1185-98.
28. Huang, D., L. Sun, L. Huang, and Y. Chen, *Nanodrug Delivery Systems Modulate Tumor Vessels to Increase the Enhanced Permeability and Retention Effect.* J Pers Med, 2021. **11**(2)
29. Singh, R. and J.W. Lillard, Jr., *Nanoparticle-based targeted drug delivery.* Exp Mol Pathol, 2009. **86**(3): p. 215-23.
30. Danaei, M., M. Dehghankhold, S. Ataei, F. Hasanzadeh Davarani, R. Javanmard, A. Dokhani, S. Khorasani, and M.R. Mozafari, *Impact of Particle Size and Polydispersity Index on the Clinical Applications of Lipidic Nanocarrier Systems.* Pharmaceutics, 2018. **10**(2)
31. Fatisson, J., I.R. Quevedo, K.J. Wilkinson, and N. Tufenkji, *Physicochemical characterization of engineered nanoparticles under physiological conditions: effect of culture media components and particle surface coating.* Colloids Surf B Biointerfaces, 2012. **91**: p. 198-204.
32. Li, Y., A. Yediler, Z. Ou, I. Conrad, and A. Kettrup, *Effects of a non-ionic surfactant (Tween-80) on the mineralization, metabolism and uptake of phenanthrene in wheat-solution-lava microcosm.* Chemosphere, 2001. **45**(1): p. 67-75.
33. Lee, E.S., Z. Gao, and Y.H. Bae, *Recent progress in tumor pH targeting nanotechnology.* Journal of Controlled Release, 2008. **132**(3): p. 164-70.
34. Fan, Y., C. Chen, Y. Huang, F. Zhang, and G. Lin, *Study of the pH-sensitive mechanism of tumor-targeting liposomes.* Colloids and Surfaces B: Biointerfaces, 2017. **151**: p. 19-25.
35. ISO10993-4, *Biological Evaluation of Medical Devices Part 4. Selection of Tests for Interactions with Blood*. 2017.
36. Miao, J., Y.-Z. Du, H. Yuan, X.-g. Zhang, and F.-Q. Hu, *Drug resistance reversal activity of anticancer drug loaded solid lipid nanoparticles in multi-drug resistant cancer cells.* Colloids and Surfaces B: Biointerfaces, 2013. **110**: p. 74-80.
37. Abbasalipourkabir, R., A. Salehzadeh, and R. Abdullah, *Cytotoxicity effect of solid lipid nanoparticles on human breast cancer cell lines.* Biotechnology, 2011. **10**(6): p. 528-33.
38. Xu, Y., S. Asghar, S. Gao, Z. Chen, L. Huang, L. Yin, Q. Ping, and Y. Xiao, *Polysaccharide-based nanoparticles for co-loading mitoxantrone and verapamil to overcome multidrug resistance in breast tumor.* International journal of nanomedicine, 2017. **12**: p. 7337.
39. Soleymani, J., M. Hasanzadeh, M.H. Somi, N. Shadjou, and A. Jouyban, *Probing the specific binding of folic acid to folate receptor using amino-functionalized mesoporous silica nanoparticles for differentiation of MCF 7 tumoral cells from MCF 10A.* Biosensors and Bioelectronics, 2018. **115**: p. 61-69.
40. Burns, C.P., B.N. Haugstad, and J.A. North, *Membrane transport of mitoxantrone by L1210 leukemia cells.* Biochem Pharmacol, 1987. **36**(6): p. 857-60.
41. Regev, R., D. Yeheskely-Hayon, H. Katzir, and G.D. Eytan, *Transport of anthracyclines and mitoxantrone across membranes by a flip-flop mechanism.* Biochemical Pharmacology, 2005. **70**(1): p. 161-69.
42. Shahabi, S., S. Döscher, T. Bollhorst, L. Treccani, M. Maas, R. Dringen, and K. Rezwan, *Enhancing cellular uptake and doxorubicin delivery of mesoporous silica nanoparticles via surface functionalization: effects of serum.* ACS applied materials & interfaces, 2015. **7**(48): p. 26880-91.
43. Yoo, H.S. and T.G. Park, *Folate receptor targeted biodegradable polymeric doxorubicin micelles.* Journal of controlled release, 2004. **96**(2): p. 273-83.

44. Kluza, J., P. Marchetti, M.-A. Gallego, S. Lancel, C. Fournier, A. Loyens, J.-C. Beauvillain, and C. Bailly, *Mitochondrial proliferation during apoptosis induced by anticancer agents: effects of doxorubicin and mitoxantrone on cancer and cardiac cells.* Oncogene, 2004. **23**(42): p. 7018-30.
45. Zhang, L., D. Zhu, X. Dong, H. Sun, C. Song, C. Wang, and D. Kong, *Folate-modified lipid-polymer hybrid nanoparticles for targeted paclitaxel delivery.* International journal of nanomedicine, 2015. **10**: p. 2101-14.
46. Setua, S., D. Menon, A. Asok, S. Nair, and M. Koyakutty, *Folate receptor targeted, rare-earth oxide nanocrystals for bi-modal fluorescence and magnetic imaging of cancer cells.* Biomaterials, 2010. **31**(4): p. 714-29.
47. Fan, Y., Y. Zhang, W. Yokoyama, and J. Yi, *Endocytosis of corn oil-caseinate emulsions in vitro: impacts of droplet sizes.* Nanomaterials, 2017. **7**(11): p. 349.
48. Sola, F., B. Canonico, M. Montanari, A. Volpe, C. Barattini, C. Pellegrino, E. Cesarini, M. Guescini, M. Battistelli, and C. Ortolani, *Uptake and Intracellular Trafficking Studies of Multiple Dye-Doped Core-Shell Silica Nanoparticles in Lymphoid and Myeloid Cells.* Nanotechnology, science and applications, 2021. **14**: p. 29.
49. Peñaloza, J.P., V. Márquez-Miranda, M. Cabaña-Brunod, R. Reyes-Ramírez, F.M. Llancalahuen, C. Vilos, F. Maldonado-Biermann, L.A. Velásquez, J.A. Fuentes, and F.D. González-Nilo, *Intracellular trafficking and cellular uptake mechanism of PHBV nanoparticles for targeted delivery in epithelial cell lines.* Journal of nanobiotechnology, 2017. **15**(1): p. 1-15.
50. Khalil, I.A., K. Kogure, H. Akita, and H. Harashima, *Uptake pathways and subsequent intracellular trafficking in nonviral gene delivery.* Pharmacological reviews, 2006. **58**(1): p. 32-45.
51. Gilleron, J., W. Querbes, A. Zeigerer, A. Borodovsky, G. Marsico, U. Schubert, K. Manygoats, S. Seifert, C. Andree, and M. Stöter, *Image-based analysis of lipid nanoparticle–mediated siRNA delivery, intracellular trafficking and endosomal escape.* Nature biotechnology, 2013. **31**(7): p. 638-46.
52. Commisso, C., *The pervasiveness of macropinocytosis in oncological malignancies.* Philosophical Transactions of the Royal Society B, 2019. **374**(1765): p. 20180153.
53. Kay, R.R., *Macropinocytosis: biology and mechanisms.* Cells & Development, 2021: p. 203713.
54. Bouallegui, Y., R. Ben Younes, R. Oueslati, and D. Sheehan, *Redox proteomic insights into involvement of clathrin-mediated endocytosis in silver nanoparticles toxicity to Mytilus galloprovincialis.* PloS one, 2018. **13**(10): p. e0205765.
55. Suen, W.-L.L. and Y. Chau, *Size-dependent internalisation of folate-decorated nanoparticles via the pathways of clathrin and caveolae-mediated endocytosis in ARPE-19 cells.* Journal of Pharmacy and Pharmacology, 2014. **66**(4): p. 564-73.
56. Barar, J., V. Kafil, M.H. Majd, A. Barzegari, S. Khani, M. Johari-Ahar, D. Asgari, G. Cokous, and Y. Omidi, *Multifunctional mitoxantrone-conjugated magnetic nanosystem for targeted therapy of folate receptor-overexpressing malignant cells.* Journal of nanobiotechnology, 2015. **13**(1): p. 1-16.
57. Bittleman, K.R., S. Dong, M. Roman, and Y.W. Lee, *Folic acid-conjugated cellulose nanocrystals show high folate-receptor binding affinity and uptake by KB and breast cancer cells.* ACS omega, 2018. **3**(10): p. 13952-59.
58. Hillaireau, H. and P. Couvreur, *Nanocarriers' entry into the cell: relevance to drug delivery.* Cellular and molecular life sciences, 2009. **66**(17): p. 2873-96.

## Supplementary data

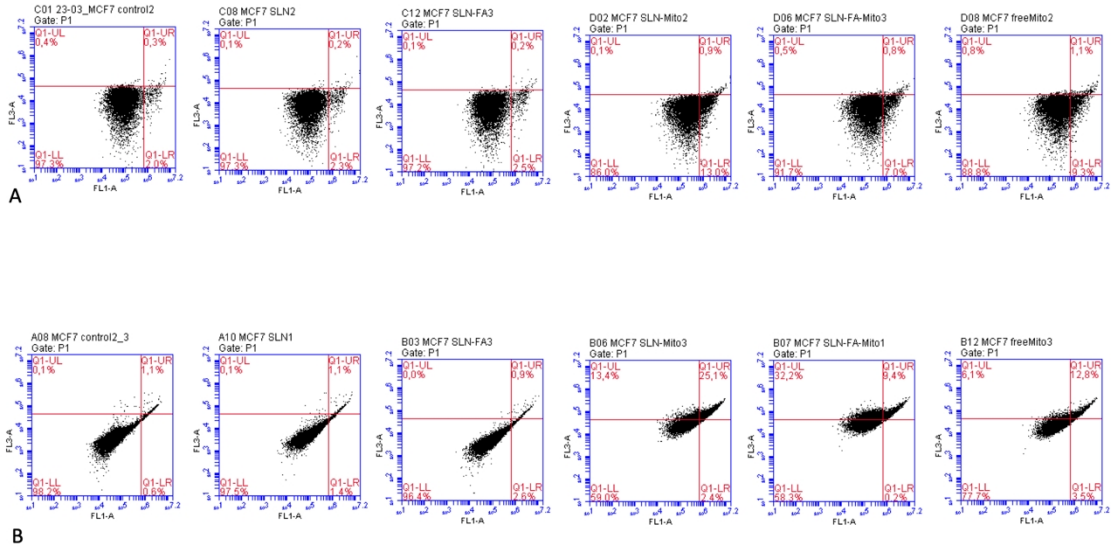



**Figure S1. Scatter plots of Annexin V (x-axis) vs 7-AAD (y-axis**) obtained by flow cytometry. MCF-7 cells were incubated with SLN, SLN-FA, SLN-Mito, SLN-FA-Mito and free Mito at a concentration of 5 µg/mL (**A**) and 50 µg/mL of lipid (**B**) and the FITC Annexin V Apoptosis assay was performed after 24h. The plots represented in A and B are independent experiments obtained in different days.

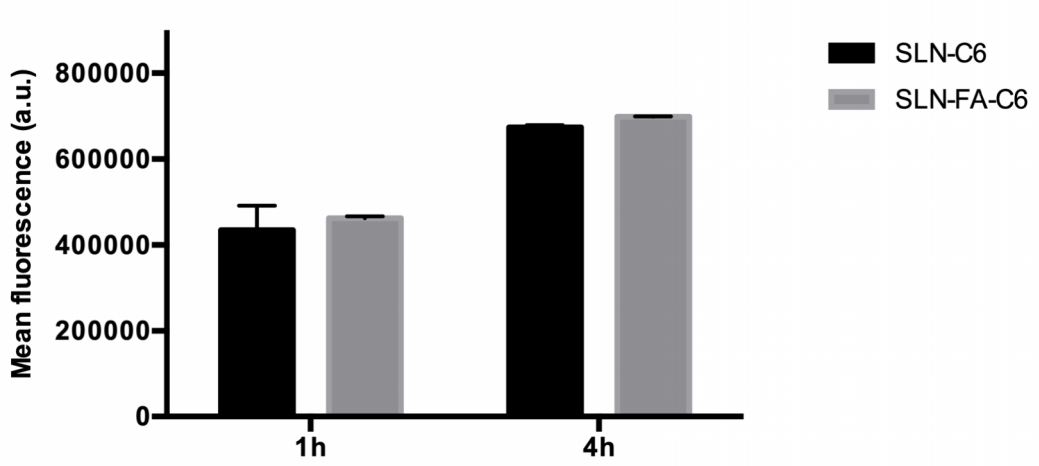
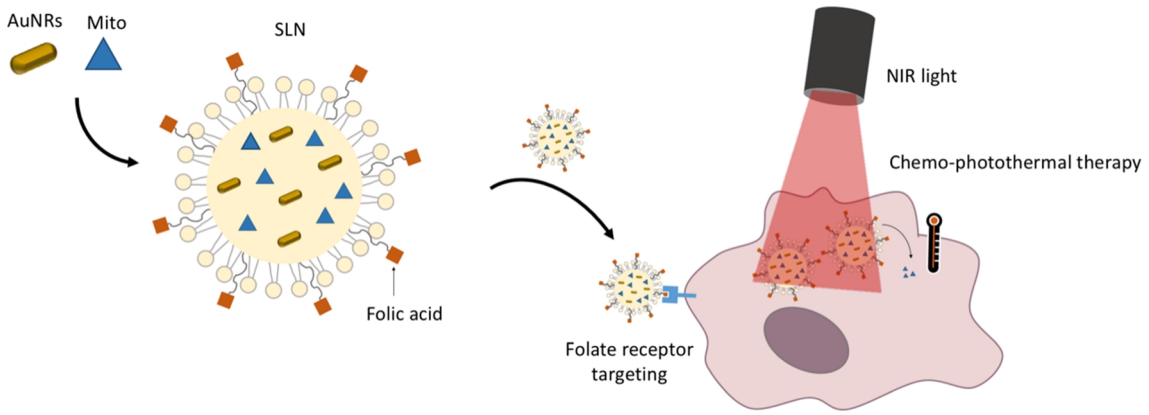



**Figure S2. Quantification of C6-labelled SLN by flow cytometry in L929 cells**. Cells were incubated with the different SLN and free drug for 1h and 4h. Data expressed as mean ± SD (n = 3). Differences between groups were evaluated using two-way ANOVA followed by Sidak post-hoc test * $p<0.05$, **** $p<0.0001$ relatively to the non-functionalized SLN at each time-point.

## 4.4. Multifunctional targeted solid lipid nanoparticles for combined photothermal therapy and chemotherapy of breast cancer

This final chapter includes the design of a more complex multifunctional nanosystem. Here, SLN were loaded with Mitoxantrone (Mito) and gold nanorods (AuNRs) for the combination of chemotherapy and photothermal therapy (PTT) in breast cancer. Based on the studies of the previous chapters, involving surface functionalization of the SLN, FA was chosen for the active cancer cell targeting of the nanosystem. Moreover, a previous work studying the heating behaviour of gold nanorods using pulsed versus continuous near infrared (NIR) laser (**Appendix I**), has led to the choice of continuous NIR laser for this particular application.



# Multifunctional targeted solid lipid nanoparticles for combined photothermal therapy and chemotherapy of breast cancer

Andreia Granja[a], Rita Lima-Sousa[b], Cátia G. Alves[b], Duarte de Melo-Diogo[b], Cláudia Nunes[a], Célia T. Sousa[c,d], Ilídio J. Correia[b,e,*] and Salette Reis[a,*]

[a]LAQV, REQUIMTE, Departamento de Ciências Químicas, Faculdade de Farmácia, Universidade do Porto, 4050-313 Porto, Portugal
[b]CICS-UBI – Centro de Investigação em Ciências da Saúde, Universidade da Beira Interior, 6200-506 Covilhã, Portugal
[c]IFIMUP and Departamento de Física e Astronomia da Faculdade de Ciências da Universidade do Porto, Rua do Campo Alegre 687, 4169-007, Porto, Portugal
[d]Departamento de Física Aplicada, Facultad de Ciencias, Universidad Autónoma de Madrid (UAM), Campus de Cantoblanco, C/ Francisco Tomás y Valiente, 7, M 12 604 - 28049, Madrid, Spain
[e]CIEPQPF – Departamento de Engenharia Química, Universidade de Coimbra, Rua Sílvio Lima, 3030-790 Coimbra, Portugal
*Corresponding authors: Ilídio J. Correia: icorreia@ubi.pt; Salette Reis: shreis@ff.up.pt;

## Abstract

Photothermal therapy (PTT) has emerged as new promising strategy for the management of cancer, either alone or combined with other therapeutics, such as chemotherapy. The use of nanoparticles for multimodal therapy can improve treatment performance and reduce drug doses and associated side-effects. Here we propose the development of a novel multifunctional nanosystem based on solid lipid nanoparticles (SLN) co-loaded with gold nanorods (AuNRs) and Mitoxantrone (Mito) and functionalized with folic acid (FA) for dual PTT and chemotherapy of breast cancer. SLN were produced using an economically affordable method and presented suitable properties for tumor passive accumulation. Upon NIR irradiation (808 nm, 1.7 W $cm^{-2}$, 5 min), nanoparticles could effectively mediate a temperature increase of more than 20˚C. Moreover, exposure to NIR light resulted in an enhanced release of Mito. Furthermore, nanoparticles were non-hemolytic and well tolerated even at high concentrations. The active targeting strategy was found to be successful, as shown by the greater accumulation of the functionalized SLN in MCF-7 cells. Finally, the combined effects of chemotherapy, NIR-induced drug release and PTT significantly enhanced breast cancer cell death. Overall, these results demonstrate that the developed lipid nanosystem is an efficient vehicle for breast cancer multimodal therapy.

**Keywords:** Solid lipid nanoparticles; Gold nanorods; Mitoxantrone; Multimodal therapy**;** Folic Acid; Breast cancer

# 1. Introduction

Breast cancer is the most common malignancy and the main cause of cancer-related deaths in women globally [1]. According to the latest GLOBOCAN report, in 2020 2.3 million women were diagnosed and 685 000 deaths occurred all over the world [1]. Given the high complexity and heterogeneity of the disease, the standard breast cancer treatment regimens generally encompass multidrug and multimodal therapy [2, 3]. However, the majority of these therapeutics are non-specific, which leads to off-target systemic toxicity and reduced efficacy [4]. To surpass some of these limitations, new treatment modalities for breast cancer management such as PTT have emerged. PTT is a safe, minimally-invasive and precise procedure based on the delivery of a PTT agent to the tumor region, followed by light irradiation, generally in the near-infrared region (NIR). The photothermal agent converts the light energy into heat, which can directly elicit cancer cell death and when combined with other modalities such as chemotherapy, improve its therapeutic effect [5]. Gold nanostructures, such as gold nanorods (AuNRs) are considered excellent photothermal agents given their high biocompatibility and versatility, along with a high light-to-heat conversion efficiency. Thus, they have been explored as photothermal agents for breast cancer therapy, either alone or in combination with other therapeutics [6-9]. The development of a multifunctional nanosystem comprising PTT and chemotherapy represents a promising therapeutic strategy, as the combined actions of the two modalities can result in higher anti-cancer efficacy, drug dosages reduction and multidrug resistance (MDR) limitation [10-12]. In addition, the incorporation of the two modalities into one single nanoplatform opens the possibility for the development of smart nanosystems, which can release their cargo upon NIR light irradiation, further improving the performance and selectivity of the treatment [13]. Different nanoplatforms co-loaded with AuNRs and chemotherapeutics have already been reported including liposomes [14, 15], dendrimers [16] mesoporous silica [17, 18], albumin [19] and polymeric [20] nanoparticles. Lipid nanoparticles, such as solid lipid nanoparticles (SLN) and nanostructured lipid carriers (NLC) emerged in the early 90's and represent a simple, biocompatible, economically affordable and versatile type of nanocarrier, which can be explored for the design of multifunctional nanosystems [21, 22]. Up to this date, only one study combining drug delivery and gold nanostructures for dual PTT and chemotherapy using lipid nanoparticles has been reported [23]. Zheng *et al*. produced NLC decorated with PEG and hyaluronic acid and loaded with doxorubicin and polyhedral gold nanoparticles, presenting encouraging results [23]. To the best of our knowledge, however, the production of SLN loaded with AuNRs for PTT has not been reported. Recently, we have designed SLN using a low-cost organic solvent-free method for the entrapment of the chemotherapeutic drug Mitoxantrone (Mito). Mito is an anthracenedione with high efficacy against different types of cancers, including breast cancer

[24]. In addition, Mito has demonstrated an enhanced cytotoxicity when combined with hyperthermia *in vitro* [25]. Thus, it may benefit from the combination with AuNRs-mediated PTT. Therefore, here we propose the development of a multifunctional SLN nanoformulation loaded with Mito and AuNRs to take advantage of the combined effects of chemotherapy and PTT. Moreover, to improve tumor accumulation and target the folate receptors (FR) overexpressed in cancer cells [26], SLN were decorated with a folic acid (FA) conjugate. SLN were produced and fully characterized and their photothermal effect and drug release behaviour upon NIR light irradiation (808 nm, 1.7 W $cm^{-2}$, 5 min) were evaluated. After that, the hemocompatibility and cytocompatibility of the nanosystem were determined and the targeting efficiency towards MCF-7 cells was studied by flow cytometry and CLSM. Finally, the combination of chemotherapy and PTT was assessed in MCF-7 cells.

# 2. Materials and Methods

## 2.1. Materials

Mitoxantrone hydrochloride, Tween® 80, Triton™ X-100, Dulbecco's Phosphate Buffered Saline, (PBS), Folic Acid (FA), Trimethylamine, Dicyclohexylcarbodiimide (DCC), N-hydroxysuccinimide (NHS), Dimethyl sulfoxide ≥ 99.9% (DMSO), Coumarin-6 (C6) (98%), Resazurin, Trypan blue solution, Propidium iodide (PI) solution and Formalin solution were purchased from Sigma-Aldrich® (St Louis, MO, USA). Cetyl Palmitate was kindly provided by Gatefossé (Nanterre, France). DSPE-$PEG_{2000}$-$NH_2$ (1,2-distearoyl-*sn*-glycero-3-phosphoethanolamine-N-[amino(polyethylene glycol)-2000 (ammonium salt) was purchased from Avanti® Polar Lipids Inc. (Merck, Darmstadt, Germany). Sodium chloride was purchased from Honeywell Fluka™ (NJ, USA). Organic-coated gold nanorods (AuNR, 10x41nm) were obtained from Nanopartz (Nanopartz, Loveland, CO, USA). Dulbecco's Modified Eagle's Medium (DMEM), Trypsin-EDTA (0.25% v/v), Penicillin-Streptomycin and Heat Inactivated Fetal Bovine Serum (FBS) were purchased from Gibco® by Life Technologies™ (UK). Hoechst 33342®, Trihydrochloride, Trihydrate and LysoTracker™ Green DND-26 were obtained from (Invitrogen, Thermo Fisher Scientific, MA, USA). MCF-7 cell line was obtained from ATCC (Middlesex, UK). Normal Human Dermal Fibroblasts (NHDF) were acquired from Promocell (Heidelberg, Germany). Ultrapure water (18.2 MΩ cm) was obtained from a water purification system (Healforce, Shanghai, China).

## 2.2. Preparation of Solid lipid nanoparticles (SLN)

SLN were prepared by the hot ultra-sonication technique, as previously described, with some adaptations [27]. Briefly, 20 mg of cetyl palmitate and 17.5 mg of Tween® 80 were heated in a water bath at 70˚C until the complete melting of the lipid. A solution of AuNRs (containing 1.6 mg) was then added to the lipid melt. Functionalized SLN were produced by adding the FA conjugate (DSPE-$PEG_{2000}$-FA), synthesized as previously reported in our group [28], to the lipid phase at a ratio of 1% of the mass of lipid+surfactant. After that, 1.1 mL of pre-heath PBS buffer (pH 8.2) was poured into the lipid phase followed by sonication for 5 min using a probe sonicator (VCX130, Sonics and Materials, 115 Newtown, CT, USA) at an amplitude of 70%. The nanoemulsion was then cooled to room temperature and stored at 4ºC until further use. For the production of Mito-loaded SLN, a drug solution in PBS buffer (470 µg/mL) was previously prepared and poured into the lipid phase.

For the cellular uptake studies performed in flow cytometry, SLN were labeled with C6, which was added to the lipid phase during the production at a ratio of 0.025% of the mass of lipid+surfactant.

### 2.3. Size, Polydispersity Index and surface charge measurements

The measurements of the mean hydrodynamic diameter, polydispersity index (PDI) and surface charge (zeta potential) of the SLN were performed by dynamic light scattering (DLS) and electrophoretic light scattering (ELS) using a ZetaPALS analyzer (Brookhaven Instruments Corporation, Holtsville, NY, USA). Nanoformulations were previously diluted at a ratio of 1:200 and measurements were performed at room temperature at a scattering angle of 90° and dust cut-off set to 30. Data are presented as mean ± standard deviation. A detailed evaluation of nanoparticle size distribution was performed using nanoparticle tracking analysis (NTA) using a NanoSight NS300 (Malvern Instruments, Worcestershire, UK) equipped with a 488 nm laser and a high sensitivity scientific CMOS camera. Each sample was diluted in distilled water (1:50,000), injected in the viewing chamber at an infusion rate of 50 and measured under constant flow at 24˚C. For each size determination, 5 videos of 20 s were captured with a camera level of 10 and detection threshold of 5. Data were analyzed using the NTA 3.4. software.

### 2.4. Entrapment Efficiency (EE%) determination

To determine the entrapment efficiency of Mito an indirect method of quantification was used. Briefly, nanoformulations were diluted in PBS at a ratio of 1:30 and transferred to centrifugal filter units (Amicon® Ultra Centrifugal Filters Ultracell-50 kDa, MERK Milipore, Ltd; Cork, Ireland) followed by centrifugation at 2851 $\times$ $g$ (Allegra X-15R Centrifuge, Beckman Coulter, Fullerton, California) until total separation of the aqueous and lipid phase. The amount of non-entrapped Mito was measured in the aqueous phase at 610 nm by UV-vis spectrophotometry (Jasco V-660 Spectrophotometer, Software: Spectra Manager v.2, Jasco Corportation, USA). A standard curve in PBS buffer previously obtained was used to determine the concentration of Mito.

EE% was determined by calculating the ratio between the entrapped drug (corresponding to the difference between the initial amount added in the nanoformulation and the non-entrapped amount) and the total amount of drug, as shown by the following equation:

$$EE\% = \frac{\text{Total amount of Mito - Non-entrapped Mito}}{\text{Total amount of Mito}} \times 100 \quad \text{(Equation 1)}$$

### 2.5. Heat stability of Mito

Prior to the PTT studies, a heat stability study of Mito was conducted using Nuclear magnetic resonance (NMR). The drug was dissolved in $D_2O$ in an NMR tube and incubated for 30 minutes at 20, 30, 40, 50, 60 and 70˚C in an NMR spectrometer (Bruker Avance III 400, operating at 400.15 MHz). $^1H$ NMR spectra were recorded and analyzed for each temperature using the standard Bruker software (version 4.01). Each spectrum was analyzed, regarding the potential formation of new signals and the variation of the chemical shifts of the protons of the drug. NMR analyses were performed at Laboratory of Structural Analysis, “Centro de Materiais da Universidade do Porto” (CEMUP) (Portugal).

### 2.6. Photothermal capacity evaluation and NIR-induced drug release

To evaluate the photothermal capacity of the AuNRs-loaded SLN, each sample (200 µL) was irradiated with a NIR laser (808 nm, 1.7 W $cm^{-2}$) for 5 minutes and the temperature variation was measured using a thermocouple thermometer. PBS solution was used as a control.

The *in vitro* drug release was performed with and without NIR laser irradiation using the dialysis method. Briefly, nanoformulations (500 µL) were placed in the upper compartment of a dialysis device (Slide-A-Lyzer™ MINI Dialysis Device, MWCO 10kDa, Thermo Scientific™, MA, USA) which was immersed into 14 mL of PBS buffer. Dialysis devices were then placed at 37˚C under stirring for 24 h. At predetermined intervals, 1 mL of each sample was collected from the external media and replaced with 1mL of pre-heated PBS. For the irradiated samples, nanoformulations were exposed to the NIR laser (808 nm, 1.7 W $cm^{-2}$) for 5 min. The amount of drug released at each time-point was quantified by UV-Vis spectrophotometry using an Evolution 201 spectrophotometer (Thermo Scientific™, MA, USA). Release data were obtained using the average of the triplicates.

### 2.7. Hemolysis assay

An *in vitro* hemolysis assay was performed using blood from human healthy volunteers. Blood samples were collected according to the principles of the declaration of Helsinki and were

kindly donated by Serviço de Hematologia from Centro Hospitalar Universitário do Porto - Hospital de Santo Antonio. Red blood cells (RBCs) were separated from the whole blood by centrifugation at 955g for 5 min at 4˚C (Allegra X-15R Centrifuge, Beckman Coulter, Fullerton, California) and were then washed 3 times with physiological saline solution (0.85% NaCl). A 4% (v/v) solution of RBCs was then prepared and incubated with the nanoformulations at ratio of 1:1 in a 96-well plate at 37˚C for 4 h. Triton X-100 (1% v/v in physiological saline) and saline solution were used as positive and negative controls, respectively. After the incubation period, supernatants were recovered and the amount of hemoglobin was quantified by UV-vis spectrophotometry at 415 nm using a microplate reader (Biotek Instruments, Winooski, VT, USA). Data were obtained using the average of three assays with blood collected from 3 different donors. The percentage of hemolysis was calculated as follows:

$$\text{hemolysis } \% = \frac{\text{Abs (sample)} - \text{Abs (negative control)}}{\text{Abs (positive control)} - \text{Abs (negative control)}} \times 100 \qquad \text{(Equation 2)}$$

### 2.8. Cytocompatibility assessment

The cytocompatibility of the lipid nanoformulations was assessed in normal (NHDF) and breast cancer cells (MCF-7) by the resazurin assay, as previously reported [29]. Cells were seeded in 96-well plates (1 x$10^4$ cells per well) in DMEM supplemented with 10% (v/v) FBS and 1% (v/v) streptomycin/gentamycin at 37˚C, 5% $CO_2$ in an humidified environment. After 24 h, cells were treated with different concentrations of the nanoformulation for 24 h and 48 h. A negative control containing cells treated with DMEM was also included. At the end of the incubation, medium was discarded and a resazurin solution (10% v/v in culture media) was added and incubated for 4 h in the dark (37˚C, 5% $CO_2$). The fluorescence of resorufin (λex = 560 nm; λem = 590 nm) was then measured in a Spectramax Gemini EM spectrofluorometer.

### 2.9. Cellular uptake studies

#### 2.9.1. Flow cytometry

Flow cytometry analysis were performed as previously described in our group [30]. MCF-7 cells were seeded in 24-well plates (2 × $10^5$ cells per well) and grown for 24 h at 37˚C, 5% $CO_2$. Cells were then incubated with functionalized and non-functionalized C6-labeled SLN (250 µg/mL of lipid) at different time-points (0.5, 1, 2, 3, 4 and 24 h) at 37˚C, 5% $CO_2$. A control

with cells incubated with only DMEM was also included. After each incubation period, cells were washed twice with PBS, detached with 0.25% trypsin-EDTA, resuspended in PBS and analysed using a BD Accuri™ C6 flow cytometer (BD Biosciences, Belgium). Staining with PI (0.01 mg/mL) was performed to exclude dead cells and trypan blue (0.004 %) was added to quench the signal from non-internalized nanoparticles. For each sample, a minimum of 10,000 events was collected. Data analysis was performed using the BD Accuri™ C6 software (BD Biosciences, Belgium). Graphpad (GraphPad Software Inc., CA, USA) was used to analyze and fit the kinetics of time of the cellular uptake to the Michaelis-Menten equation:

$$V = \frac{V_{max} \times t}{k + t} \qquad \text{(Equation 3)}$$

where V is the cellular uptake in real time, $t$ is the incubation time, $V_{max}$ is the value of saturated cellular uptake and k is the time of half maximum uptake.

### 2.9.2. Confocal microscopy

For Confocal Laser Scanning Microscopy (CLSM) imaging, MCF-7 cells were seeded in µ-slide 8-well imaging plates (Ibitreat, Ibidi GmbH, Munich, Germany) at a density of $1x10^4$ cells per well and incubated at 37˚C, 5% $CO_2$. After 24 h, the different Mito-loaded nanoformulations (5 µg/mL of lipid) were incubated for 4 h and 24 h in a humidified atmosphere, at 37˚C, 5% $CO_2$. At the end of the incubation, cells were washed three times with PBS and stained with Lysotracker™ Green (60 nM) followed by incubation for 30 min at 37˚C, 5% $CO_2$. Cells were then washed three times with PBS and fixed with formalin solution for 30 min at room temperature. After rinsed three times with PBS, cells were stained with Hoechst 33342® (8 µM) for 10 min at room temperature protected from light and, finally, washed three times with PBS. CLSM images were acquired on a Leica Stellaris 8 confocal microscope (LeicaMicrosystems, Wetzlar, Germany) equipped with the Leica Application Suite X package (LAS X) using a $\lambda_{ex}/\lambda_{em}$ of 350⁄461 nm (Hoechst 33342®), $\lambda_{ex}/\lambda_{em}$ of 504⁄511 nm (LysoTracker™ Green) and $\lambda_{ex}/\lambda_{em}$ of 610/630 nm (Mito) with a resolution of 1024×1024 using a 63X/1.4 oil immersion objective. Images were analysed using Fiji ImageJ software (version 2.0, National Institutes of Health).

Time-lapse live cell imaging of SLN uptake was also performed using CLSM. MCF-7 cells were seeded on 35 mm µ-Dishes (polymer coated, Ibidi GmbH, Munich, Germany) at a density of $3.6 \times 10^4$ cells per dish for 24. After that, cells were stained with Hoechst 33342® (8 µM) for 10 min at room temperature. Cell culture dishes were then placed on the confocal incubator

chamber, at 37˚C, 5% $CO_2$. Nanoformulations (5 µg/mL of lipid) were then added and immediately observed in CLSM. Images were automatically collected for up to 30 min with a time interval of 5 min between frames on a Leica Stellaris 8 confocal microscope (LeicaMicrosystems, Wetzlar, Germany) using a $\lambda_{ex}/\lambda_{em}$ of 610/630 nm (Mito) with a resolution of 1024×1024 using a 63X/1.4 oil immersion objective. CLSM studies were performed at the Imaging by confocal and fluorescence lifetime laboratory, CEMUP, Portugal.

### 2.10. Combined chemo and photothermal therapy effects *in vitro*

The combinatorial effects of chemotherapy and PTT mediated by the nanoformulations were assessed in MCF-7 cells by the resazurin assay, as reported previously [29]. Briefly, cells were grown in 96-well plates (1 x$10^4$ cells per well) for 24 h at 37˚C, 5% $CO_2$, and incubated with the different nanoformulations (SLN-Au and SLN-Au-Mito) at an equivalent concentration of 24 and 32 µg/mL of AuNRs. After 4 h, cells were irradiated with NIR light (808 nm, 1.7 W $cm^{-2}$) for 5 min. Cells incubated with only DMEM with and without NIR irradiation were used as a control. Cell viability was then evaluated 24 h after nanoparticle incubation, as described in **section 2.8**.

### 2.11. Statistical analysis

Statistical analysis was performed using Graphpad Prism6 Software (GraphPad Software Inc., CA, USA). Differences between groups were assessed by two-way ANOVA with a *p*-value < 0.05 considered statistically significant. All data are expressed as mean ± SD.

# 3. Results

## 3.1. Physicochemical characterization

Two different SLN nanoformulations were produced by the hot ultra-sonication technique. Formulations appeared milky, homogeneous with light brown color due to the loading of AuNRs. After Mito entrapment, color changed to dark blue. Their main physicochemical characteristics are summarized in **Figure 1**. The hydrodynamic size of the SLN varied between 206 to 212 nm, for SLN Au-FA and SLN Au-Mito-FA, respectively, as measured by DLS. Measurements obtained through NTA, however, showed a relatively smaller particle size of around 174 and 162 nm, respectively. The differences obtained with the two techniques are related with the ability of NTA to track each nanoparticle individually, while DLS determinations can be biased by the presence of agglomerated particles, as previously highlighted [27]. In general, the results obtained for particle size suggest that SLN are suitable for intravenous administration and tumor passive targeting [31, 32]. Polydispersity index (PDI) was below 0.2, confirming the presence of a monodisperse population for lipid-based nanoparticles [33], which is also corroborated by the particle size distribution graphs obtained through NTA. The low values of zeta potential of approximately -10 mV may be related to the ionic strength of the solvent (PBS), which is much higher than double deionized water [34]. Slightly negative surface charges have been found to preferentially accumulate in the tumor region while having limited uptake in normal organs such as liver [35]. Loading of Mito was efficient, as shown by EE% of 88% obtained for this nanoformulation.

**A**

| | Size | PdI | ζ-potential | EE% |
|---|---|---|---|---|
| **SLN Au-FA** | 212 ± 1 | 0.10 ± 0.03 | -11 ± 2 | |
| **SLN Au-Mito-FA** | 206 ± 3 | 0.12 ± 0.01 | -10 ± 1 | 88 ± 3 |

**B**

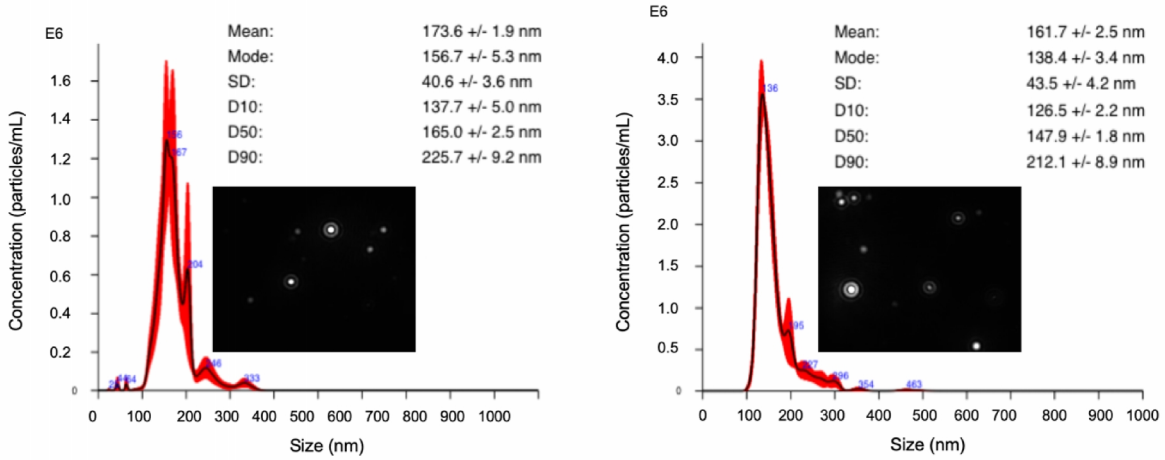



**Figure 1. Physicochemical characterization of SLN Au-Mito-FA and corresponding unloaded nanoformulation (SLN Au-FA)**. (**A**) Hydrodynamic size, PDI and zeta potential determined by DLS and EE%. (**B**) Particle size distribution measured through NTA and corresponding video frames of SLN-Au-FA (left) and SLN Au-Mito-FA (right).

### 3.2. Photothermal effect and NIR-induced drug release

Prior to the PTT studies, the heat stability of Mito was evaluated through NMR. Overall, the obtained data confirmed that no structural changes occurred in the molecule for temperatures up to 70 °C, suggesting that Mito is suitable for the subsequent studies of PTT (**Figure S1**).

The temperature variation achieved upon NIR light exposure was addressed at two different concentrations of AuNRs (**Figure 2A**). At the lowest concentration tested (24 μg/mL) temperature was elevated more than 20˚C, while at 32 μg/mL an elevation of 25˚C was observed. No differences were found between loaded and unloaded nanoformulations, which suggests that the entrapment of Mito did not affect the light-to-heat conversion efficiency of the nanosystem. PBS buffer, the solvent used for the production of the SLN, was used as a control, demonstrating only a very limited temperature variation of approximately 2˚C. Overall, these data suggest that the developed nanosystem is suitable for an effective PTT application at the two concentrations tested.

The release of Mito was investigated in physiological PBS with 5 minutes of NIR irradiation and without irradiation (**Figure 2B)**. As shown in the graph, a controlled release was obtained

at the first 6 h of the study, with only 22% of Mito released to the external media. After NIR irradiation, a higher release of Mito occurred (28%). This difference between irradiated and non-irradiated samples increased over time. At the end of the assay after 48 h, 76% of Mito was released, in contrast to the 68% released from the non-irradiated SLN. These data suggest that the temperature increase occurring following NIR irradiation led to the partial melting of the lipid matrix of the SLN, thus enhancing the release of the drug. Therefore, a higher cancer cell death may be predicted from the combined effects of hyperthermia and enhanced drug release.

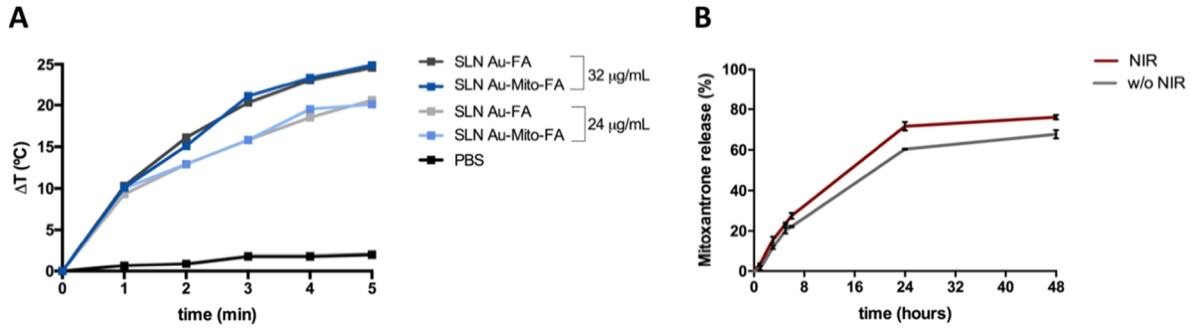



**Figure 2. NIR light irradiation effect on the temperature variation (ΔT) and drug release of the nanoformulations** (**A**) ΔT of SLN Au-FA and SLN Au-FA-Mito at two different concentrations of AuNRs upon irradiation with NIR laser (808 nm, 1.7 W $cm^{-2}$) for 5 min. PBS was used as a control. (**B**) Cumulative release of Mito from SLN Au-Mito-FA with and without NIR laser irradiation for 5 min. Data are expressed as mean ± SD (n = 3).

### 3.3. Hemolysis

To evaluate the potential of the nanoformulations for intravenous injection, a hemolysis assay was conducted using human blood. Nanoformulations were tested at a concentration range of 8 to 40 µg/mL of AuNRs (corresponding to 97 to 485 µg/mL of lipid). As shown in **Figure 3,** nanoparticles induced less than 1% hemolysis, even at the highest lipid concentration (**Figure 3** and **Figure S2**). Therefore, according to ISO 10993-4 [36], those are considered safe for intravenous administration. These results demonstrate that the range of concentration of AuNRs found to be suitable for PTT applications is non-hemolytic.

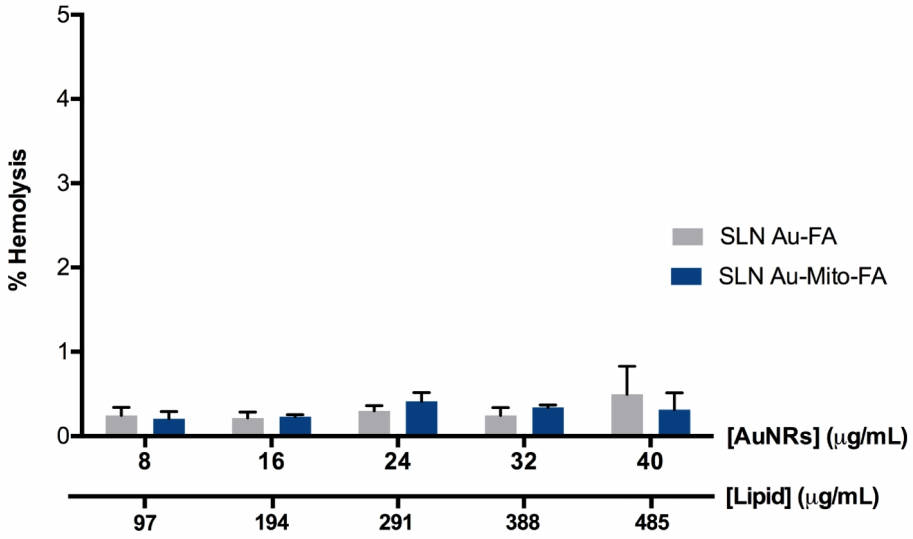



**Figure 3. Hemolytic activity of the nanoformulations at different concentrations**. Data represent the average of 3 assays using RBCs from 3 human donors.

### 3.4. Cytocompatibility assessment

The cytocompatibility of SLN Au-FA was also evaluated in normal cells (NHDF) and tumoral cells (MCF-7) following incubation for 24 and 48 h. The nanoparticles were found to be well tolerated by NHDF up to concentrations of 388 μg/mL of lipid. The same trend was observed for MCF-7 cells following incubation for 24 h. After incubation for 48 h, however, the two highest concentrations (291 μg/mL and 388 μg/mL) induced a reduction in MCF-7 cell viability. These results are in agreement with previous works with similar types of nanoparticles, where NHDF were found to have a high tolerability at a similar or higher range of SLN concentrations [37, 38], while MCF-7, presented lower tolerability with values of $IC_{50}$ ranging from 175 μg/mL to 560 μg/mL of SLN after 48 h incubation [39, 40]. Moreover, due to the FA active targeting, a higher internalization is prone to occur in MCF-7 cells, which overexpress the FR, in opposite to NHDF [41, 42].

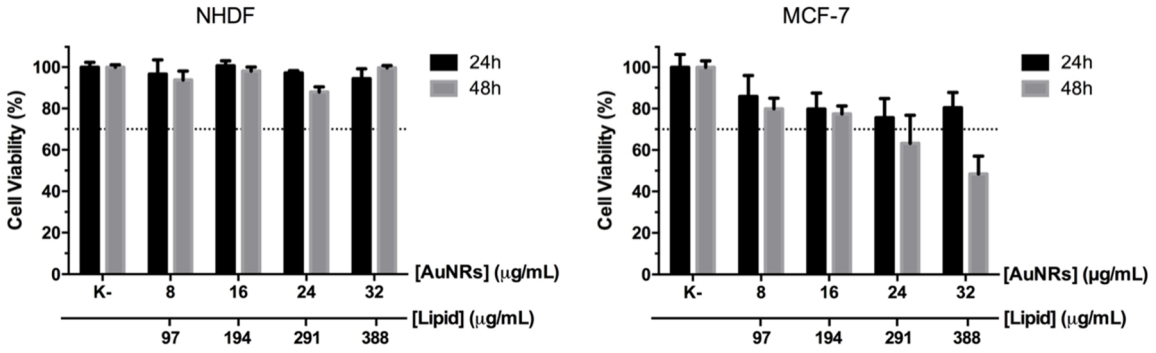


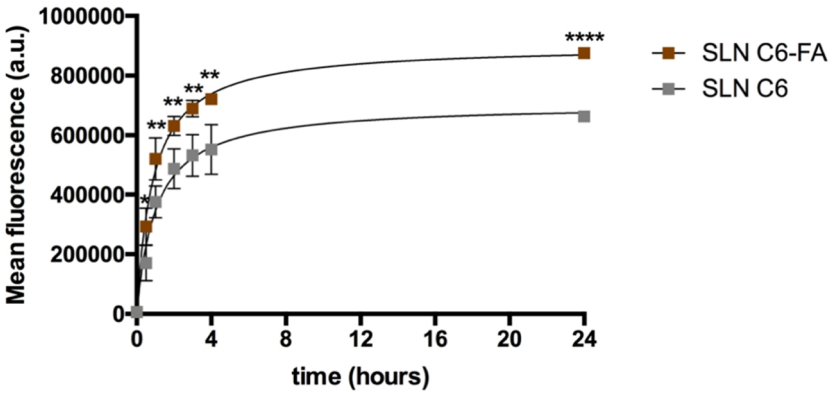

**Figure 4. Cytocompatibility of unloaded SLN.** Cell viability was evaluated following incubation with SLN Au-FA at different concentrations in normal (NHDF) and breast cancer cells (MCF-7) after 24 h and 48 h incubation. Data are expressed as mean ± SD (n = 5).

### 3.5. Cellular uptake

The effect of the functionalization on breast cancer cell targeting ability was evaluated by analysing MCF-7 cellular uptake of functionalized and non-functionalized SLN by flow cytometry and CLSM.

For the flow cytometry studies, C6-labelled SLN with and without the DSPE-PEG-FA conjugate (SLN C6-FA and SLN C6) were produced. Nanoparticles were then characterized to ensure that their main physicochemical characteristics were not considerably affected (**Table S1**). After that, SLN were incubated with MCF-7 for different incubation periods up to 24 h. The time-dependent cellular uptake in depicted in **Figure 5A.** After incubation with the two types of SLN, a rapid internalization occurred during the first 4 h, followed by a plateau. Moreover, a significantly higher cellular uptake was obtained for SLN C6-FA for all of the studied time-points, thus confirming the efficacy of the active targeting strategy. Additionally, the cellular uptake was found to follow Michaelis-Menten kinetics (**Figure 5B**). SLN C6-FA exhibited a 1.3-fold higher saturated cellular uptake ($V_{max}$) than non-functionalized SLN and a 1.2-fold lower k value, suggesting a higher and quicker cellular internalization, comparing to the non-functionalized SLN.

**A**




**B**

| | $V_{max}$ | k |
|---|---|---|
| **SLN C6** | 704691 ± 32091 | 1.04 ± 0.17 |
| **SLN C6-FA** | 901008 ± 24190 | 0.88 ± 0.09 |

**Figure 5. Cellular uptake of C6-labelled SLN in MCF-7 cells using flow cytometry. (A)** Time-dependent uptake of functionalized (SLN C6-FA) and non-functionalized (SLN C6) C6-labelled SLN for 24 h. Values represent mean ± SD; n = 3. Differences between groups were assessed using two-way ANOVA followed by Sidak post-hoc test. **p*<0.05, ***p*<0.01, *****p*<0.0001 (**B**) Michaelis-Menten kinetics parameters for SLN C6 and SLN C6-FA.

Cellular uptake was also evaluated through CLSM, using the intrinsic fluorescence of Mito for visualization. MCF-7 cells were incubated with the functionalized and non-functionalized SLN for 4 and 24 h. The CLSM images are presented in **Figure 6**. After incubation for 4 h, it is possible to observe a high red fluorescence in the cytoplasm of the cells, including in the endosomes and lysosomes, as suggested by the co-localisation of the green channel (Lysotracker) and the red channel (Mito). It is also evident that incubation with functionalized SLN results in a stronger fluorescence inside the cell comparing to their non-functionalized counterparts, suggesting a quicker and higher internalization of the functionalized SLN, mediated by the FR overexpressed in MCF-7 cells [42]. After 24 h (**Figure S3**), as expected, a much higher signal of the red channel was observed, with a translocation of Mito to the nucleus, which is its local of action, as denoted by the co-localization of the blue and red fluorescence. This effect can be attributed to a time-dependent cellular uptake and also to the

gradual release of Mito over time as shown in **Figure 2B**. Moreover, a higher accumulation of the functionalized SLN in cytoplasm could also be observed, although less evident that at 4 h incubation, which may reflect a saturation of the cellular uptake at 24 h. Additionally, a higher signal in the cell nucleus is also noticeable in the cells incubated with functionalized SLN-FA-Mito, once again suggesting a higher internalization. Overall CLSM data corroborate the flow cytometry results, demonstrating a higher cellular uptake of the functionalized SLN, comparing to their non-functionalized counterparts, suggesting a successful active targeting strategy.

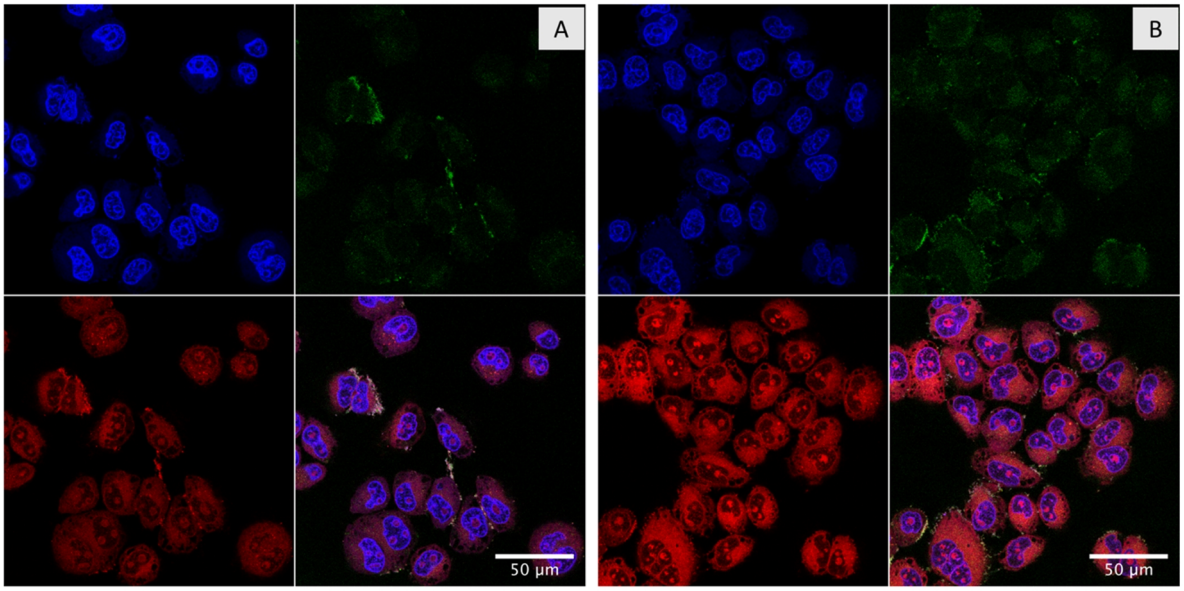



**Figure 6. CLSM images of SLN uptake in MCF-7 cells**. Cellular uptake of non-functionalized (**A**) and functionalized SLN (**B**) after incubation for 4 h. Blue channel: Hoechst 33342® (nucleus). Green channel: LysoTracker™ Green DND-26. Red channel: Mito.

To study the dynamics of cellular uptake in real-time, time-lapse CLSM was performed (**Figure 7**). MCF-7 cells were incubated with free Mito, SLN-Mito and SLN-FA-Mito for 30 min and images were recorded at pre-determined time-points. As it can be observed in **Figure 7**, nanoparticle uptake occurs approximately at 20 min of incubation. A higher red fluorescence intensity is observed following treatment with functionalized SLN for all the studied time-points, which suggests the occurrence of a faster and higher cancer cell internalization of these nanoparticles. Interestingly, both SLN and SLN-FA led to an enhanced Mito uptake in comparison with incubation with the free drug. Similar facts have been reported in other studies for the Mito analogue doxorubicin [43, 44]. This fact can be related to the lipophilicity of SLN, which enhance the interaction with the cell membranes, thus improving drug intracellular delivery [43, 45]. Moreover, free drug and drug-loaded nanoparticles may enter cells through different mechanisms. Free Mito internalization occurs mainly through passive [46] or flip-flop diffusion [47], being subjected to P-glycoprotein (P-gp)-mediated efflux [47]. In

contrast, nanoparticles are generally internalized via endocytosis, which may improve the intracellular drug delivery and evade the P-gp-mediated drug efflux [44, 48].

Overall these data support that FA functionalization resulted in a faster and higher cancer cell uptake for the first 30 minutes of incubation with the nanoparticles, demonstrating the efficacy of the functionalization.

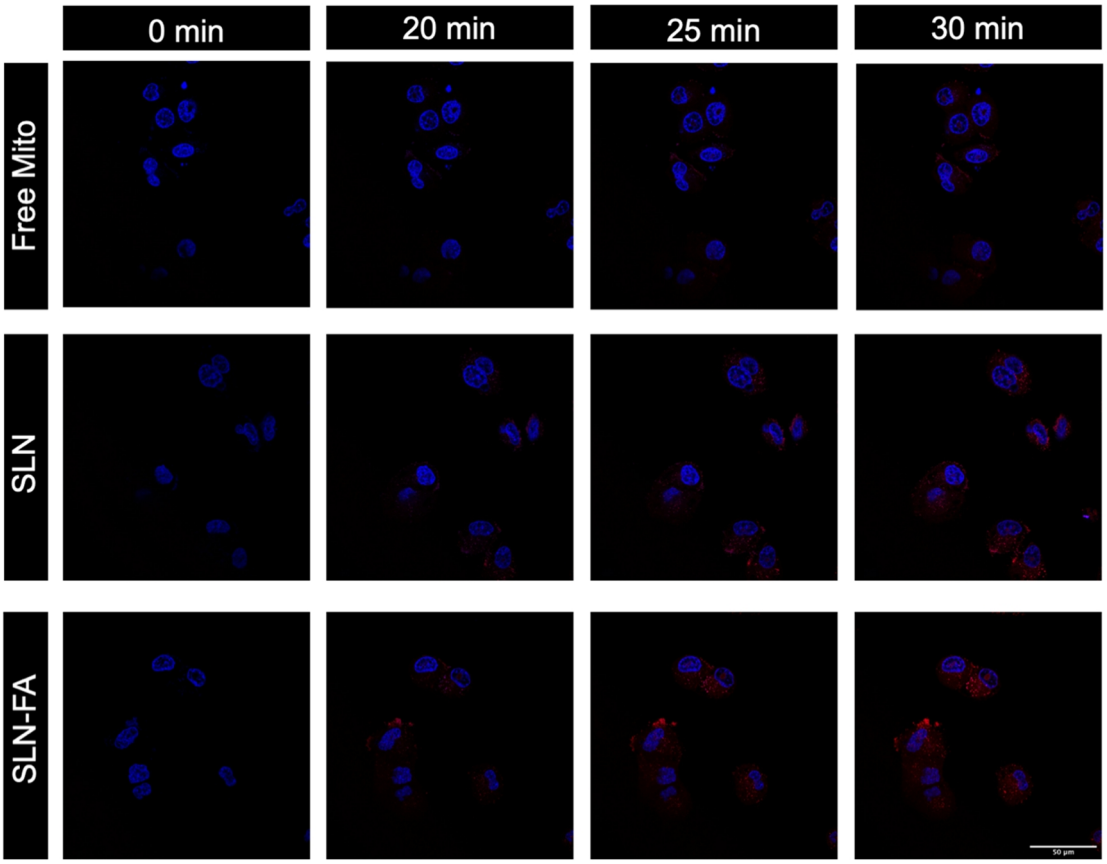



**Figure 7. Time-lapse CLSM of the MCF-7 cellular uptake of free Mito, SLN-Mito and SLN-Mito-FA**. Cells were incubated under the different conditions at 37 ˚C for 30 min in the confocal incubator chamber and images were acquired every 5 min. The cellular uptake of free Mito, SLN and SLN-FA in MCF-7 cells was followed for 30 min.

### 3.6. Chemo and Phototherapeutic combined effects

After evaluating the cytocompatibility of the nanosystem and the targeting efficiency towards MCF-7 cells, the phototherapeutic and chemotherapeutic combined effects of the nanoformulation were analysed at two different concentrations of AuNRs (**Figure 8**). Cells were incubated with the nanoformulations and after 4 h, exposed to NIR light for 5 min. A

control comprising cells treated with only DMEM exposed to NIR light was also included. As shown in **Figure 8**, there were no differences between irradiated and non-irradiated control cells, demonstrating that NIR irradiation *per se*, did not induce any alterations in cancer cell viability. In contrast, NIR light induced a significant reduction in cancer cell viability after treatment with SLN Au-FA at the highest concentration tested (corresponding to 32 µg/mL of AuNRs), demonstrating the PTT effect of the nanosystem. Moreover, for Mito-loaded SLN, both concentrations tested were able to elicit a higher cancer cell death following exposure to NIR light. At the highest concentration tested (32 µg/mL of AuNRs and equivalent 10 µg/mL of Mito), cell viability decreased from 22 to 8%, which can be attributed to the combined actions of PTT, chemotherapy and NIR-induced drug release. Zheng *et al*. has developed a nanoformulation based on NLC loaded with doxorubicin and polyhedral gold nanoparticles aiming to combine chemotherapy, PTT and drug release. The authors could achieve a demarked reduction in cancer cell viability from approximately 20 to 10% at a concentration of 20 µg/mL of doxorubicin and 500 µg/mL of NLC. Nevertheless, in this study a high laser dose was used (20 W $cm^{-2}$) with an irradiation time of 10 min [23]. In our work, similar results were obtained using a much lower power (1.7 W $cm^{-2}$) and only 5 min of irradiation. Overall, our data suggest that the multifunctional lipid nanosystem here developed is a promising strategy for breast cancer multimodal therapy.

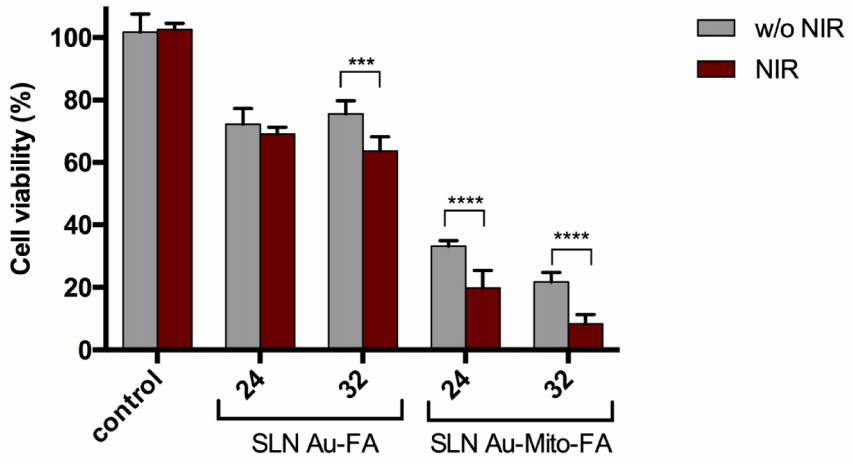



**Figure 8.** Phototherapeutic and combined PTT-chemotherapy effects of the nanoformulations in MCF-7 cells upon NIR irradiation (808 nm, 1.7 W $cm^{-2}$) for 5 min. Cells were treated for 24 h. Data are expressed as mean ± SD (n = 5). Differences between groups were assessed using two-way ANOVA followed by Sidak post-hoc test ***$p$<0.001, ****$p$<0.0001.

## 4. Conclusion

In this work, novel multifunctional lipid nanoparticles co-loaded with Mito and AuNRs were produced for combined PTT-chemotherapy of breast cancer. Nanoparticles presented adequate physicochemical characteristics for intravenous injection and tumor passive accumulation. Additionally, an active targeting strategy was implemented by functionalizing the SLN surface with DSPE-PEG-FA conjugate. A temperature increase up to 20˚C was mediated by the nanoformulation upon NIR laser irradiation, demonstrating its suitability for PTT applications. Additionally, an increased drug release occurred following NIR light exposure for 5 min, suggesting that the temperature variation was enough to destabilize the lipid matrix structure. Moreover, nanoparticles were found to be non-hemolytic and well tolerated by normal and tumoral cells. The functionalization was found to be effective, leading to higher nanoparticle accumulation in MCF-7 cells, as demonstrated by flow cytometry and CLSM studies. Finally, the chemo-phototherapeutic effect of the nanoformulation was evaluated in MCF-7 cells. NIR irradiation induced a significant reduction in cancer cell viability following incubation with drug-loaded and unloaded SLN demonstrating the PTT effect of the nanosystem. Furthermore, a demarked increase of cancer cell death was obtained due to the combined effects of chemotherapy, NIR-induced drug release and PTT. Overall these data suggest that the developed lipid nanosystem combining active cancer cell targeting, PTT, NIR-induced drug release and chemotherapy represents an economically viable and effective approach for the multimodal therapy of breast cancer.

## Acknowledgments

This work received financial support from PT national funds (FCT/MCTES, Fundação para a Ciência e Tecnologia and Ministério da Ciência, Tecnologia e Ensino Superior) through the project UIDB/50006/2020 (LAQV-REQUIMTE). This work was also financed by CENTRO-01-0145-FEDER-028989 and POCI-01-0145-FEDER-031462. Andreia Granja acknowledges FCT (Fundação para a Ciência e Tecnologia) and ESF (European Social Fund) for her PhD grant SFRH/BD/130147/2017. Rita Lima-Sousa and Cátia G. Alves acknowledge funding from individual PhD fellowships from FCT (SFRH/BD/144922/2019 and SFRH/BD/145386/2019). Duarte de Melo-Diogo acknowledges CENTRO-01-0145-FEDER-028989 for the funding given in the form of a research contract. Célia T. Sousa thanks FCT for financial support through the Investigador FCT program (contract no. IF/01159/2015), to the program Atraccion de Talento (CAM), ref. 2020-T1/IND-19889 and the UE's Horizon 2020 research and

innovation program under the Marie Sklodowska-Curie grant no. 734801. The authors are also grateful for the technical support from the CLSM studies were performed at the Imaging by confocal and fluorescence lifetime laboratory, CEMUP, Portugal.

## References


1. Sung, H., J. Ferlay, R.L. Siegel, M. Laversanne, I. Soerjomataram, A. Jemal, and F. Bray, *Global Cancer Statistics 2020: GLOBOCAN Estimates of Incidence and Mortality Worldwide for 36 Cancers in 185 Countries.* CA Cancer J Clin, 2021. **71**(3): p. 209-249.
2. Polyak, K., *Heterogeneity in breast cancer.* The Journal of clinical investigation, 2011. **121**(10): p. 3786-3788.
3. Tan, P.H., I. Ellis, K. Allison, E. Brogi, S.B. Fox, S. Lakhani, A.J. Lazar, E.A. Morris, A. Sahin, and R. Salgado, *The 2019 World Health Organization classification of tumours of the breast.* Histopathology, 2020. **77**(2): p. 181-185.
4. Bai, X., J. Ni, J. Beretov, P. Graham, and Y. Li, *Cancer stem cell in breast cancer therapeutic resistance.* Cancer Treatment Reviews, 2018. **69**: p. 152-163.
5. Lee, J. and J.-C. Kim, *Photothermally triggerable solid lipid nanoparticles containing gold nanospheres.* Colloids and Surfaces A: Physicochemical and Engineering Aspects, 2015. **484**: p. 441-448.
6. Abadeer, N.S. and C.J. Murphy, *Recent progress in cancer thermal therapy using gold nanoparticles.* The Journal of Physical Chemistry C, 2016. **120**(9): p. 4691-4716.
7. Manivasagan, P., S. Bharathiraja, M. Santha Moorthy, S. Mondal, T.P. Nguyen, H. Kim, T.T.V. Phan, K.D. Lee, and J. Oh, *Biocompatible Chitosan Oligosaccharide Modified Gold Nanorods as Highly Effective Photothermal Agents for Ablation of Breast Cancer Cells.* Polymers, 2018. **10**(3): p. 232.
8. Xu, W., J. Qian, G. Hou, Y. Wang, J. Wang, T. Sun, L. Ji, A. Suo, and Y. Yao, *PEGylated hydrazided gold nanorods for pH-triggered chemo/photodynamic/photothermal triple therapy of breast cancer.* Acta Biomaterialia, 2018. **82**: p. 171-183.
9. Nguyen, V.D., H.-K. Min, D.-H. Kim, C.-S. Kim, J. Han, J.-o. Park, and E. Choi, *Macrophage-Mediated Delivery of Multifunctional Nanotherapeutics for Synergistic Chemo-photothermal Therapy of Solid Tumors.* ACS Applied Materials & Interfaces, 2020.
10. Xing, Y., J. Zhang, F. Chen, J. Liu, and K. Cai, *Mesoporous polydopamine nanoparticles with co-delivery function for overcoming multidrug resistance via synergistic chemo-photothermal therapy.* Nanoscale, 2017. **9**(25): p. 8781-8790.
11. Peng, Y., J. Nie, W. Cheng, G. Liu, D. Zhu, L. Zhang, C. Liang, L. Mei, L. Huang, and X. Zeng, *A multifunctional nanoplatform for cancer chemo-photothermal synergistic therapy and overcoming multidrug resistance.* Biomaterials science, 2018. **6**(5): p. 1084-1098.
12. Fan, W., B. Yung, P. Huang, and X. Chen, *Nanotechnology for multimodal synergistic cancer therapy.* Chemical reviews, 2017. **117**(22): p. 13566-13638.
13. Siafaka, P.I., N. Üstündağ Okur, E. Karavas, and D.N. Bikiaris, *Surface modified multifunctional and stimuli responsive nanoparticles for drug targeting: current status and uses.* International journal of molecular sciences, 2016. **17**(9): p. 1440.
14. Li, Y., D. He, J. Tu, R. Wang, C. Zu, Y. Chen, W. Yang, D. Shi, T.J. Webster, and Y. Shen, *The comparative effect of wrapping solid gold nanoparticles and hollow gold nanoparticles with doxorubicin-loaded thermosensitive liposomes for cancer thermo-chemotherapy.* Nanoscale, 2018. **10**(18): p. 8628-8641.
15. Nguyen, V.D., H.K. Min, C.S. Kim, J. Han, J.O. Park, and E. Choi, *Folate receptor-targeted liposomal nanocomplex for effective synergistic photothermal-chemotherapy of breast cancer in vivo.* Colloids Surf B Biointerfaces, 2019. **173**: p. 539-548.
16. Hashimoto, T., E. Yuba, A. Harada, and K. Kono, *Preparation of photothermal-chemotherapy nanohybrids by complexation of gold nanorods with polyamidoamine dendrimers having poly (ethylene glycol) and hydrophobic chains.* Journal of Materials Chemistry B, 2020. **8**(14): p. 2826-2833.
17. Wu, J., Y. Liu, Y. Tang, S. Wang, C. Wang, Y. Li, X. Su, J. Tian, Y. Tian, J. Pan, et al., *Synergistic Chemo-Photothermal Therapy of Breast Cancer by Mesenchymal Stem Cell-Encapsulated Yolk-Shell GNR@HPMO-PTX Nanospheres.* ACS Appl Mater Interfaces, 2016. **8**(28): p. 17927-35.
18. Monem, A.S., N. Elbialy, and N. Mohamed, *Mesoporous silica coated gold nanorods loaded doxorubicin for combined chemo–photothermal therapy.* International journal of pharmaceutics, 2014. **470**(1-2): p. 1-7.
19. Encinas-Basurto, D., J. Ibarra, J. Juarez, A. Pardo, S. Barbosa, P. Taboada, and M.A. Valdez, *Hybrid folic acid-conjugated gold nanorods-loaded human serum albumin nanoparticles for*

*simultaneous photothermal and chemotherapeutic therapy.* Materials Science and Engineering: C, 2018. **91**: p. 669-678.
20. Darwish, W.M., A.S. Abdoon, M.S. Shata, and M. Elmansy, *Vincristine-loaded polymeric corona around gold nanorods for combination (chemo-photothermal) therapy of oral squamous carcinoma.* Reactive and Functional Polymers, 2020. **151**: p. 104575.
21. Albuquerque, J., C.C. Moura, B. Sarmento, and S. Reis, *Solid lipid nanoparticles: a potential multifunctional approach towards rheumatoid arthritis theranostics.* Molecules, 2015. **20**(6): p. 11103-11118.
22. Ong, Y.S., M. Bañobre-López, S.A.C. Lima, and S. Reis, *A multifunctional nanomedicine platform for co-delivery of methotrexate and mild hyperthermia towards breast cancer therapy.* Materials Science and Engineering: C, 2020. **116**: p. 111255.
23. Zheng, S., V.D. Nguyen, S.Y. Song, J. Han, and J.O. Park, *Combined photothermal-chemotherapy of breast cancer by near infrared light responsive hyaluronic acid-decorated nanostructured lipid carriers.* Nanotechnology, 2017. **28**(43): p. 435102.
24. Varadwaj, P., K. Misra, A. Sharma, and R. Kumar, *Mitoxantrone: an agent with promises for anticancer therapies.* Electronic Journal of Biology, 2010. **6**(2): p. 36-42.
25. Herman, T.S., *Effect of Temperature on the Cytotoxicity of Vindesine, Amsacrine, and Mitoxantrone1, 2.* Cancer treatment reports, 1983. **67**(11): p. 1019.
26. Assaraf, Y.G., C.P. Leamon, and J.A. Reddy, *The folate receptor as a rational therapeutic target for personalized cancer treatment.* Drug Resistance Updates, 2014. **17**(4-6): p. 89-95.
27. Granja, A., R. Lima-Sousa, C.G. Alves, D. de Melo-Diogo, M. Pinheiro, C.T. Sousa, I.J. Correia, and S. Reis, *Mitoxantrone-loaded lipid nanoparticles for breast cancer therapy–quality-by-design approach and efficacy assessment in 2D and 3D in vitro cancer models.* International Journal of Pharmaceutics, 2021: p. 121044.
28. Lopes-de-Araújo, J., A.R. Neves, V.M. Gouveia, C.C. Moura, C. Nunes, and S. Reis, *Oxaprozin-Loaded Lipid Nanoparticles towards Overcoming NSAIDs Side-Effects.* Pharmaceutical research, 2016. **33**(2): p. 301-314.
29. Lima-Sousa, R., D. de Melo-Diogo, C.G. Alves, C.S. Cabral, S.P. Miguel, A.G. Mendonça, and I.J. Correia, *Injectable in situ forming thermo-responsive graphene based hydrogels for cancer chemo-photothermal therapy and NIR light-enhanced antibacterial applications.* Materials Science and Engineering: C, 2020. **117**: p. 111294.
30. Silva, M.I., A.I. Barbosa, S.A. Costa Lima, P. Costa, T. Torres, and S. Reis, *Freeze-dried Softisan® 649-based lipid nanoparticles for enhanced skin delivery of cyclosporine A.* Nanomaterials, 2020. **10**(5): p. 986.
31. Singh, R. and J.W. Lillard Jr, *Nanoparticle-based targeted drug delivery.* Experimental and molecular pathology, 2009. **86**(3): p. 215-223.
32. Wang, S., Z. Liu, Y. Tong, Y. Zhai, X. Zhao, X. Yue, Y. Qiao, Y. Liu, Y. Yin, and R. Xi, *Improved cancer phototheranostic efficacy of hydrophobic IR780 via parenteral route by association with tetrahedral nanostructured DNA.* Journal of Controlled Release, 2021. **330**: p. 483-492.
33. Danaei, M., M. Dehghankhold, S. Ataei, F. Hasanzadeh Davarani, R. Javanmard, A. Dokhani, S. Khorasani, and M. Mozafari, *Impact of particle size and polydispersity index on the clinical applications of lipidic nanocarrier systems.* Pharmaceutics, 2018. **10**(2): p. 57.
34. Brown, M.A., A. Goel, and Z. Abbas, *Effect of electrolyte concentration on the stern layer thickness at a charged interface.* Angewandte Chemie, 2016. **128**(11): p. 3854-3858.
35. Xiao, K., Y. Li, J. Luo, J.S. Lee, W. Xiao, A.M. Gonik, R.G. Agarwal, and K.S. Lam, *The effect of surface charge on in vivo biodistribution of PEG-oligocholic acid based micellar nanoparticles.* Biomaterials, 2011. **32**(13): p. 3435-3446.
36. ISO10993-4, *Biological Evaluation of Medical Devices Part 4. Selection of Tests for Interactions with Blood*. 2017.
37. Ruktanonchai, U., U. Sakulkhu, P. Bejrapha, P. Opanasopit, N. Bunyapraphatsara, V. Junyaprasert, and S. Puttipipatkhachorn, *Effect of lipid types on physicochemical characteristics, stability and antioxidant activity of gamma-oryzanol-loaded lipid nanoparticles.* Journal of microencapsulation, 2009. **26**(7): p. 614-626.
38. Schubert, M. and C. Müller-Goymann, *Characterisation of surface-modified solid lipid nanoparticles (SLN): influence of lecithin and nonionic emulsifier.* European journal of pharmaceutics and biopharmaceutics, 2005. **61**(1-2): p. 77-86.
39. Ying, X.-Y., D. Cui, L. Yu, and Y.-Z. Du, *Solid lipid nanoparticles modified with chitosan oligosaccharides for the controlled release of doxorubicin.* Carbohydrate polymers, 2011. **84**(4): p. 1357-1364.

40. Doktorovova, S., E.B. Souto, and A.M. Silva, *Nanotoxicology applied to solid lipid nanoparticles and nanostructured lipid carriers–a systematic review of in vitro data.* European Journal of Pharmaceutics and Biopharmaceutics, 2014. **87**(1): p. 1-18.
41. Faria, R., A. Sousa, A.R. Neves, J.A. Queiroz, and D. Costa, *Methotrexate-plasmid DNA polyplexes for cancer therapy: Characterization, cancer cell targeting ability and tuned in vitro transfection.* Journal of Molecular Liquids, 2019. **292**: p. 111391.
42. Soleymani, J., M. Hasanzadeh, M.H. Somi, N. Shadjou, and A. Jouyban, *Probing the specific binding of folic acid to folate receptor using amino-functionalized mesoporous silica nanoparticles for differentiation of MCF 7 tumoral cells from MCF 10A.* Biosensors and Bioelectronics, 2018. **115**: p. 61-69.
43. Mussi, S.V., R.C. Silva, M.C. de Oliveira, C.M. Lucci, R.B. de Azevedo, and L.A.M. Ferreira, *New approach to improve encapsulation and antitumor activity of doxorubicin loaded in solid lipid nanoparticles.* European journal of pharmaceutical sciences, 2013. **48**(1-2): p. 282-290.
44. Yoo, H.S. and T.G. Park, *Folate receptor targeted biodegradable polymeric doxorubicin micelles.* Journal of controlled release, 2004. **96**(2): p. 273-283.
45. Wong, H.L., A.M. Rauth, R. Bendayan, J.L. Manias, M. Ramaswamy, Z. Liu, S.Z. Erhan, and X.Y. Wu, *A new polymer–lipid hybrid nanoparticle system increases cytotoxicity of doxorubicin against multidrug-resistant human breast cancer cells.* Pharmaceutical research, 2006. **23**(7): p. 1574-1585.
46. Burns, C.P., B.N. Haugstad, and J.A. North, *Membrane transport of mitoxantrone by L1210 leukemia cells.* Biochem Pharmacol, 1987. **36**(6): p. 857-60.
47. Regev, R., D. Yeheskely-Hayon, H. Katzir, and G.D. Eytan, *Transport of anthracyclines and mitoxantrone across membranes by a flip-flop mechanism.* Biochemical Pharmacology, 2005. **70**(1): p. 161-169.
48. Shahabi, S., S. Döscher, T. Bollhorst, L. Treccani, M. Maas, R. Dringen, and K. Rezwan, *Enhancing cellular uptake and doxorubicin delivery of mesoporous silica nanoparticles via surface functionalization: effects of serum.* ACS applied materials & interfaces, 2015. **7**(48): p. 26880-26891.

## Supplementary data

### Thermostability studies of mitoxantrone by NMR

The NMR spectrum of the mitoxantrone hydrochloride at 20°C confirmed the chemical structure and the purity of the drug, according to the supplier's specifications (**Figure S1**, bottom). The expected protons were possible to register and the presence of two set of signals in the low field region (high chemical shift values) evidenced that the molecule is present in the cationic form in aqueous solution.

In the defined experimental conditions, no evidence of the formation of new signals was possible to determine, nor changes in the integral intensities or in the signals' multiplicity, at any of the tested temperature values. Also, the chemical shift of the characteristic protons remained unaltered, specially the aliphatic protons from the carbonated lateral chains. Only a negligible effect on the chemical shift of aromatic protons was verified, however the maximum variation of these values was about 0.13 ppm, from 20 to 70 °C (**Figure S1**).

Globally, the NMR studies confirmed that no structural changes occurred in the molecule for temperature values up to 70 °C, suggesting that mitoxantrone is suitable for the subsequent studies of PTT.

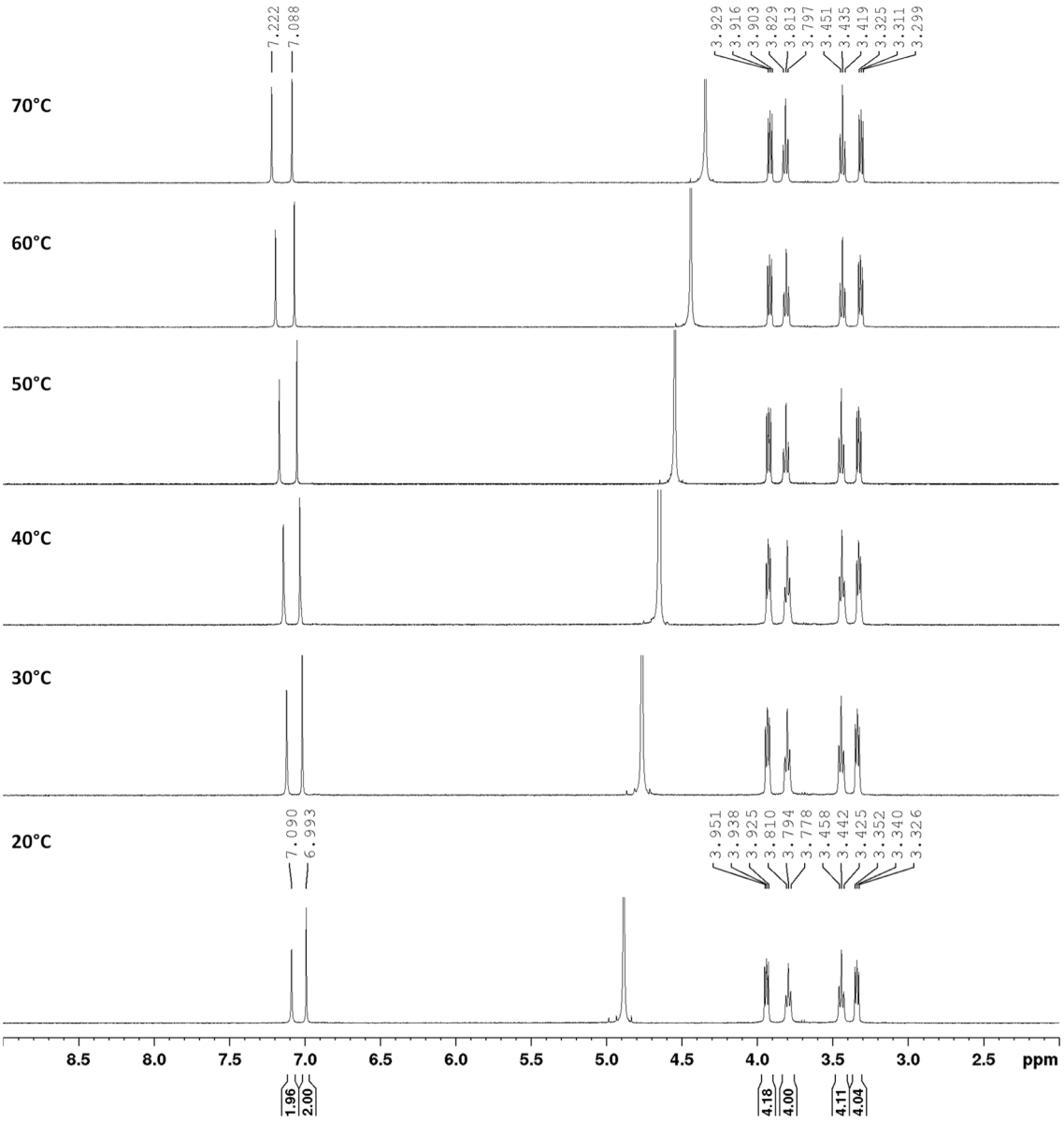



**Figure S1**. $^{1}$H NMR spectra of Mito after incubation during 30 min at 20, 30, 40, 50, 60 and 70˚C.

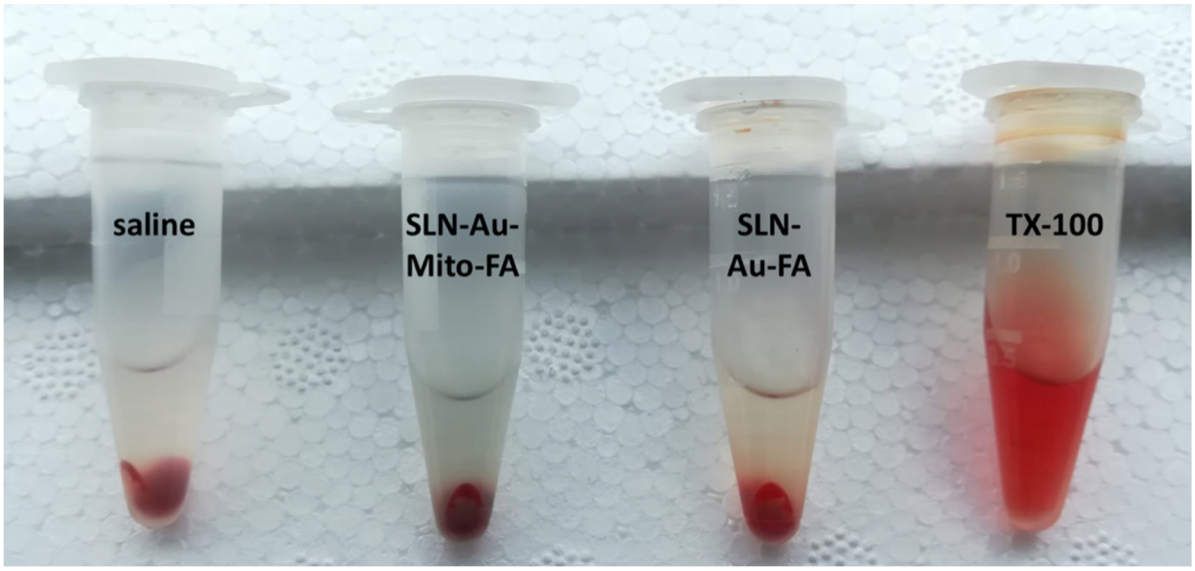



**Figure S2. Hemolysis assay.** Image of the samples treated with the highest concentration of nanoformulation tested (40 µg/mL of AuNRs) of SLN-Au-Mito-FA, SLN-Au-FA and controls - negative (saline solution) and positive (TX-100 - 1% v/v) following 4 h incubation.

**Table S1.** Physicochemical characterization of C6-loaded SLN

| | Size (nm) | PDI | Zeta potential (mV) |
|---|---|---|---|
| **SLN C6** | 212 ± 1 | 0.11 ± 0.01 | -8 ± 2 |
| **SLN C6-FA** | 230 ± 2 | 0.06 ± 0.01 | -10 ± 2 |

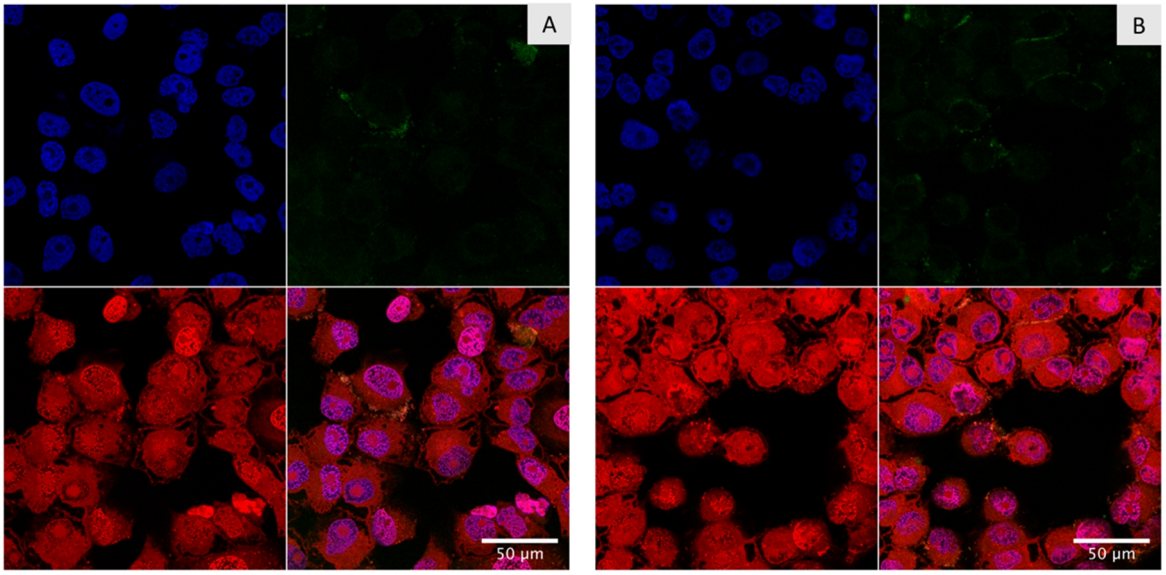



**Figure S3. CLSM images of SLN uptake in MCF-7 cells**. Cellular uptake of non-functionalized (**A**) and functionalized SLN (**B**) after incubation for 24 h. Blue channel: Hoechst 33342 (nucleus). Green channel: LysoTracker™ Green DND-26. Red channel: Mito.

# Chapter 5

## Concluding remarks and future perspectives

According to the latest 2020 statistics, breast cancer is the most common and the deathliest cancer in women all over the world [1]. The disease has also a significant impact in the patients' quality of life, being the leading cause of DALYs in women in 2017 [2]. Moreover, breast cancer has a high economic burden, with elevated economic and healthcare costs [3, 4]. The standard treatment regimens include local (surgery and radiotherapy) and adjuvant systemic therapies (hormonal therapy, targeted therapy and chemotherapy). Local therapies, however, are generally ineffective for the most advanced stages of disease, while hormonal and targeted therapies are only suitable for specific breast cancer subtypes. In this way, chemotherapy is the only adjuvant therapeutic that can be used to every breast cancer subtype and also one of the major therapeutics for advanced and metastatic disease [5, 6]. Chemotherapy efficacy, however, is compromised by its limited cancer cell-selectivity, which causes dose-limiting systemic side-effects [7]. In addition, cancer cells may develop MDR [8]. These limitations can result in treatment failure, disease recurrence, metastasis and eventual death of the patients. Therefore, new treatment options with less side-effects and improved efficacy are needed.

In this thesis, nanomedicine strategies were applied to improve breast cancer therapy. First, a literature review addressing the potential of nanomedicine and, particularly, lipid nanoparticles in the context of breast cancer therapy was performed (**Chapter 2.1**). Here, a deeper understanding of the pathophysiology of the disease and its current therapeutics and limitations was obtained. Additionally, the benefits of nanomedicine and, lipid nanoparticles in particular, for the specific therapeutic purpose were identified. It was also found that only a very limited amount of studies, have reported the development of multifunctional and multimodal lipid nanoparticles. Secondly, after identifying the potential of combining conventional chemotherapy with other treatment modalities such as hyperthermia, a literature review describing the latter was conducted (**Chapter 2.2**). The aim of this review was to gather more information on the molecular and clinical aspects of hyperthermia and understand the benefits of nanoparticle-mediated hyperthermia, particularly photothermal therapy (PTT). During the execution of this literature review it was also found that PTT could enhance the cytotoxicity of common chemotherapeutic drugs, including Mito.

The theoretical knowledge acquired in the abovementioned chapters was then used to design the main experimental goals of this thesis. First, a lipid nanodelivery system was developed and optimized for the entrapment of the chemotherapeutic drug Mito (**chapter 4.1**); after that, the anti-cancer efficacy of the nanosystem was evaluated in 2D and 3D breast cancer models (**chapter 4.1**); subsequently, the selectivity towards breast cancer cells was improved by exploring two different active targeting strategies based on hyaluronic acid (**chapter 4.2**) and folic acid (**chapter 4.3**) and, ultimately, a cancer cell-targeted multifunctional nanosystem combining chemotherapy and PTT was developed (**chapter 4.4**).

In order to achieve the first goal, solid lipid nanoparticles were produced using a simple, low-cost, organic-solvent-free method for the entrapment of Mito (**chapter 4.1**). For a cost-effective, rational and systematic optimization of the nanoformulation, a Box-Behnken design, a tool frequently used in the pharmaceutical industry, was implemented [9]. Nanoparticles presented adequate physicochemical properties for intravenous injection and tumor passive accumulation along with a high drug entrapment efficiency. The release of Mito was found to occur at a much faster rate at acidic than physiological pH. These findings suggested that once in the circulation, only a limited amount of drug will be released, thus minimizing systemic side effects. On the other hand, when in the presence of an acidic environment, such as the tumor region and the cellular endosomal compartments, a faster and higher drug release may occur, where free Mito can exert its action in the nucleus. Moreover, the nanoformulation was stable for at least 6 months of storage. After these studies, the hemocompatibility of the SLN in human RBCs was demonstrated, suggesting, once again, its suitability for circulation in the bloodstream. The lipid nanocarrier was also found to have a high tolerability in both normal (NHDF) and breast cancer cell line MCF-7. Finally, the anti-cancer activity of the nanosystem was evaluated in 2D and 3D cancer cell models. The latter were produced due to their capacity to replicate with higher accuracy the heterogeneity, cell and extracellular matrix interactions, nutrient access and drug and nanoparticle permeability [10]. The nanoformulation was found to maintain the high anti-tumoral effects of the free drug in both models and was also able to penetrate the developed three-dimensional structure. This work demonstrated that an effective Mito drug delivery vehicle with a high anti-cancer activity was possible to build using solid lipid nanoparticles produced with a simple economically affordable method.

After the development of the Mito-loaded SLN, there was the need to rely not only on the EPR effect for nanoparticle tumor accumulation, but also on an active targeting strategy to improve the selectivity of the nanosystem towards cancer cells. Two different conjugates were synthesized. First SLN were surface decorated with a DPPE-HA conjugate (**chapter 4.2**), taking advantage of the overexpression of the CD44 receptor overexpressed in several types

of cancer, including breast cancer [11, 12]. HA is glycosaminoglycan with a set of beneficial properties, such as biodegradability, biocompatibility and non-immunogenicity, which make it a promising cancer cell active targeting ligand [13, 14]. Despite its affinity towards CD44 receptor, due its hydrophilicity, HA can also limit protein absorption and opsonisation [15]. Since its binding affinity towards CD44 is influenced by different factors, including the HA molecular weight [16, 17], in this study two different conjugates with a low (20-60 kDa) and high HA (1000-1800 kDa) molecular weight were studied to evaluate their influence on breast cancer cell targeting ability. Nanoparticles main characteristics, release profile, hemolytic activity and storage stability were not considerably affected after functionalization. The cell viability studies pointed to a tendency of the high molecular weight HA- functionalized SLN to elicit a higher anti-tumoral activity, as shown by the values of $IC_{50}$. Cellular uptake studies in confocal microscopy pointed to an enhanced internalization following decoration with the two conjugates, suggesting the efficacy of the developed active targeting strategy. Comparing the two HA molecular weights, the high HA seemed to induce an enhanced cellular uptake. Moreover, after 24h a nuclear translocation was observed, suggesting that Mito could be effectively delivered to its cellular target. Flow cytometry studies also pointed to a time-dependent cellular uptake, which was improved after functionalization with the high molecular weight HA. Overall these findings suggested that a HA of a higher molecular weight was the most suitable for breast cancer cell active targeting.

A second active targeting strategy was developed based on FA (**chapter 4.3)**. A DSPE-PEG-FA conjugate was produced and used for the surface functionalization of the SLN, aiming to prolong its blood circulation and enhance breast cancer cell targeting, due to the effects of PEG and FA, respectively [18, 19]. The use of small molecules such as FA as targeting agents is an appealing approach given their low cost, conjugation through simple and easy methods, facility of large-scale production and high affinity towards the FR [20]. Due to the overexpression of the FR in most solid tumors and negligible expressing in most normal tissues, the targeting of the FR may improve cancer drug delivery, while limiting non-specific tissue distribution [21, 22]. Similarly to the previous studies, SLN retained their physicochemical characteristics, drug release profile, stability and non-hemolytic potential. Moreover, FA-functionalized SLN induced a higher cytotoxicity towards MCF-7 cells, as shown by the value of $IC_{50}$, which was comparatively smaller than the value determined after treatment with SLN functionalized with HA of a high molecular weight. Additionally, an enhanced cellular uptake occurred after functionalization with the DSPE-PEG-FA conjugate, as assessed by confocal microscopy and flow cytometry. The uptake of these nanoparticles was also showed to be mediated by clathrin and macropinocytosis.

Following the two active targeting strategies, FA was selected to proceed with further studies. Moreover, a previous work studying the heating behaviour of gold nanorods using pulsed versus continuous near infrared (NIR) laser (**Appendix I**), has led to the choice of continuous NIR laser for this particular application. After developing an effective Mito nanocarrier with suitable characteristics and high selectivity towards breast cancer cells, a multifunctional SLN co-loaded with Mito and AuNRs was produced for combination of chemotherapy and PTT. The nanosystem was able to induce a temperature increase of more than 20˚C and could release the drug at higher rate following NIR light irradiation. Nanoparticle functionalization resulted in a quicker and higher cancer cellular internalization. Similar outcomes were obtained using time-lapse live cell imaging in confocal microscopy, where functionalized SLN were found to be internalized after 30 min, demonstrating a faster and higher uptake than non-functionalized SLN and free Mito. This effect is in agreement with the findings found in the previous chapters, where Mito-loaded SLN and, particularly, functionalized Mito-loaded SLN led to an enhanced anti-cancer activity than the free drug. This can be related to the lipophilicity of the SLN, which can more easily interact with the cell membranes [23] and also to the different cellular uptake mechanisms that occur for the SLN and free drug, which are generally endocytosis and passive or flip-flop diffusion, respectively [24, 25]. Endocytosis may promote a higher drug uptake and also evade efflux mediated by the drug efflux pumps, in contrast to what occurs with the free drug [26, 27]. Finally, the combined effects of chemotherapy, NIR light-induced drug release and PTT resulted in a higher breast cancer cell death, proving the efficacy of the multimodal therapy.

To conclude, in this thesis a lipid nanosystem was developed to improve breast cancer therapy, starting from the design and optimization of a simple SLN drug delivery system, until the development of a more complex multimodal nanosystem for dual chemo and PTT. Taking into account the advantages of these nanosystems, namely their economically affordable production and functionalization strategies, a scale-up and a clinical translation may be feasible, after the appropriate *in vivo* and clinical studies.

**Limitations and future perspectives**

Despite the interesting results of the experimental work here reported, there are also several limitations that need to be identified and future work that should be conducted. First, the stability of the nanoparticles in more complex media, such as human plasma or blood remains to be evaluated. One possibility is to use NTA, as reported previously [28]. It would also be important to evaluate the anti-cancer activity and the targeting efficiency of the

nanoformulations in other breast cancer 2D and 3D cell models, including the ones with breast cancer subtypes that are more challenging to treat, such as TNBC, for instance the MDA-MB-231 cell line, which also overexpresses the FR [29, 30]. Also, taking into account the results obtained in terms of enhanced anti-tumoral activity and internalization, comparing to the free drug and the possible drug efflux pump evasion mediated by the nanoparticles, it would also be interesting to evaluate the efficacy of these nanoformulations in MDR cell lines, such as the MCF7/VP cell line [31]. Moreover, the selectivity of the functionalized SLN needs to be elucidated, by evaluating cellular uptake in normal cells that do not express or have a reduced expression of FR, such as the human breast epithelial cell line MCF10A [32]. Finally, the lack of *in vivo* biodistribution, toxicity and efficacy studies is also a major limitation of this scientific work and an issue that is already being addressed. Regarding this fact, some preliminary results were added to the Appendix section (**Appendix II**).

## References

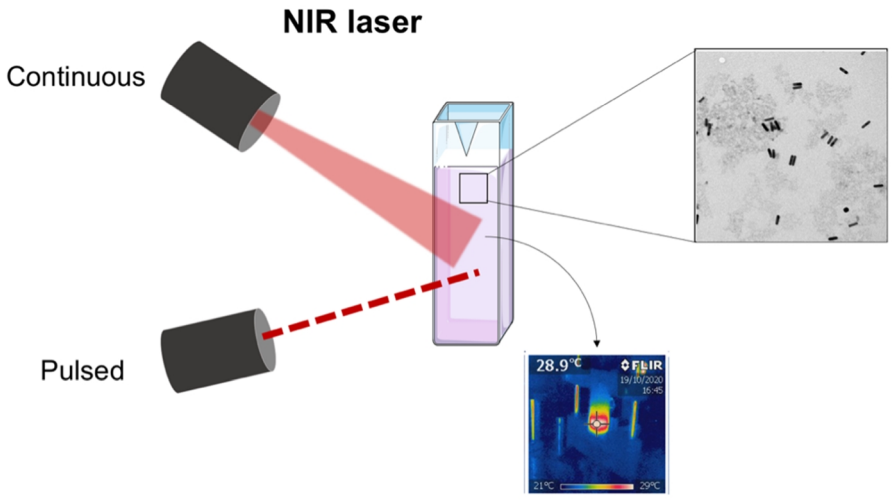

1. Sung, H., J. Ferlay, R.L. Siegel, M. Laversanne, I. Soerjomataram, A. Jemal, and F. Bray, *Global cancer statistics 2020: GLOBOCAN estimates of incidence and mortality worldwide for 36 cancers in 185 countries.* CA: a cancer journal for clinicians, 2021. **71**(3): p. 209-49
2. Global Burden of Disease Cancer, C., C. Fitzmaurice, D. Abate, N. Abbasi, H. Abbastabar, F. Abd-Allah, O. Abdel-Rahman, A. Abdelalim, A. Abdoli, I. Abdollahpour, et al., *Global, Regional, and National Cancer Incidence, Mortality, Years of Life Lost, Years Lived With Disability, and Disability-Adjusted Life-Years for 29 Cancer Groups, 1990 to 2017: A Systematic Analysis for the Global Burden of Disease Study.* JAMA oncology, 2019. **5**(12): p. 1749-68.
3. Luengo-Fernandez, R., J. Leal, A. Gray, and R. Sullivan, *Economic burden of cancer across the European Union: a population-based cost analysis.* Lancet Oncol, 2013. **14**(12): p. 1165-74.
4. Mariotto, A.B., K. Robin Yabroff, Y. Shao, E.J. Feuer, and M.L. Brown, *Projections of the cost of cancer care in the United States: 2010–2020.* Journal of the National Cancer Institute, 2011. **103**(2): p. 117-28.
5. Mayer, E.L. and H.J. Burstein, *Chemotherapy for metastatic breast cancer.* Hematology/oncology clinics of North America, 2007. **21**(2): p. 257-72.
6. Goldhirsch, A., J.N. Ingle, R. Gelber, A. Coates, B. Thürlimann, and H.-J. Senn, *Thresholds for therapies: highlights of the St Gallen International Expert Consensus on the primary therapy of early breast cancer 2009.* Annals of oncology, 2009. **20**(8): p. 1319-29.
7. Shapiro, C.L. and A. Recht, *Side effects of adjuvant treatment of breast cancer.* New England Journal of Medicine, 2001. **344**(26): p. 1997-2008.
8. Bai, X., J. Ni, J. Beretov, P. Graham, and Y. Li, *Cancer stem cell in breast cancer therapeutic resistance.* Cancer Treatment Reviews, 2018. **69**: p. 152-63.
9. Mishra, V., S. Thakur, A. Patil, and A. Shukla, *Quality by design (QbD) approaches in current pharmaceutical set-up.* Expert opinion on drug delivery, 2018. **15**(8): p. 737-58.
10. Costa, E.C., A.F. Moreira, D. de Melo-Diogo, V.M. Gaspar, M.P. Carvalho, and I.J. Correia, *3D tumor spheroids: an overview on the tools and techniques used for their analysis.* Biotechnology advances, 2016. **34**(8): p. 1427-41.
11. Xu, H., M. Niu, X. Yuan, K. Wu, and A. Liu, *CD44 as a tumor biomarker and therapeutic target.* Exp Hematol Oncol, 2020. **9**(1): p. 36.
12. Chang Hyun Kim, S.G.L., Myung Joo Kang, Sangkil Lee & Young Wook Choi, *Surface modification of lipid-based nanocarriers for cancer cell-specific drug targeting.* Journal of Pharmaceutical Investigation, 2017.
13. Tiwari, S. and P. Bahadur, *Modified hyaluronic acid based materials for biomedical applications.* International journal of biological macromolecules, 2019. **121**: p. 556-71.

14. Marinho, A., C. Nunes, and S. Reis, *Hyaluronic Acid: A Key Ingredient in the Therapy of Inflammation.* Biomolecules, 2021. **11**(10): p. 1518.
15. Santhanam, S., J. Liang, R. Baid, and N. Ravi, *Investigating thiol-modification on hyaluronan via carbodiimide chemistry using response surface methodology*. Journal of biomedical materials research. Part A, 2015. **103**(7): p. 2300-08.
16. Tavianatou, A.G., Z. Piperigkou, C. Barbera, R. Beninatto, V. Masola, I. Caon, M. Onisto, M. Franchi, D. Galesso, and N.K. Karamanos, *Molecular size-dependent specificity of hyaluronan on functional properties, morphology and matrix composition of mammary cancer cells.* Matrix Biol Plus, 2019. **3**: p. 100008.
17. Jordan, A.R., R.R. Racine, M.J. Hennig, and V.B. Lokeshwar, *The role of CD44 in disease pathophysiology and targeted treatment.* Frontiers in immunology, 2015. **6**: p. 182.
18. Shah, N.B., G.M. Vercellotti, J.G. White, A. Fegan, C.R. Wagner, and J.C. Bischof, *Blood–nanoparticle interactions and in vivo biodistribution: impact of surface PEG and ligand properties.* Molecular pharmaceutics, 2012. **9**(8): p. 2146-55.
19. Sudimack, J. and R.J. Lee, *Targeted drug delivery via the folate receptor.* Advanced drug delivery reviews, 2000. **41**(2): p. 147-62-
20. Pearce, A.K. and R.K. O'Reilly, *Insights into active targeting of nanoparticles in drug delivery: Advances in clinical studies and design considerations for cancer nanomedicine.* Bioconjugate chemistry, 2019. **30**(9): p. 2300-11.
21. Zwicke, G.L., G.A. Mansoori, and C.J. Jeffery, *Utilizing the folate receptor for active targeting of cancer nanotherapeutics.* Nano Reviews & Experiments, 2012. **3**.
22. Kue, C.S., A. Kamkaew, K. Burgess, L.V. Kiew, L.Y. Chung, and H.B. Lee, *Small molecules for active targeting in cancer.* Medicinal research reviews, 2016. **36**(3): p. 494-575.
23. Mussi, S.V., R.C. Silva, M.C. de Oliveira, C.M. Lucci, R.B. de Azevedo, and L.A.M. Ferreira, *New approach to improve encapsulation and antitumor activity of doxorubicin loaded in solid lipid nanoparticles.* European journal of pharmaceutical sciences, 2013. **48**(1-2): p. 282-90.
24. Burns, C.P., B.N. Haugstad, and J.A. North, *Membrane transport of mitoxantrone by L1210 leukemia cells.* Biochem Pharmacol, 1987. **36**(6): p. 857-60.
25. Regev, R., D. Yeheskely-Hayon, H. Katzir, and G.D. Eytan, *Transport of anthracyclines and mitoxantrone across membranes by a flip-flop mechanism.* Biochemical Pharmacology, 2005. **70**(1): p. 161-69.
26. Shahabi, S., S. Döscher, T. Bollhorst, L. Treccani, M. Maas, R. Dringen, and K. Rezwan, *Enhancing cellular uptake and doxorubicin delivery of mesoporous silica nanoparticles via surface functionalization: effects of serum.* ACS applied materials & interfaces, 2015. **7**(48): p. 26880-91.
27. Yoo, H.S. and T.G. Park, *Folate receptor targeted biodegradable polymeric doxorubicin micelles.* Journal of controlled release, 2004. **96**(2): p. 273-83.
28. Montes-Burgos, I., D. Walczyk, P. Hole, J. Smith, I. Lynch, and K. Dawson, *Characterisation of nanoparticle size and state prior to nanotoxicological studies.* Journal of Nanoparticle Research, 2010. **12**(1): p. 47-53.
29. Marshalek, J.P., P.S. Sheeran, P. Ingram, P.A. Dayton, R.S. Witte, and T.O. Matsunaga, *Intracellular delivery and ultrasonic activation of folate receptor-targeted phase-change contrast agents in breast cancer cells in vitro.* Journal of Controlled Release, 2016. **243**: p. 69-77.
30. Soleymani, M., M. Velashjerdi, Z. Shaterabadi, and A. Barati, *One-pot preparation of hyaluronic acid-coated iron oxide nanoparticles for magnetic hyperthermia therapy and targeting CD44-overexpressing cancer cells.* Carbohydrate polymers, 2020. **237**: p. 116130.
31. Diah, S.K., P.K. Smitherman, J. Aldridge, E.L. Volk, E. Schneider, A.J. Townsend, and C.S. Morrow, *Resistance to mitoxantrone in multidrug-resistant MCF7 breast cancer cells: evaluation of mitoxantrone transport and the role of multidrug resistance protein family proteins.* Cancer Res, 2001. **61**(14): p. 5461-7.
32. Soleymani, J., M. Hasanzadeh, M.H. Somi, N. Shadjou, and A. Jouyban, *Probing the specific binding of folic acid to folate receptor using amino-functionalized mesoporous silica nanoparticles for differentiation of MCF 7 tumoral cells from MCF 10A.* Biosensors and Bioelectronics, 2018. **115**: p. 61-69.

# Appendix

# Appendix I

**Preliminary results of a study conducted to evaluate the most suitable NIR laser (Pulsed versus continuous) and other key parameters in the heating behavior of gold nanoparticles for photothermal therapy applications**




In the first study, a pulsed femtosecond laser (Femtosecond Ti:Sapphire amplifier (FemtopowerTM) running with 1kHz repetition rate, pulse duration of 30 fs, wavelength 800 nm) was used. Two different gold nanostructures geometries were evaluated (spherical and rods),with the latter being selected to proceed with further studies. Different parameters which could influence gold nanorods heating behavior were then studied, including nanorod concentration, laser output power, laser spot size, use of a laser pulse amplification and irradiation time. In **Figure A1**, a summary of study of laser output power and concentration of nanorods on their heating behavior is presented. The temperature increase over time was measured using both a type-K thermocouple and FLIR i7 Infrared Thermal camera. Additionally, the SPR band of the gold nanorods was measured by UV-VIS spectroscopy after laser exposure. As observed in the graphs of **Figure A1**, the temperature did not rise more than 10ºC, using a very high concentration of AuNRs. This may occur due to a more localized heating of the nanorods, which, does not result in a temperature increase of the surrounding media [1]. In addition, the surface plasmon resonances band of the AuNRs at 800 nm, disappeared after one single laser irradiation, possibly indicating the reshaping of the AuNRs

induced by the high power laser [2]. Taking into account the final purpose of the work, which was the encapsulation of the nanorods into lipid nanoparticles able to generate a reasonable temperature increase to promote the melting of the solid lipid, a continuous NIR laser was then evaluated.

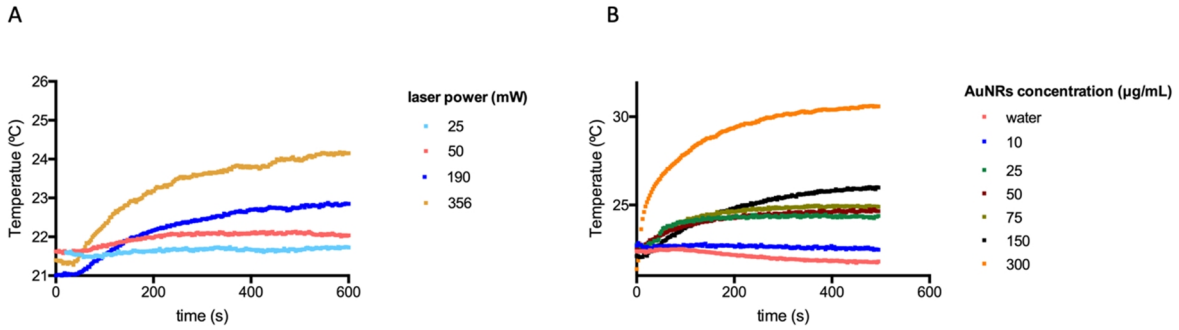



**Figure A1.** Study of the influence of pulser laser output power (**A**) and AuNRs concentration (**B**) on the heating behaviour of AuNRs over time.

An infrared continuous laser (MDL-III-808/1~2500mW) operating at 808 nm was selected to proceed with further studies using AuNRS. In this work, several relevant parameters were also studied, such as the concentration of AuNRs, the volume of the solution, the laser output power and the laser spot area. In this study, the values of the Specific Absorption Rate (SAR) based on the temperature heating curves obtained were also calculated. **Figure A2** presents a summary of the influence of the AuNRs concentration and output power of the NIR laser on the heating curves of the AuNRs. The most relevant parameter in the heating of the AuNRs was the laser output power. A much higher temperature variation was also obtained when compared to the heating curves of the pulsed laser, even at much lower concentrations. The thermal images obtained using an infrared camera displayed in **Figure A3** showing the maximum temperature reached for the two laser types using the same concentration of AuNRs, also highlight this fact. Therefore the continuous laser was found to be the most suitable for the desired application in the context of this PhD thesis.

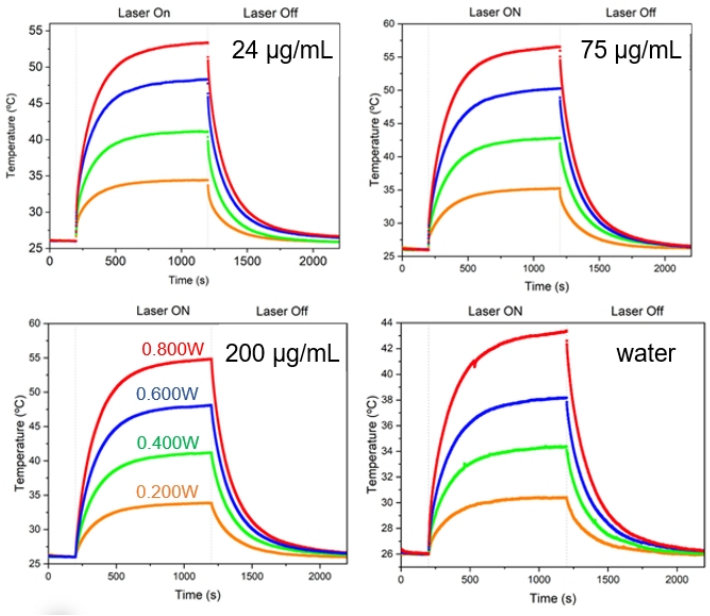



**Figure A2.** Study of the influence of the output power of a continuous laser (800 nm) and concentration of AuNRS on the heating behaviour of AuNRs over time.

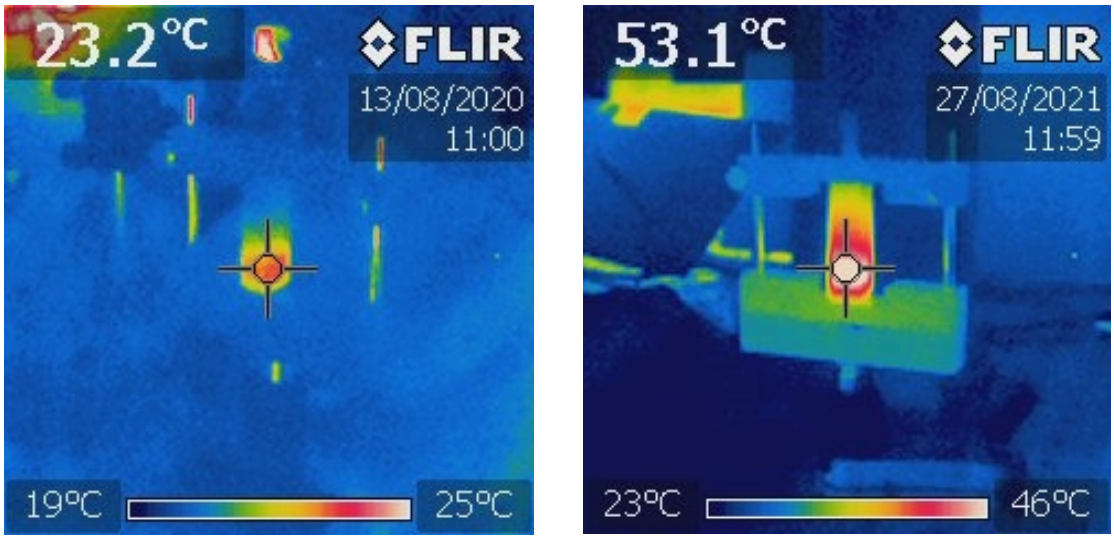



**Figure A3.** Maximum temperature reached following pulsed (left) and continuous (right) NIR laser irradiation of the gold nanorods at a concentration of 75 µg/mL at the maximum power for the two laser types measured using a FLIR i7 Infrared Thermal camera. Pulsed laser specifications: Femtosecond Ti:Sapphire amplifier (FemtopowerTM) running with 1kHz repetition rate, pulse duration of 30 fs, wavelength 800 nm. Continuous wave laser: 808 nm with a maximum output power of 2.5W.

# Appendix II

**Preliminary results of an *in vivo* biodistribution assay using IVIS**

SLN were produced has described in **Chapter 4.4** and labelled with Cyanine 5 (Cy5) at an amount corresponding to 0.025% and 0.1% of the total lipid mass (size 221 nm; PDI 0.10; EE%: 97; size 199 nm; PDI 0.13; EE%: 96, respectively) for visualization in the IVIS system.

In this pilot study, two different administration routes were evaluated, the retro-orbital and the intraperitoneal injection, using healthy wild-type C57BL/6 mice. In addition, two nanoformulations with different concentrations of Cy5 were tested. With both injection routes, concentrations up to 200 mg/Kg (nanoparticles per kilogram of mouse) were possible to be administered, which demonstrated the high biocompatibility of the nanoparticles. The biodistribution of the nanoparticles was observed using IVIS immediately after administration and 1h later, as shown in **Figure A4** for one of the administration routes and one of the Cy5 concentrations. After 1h, the nanoparticles seem to distribut all over the animal body, with a higher accumulation in the liver region. Depending on the concentration and administration routes, slighly different elimination times (occuring mainly via bladder) occurred.

Future work will focus on performing biodistribution studies after selection of the most adequate administration route and concentration of Cy5. Also, a xenografted tumor model will be developed and the nanoparticles biodistribution will then be evaluated and compared to that of the healthy mice. After that, the anti-tumoral activity of the nanoformulations *in vivo* will be assessed, with and without NIR laser irradiation.

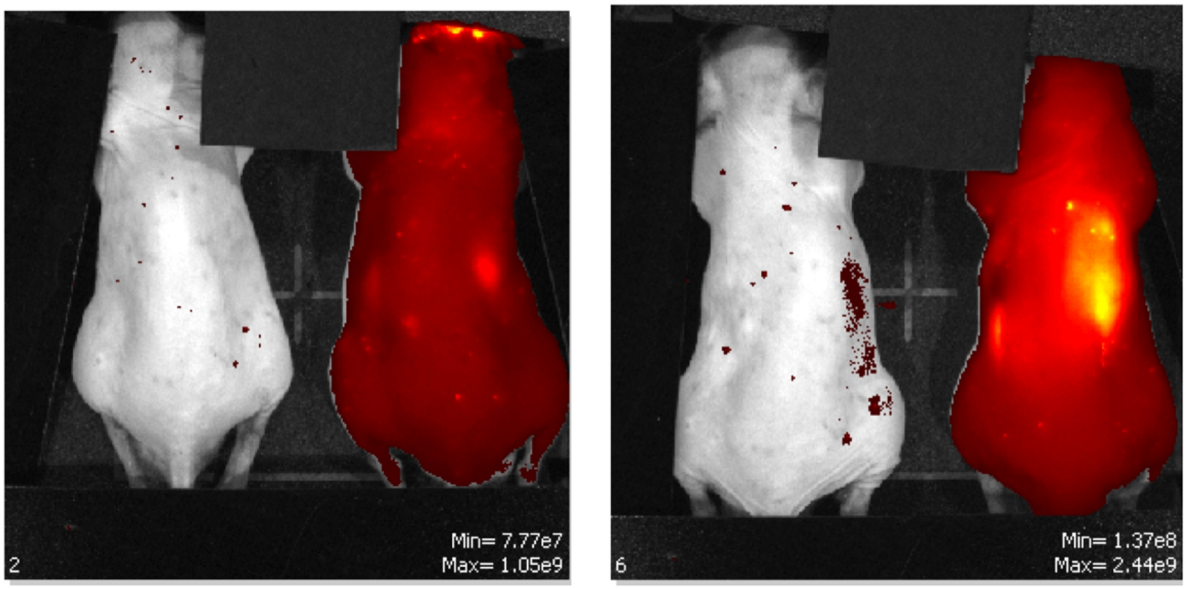



**Figure A4**. SLN biodistribution 0h (left) and 1h (right) after retro-orbital injection in healthy wild-type C57BL/6 mice. Left mouse injected with saline solution (control), right mouse injected with the SLN-FA-Cy5 nanoformulation. Data were obtained suing an IVIS Spectrum 200 In vivo Imaging System (Perkin Elmer, MA, USA). Exposure time 20, binning factor 2, excitation filter 620, emission filter 670, f number 1, field of view 10.

## References


1. Sahu, A., M. Kim, J. Ryu, J.-G. Son, E. Lee, and G. Tae, *Nanographene oxide as a switch for CW/pulsed NIR laser triggered drug release from liposomes.* Materials Science and Engineering: C, 2018. **82**: p. 19-24,
2. González-Rubio, G., A. Guerrero-Martínez, and L.M. Liz-Marzán, *Reshaping, fragmentation, and assembly of gold nanoparticles assisted by pulse lasers.* Accounts of chemical research, 2016. **49**(4): p. 678-86,